Langley Aerospace Test Highlights 1988

NASA

National Aeronautics and
Space Administration

Langley Research Center
Hampton, Virginia 23665-5225

NASA Technical Memorandum 101579

Langley Research Center

Foreword

The role of the Langley Research Center is to perform basic and applied research necessary for the advancement of aeronautics and space flight, to generate new and advanced concepts for the accomplishment of related national goals, and to provide research advice, technological support, and assistance to other NASA installations, other government agencies, and industry. This report highlights some of the significant tests that were performed during calendar year 1988 in Langley Research Center test facilities, a number of which are unique in the world. The report illustrates both the broad range of the research and technology activities at the Langley Research Center and the contributions of this work toward maintaining United States leadership in aeronautics and space research. Other highlights of Langley research and technology for 1988 are described in *Research and Technology 1988 Annual Report of the Langley Research Center.* Further information about both reports is available from the Office of the Chief Scientist, Mail Stop 105-A, Langley Research Center, Hampton, Virginia 23665 (804-864-6062).

Richard H. Petersen
Director

Availability Information

For additional information on any highlight, contact one of the individuals identified with the highlight. This individual is either a member or a leader of the research group. Commercial telephone users may dial the listed extension preceded by (804) 864. Telephone users with access to the Federal Telecommunications System (FTS) may dial the extension preceded by 928.

Contents

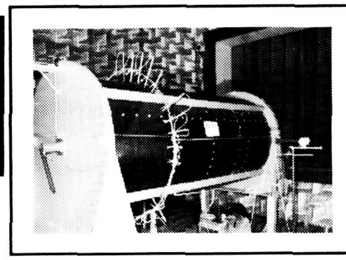

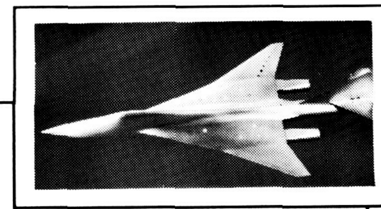

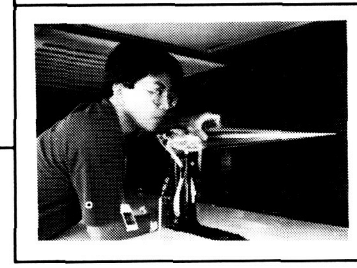

30- by 60-Foot Tunnel

The Langley 30- by 60-Foot Tunnel is a continuous-flow open-throat double-return tunnel powered by two 4000-hp electric motors, each driving a four-blade 35.5-ft-diameter fan. The tunnel test section is 30 ft high and 60 ft wide and is capable of speeds up to 100 mph. The tunnel was first put into operation in 1931 and has been used continuously since then to study the low-speed aerodynamics of commercial and military aircraft. The large open-throat test section lends itself readily to tests of large-scale models and to unique test methods with small-scale models.

Large-scale and full-scale aircraft tests are conducted with the strut mounting system. This test method can handle airplanes up to the size of present-day light twin-engine airplanes. Such tests provide static aerodynamic performance and stability and control data, including the measurement of power effects, wing pressure distributions, and flow visualization.

Small-scale models can be tested to determine both static and dynamic aerodynamics. For all captive tests, the models are sting mounted with internal strain-gauge balances. The captive test methods include conventional static tests for performance and stability and control, forced-oscillation tests for aerodynamic damping, and rotary tests for spin aerodynamics. Dynamically scaled subscale models, properly instrumented, are also freely flown in the large test section with a simple tether to study their dynamic stability characteristics at low speed and at high angles of attack. A small computer is used in this free-flight test technique to represent the important characteristics of the airplane flight control system.

The Langley 12-Foot Low-Speed Tunnel, which is used extensively for static tests prior to entry in the 30- by 60-Foot Tunnel, is an atmospheric wind tunnel with a 12-ft octagonal cross section for model testing. The tunnel serves as a diagnostic facility for exploratory research primarily in the area of high-angle-of-attack stability and control studies of various airplane and spacecraft configurations. Preliminary tests are conducted in the 12-Foot Low-Speed Tunnel on simple models prior to testing in higher speed facilities on more sophisticated models to obtain more efficient test planning and effective use of occupancy time in such facilities.

Forebody Controls Research

One factor that limits the maneuvering effectiveness of current fighter aircraft is the degradation of aerodynamic control effectiveness at stall and poststall angles of attack. As a result, a number of new technologies are being developed, including advanced aerodynamic and propulsive control concepts, in order to enhance the maneuverability and agility of future fighter aircraft. One of these concepts, the use of actuated strakes on the aircraft forebody, is designed to take advantage of the long moment arm to the aircraft center of gravity and the existence of the powerful forebody vortex flow field at high angles of attack. The actuated

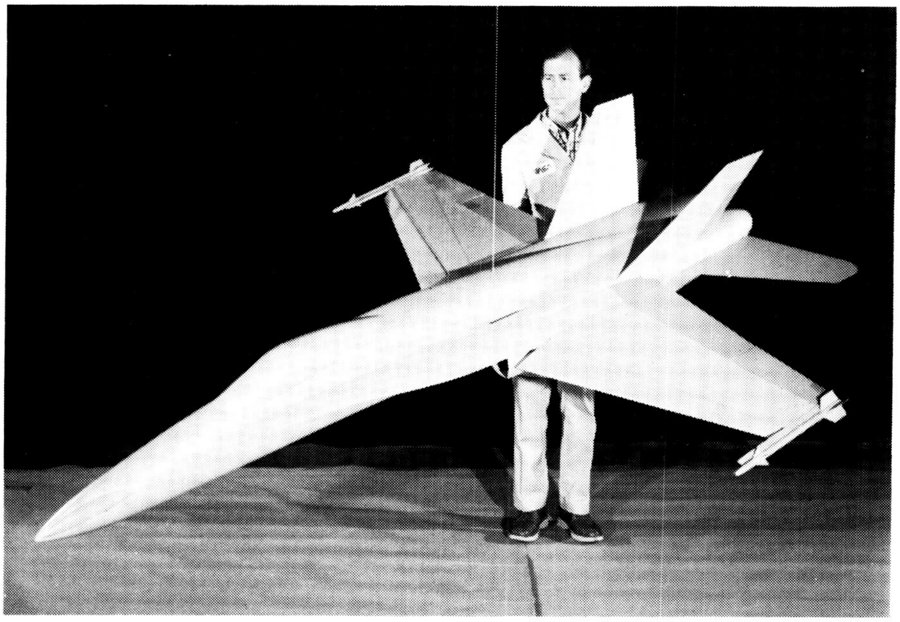

16-percent-scale F-18 free-flight model that incorporates actuated forebody strakes. L-88-3358

forebody strakes are designed to control this strong vortex flow field to provide enhanced yaw control at high angles of attack where a conventional rudder becomes ineffective.

Preliminary tests conducted with a generic fighter wind tunnel model have verified the potential of this concept. Results from these tests indicated that the actuated forebody strakes could provide greatly improved levels of yaw control at high angles of attack and would significantly enhance aircraft maneuverability. Research is currently under way to develop and demonstrate this concept during flight tests using the NASA F-18 High-Angle-of-Attack Research Vehicle (HARV). The figure shows a 16-percent scale model of the F-18 which has been modified to include a pair of conformal actuated forebody strakes. Results obtained with this model during static and free-flight tests in the 30- by 60-Foot Tunnel have shown similar promising results. During the wind tunnel free-flight tests, the model modified with the actuated forebody strakes was more maneuverable and was found to be controllable to much higher angles of attack than the unmodified configuration. The results of these and additional planned tests will be used to determine the best actuated forebody strake design for flight tests using the F-18 HARV aircraft.

(D. G. Murri, 41160)

Advanced Turboprop

A joint NASA/industry cooperative program was developed to investigate the low-speed static and dynamic stability and control characteristics and the flying qualities of a representative advanced turboprop (twin-engine pusher) business/commuter aircraft configuration. Previous tests, which were conducted on a 17.5-percent unswept, two-surface design in the 30- by 60-Foot Tunnel, showed that wing stall was accompanied by pronounced unstable roll damping, large asymmetrical rolling moments, and a marked degradation in aileron effectiveness. The in-

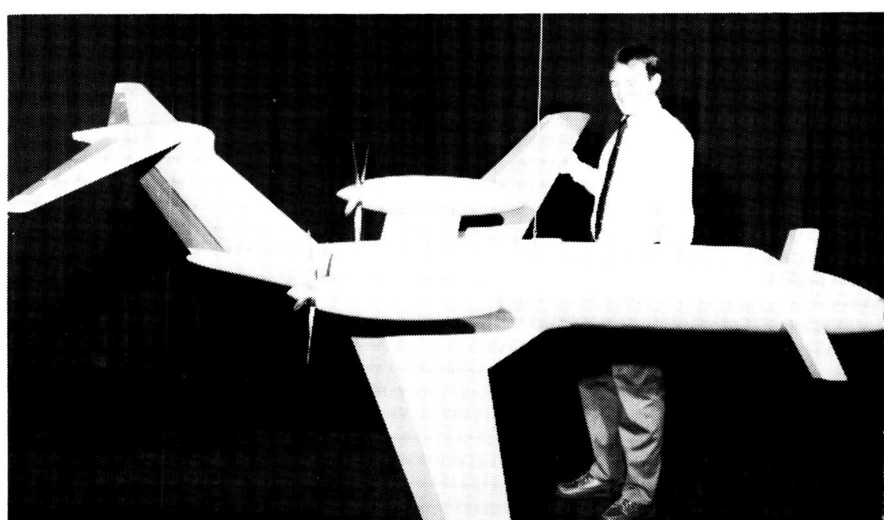

Advanced turboprop forward-swept wing configuration. L-89-3

vestigation showed significant effects of power in the poststall angle-of-attack range and the existence of a deep-stall trim point for engine-out conditions with a far-aft center-of-gravity location.

Based on the static and dynamic tests, wing leading-edge devices were designed to provide an increased stall margin in addition to improved roll damping and increased roll control in the stall/poststall angle-of-attack region. Tethered free-flight tests demonstrated that these modifications were effective and that the model exhibited satisfactory stability, control, and flying qualities.

Present tests include follow-on studies of various two- and three-surface designs to investigate configuration and power effects on stability and control and general flight behavior. The model has provisions for two locations of the main wing for two- and three-surface testing. The current test configuration features a 15° forward-swept wing and a 10° forward-swept canard. Future plans include free-flight tests for over-the-tail and over-the-wing propeller designs.

(P. L. Coe, 41150, D. B. Owens, and S. G. Turner)

Wind Tunnel Free-Flight Tests of Yaw Vectoring Applied to STOL and Maneuver Technology Demonstrator

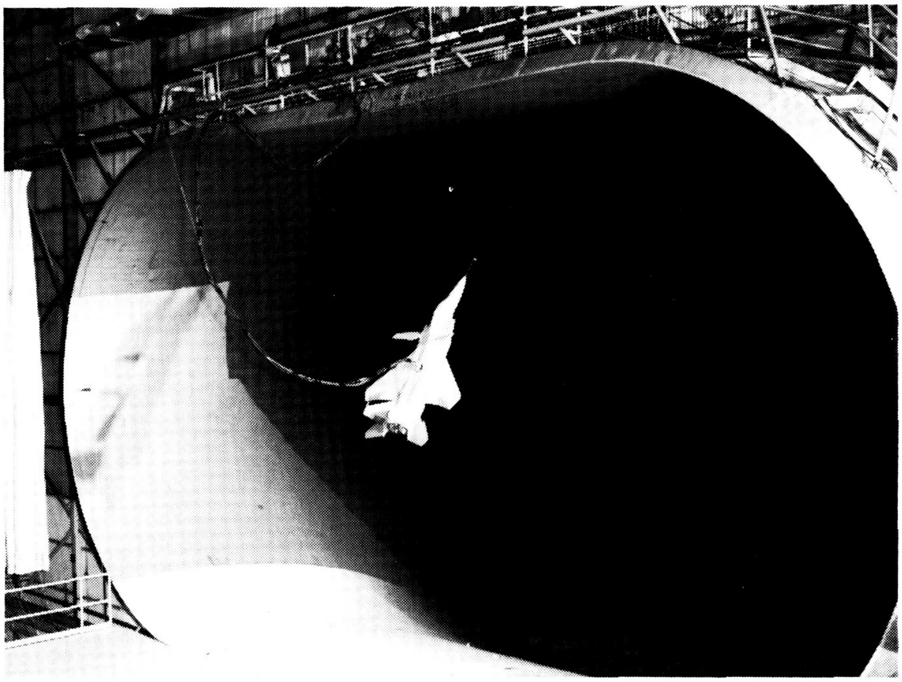

13-percent-scale modified F-15 S/MTD model during wind tunnel free-flight tests. L-88-1075

A series of wind tunnel free-flight tests have been conducted in the 30- by 60-Foot Tunnel in order to investigate the low-speed flight dynamic behavior of a model of the STOL (Short Takeoff and Landing) and Maneuver Technology Demonstrator (S/MTD) modified to include thrust vectoring in the yaw axis. The primary objective of the original United States Air Force sponsored S/MTD program is to investigate, develop, and validate technology areas related to providing current and future fighter aircraft with STOL capability and enhanced maneuvering performance. Wind tunnel free-flight tests were previously conducted using a 13-percent scale model of the baseline S/MTD configuration, which is an F-15 aircraft modified to include canards and two-dimensional exhaust nozzles incorporating pitch vectoring and thrust reversing. The current tests were conducted in order to investigate the additional maneuver enhancements that could be obtained with the addition of thrust vectoring in the yaw axis.

Free-flight tests conducted previously showed that the baseline model exhibited good flying characteristics to an angle of attack α of approximately 25°. These tests also showed that the thrust vectoring in the pitch axis provided excellent pitch control effectiveness. However, at angles of attack above 25°, yaw control degraded rapidly due to loss of rudder effectiveness such that the model could not be flown above an angle of attack of approximately 40°. These results indicate that the baseline S/MTD airplane will have good low-speed flight dynamic characteristics within its nominal test envelope ($\alpha < 30°$) but the flight behavior in the stall region will still be poor due to loss of rudder effectiveness.

The current free-flight tests were conducted with the 13-percent scale model modified to include thrust vectoring in the yaw axis. For these tests, the

aircraft flight control laws were modified to command blended rudder and yaw vectoring deflections to provide the desired yaw-control power. Results from the current free-flight tests showed that the addition of the thrust vectoring in yaw greatly enhanced the yaw control effectiveness at high angles of attack. With the addition of the yaw vectoring, the model was much easier to fly above an angle of attack of 25° and was flown to angles of attack well in excess of 40°.

(D. G. Murri, 41160)

Low-Turbulence Pressure Tunnel

The Langley Low-Turbulence Pressure Tunnel (LTPT) is a single-return closed-circuit tunnel that can be operated at pressures from near vacuum to 10 atm. The test section is rectangular in shape (3 ft wide and 7.5 ft in height and length), and the contraction ratio is 17.6:1. The LTPT is capable of testing at Mach numbers from 0.05 to 0.50 and unit Reynolds numbers from 0.1×10^6/ft to 15×10^6/ft. The tunnel has provisions for removal of the sidewall boundary layer by means of a closed-loop suction system mounted inside the pressure chamber. This system utilizes slotted vertical sidewalls just ahead of the model test section, and the removed air is reinjected through an annular slot downstream of the test section. A flow control system allows the flow and pressure requirements to be varied as dictated by tunnel operation. This system can be used to provide boundary-layer control (BLC) for low-drag airfoil research.

A BLC system for high-lift airfoil testing is also available. This system utilizes compressed dry air and involves tangential blowing from slots located on the sidewall mounting end plates. Flowmeters can be used to monitor the amount of air blown into the tunnel. An automatically controlled vent valve is utilized to remove the air injected into the tunnel by this system. A high-lift model support and force balance system is provided to handle both single-element and multiple-element airfoils. The LTPT has been modified to add a passive suction BLC system for high-lift testing and a three-component laser Doppler velocimeter (LDV).

The measured turbulence level of the LTPT is very low due to the large contraction ratio and the many fine-mesh antiturbulence screens. The excellent flow quality of this facility makes it particularly suitable for testing low-drag airfoils. Recent flow quality measurements in the LTPT indicate that the velocity fluctuations in the test section range from 0.025 percent at Mach 0.05 to 0.30 percent at Mach 0.20 at the highest unit Reynolds number.

The drive system is a 2000-hp direct-current motor with power supplied from a motor-generator set. The tunnel stagnation temperature is controlled by a heat exchanger, which provides both heating and cooling via steam injectors and modulated valves that control the flow volume of water through a set of coils.

Airfoil Drag Measurements at Low Reynolds Numbers

Recent interest in low Reynolds number aerodynamics has increased for both military and civil applications with emphasis on providing improved vehicle performance. Applications are varied and include remotely piloted vehicles, wind

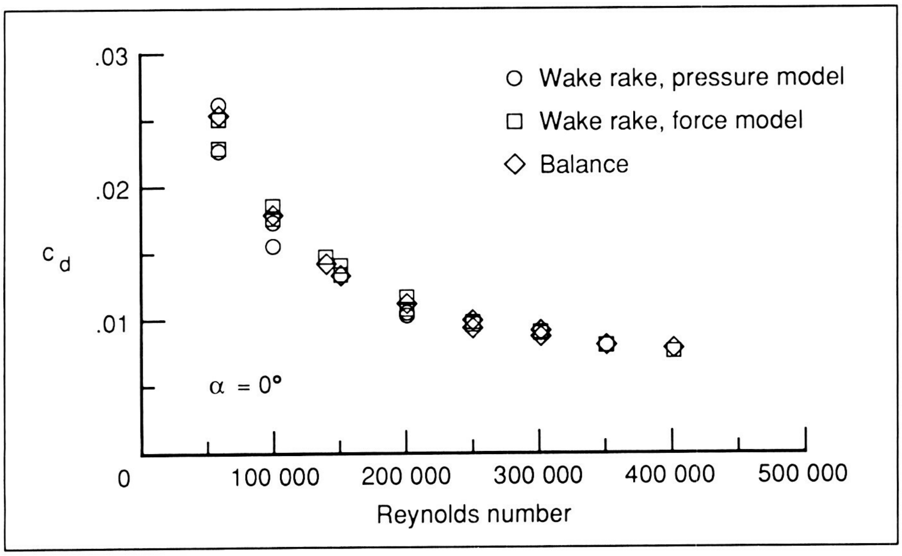

Comparison of drag data from wake rake and balance for Eppler 387 airfoil.

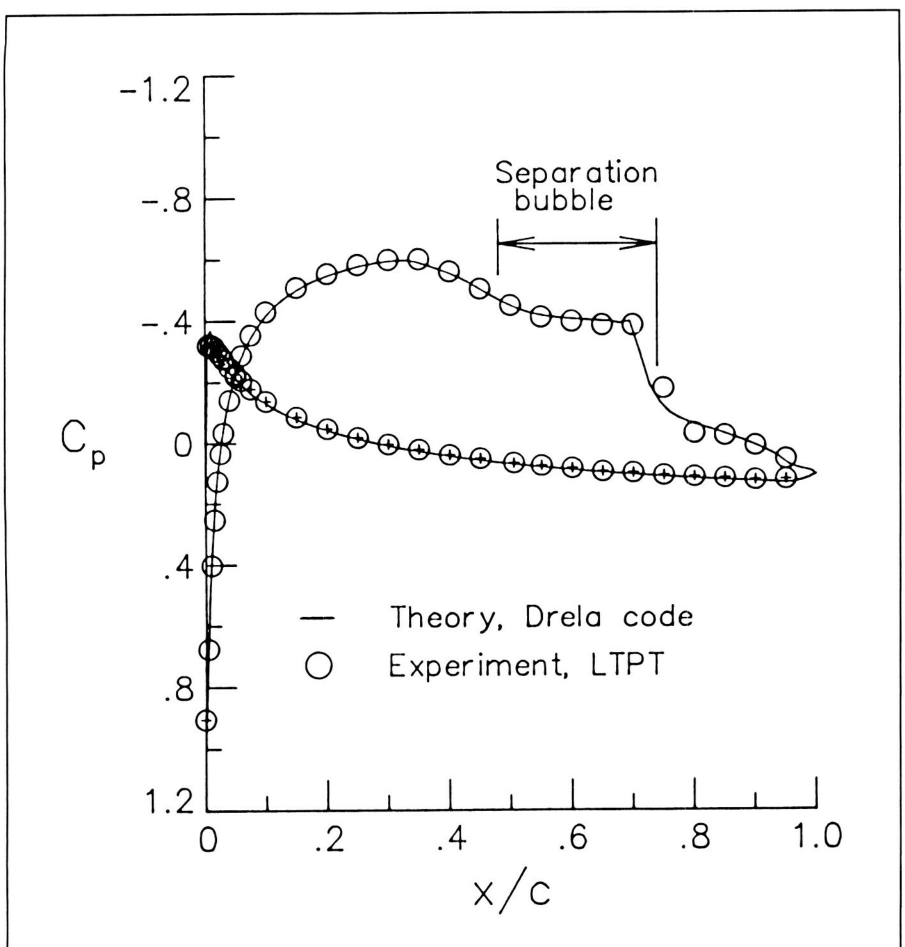

Comparison of theory and experiment for Eppler 387 airfoil at R_N = 200,000 and C_L = 0.35.

turbines, and propellers. Also, wind tunnel results from several European facilities on the Eppler 387 airfoil have shown large differences in airfoil performance at low Reynolds numbers ($R_N \leq 500,000$). The objective of this research was to obtain performance measurements on both force and pressure models of an Eppler 387 airfoil in the LTPT to evaluate the measurement of drag and to verify codes. The LTPT was selected because of its good flow quality, variable pressure capability, and precision pressure instrumentation.

The first figure shows a comparison of the drag data using the wake-rake technique (pressure) and balance (force) at an angle of attack of 0°. At a Reynolds number less than approximately 100,000, where large laminar separation bubbles and unsteady wake occur, the wake-rake data indicate large variations in drag coefficients. The second figure illustrates a pressure data comparison between experiment and theory for a Reynolds number of 200,000 and a lift coefficient C_L of 0.35. The theory was developed by Mark Drela at the Massachusetts Institute of Technology and, as indicated in the figure, has the ability to predict flows in which laminar separation bubbles are present.

Results obtained from this ongoing research illustrate the importance of test measurement technique, tunnel flow quality, and model contour accuracy to determine aerodynamic performance of airfoils for Reynolds numbers less than approximately 500,000.

(R. J. McGhee, 41005)

20-Foot Vertical Spin Tunnel

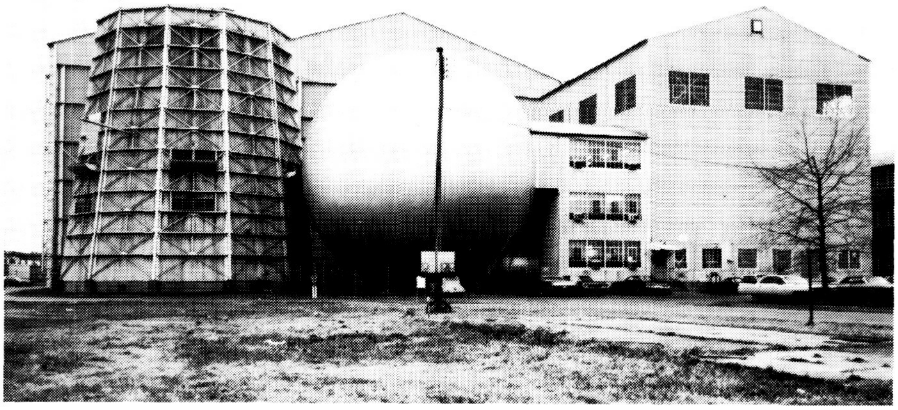

The Langley 20-Foot Vertical Spin Tunnel is the only operational spin tunnel in the United States and one of only two such tunnels in the free world. The tunnel, which is used to investigate spin characteristics of dynamically scaled aircraft models, is a vertical tunnel with a closed-circuit annular return passage. The vertical test section has 12 sides and is 20 ft wide and 25 ft high. The test medium is air. Tunnel speed can be varied from 0 ft/s to 90 ft/s with accelerations to 15 ft/s^2. This facility is powered by a 1300-hp main drive.

Spin recovery characteristics are studied by remote actuation of the aerodynamic controls of models to predetermined positions. Force and moment testing is performed with a gooseneck rotary-arm model support, which permits angles of attack from 0° to ±90° and sideslip angles from 0° to ±20°. Motion picture and video records are used to record the spinning and recovery characteristics in the spin tunnel tests. Force and moment data from the rotary balance tests are recorded in coefficient form and stored on magnetic tapes.

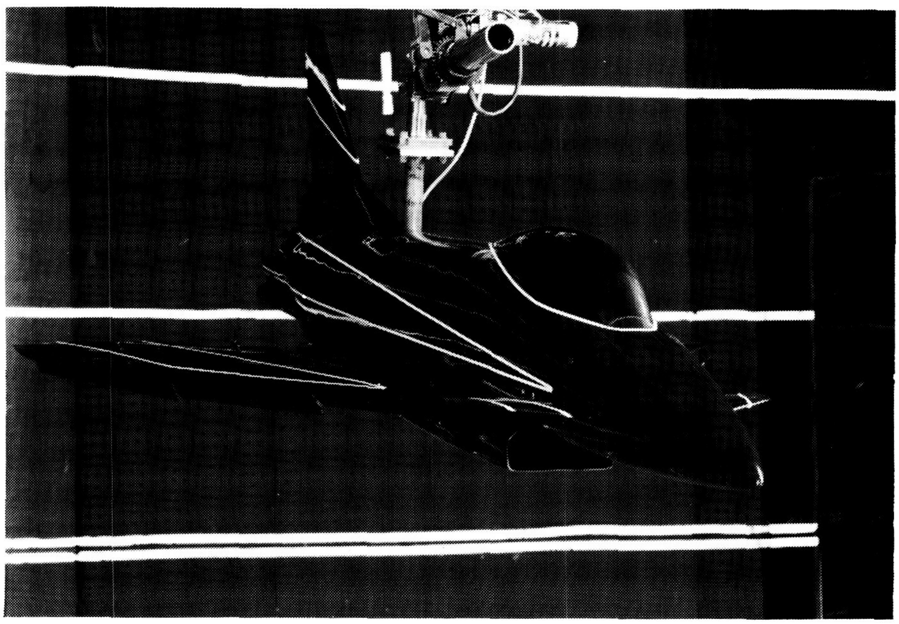

X-31 model on Rotary Balance Apparatus.

X-31 Rotary Balance and Free-Spinning Tests

The X-31 is a research airplane being developed by Rockwell International Corporation and Messerschmitt-Bölkow-Blohm to demonstrate in flight the enhanced maneuvering capability for fighter aircraft, particularly at high-angle-of-attack conditions. The program is jointly sponsored by the United States Defense Advanced Research Projects Agency and the German Federal Min-

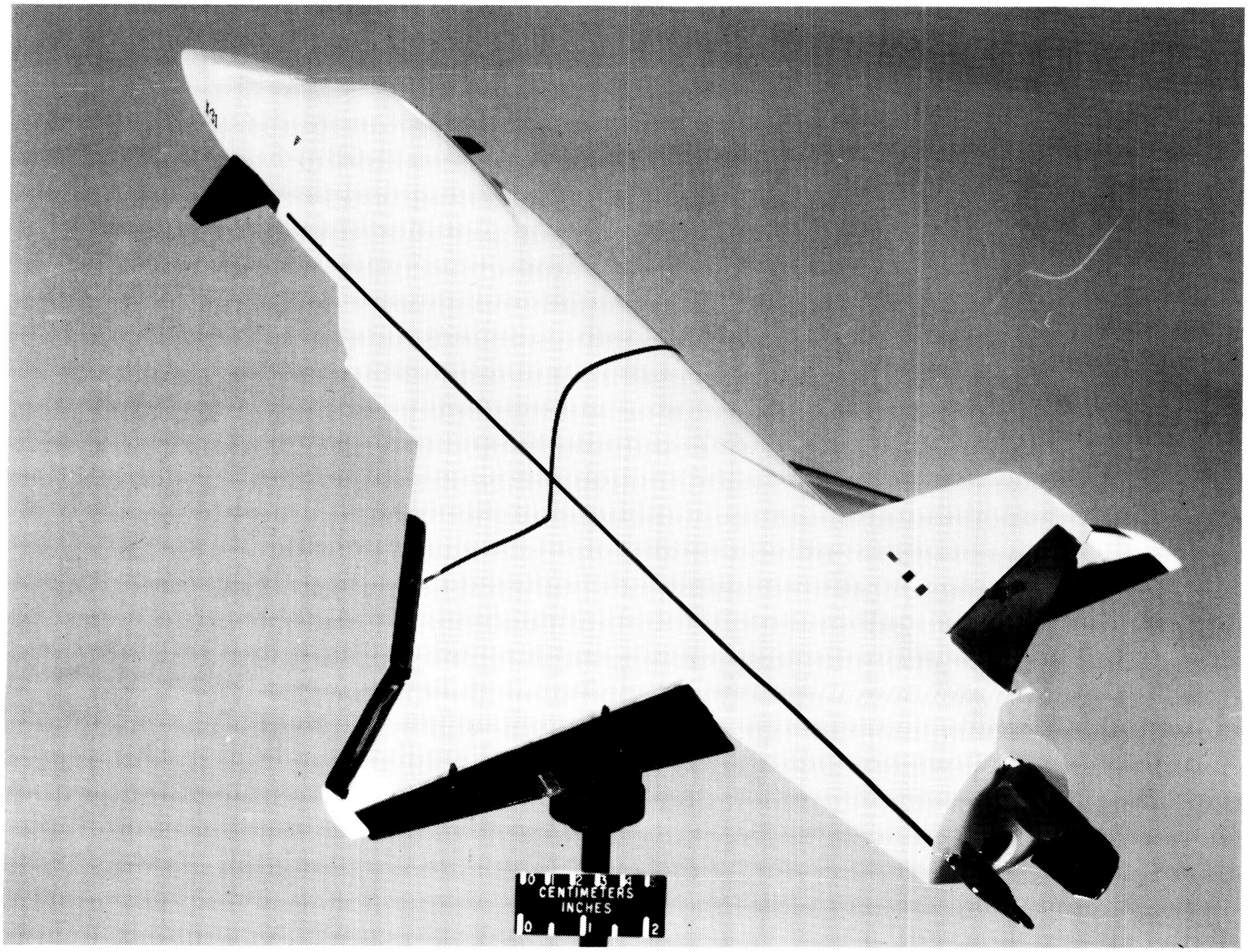

X-31 model used in free-spinning tests. L-88-11300

istry of Defence, with the United States Naval Air Systems Command acting as the program manager. Because knowledge of the high-angle-of-attack aerodynamics is vital to the successful development of the X-31, rotary balance tests and free-spinning tests were conducted to define the static and rotational aerodynamic characteristics and to identify the spin and spin-recovery characteristics of the configuration. In addition, the free-spinning tests were used to size the emergency spin-recovery parachute system. Earlier free-spinning tests on a preliminary design showed moderately fast erect spins for most control settings with good to marginal recoveries obtained by the use of available aileron and rudder controls. Pitch control had little effect on the model behavior. No inverted spin modes were identified in these tests.

Subsequent design changes to the X-31, including a different fuselage and canopy, and modifications to the empennage and engine inlet necessitated the fabrication of a new model and additional spin tunnel testing. Spin results on this new design indicate a more damped configuration with reduced spin rates and improved recoveries. Rotary balance tests provided aerodynamic data for use in predicting steady spin characteristics and for developing a mathematical model of the airplane aerodynamics for use in piloted simulation studies.

(M. S. Hungness, J. S. Bowman, Jr., 41195, and E. G. Dickes)

7- by 10-Foot High-Speed Tunnel

The Langley 7- by 10-Foot High-Speed Tunnel is a closed-circuit single-return continuous-flow atmospheric tunnel with a test section 6.6 ft high, 9.6 ft wide, and 10 ft long. The tunnel is fan driven and is powered by a 14,000-hp electric motor. It operates over a Mach number range from 0.2 to 0.9 to produce a maximum Reynolds number of 4×10^6/ft. In addition to static testing of models to high angles of attack and large sideslip angles, the facility is equipped for both steady-state roll and oscillatory stability testing.

The facility has an important role in a wide range of basic and applied aerodynamic research, including advanced vortex lift concepts, drag reduction technology, highly maneuverable aircraft concepts, and the development of improved aerodynamic theories, such as the difficult separated-flow and jet interaction effects needed for computer-aided design and analysis.

The facility resumed testing in January 1989 after the installation of new fan blades.

14- by 22-Foot Subsonic Tunnel

The Langley 14- by 22-Foot Subsonic Tunnel (formerly the 4- by 7-Meter Tunnel) is used for low-speed testing of powered and unpowered models of various fixed- and rotary-wing civil and military aircraft. The tunnel is powered by an 8000-hp electrical drive system, which can provide precise tunnel speed control from 0 ft/s to 318 ft/s with the Reynolds number per foot ranging from 0 to 2.1×10^6. The test section is 14.5 ft high, 21.8 ft wide, and approximately 50 ft long. The tunnel can be operated as a closed tunnel with slotted walls or as one or more open configurations when the sidewalls and ceiling are removed to allow extra testing capability, such as flow visualization and acoustic tests. The tunnel is equipped with a two-component laser velocimeter system. Furthermore, boundary-layer suction on the floor at the entrance to the test section and a moving-belt ground board for operation at test section flow velocities to 111 ft/s can be installed for ground effect tests.

Langley Research Center has completed significant modifications to the 14- by 22-Foot Subsonic Tunnel to improve and expand its aerodynamic and acoustic test capability. One of the more significant aerodynamic improvements was achieved through

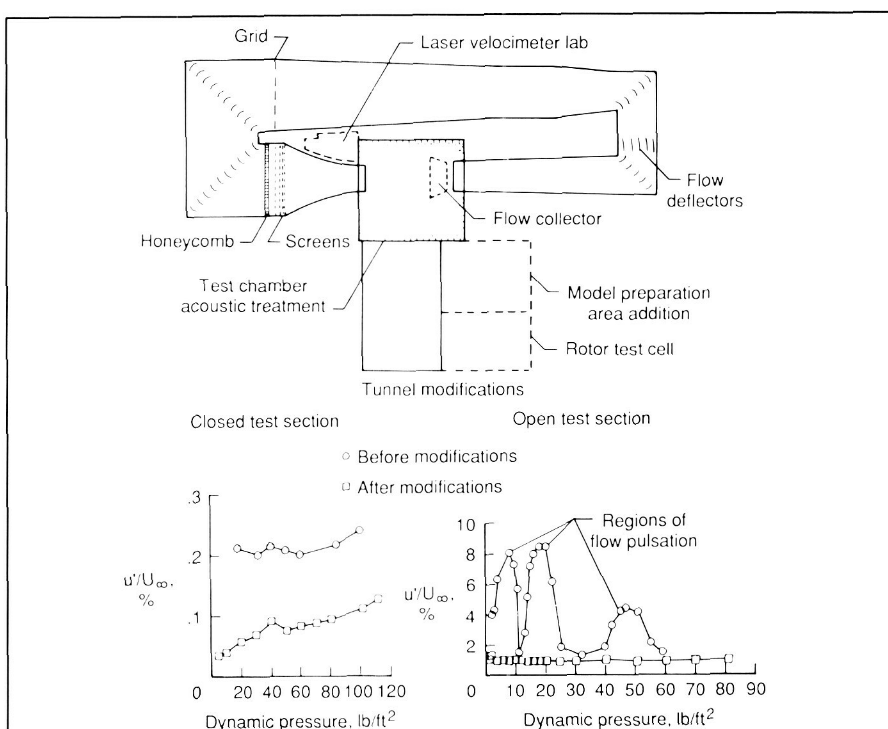

Effect of flow improvement modifications on longitudinal turbulence intensity (u'/U_∞).

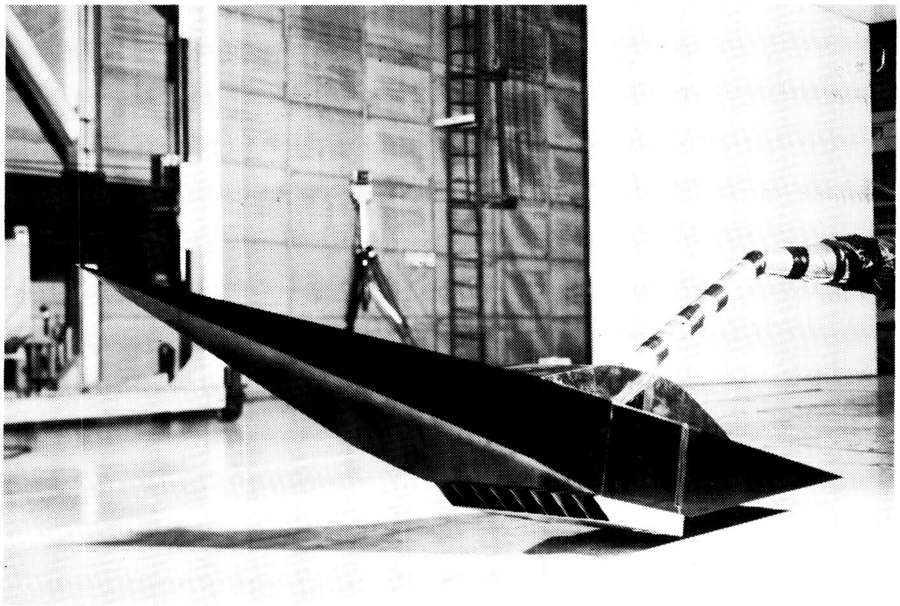

GEM in 14- by 22-Foot Subsonic Tunnel. L-88-13521

the use of flow deflectors installed downstream of the first corner of the tunnel circuit to improve the performance of the tunnel fan. The deflectors resulted in a more uniform velocity distribution into the tunnel drive system and eliminated regions of large-scale flow separation in the return leg of the tunnel circuit.

A turbulence reduction system consisting of a grid, a honeycomb, and four fine-mesh screens dramatically reduced the level of longitudinal turbulence intensity in the tunnel test section. This system provided a reduction in turbulence of 50 percent or more for the closed test section configuration. Periodic flow pulsations that occurred at several speeds in the unmodified configuration of the open test section were eliminated by installation of a new flow collector.

Acoustic reverberations in the open test section were reduced through the use of sound-absorbing panels on the test chamber walls. A major operational improvement was achieved through the construction of a specially designed laser velocimeter laboratory for setup and maintenance of the two-component laser velocimetry system. Finally, an addition to the model preparation area, which includes a support system and rotor test cell, provides the capability to assemble and test rotor models in hovering conditions prior to actual entry into the tunnel.

NASP Generic Ground Effects Model Tests

An extensive wind tunnel investigation using the 14- by 22-Foot Subsonic Tunnel has been conducted to determine the ground effects of a generic NASP-like (National Aero-Space Plane) configuration. The generic ground effects model (GEM) shown in the figure was developed for powered ground effects testing using a top-mounted air sting. This sting provided high-pressure air to the ejector-powered engine simulators while allowing an unobstructed lower surface.

Six-component force and moment data as well as flow visualization photographs were obtained over a wide range of test conditions including thrust settings from power-off to thrust coefficients of 0.8, angles of attack from -4° to 18°, and ground heights from as low as 0.01 body lengths (1-in.) from the tunnel floor to 0.76 body lengths above the floor (representing conditions out of ground effect). Thrust coefficients were varied by changing engine supply pressure and mass flow and by changing tunnel dynamic pressure from 10 lb/ft^2 to 70 lb/ft^2. Initial data confirmed that because of the sharp corners on the model geometry, Reynolds number effects were minimal above a free-stream dynamic pressure $q = 10$ lb/ft^2.

Preliminary results indicate that while this configuration exhibits a lift increase as the ground plane is approached without power, it experiences a significant loss of lift in ground effect under powered conditions. This loss of lift is present up to and beyond a representative takeoff angle of attack of 12°.

(G. M. Gatlin, 45065, P. F. Quinto, and J. W. Paulson, Jr.)

Advanced Turboprop Integration Research

An exploratory research program has been conducted in the 14- by 22-Foot Subsonic Tunnel to investigate propeller installation effects on the low-speed

ORIGINAL PAGE
BLACK AND WHITE PHOTOGRAPH

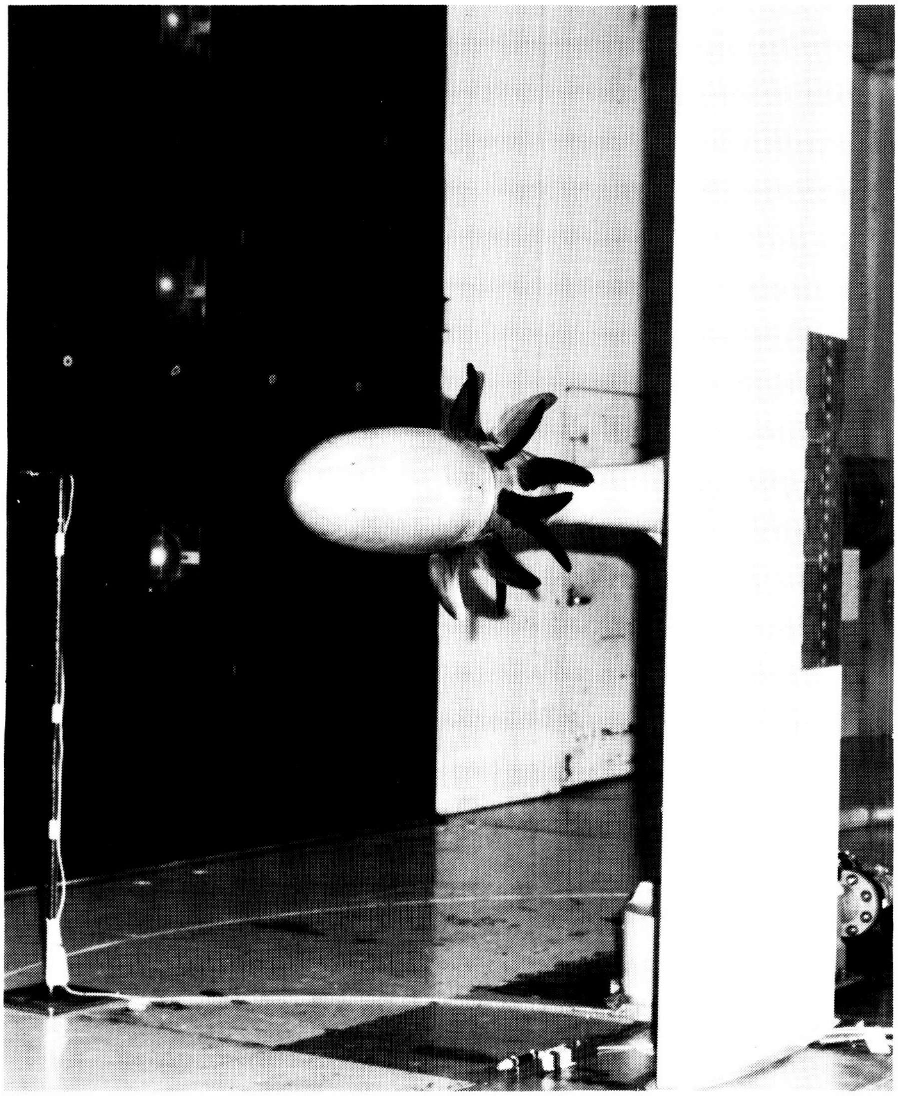

UDF/semispan wing mounted for testing in 14- by 22-Foot Subsonic Tunnel. L-88-05260

aerodynamic characteristics of an advanced counterrotation turboprop configuration mounted in several different chordwise locations above and behind a wing. A 2-ft-diameter model of the General Electric Unducted Fan (UDF) was used in combination with a 1-m by 3-m semispan wing, as shown in the figure. Tests were conducted for simulated takeoff, cruise, and landing configurations. A total of seven different propeller/wing positions were tested for angles of attack ranging from −4° to 20°.

Aerodynamic loads were measured on the wing with a six-component balance, and oscillatory blade stresses were measured on each row of the UDF simulator by means of blade-mounted strain gauges. Several hundred pressure measurements were made on the surfaces of both the wing and nacelle to aid in identifying the sources of the aerodynamic interference effects.

Early analysis of the results of the experiments indicated that blade stresses were very high for those configurations where the wing wake passed through a significant portion of the propeller disk, but the stresses were reduced as the wake was moved toward the outer edges of the disk. When the propeller was positioned over the wing forward of the wing trailing edge, increases in power caused increases in the basic wing lift which increased the overall lift for the wing-propeller combination. An analysis of the pressure data indicated a favorable effect of the propeller on the wing upper-surface pressure distribution for those cases, but the measured propeller performance was essentially unaffected by the wing pressures.

Data from this investigation are being incorporated into a data base that is being used to identify and develop needed improvements in computational fluid dynamics (CFD) capabilities for design and analysis.

(D. Dunham, 45061, Z. Applin, G. Gentry, A. Hsing, and L. Huang)

Low-Speed Aerodynamic Investigation of Generic Accelerator Configuration

As part of the NASP Program, an investigation was conducted in the 14- by 22-Foot Subsonic Tunnel to determine the low-speed aerodynamic characteristics of a generic accelerator-type configuration. The model incorporated a conical forebody with a 5° semiapex angle, a truncated conical afterbody, a simulated wraparound engine package, and a 76° swept delta wing. Six-component force and moment

data were obtained over an angle-of-attack range from −4° to 30° at 0° sideslip, and surface pressure data were obtained on the forebody. In addition to tests of the basic configuration, component buildup tests were conducted, and the effects of power, forebody nose bluntness, a canard surface, and flap deflections were determined. Testing was also conducted with the simulated engine package only on the lower half of the model.

Results indicate that the large asymmetric yawing moments resulting from a sharp nose configuration were significantly reduced as nose bluntness was increased. Testing with the engine simulation system shows that flap effectiveness was significantly increased during power-on conditions. A flow visualization technique incorporating a propylene glycol vapor generator successfully produced good visible smoke in the test section at a free-stream dynamic pressure of 49 lb/ft^2, whereas previously, smoke flow visualization had only been possible at free-stream dynamic pressures of 4 lb/ft^2 or below. The propylene glycol vapor smoke identified areas of vortical flow over the model.

(G. M. Gatlin, 45065, P. F. Quinto, and J. W. Paulson, Jr.)

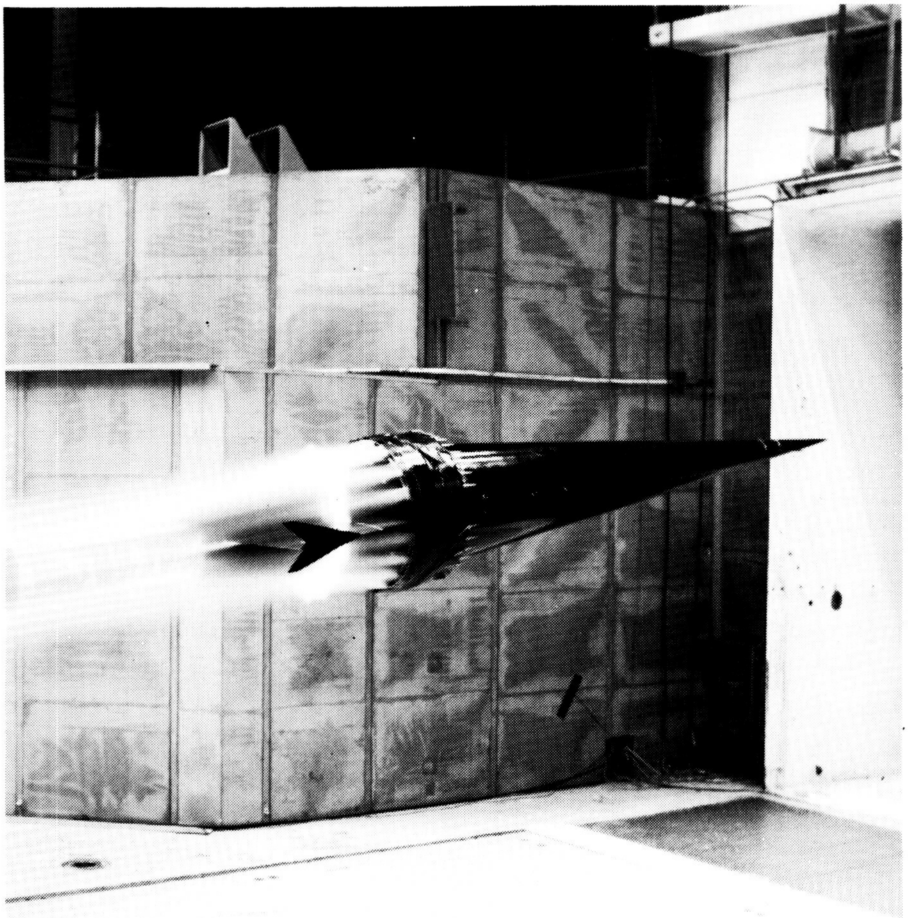

Flow visualization of NASP accelerator-type engine exhaust flow with water vapor injected into engine simulators illuminated by thin sheet of laser light to highlight flow over tail cone.

High-Angle-of-Attack Aerodynamic Characteristics of Crescent and Elliptic Wings

Recent wind tunnel experiments were conducted to investigate the influence of highly swept wing tip shapes on the high-angle-of-attack aerodynamic characteristics of a wing with a moderate aspect ratio AR of 7. The experiments were conducted in the 14- by 22-Foot Subsonic Tunnel for a model with various wing planform shapes. Static longitudinal and lateral-directional forces and moments were measured for elliptic and crescent wing configurations of identical span and area. The forces and moments were obtained for an angle-of-attack range including stall and poststall conditions at a Reynolds number, based on the average wing chord, of 1.8×10^6. Flow visualization using a mixture of oil and titanium-dioxide was performed for several incidence angles.

The force and moment data and the flow visualization results demonstrated that the crescent planform with its highly swept tips produced better high-angle-of-attack aerodynamic characteristics than the unswept elliptic planform, as shown in the figure. Leading-edge separation-

ORIGINAL PAGE
BLACK AND WHITE PHOTOGRAPH

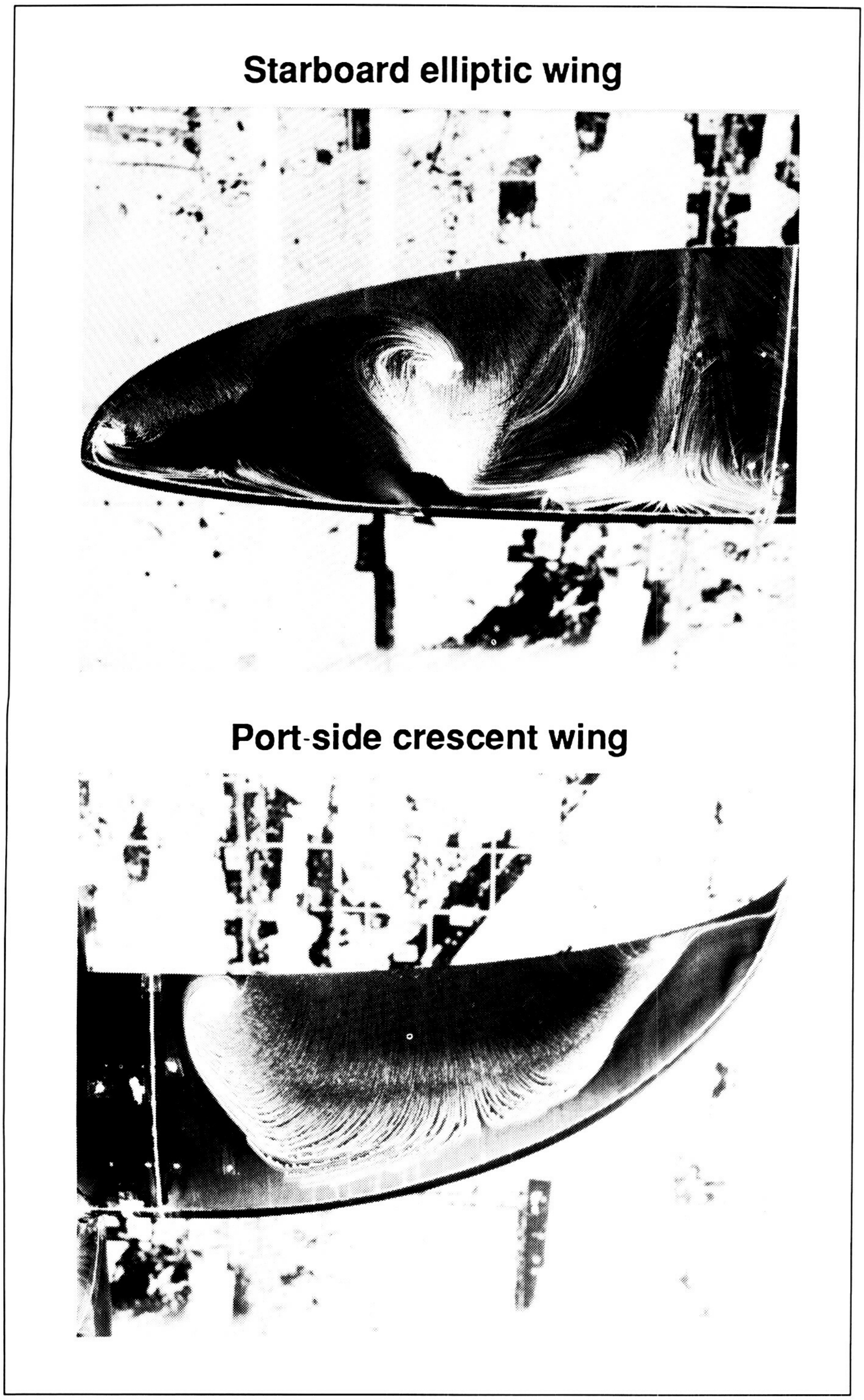

Oil-surface flow visualization of stall patterns on starboard elliptic wing (top) and port crescent wing (bottom) planforms at angle of attack of 21°.

induced vortex flow over these highly swept tips is thought to produce this improved behavior at high angles of attack. The unique planform design may result in safer and more efficient low-speed airplanes.

(P. M. H. W. Vijgen and P. Stough, 43860)

Cross Flow Vorticity Experiments on Swept Cylinder Model

Flow visualization experiments were conducted in the 14- by 22-Foot Subsonic Tunnel on a large-scale swept cylinder model. This model, which had an untapered 3-ft chord and a 10-ft span, was designed to provide a favorable environment for studying the development of cross flow within the laminar boundary layer. Streamwise vorticity is one of several types of boundary-layer flow phenomena that can cause a premature transition of the boundary layer from laminar to turbulent flow. Little is known about the actual development and subsequent breakdown of these vortical structures. Thus, current research is being directed toward gaining a better understanding of the physics that control these flow disturbances.

This swept cylinder model was tested at leading-edge sweep angles from 15° to 75° and tunnel speeds up to 190 mi/h. Sublimating chemical and liquid-crystal flow visualization techniques were used to identify the presence of cross flow disturbances. Preliminary results indicated that cross flow vortices were produced on the model surface for a variety of sweep angle and tunnel flow speeds. Vortex

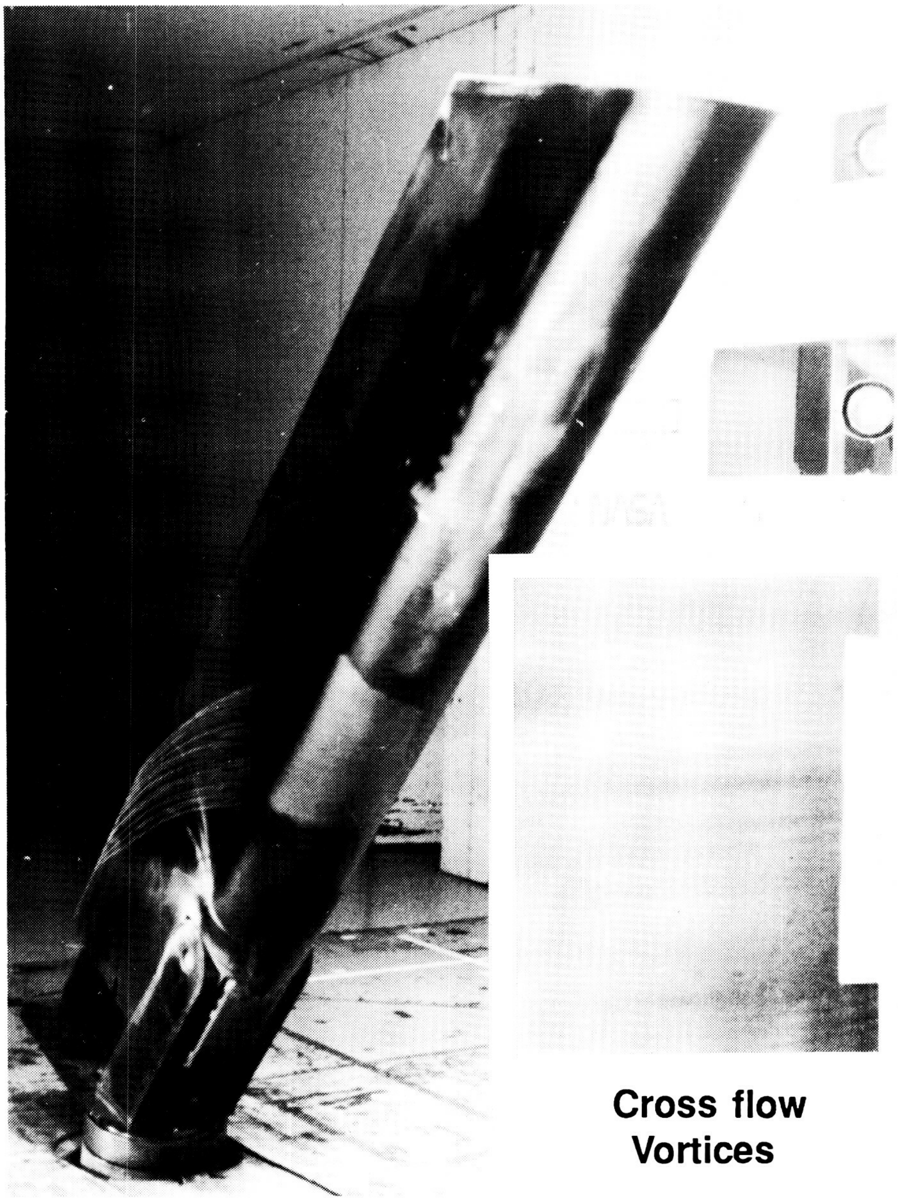

Swept cylinder model in 14- by 22-Foot Subsonic Tunnel.

spacing appeared to be approximately 8 to 10 vortices per in. Results from these tests have defined an operating envelope for future experiments in which a surface-mounted hot-film sensor will be used to electronically detect cross flow disturbances on the swept cylinder model. Ultimately, these results will be used to improve and validate computer codes for predicting laminar to turbulent boundary-layer transition.

(M. Wusk and P. Stough, 43860)

8-Foot Transonic Pressure Tunnel

ORIGINAL PAGE
BLACK AND WHITE PHOTOGRAPH

The Langley 8-Foot Transonic Pressure Tunnel is a closed-circuit single-return variable-density continuous-flow wind tunnel. The test section walls are slotted (5-percent porosity) at the top and bottom, with solid sidewalls fitted with windows for schlieren flow visualization. In 1982, the facility was modified for flow-quality improvements and reconfigured for low-drag testing of a large-chord swept laminar-flow control airfoil at transonic speeds. A honeycomb and screens were permanently installed in the settling chamber to suppress the turbulence level in the test section.

Following completion of the laminar-flow-control experiment in the fall of 1988, the contoured liner was removed and the test section was restored to its original slotted three-dimensional test configuration. After completion of operational shakedown runs and empty tunnel calibrations, the tunnel is scheduled to be fully operational in the transonic test mode in 1989.

The Basic Aerodynamic Research Facility is an integral part of the 8-Foot Transonic Pressure Tunnel (8-Foot TPT) research complex. Utilizing two of the 8-Foot TPT 100,000 ft^3/min compressors, this facility can

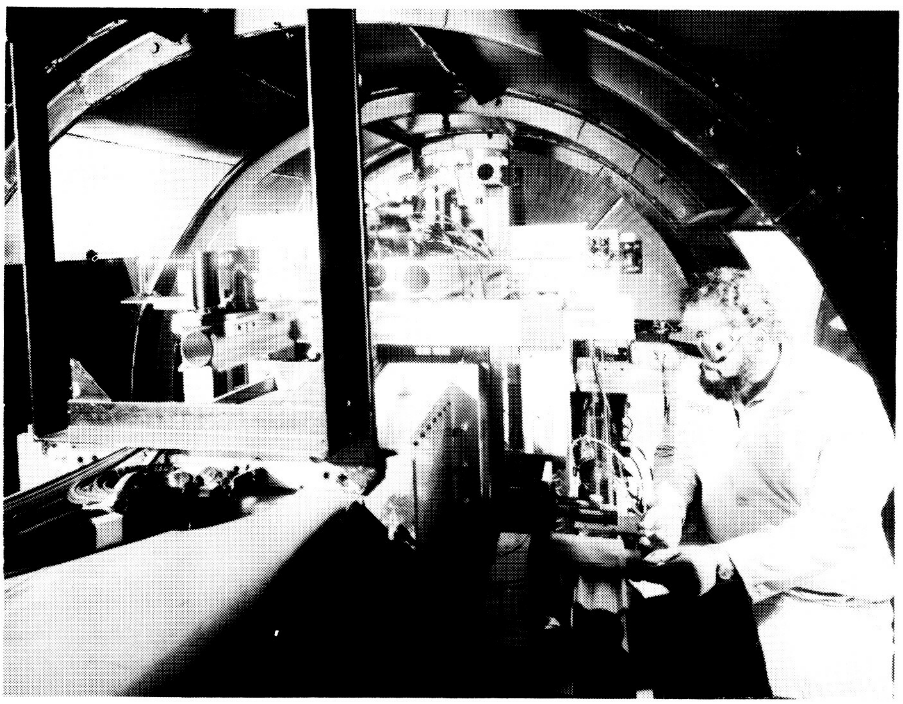

L-87-2294

Basic Aerodynamic Research Facility 3-D laser velocimeter system.

ORIGINAL PAGE
BLACK AND WHITE PHOTOGRAPH

Slotted test section. L-88-11585

achieve continuous-flow Mach numbers to 1.25 in its 18-in. by 18-in. test section. Historically, this facility has been used as a test bed for research to be performed in the larger and more costly wind tunnels. To expand the capability of this facility, the test section has been configured to accommodate an orthogonal, three-dimensional laser velocimeter system. This small wind tunnel is ideal for direct comparisons of different transonic flow diagnostic techniques.

Laminar-Flow-Control Tests

A hybrid laminar-flow-control (HLFC) experiment has been completed in the 8-Foot Transonic Pressure Tunnel as the third and final experiment in the Laminar-Flow-Control (LFC)

View of hybrid airfoil looking upstream from trailing edge. L-88-07992

Project. This experiment utilized the same model slotted bottom and perforated top forward segment as the perforated LFC test. However, the middle and aft segments on the top side were solid and were contoured differently from the baseline LFC airfoil to provide a favorable pressure gradient back to 60 percent of the chord. The perforated top forward panel enabled suction to be applied from 3 percent to as far back as 26 percent of the chord. On the bottom, suction was applied back to 85 percent of the chord by use of the original slotted panels in order to keep the flow attached and thus attain the design lift coefficient.

The test setup and the pressure and velocity capability of the 8-Foot TPT permitted variations in both the level and extent of suction, Reynolds number variations to 24×10^6, and Mach numbers from 0.4 to 0.8. Changes in the angles of the trailing-edge flaps enabled some experimentation with off-design pressure distributions.

The data are now being reduced, and the tunnel has been restored to its original configuration.
(J. C. Ferris, 42862)

Transonic Dynamics Tunnel

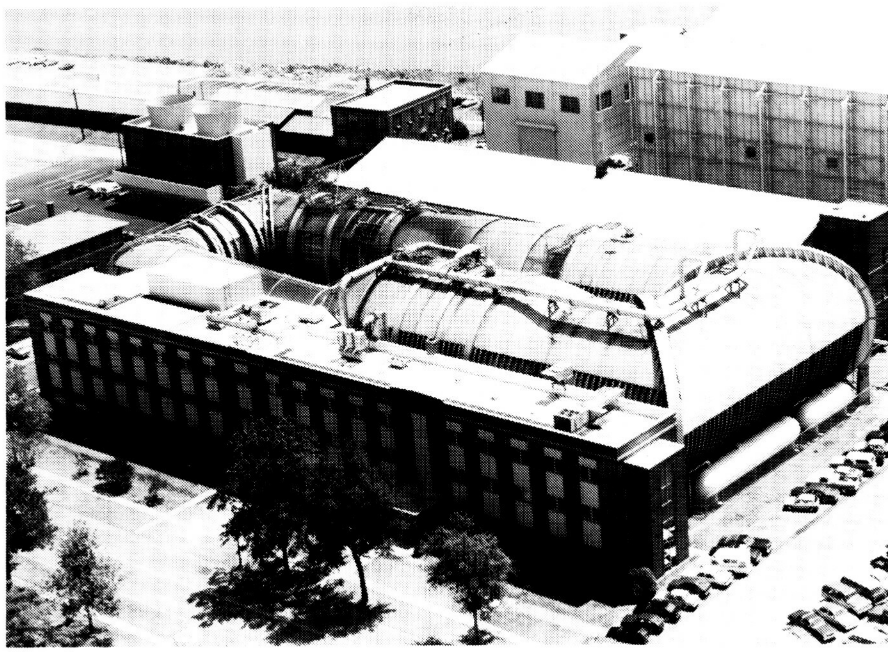

Conversion of the original Langley 19-Foot Pressure Tunnel into the Transonic Dynamics Tunnel (TDT) was begun in the late 1950's to satisfy the need for a large transonic wind tunnel dedicated specifically to work on the dynamics and aeroelastic problems associated with the development of high-speed aircraft. Since the facility became operational in 1960, it has been used almost exclusively to clear new designs for safety from flutter and buffet, to evaluate solutions to aeroelastic problems, and to research aeroelastic phenomena at transonic speeds.

The tunnel is a slotted-throat single-return closed-circuit wind tunnel with a **16-ft** *by* **16-ft** *test section. The stagnation pressure can be varied from slightly above atmospheric to near vacuum, and the Mach number can be varied from 0 to 1.2. Both test section Mach number and density are continuously controllable. The facility can use either air or a heavy gas (R12) as the test medium. The heavy gas is usually used because it has several advantages over air as a test medium for dynamically scaled aeroelastic model testing. The tunnel has a reclamation system so that the heavy gas can be purified and reused.*

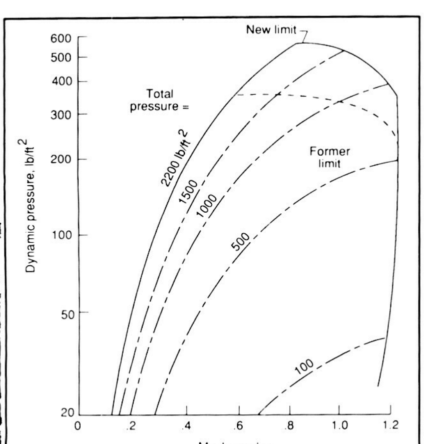

Former and present operational boundaries of TDT.

The facility is equipped with many features uniquely suited to dynamic and aeroelasticity testing. These include a new computerized data acquisition system especially designed to rapidly process large quantities of dynamic data, a means of rapidly reducing test section Mach number and dynamic pressure to protect models from damage when aeroelastic instabilities occur, a system of oscillating vanes to generate sinusoidal variations in tunnel flow angle for use in gust response studies, and special mount systems that enable simulation of airplane free-flight dynamic motions.

During much of 1985, the tunnel complex was modified to provide 50-percent higher test dynamic pressures in the transonic speed range. The test medium density capability was increased by 50 percent in that speed range, which allows models to be built 50 percent heavier and still meet the mass density scaling ratios required for proper modeling of full-size aircraft. For strength considerations, this becomes very significant as full-size aircraft become

more structurally efficient. To provide this increased density capability, the existing fan motor was rewound to increase the power rating from 20,000 hp to 30,000 hp. Additional tunnel cooling capacity was provided to accommodate the increased tunnel power limit. Other major modifications included changes to the electrical power distribution system and installation of a new speed control system.

Microphone frequency response in heavy gas atmosphere.

The TDT is one of the prime facilities at Langley Research Center for testing aeroelastic properties of model rotorcraft. An experiment was performed to determine if the tunnel was also suitable for acoustic testing. In the TDT, tests are performed in a heavy gas (R12) at one-half atmospheric pressure and ambient temperature for dynamic scaling of the rotor system. This test environment results in an acoustic impedance (which is the product of density and the speed of sound in a gas) approximately 93 percent that of air at atmospheric pressure. Thus, an important question is whether a standard microphone designed for use in air at atmospheric pressure can be used to measure sound in the heavy gas at one-half atmospheric pressure. To address this question, a calibration of the effects of a heavy gas atmosphere on microphone frequency response and sensitivity was performed in the Flow Impedance Test Laboratory.

A small pressure vessel containing a microphone and an electrostatic actuator was constructed to allow introduction of air or the heavy gas at various pressures. An electrostatic actuator is a device used for microphone calibration in which an electrostatic charge moves the microphone diaphragm in a manner similar to sound pressure waves. Frequency response of the microphone was determined by sweeping a sinusoidal input signal to the actuator through the frequency range of interest and measuring the output response of the microphone. Results from frequency sweeps using air at standard atmospheric pressure and the heavy gas at one-half atmospheric pressure were used to determine the difference in microphone sensitivity due to the change in gases. Once the relative sensitivity of the microphone system was established, the data were used to construct a correction curve to relate measurements between the two environments. The correction curve in the figure shows that microphone response in the heavy gas is very close to the response of the microphone in air at standard pressure for the frequency range from 20 Hz to 20 kHz. Thus, standard microphones can be used in the heavy gas without additional calibration for rotorcraft testing in the TDT.

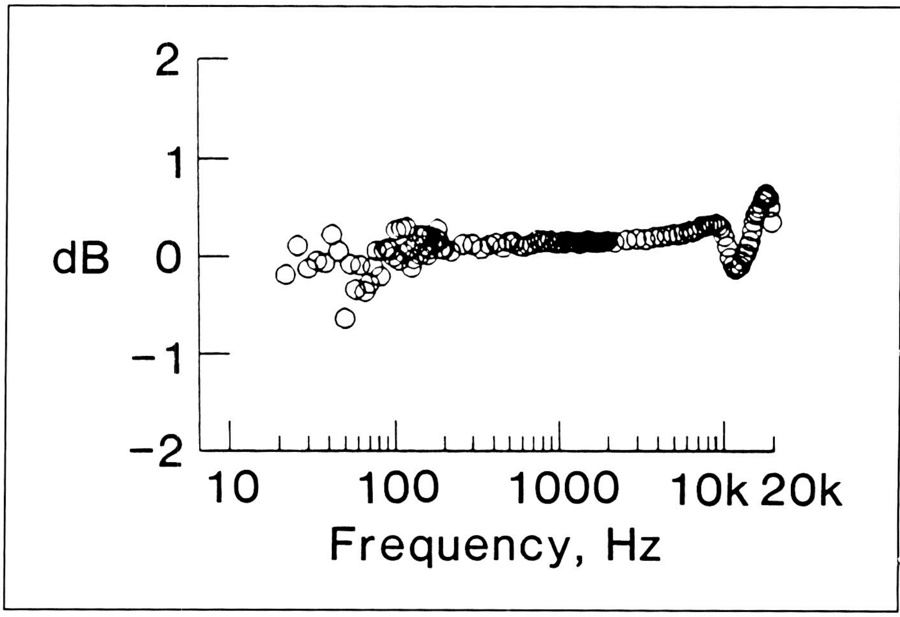

Frequency response in heavy gas relative to air.

(E. R. Booth, Jr., 43627)

Effects on Flutter of New Leading-Edge Flaps and New Air Defense Pylons for F-16

Because the F-16 has been one of the United States Air Force's most versatile fighters since it entered the inventory in the mid-1970's, it is continuously being modified to satisfy new mission requirements and to take advantage of new technology for improving its performance. Two modifications being planned are a new composite leading-edge flap and a new air defense pylon. The new leading-edge flaps will contain advanced antennas and

avionics and will be heavier than the flaps they replace. This modification is planned for future F-16's. Existing National Guard F-16's will be modified with the new air defense pylon for carrying AIM-7 and AIM-120 missiles under the wing.

Because modifications such as these can have an adverse impact on airplane flutter characteristics, a 1/4-scale aeroelastic model of the F-16 airplane was tested to determine the effects on flutter of these modifications. A photograph of the cable-mounted model with the new leading-edge flaps and with an AIM-7 missile mounted on the new pylon is shown in the figure. Tests were conducted with the new leading-edge flaps and the current leading-edge flaps and their respective actuators for comparison. Systematic variations in external stores mounted to the air defense pylon were also made during the test. Thirty-eight configurations were tested.

The data showed that the flutter characteristics of the wing with the new composite leading-edge flap were not significantly different from the flutter characteristics of the wing with the current flap. Test results for configurations with external stores mounted on the new pylon indicated an adverse effect on flutter. This result is consistent with that obtained by analysis. These wind tunnel test results will be used together with analytical results to guide flight tests and to establish flight operation procedures and restrictions for the modified aircraft.

(M. G. Farmer and J. A. Rivera, Jr., 41263)

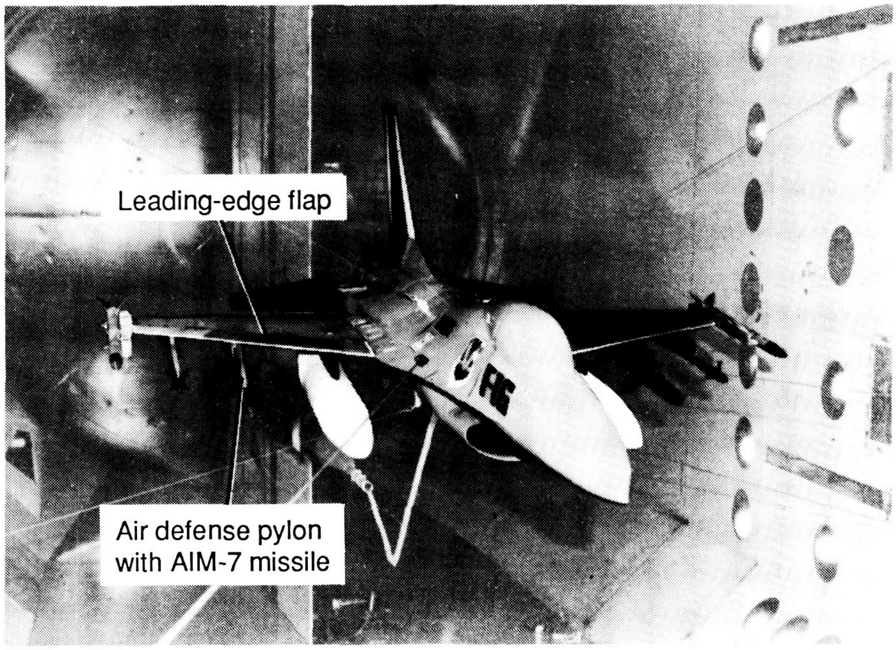

F-16 with composite flaps in TDT. L-88-6264

MILSTAR Radome Test for Panel Flutter

The United States Air Force is currently developing a new radome for the MILSTAR program. The radome, which will contain satellite communication hardware and will be flown on five airplanes (namely, the C-18, EC-135, RC-135, E-3, and E-4), will be located on top of the aircraft as shown in the figure. This radome is a thin Kevlar shell approximately 18 ft long. During initial flight tests conducted in the spring of 1988, lowly damped responses were observed for several of the radome's structural modes. In addition, analyses predicted that panel flutter might occur when the local flow on the radome was supersonic. Consequently, the flight test program was halted until an assessment could be made of the panel flutter characteristics. To provide the needed flutter data and other response and aerodynamic data for fatigue analysis and analysis correlation, a wind tunnel test was conducted using an actual radome.

The radome was mounted on a turntable to allow simulation of flight sideslip angles. A photograph of the radome is shown at the left in the figure. The radome was instrumented to monitor the response for panel flutter and to measure accelerations, strains, and steady and unsteady pressures. Tests were conducted at transonic Mach numbers up to a dynamic pressure of 500 lb/ft^2 for sideslip angles of 0°, 3°, and 6° and to 350 lb/ft^2 for sideslip angles of 9°. No panel flutter occurred over the range of test parameters. Static aerodynamic data were obtained in the transonic region; these pressure data correlated reasonably well with analytical results.

Because no panel flutter occurred during the tunnel test, the Air Force has resumed flight testing of the new radome. The

ORIGINAL PAGE
BLACK AND WHITE PHOTOGRAPH

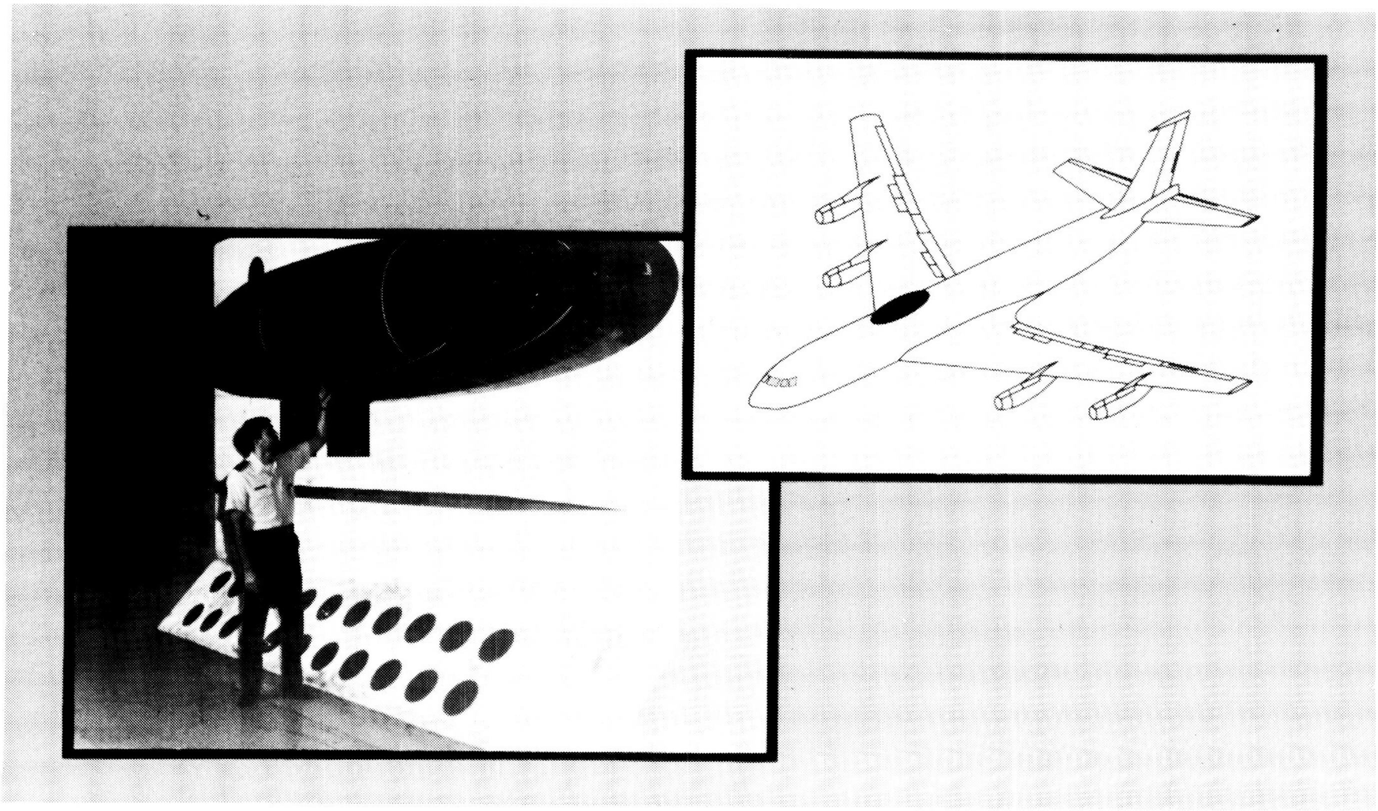

MILSTAR radome in TDT.

L-88-09068

Air Force will use the wind tunnel test results along with both the analytical results and flight test data to establish further flight test procedures and to determine possible operating envelope restrictions on radome-equipped aircraft.

(M. G. Farmer, 41263, and D. F. Keller)

Aeroelastic Characteristics Study of Atlas-Centaur Large Payload Fairing

Increasing demands for space launches using expendable vehicles have resulted in the design of a larger payload capability for the Atlas-Centaur vehicle. Because of concerns over possible buffet load limitations or aeroelastic instabilities associated with a large payload fairing (bulbous nose), an experimental study was conducted using a 1/10-size dynamically scaled aeroelastic model to examine the effects of various fairing length-to-diameter (L/D) ratios. The model, shown in the photograph (on page 23) consisted of a rigid shell simulating the forward portion of the Atlas-Centaur vehicle with adjustable internal structure to simulate the flexibility of the actual vehicle. Simulation of either of the first two bending modes could be made. Because the majority of potential buffeting flows occur near the nose of a typical "bulbous nose" vehicle, simulation of only the forward portion of the vehicle was considered to be sufficient.

The effects of L/D ratios of 0.3, 0.6, 0.8, 1.0, and 1.2 were studied over a Mach number range of 0 to 1.2 and at several dynamic pressure levels. These L/D ratios were tested on both the first and second bending mode configurations. The model was found to be free of aeroelastic instabilities. Additionally, the model buffet responses that were scaled to full-scale values were at acceptable levels. The buffet response was remarkably similar for most of the fairing L/D ratios, except that, as shown by the data in the figure, the response in the second mode for L/D = 0.3 was substantially greater than that of the other L/D configurations. The wind tunnel test demonstrated that the proposed flight vehicle fairing, L/D = 1.0, will be free of detrimental aeroelastic buffet response and insta-

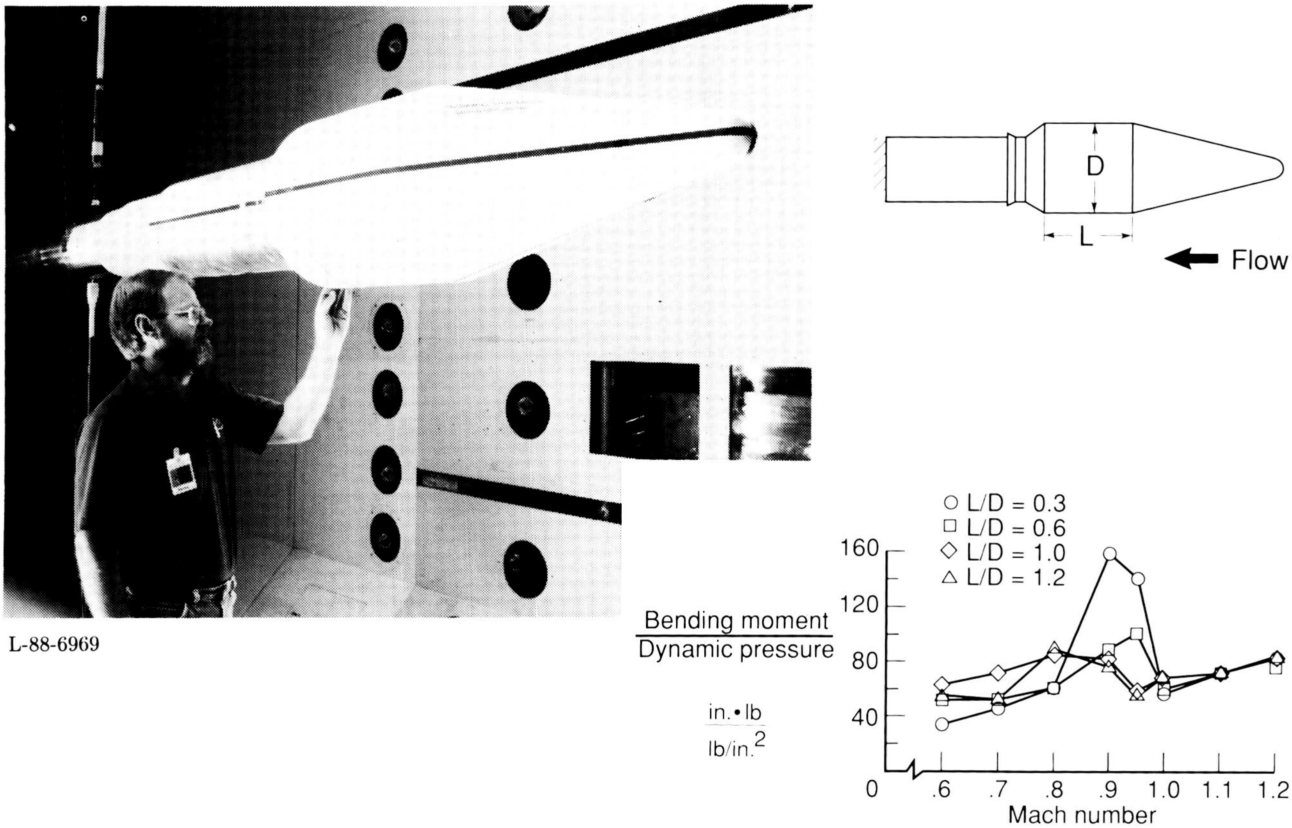

L-88-6969

Atlas-Centaur large payload fairing model (upper left), characteristic dimensions of model (upper right), and buffet response for bending mode 2 (bottom).

bilities. The parametric study of fairing configurations has resulted in a data base of response information on fairing L/D ratios.

(S. R. Cole and M. G. Farmer, 41267)

Evaluation of Performance Characteristics of Advanced-Design Rotor Blades

A study of the coupling of advanced aerodynamic shapes with a blade structure designed for minimum hub vibratory loads is in progress. One objective

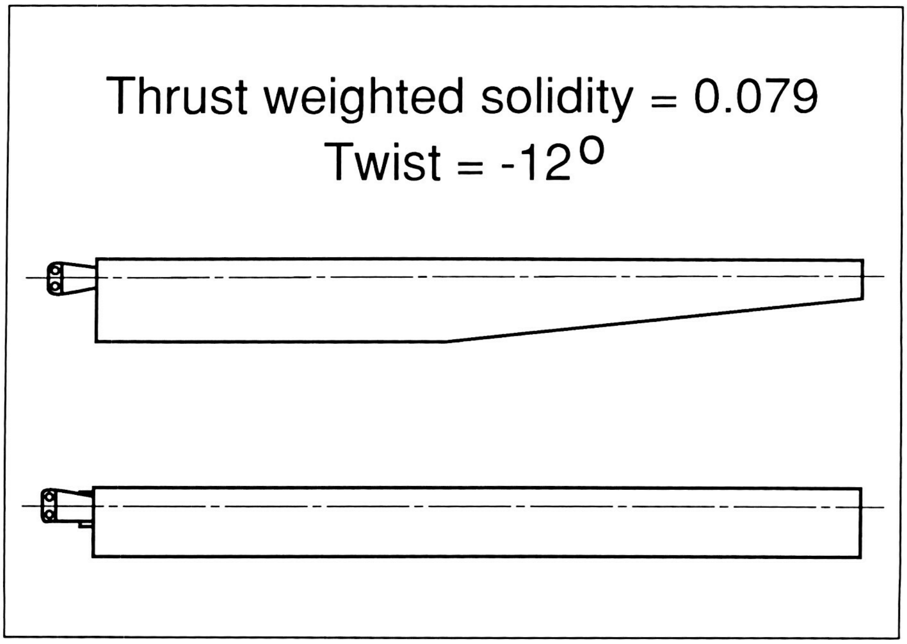

Geometry of rotor blades.

of this joint effort among the United States Army, NASA, and Bell Helicopter Textron is to evaluate the effects of rotor planform shape on aerodynamic performance.

As part of this evaluation, wind tunnel tests were conducted using two sets of rotor blades designed for specified aerodynamic performance requirements. These two sets include a rectangular planform blade designed by Bell Helicopter Textron and a tapered planform blade designed by the Army Aerostructures Directorate personnel at Langley Research Center. Each blade set was also structurally designed for minimum hub shears and moments. The thrust-weighted solidity, twist distribution, and inboard airfoil section were the same for both blade sets (shown in the first figure). Both rotors were 1/5-size aeroelastically scaled models and were tested at conditions simulating various rotor tasks defined by aircraft gross weight and propulsive force requirements to an advance ratio of 0.425. Main-rotor torque measurements were made to evaluate performance between the two configurations.

The illustrative results shown in the second figure were obtained for a hover tip Mach number of 0.646, which represents sea-level standard conditions. The hover data indicate that the tapered planform provides a performance improvement for thrust coefficients both above and below the design value of 0.0051. The forward flight data also indicate a performance advantage for the tapered blades at advance ratios above 0.15. Analytical results, not shown, yielded trends consistent with the experimental results for the hover condition but did not yield as consistent trends for the forward flight case. These results show that the use of a highly tapered rotor blade can result in hover improvements without degradation of forward flight performance relative to a rectangular blade.

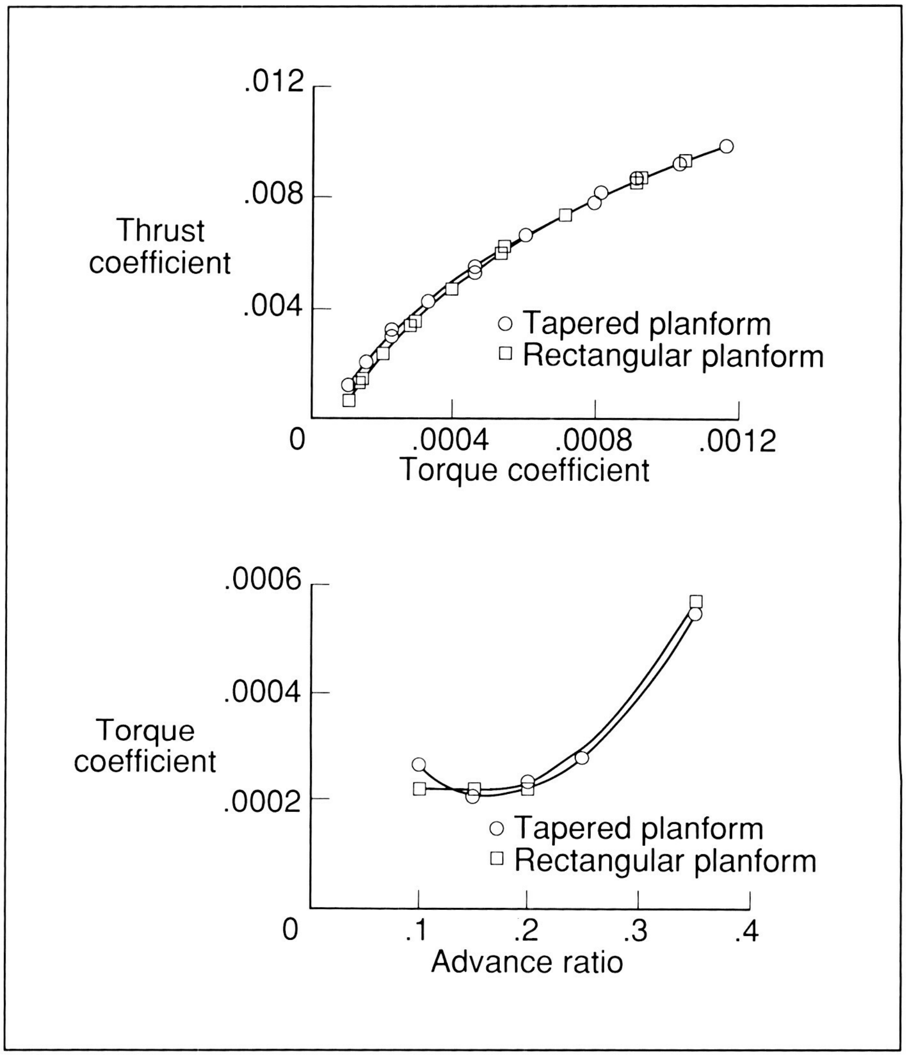

Hover and forward flight performance data. Tip Mach number is 0.646 (top and bottom figures); lift coefficient is 0.005, and equivalent parasite area is 20.65 ft^2 (bottom figure).

(K. W. Noonan, 43967, W. T. Yeager, Jr., M. L. Wilbur, and P. H. Mirick)

16-Foot Transonic Tunnel

The Langley 16-Foot Transonic Tunnel is a closed-circuit single-return continuous-flow atmospheric tunnel. Speeds up to Mach 1.05 are obtained with the tunnel main-drive fans, and speeds from Mach 1.05 up to Mach 1.30 are obtained with a combination of main-drive and test section plenum suction. The slotted octagonal test section measures 15.5 ft across the flats. The tunnel is equipped with an air exchanger with adjustable intake and exit vanes to provide some temperature control. This facility has a main-drive power of 60,000 hp, and a 36,000-hp compressor provides test section plenum suction.

The tunnel is used for force, moment, pressure, flow visualization, and propulsion-airframe integration studies. Model mounting consists of sting, sting-strut, and fixed-strut arrangements; propulsion simulation studies are made with dry, cold, high-pressure air.

The 16-Foot Transonic Tunnel has undergone several major modifications. These include a floor-mount system to facilitate semispan model testing and a model preparation area for model buildup and calibration.

B-1B Nozzle/Afterbody Aeroacoustics

The outer nozzle flaps of the B-1B aircraft are experiencing high wear rates resulting in unacceptable maintenance downtime and excessive replacement costs. The unacceptable structural life of the outer flaps and associated hardware are caused by high turbulence and dynamic pressure fluctuations occurring in the internozzle fairing region during flight and ground operations of the B-1B aircraft. Other aircraft with closely spaced engines such as the F-18 and F-15 are also known to have suffered fatigue failures in the internozzle region. Recent studies at Langley Research Center have identified the phenomenon of twin supersonic jet plume resonance as a source of significantly higher internozzle dynamic pressures. An investigation has been conducted recently on a 6-percent scale model of the B-1B aircraft to ascertain the existence of twin plume resonance and to explore some passive methods of load suppression in the outer nozzle region. This investigation has been conducted at Mach numbers from 0.2 to 0.9, angles of attack up to 6°, and nozzle pressure ratios up to 3.5.

The results of this investigation indicate that amplitude levels associated with this phenomenon were found to dominate the dynamic pressure fluctua-

B-1B model installed in 16-Foot Transonic Tunnel. L-87-11046

tions in the internozzle region at some Mach numbers. However, at other flight conditions and especially at Mach number 0.85, vortices separating from an over-the-wing fairing located between the nozzles were the major source of high dynamic loadings. Shock noise levels were reduced by utilizing an air jet injection technique.

(F. J. Capone, 43013, J. M. Seiner, and O. C. Pendergraft, Jr.)

Transonic Characteristics of High Mach Number Nozzle Designs

An experimental investigation has been conducted to assess the off-design performance of nozzles designed for operation at hypersonic speeds. Transonic wind tunnel tests have been conducted on a series of two-dimensional external expansion ramp nozzles. A typical high-speed nozzle configuration installed in the 16-Foot Transonic Tunnel test section is shown in the figure.

High-pressure air was used to simulate jet exhaust. Forces and moments on the nozzle/afterbody (downstream of the metric seal) were measured with a six-component strain-gauge balance. Internal static pressure orifices were located on the ramp. Model variables included ramp chordal angle, length, and curvature; cowl (short flap) geometry; and ramp internal convergent section geometry. Tests were conducted at $\alpha = 0°$ over a Mach number range from 0 to 1.2 and a nozzle pressure ratio from 1.0 (jet off) to approximately 10.

Preliminary results indicate that the longer curved ramps tended to provide better thrust-minus-drag performance than the short steep-angle ramps. Sizable thrust vector angles were generated by all ramp/cowl combinations. As a result, large nose-up pitching moments were measured. The magnitude of these thrust vector angles (6° to 13° at static conditions) was directly related to the ramp

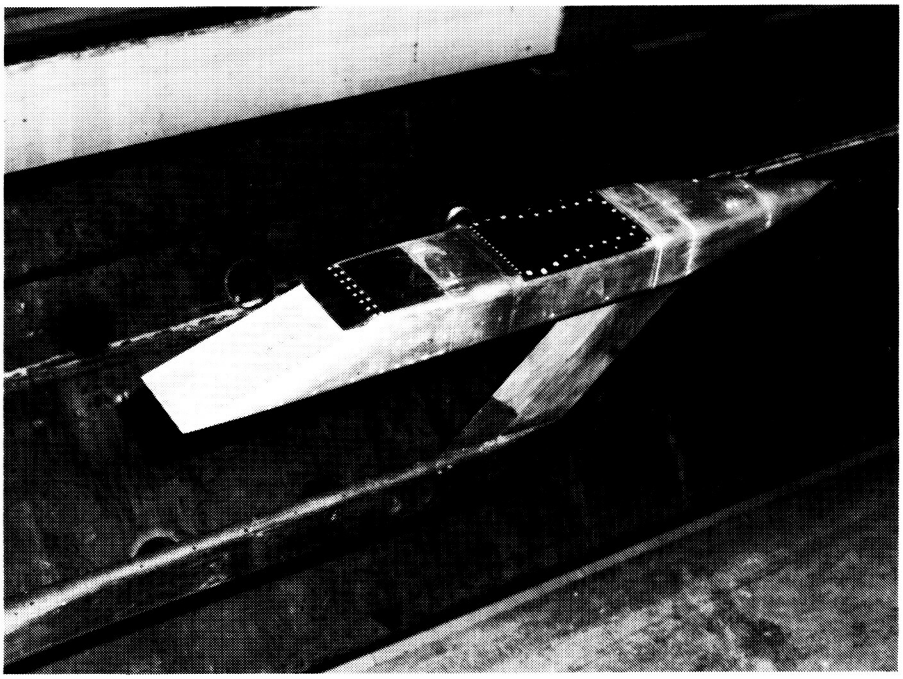

Isolated afterbody nozzle model. L-88-06814

terminal angle (6° to 16°). Straight ramp configurations generated substantially larger thrust vector angles (nose-up moments) than did the curved ramps.

(L. D. Leavitt, 43017, and M. Lamb)

External Flow Effects on Multiaxis Thrust Vectoring Nozzle Concepts

A wind tunnel investigation was conducted to determine external flow effects on several multiaxis thrust vectoring nozzle concepts. Pitch thrust vector angles up to 15° and yaw vector angles up to 20° were tested. The baseline nozzle concept utilized for this investigation was a nonaxisymmetric convergent-divergent type with throat area and expansion ratio values representative of subsonic, dry power operation. Several different yaw vectoring concepts were tested. These concepts included nozzle sidewall ports, nozzle sidewall flaps (as shown in the figure), and vanes downstream of the nozzle exit. High-pressure air was used to simulate jet exhaust flow at nozzle pressure ratios up to 7.0. The test was conducted in the 16-Foot Transonic Tunnel at Mach numbers from 0.2 to 0.9 and angles of attack to 14.5°. Six-component force and moment data were obtained from an internal strain-gauge balance.

Results from this test indicate that several of the yaw vector concepts could provide greater control power at low Mach numbers (< 0.4) than conventional rudder controls. Large control power increments were also realized at Mach numbers > 0.4. Based on these results, it is believed that conventional control surfaces on future aircraft could be considerably smaller than control surfaces on current aircraft, thus providing substantial drag and weight reductions. In addition, several of the yaw vector concepts (vanes downstream of the nozzle exit, in particular) have significant external flow effects on the resulting control power. This result indicates that thrust-generated control moments are not only a function of nozzle internal design but also of airplane external aerodynamics.

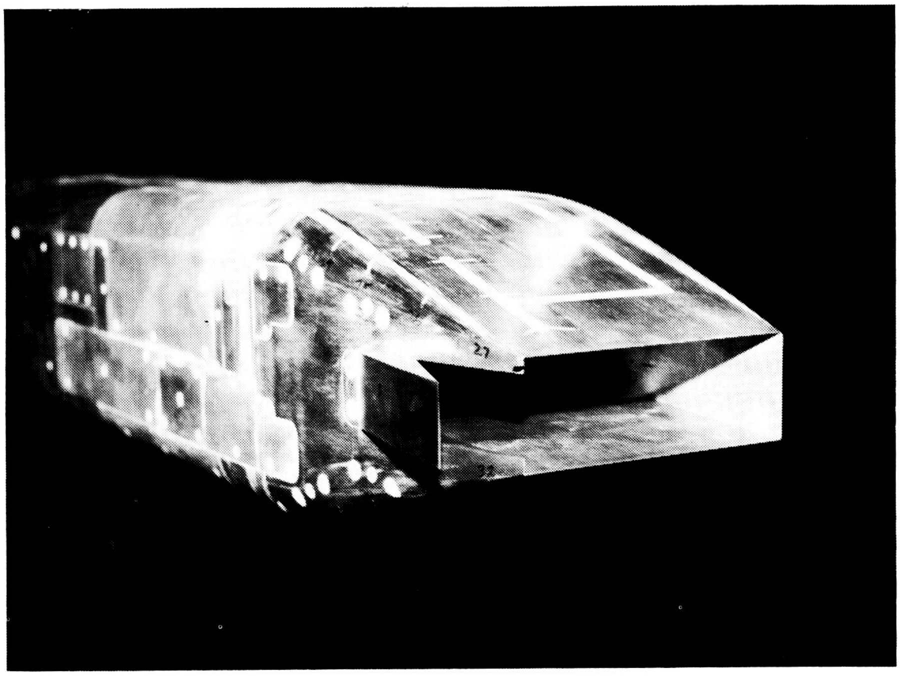

Sidewall flap. L-87-2270

(B. L. Berrier, 43003, M. L. Mason, and J. G. Taylor)

Investigation of Tail-Size Reductions on Modified F-15 Equipped With Multiaxis Thrust Vectoring

A wind tunnel investigation was conducted in the 16-Foot Transonic Tunnel to quantify the drag savings of reduced horizontal and vertical tails on a fighter aircraft utilizing thrust vectoring nozzles for control. Tests were conducted on a 1/12-scale model of the F-15 STOL (Short Takeoff and Landing) and Maneuver Technology Demonstrator (S/MTD) aircraft that uses canards and thrust vectoring nozzles for increased maneuverability. Results were obtained at Mach numbers from 0.4 to 1.2, angles of attack up to 10°, and nozzle pressure ratios up to 7.5. An internal balance and static pressure distributions were used to obtain force and moment data on both the fuselage and nozzles. The effects of reduced

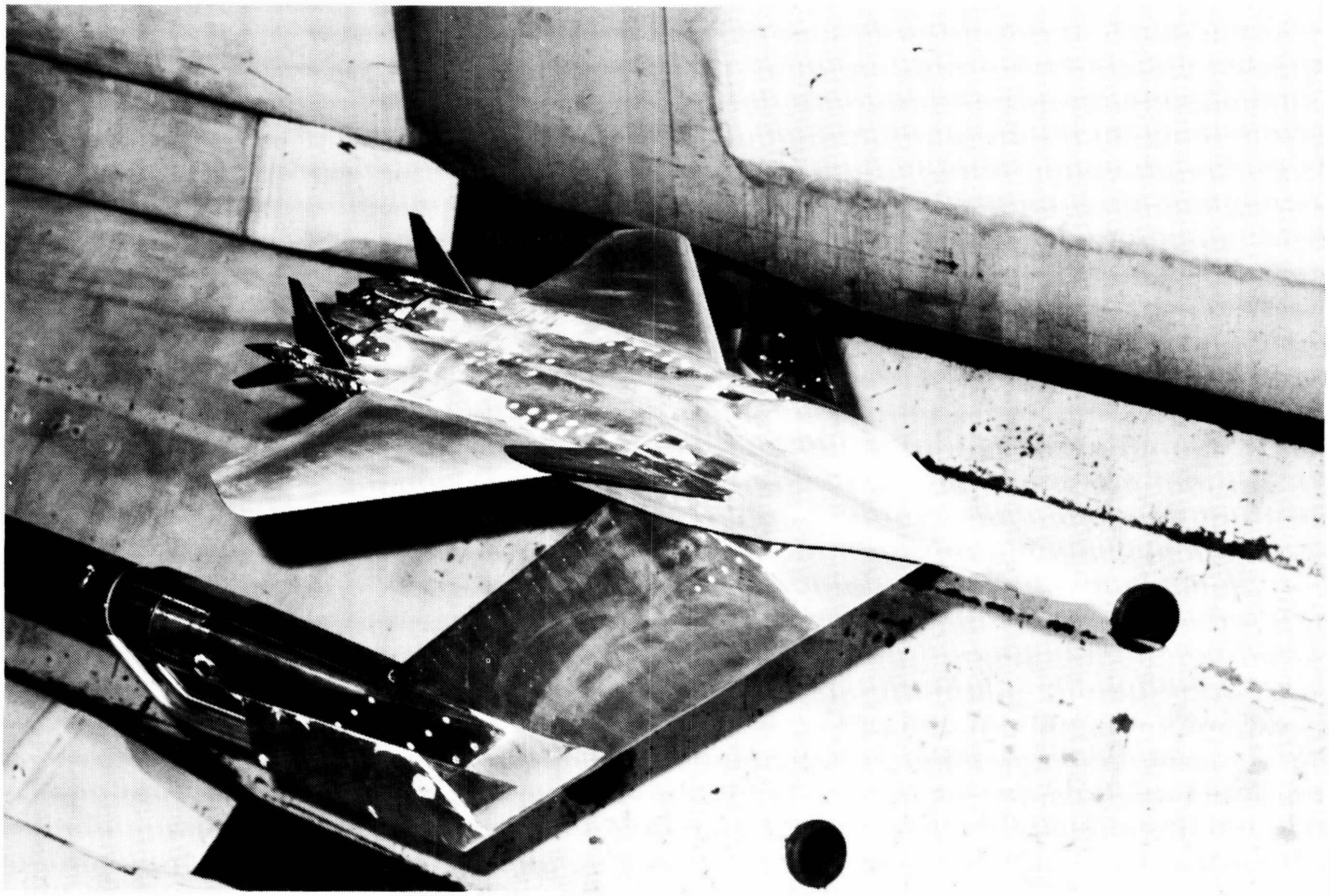

F-15 STOL configuration with reduced tails in 16-Foot Transonic Wind Tunnel. L-88-11482

tail size were obtained by testing combinations of horizontal and vertical tails at 100, 75, 50, 25, and 0 percent of the original sizes.

Previous studies showed that by utilizing thrust vectoring for maneuvering and control, the size of conventional aerodynamic surfaces (such as the horizontal and vertical tails) could be significantly reduced without decreasing aircraft effectiveness. In addition, tail-size reduction or elimination could substantially decrease drag and weight, thus greatly increasing aircraft range and fuel savings.

Results from this test quantified the significant drag savings achievable through the use of thrust vectoring nozzles to reduce or replace conventional control surfaces. Critical data were also provided which will greatly impact the future flight test program of the F-15 S/MTD aircraft, as will several configurations tested to provide data useful for the validation of transonic wing/body computational codes.

(M. Frassinelli, 43019, and T. Carson)

National Transonic Facility

The National Transonic Facility (NTF) is a cryogenic fan-drive transonic wind tunnel designed to provide full-scale Reynolds number simulation in the critical flight regions of most current and planned aircraft. The NTF can operate at Mach numbers from 0.2 to 1.2, stagnation pressures from 1 to 9 atm, and stagnation temperatures from 340 K to 80 K. The maximum Reynolds number capability is 120 × 10^6 at a Mach number of 1.0, based on a reference length of 0.25 m.

Construction of the NTF was completed in September 1982. The tunnel was declared operational in August 1984, and aerodynamic calibration and research and development testing were begun in that year.

Boeing 767-200 Research Program

A test program has been conducted as part of a Memorandum of Agreement among NASA Langley Research Center, NASA Ames Research Center, and the Boeing Commercial Airplane Company. Objectives of the program are to compare data obtained at comparable conditions in three different transonic wind

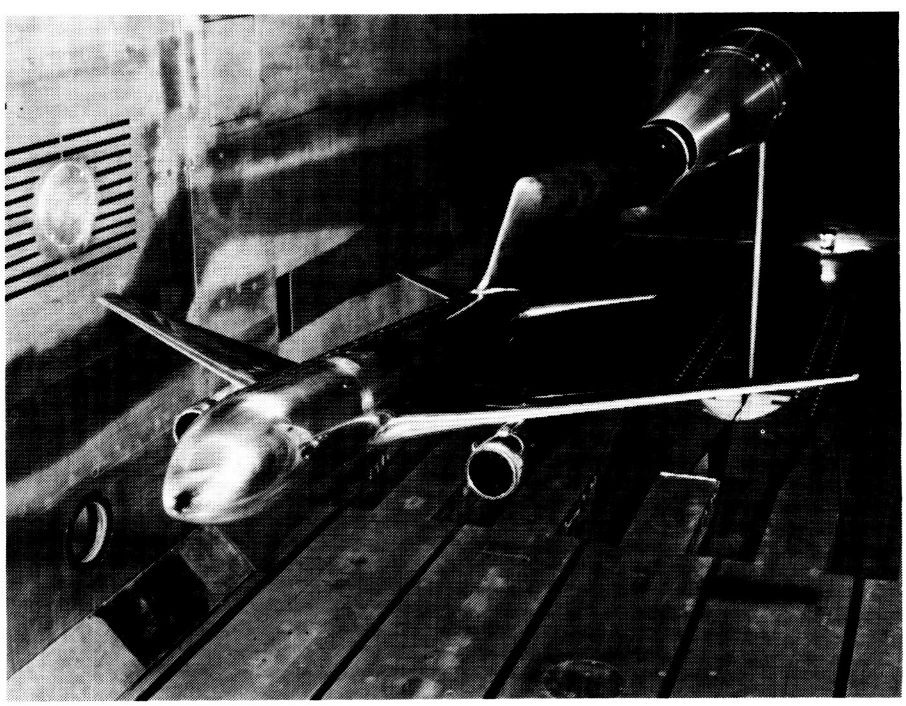

Boeing 767-200 model in NTF. L-87-4167

ORIGINAL PAGE
BLACK AND WHITE PHOTOGRAPH

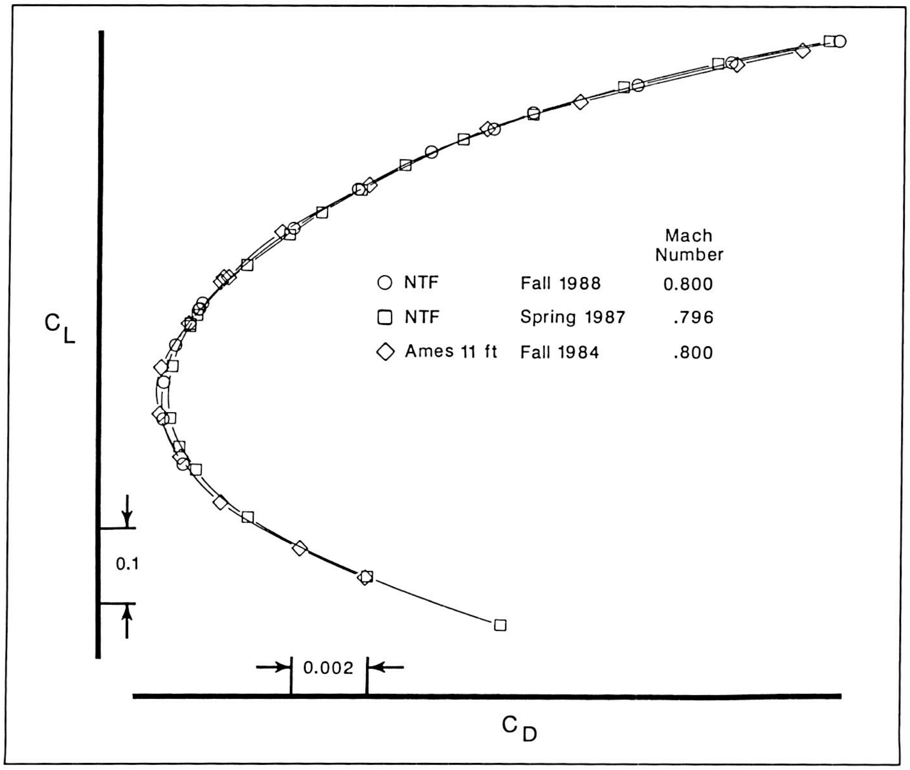

Variation of drag coefficient at Reynolds number of 7.5×10^6/*ft.*

tunnels, to compare Reynolds number effects on the model, and to compare data obtained in the NTF at a full-scale cruise Reynolds number to available airplane flight data. The wind tunnel investigations use an 0.03-scale model of the Boeing 767-200 airplane. The first figure shows the model installed in the NTF.

The data shown in the second figure are for three separate wind tunnel investigations at nearly identical test conditions. The maximum variation of drag coefficient C_D at a given lift coefficient C_L (for the three sets of data) is approximately 0.0003. This excellent repeatability has increased the level of confidence in the data from all the facilities.

The latest test in the NTF was mainly conducted at a temperature of −260°F (using cryogenic nitrogen), and at the airplane cruise flight Reynolds number of 67.4×10^6/ft. Data were obtained with the horizontal tail removed and at a series of fixed angles. These data are being converted into engineering form in order to conduct stability, control, and performance analyses; the initial study indicated that the repeatability of these data is very good. **(S. G. Flechner, 45108, and B. B. Gloss)**

Transonic Reynolds Number Effects for Slender Wing/Body Configuration

A wind tunnel investigation was conducted in the NTF to determine the Reynolds number effects on the transonic aerodynamics of a slender wing/body configuration. The model was comprised of a cone-cylinder-frustum body along with a unit-aspect-ratio delta wing and was representative of a class of vehicles capable of very high-speed

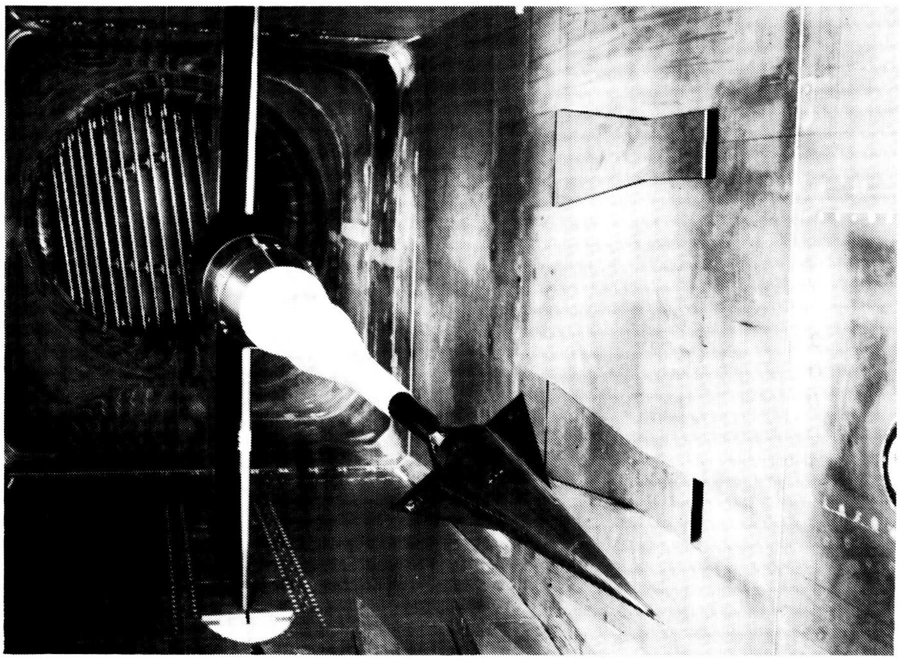

Slender wing/body configuration mounted in NTF. L-88-1551

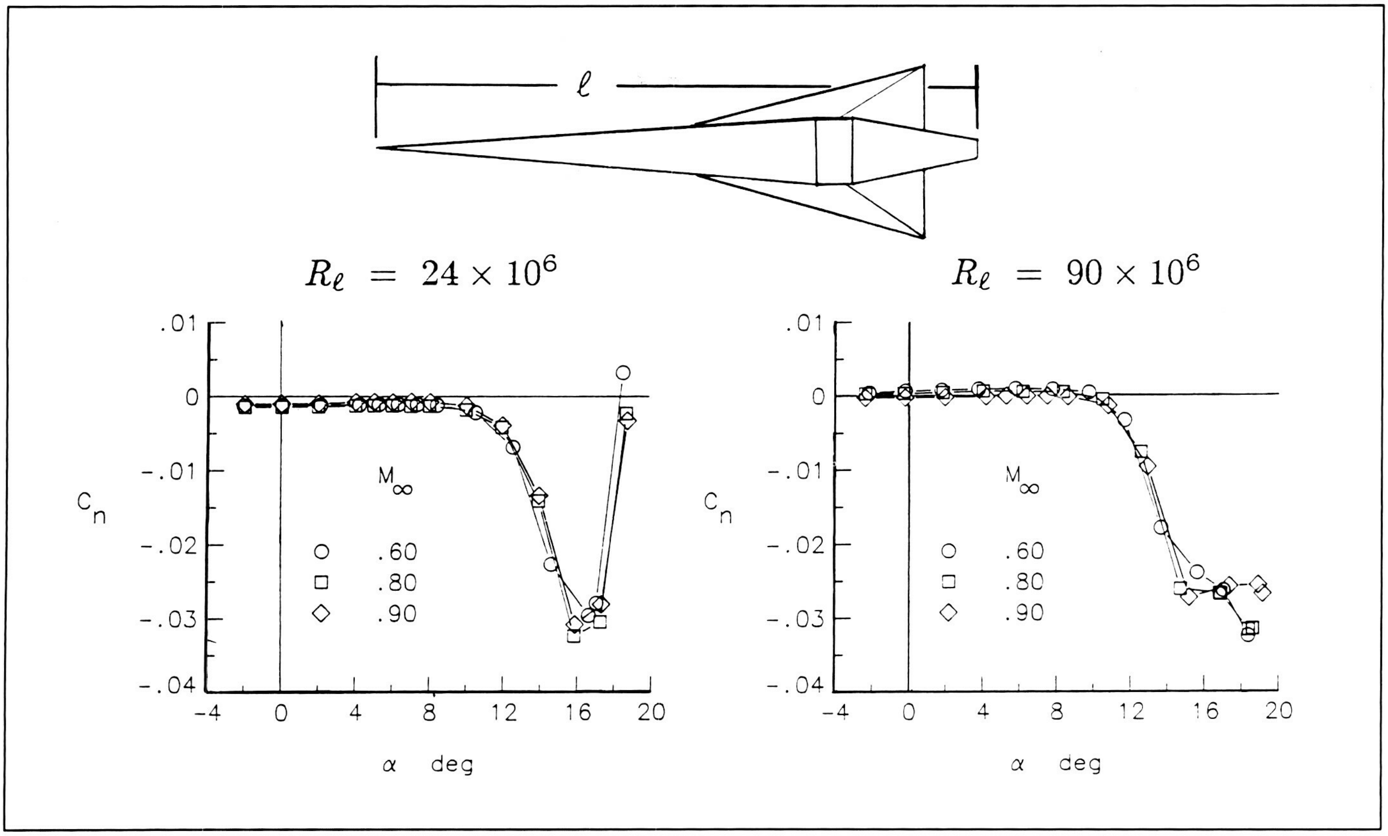

Reynolds number effect on yawing moment.

flight. The transonic data were obtained in the NTF as part of a broader experimental program for this model which included low-speed Reynolds number studies conducted in the Low-Turbulence Pressure Tunnel as well as supersonic compressibility studies conducted in the Unitary Plan Wind Tunnel. The first figure shows the configuration mounted in the NTF.

Tests were conducted in the NTF for Mach numbers ranging from 0.3 to 1.15 and Reynolds numbers ranging from 18×10^6 to 180×10^6 (based upon body length) such that Mach and Reynolds number effects could be isolated. Both longitudinal and lateral-directional force and moment data were obtained. At 0° sideslip and high angles of attack, asymmetric flow separation occurred causing significant lateral-directional forces and moments. A sample result is presented in the second figure for the yawing moment at 0° sideslip. The data demonstrate significant Reynolds number effects above an angle of attack of approximately 14°. The low Reynolds number data show a nonlinear reversal in the yawing moment trend with angle of attack above this angle, whereas the high Reynolds number data do not evidence this effect in the angle-of-attack range investigated. The high Reynolds number data also show increased compressibility effects at the high angles of attack as compared to the low Reynolds number data. **(J. M. Luckring, 42869, and C. H. Fox, Jr.)**

0.3-Meter Transonic Cryogenic Tunnel

ORIGINAL PAGE
BLACK AND WHITE PHOTOGRAPH

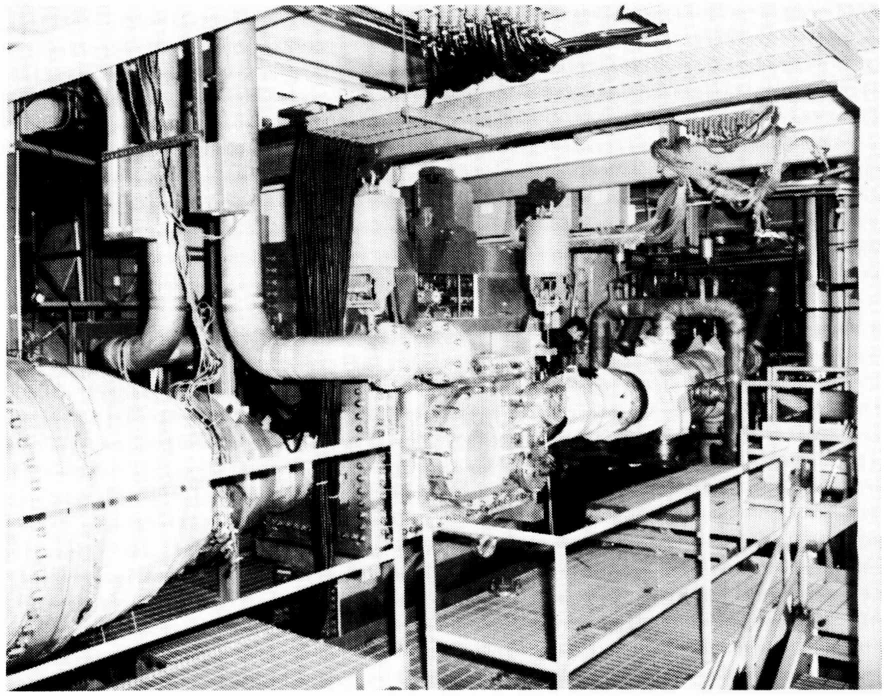

The Langley 0.3-Meter Transonic Cryogenic Tunnel (TCT) is a continuously operating cryogenic pressure tunnel. The test section Mach number is continuously variable between 0.2 and approximately 1.3, with suitable adjusted test section shapes. The stagnation pressure can vary from slightly over 1 bar up to 6 bars and the stagnation temperature from 340 K down to approximately 77 K (−196° C). The test gas is nitrogen. The wide ranges of pressure and tem-

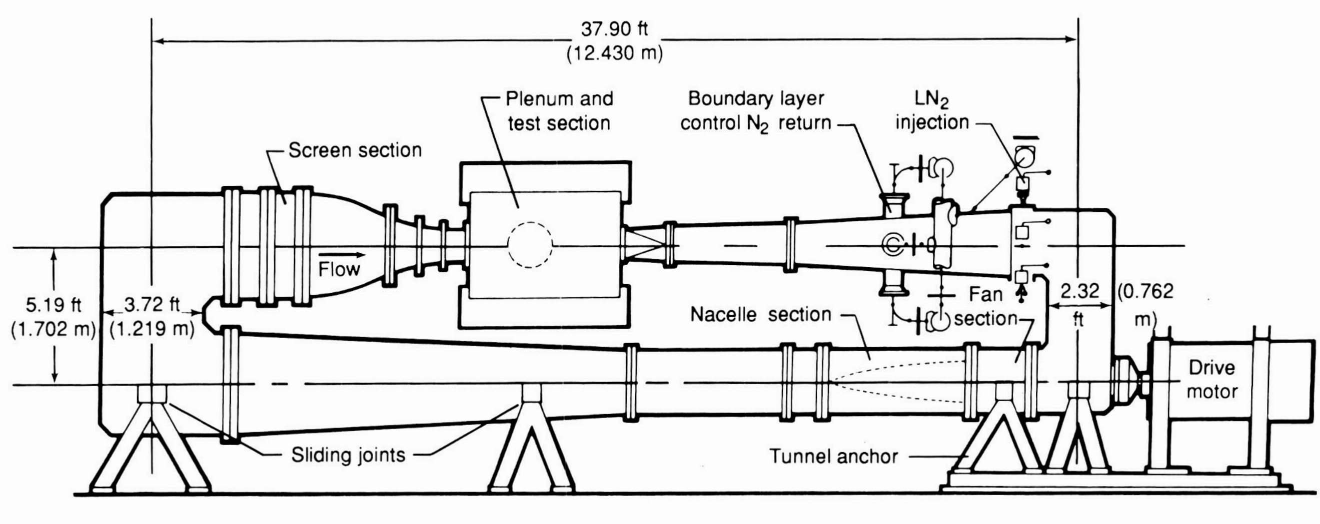

Sketch of 0.3-Meter TCT with 13-in. by 13-in. two-dimensional Adaptive Wall Test Section installed.

perature allow the study of approximately a 30-to-1 range in Reynolds number effects. A maximum Reynolds number of more than 100 × 10^6/ft is possible. The 0.3-Meter TCT has automatic control of Mach number, pressure, and temperature.

The tunnel was placed in operation in 1973 as a three-dimensional pilot tunnel to demonstrate the cryogenic wind tunnel concept at transonic speeds. The successful demonstration of the cryogenic concept in the 0.3-Meter TCT played a major role in the decision to build the United States National Transonic Facility (NTF). Subsequently, the 0.3-Meter TCT has played a major part in the Advanced Technology Airfoil program because the tunnel allows Reynolds number effects to be studied in two-dimensional testing. The 0.3-Meter TCT is currently involved in the evaluation of testing techniques for improving data quality (by minimizing boundary interferences) in both two- and three-dimensional testing. The combination of flight Reynolds number capability and minimal boundary interferences makes the 0.3-Meter TCT a powerful tool for aeronautical research at transonic speeds.

During more than 15 years of operation, the 0.3-Meter TCT has run with three different test sections. The original test section was octagonal with a sting-type model support system. In 1975, an 8-in. by 24-in. two-dimensional test section was installed with slotted top and bottom walls. In 1985, a new Adaptive Wall Test Section was installed.

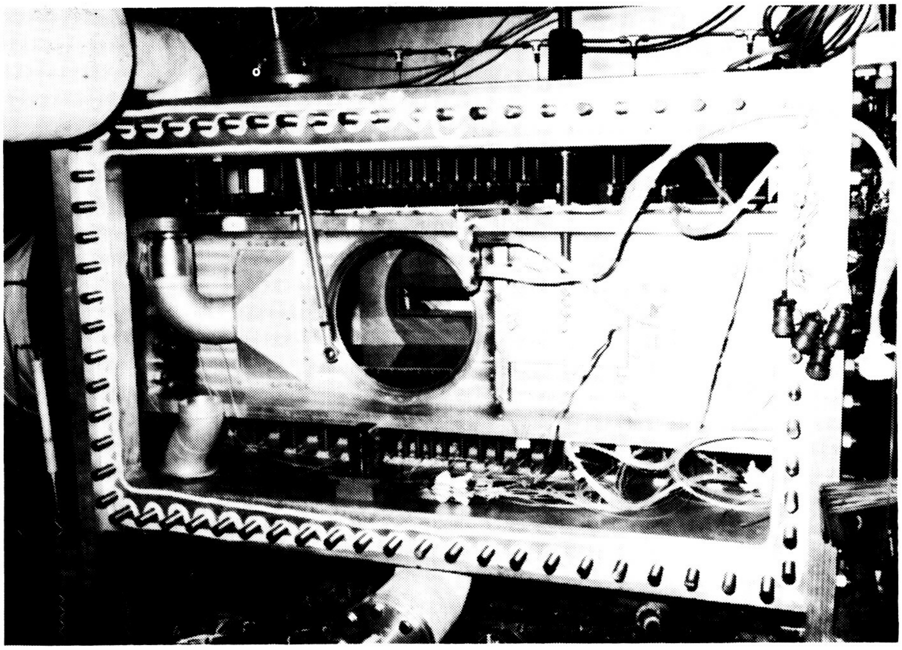

View of 0.3-Meter TCT AWTS with left side of surrounding pressure shell removed.

Adaptive Wall Test Section.

The Adaptive Wall Test Section (AWTS) is nominally 13 in. square and has an effective length of 55.8 in. This unusual transonic test section has four solid walls with a flexible floor and ceiling. The complete test section is enclosed in a pressure shell that forms a 73.2-in.-long insert into the 0.3-Meter TCT tunnel circuit.

A system of 21 computer-controlled jacks supports each flexible wall. These flexible walls are made of 308 stainless steel. The AWTS has motorized model support turntables and a traversing wake survey probe, both of which are computer controlled.

For each data point, the flexible walls are adapted to shapes that drastically minimize wall interferences that would otherwise exist. In two-dimensional testing, the walls follow streamline shapes that would exist around the model if it were in free air. The floor and ceiling of the test section in effect become invisible to the model. With wall interferences minimized, the model size and therefore the Reynolds number capability of the tunnel can be increased. In addition, the removal of noisy slots in the test section gives the added benefit of much improved data quality.

For two-dimensional testing, the AWTS has provisions for both active and passive sidewall boundary-layer control (BLC). Porous plates can be fitted into the rigid sidewalls just upstream of the model location. This BLC system allows the investigation of another source of boundary interference.

Initial AWTS evaluation was performed with two-dimensional airfoils ranging in chord from 6 in. to 13 in. A record chord Reynolds number of 74 × 10^6

has been achieved. The walls have been successfully adapted with lift coefficients up to 1.5 and Mach numbers up to 0.82. More recently, the sidewall mounted wings have been tested to investigate the testing technique for minimizing three-dimensional wall interferences by two-dimensional wall adaptation. These tests also allowed the demonstration of the supersonic capability of the 0.3-Meter TCT.
(S. W. D. Wolf, 45008)

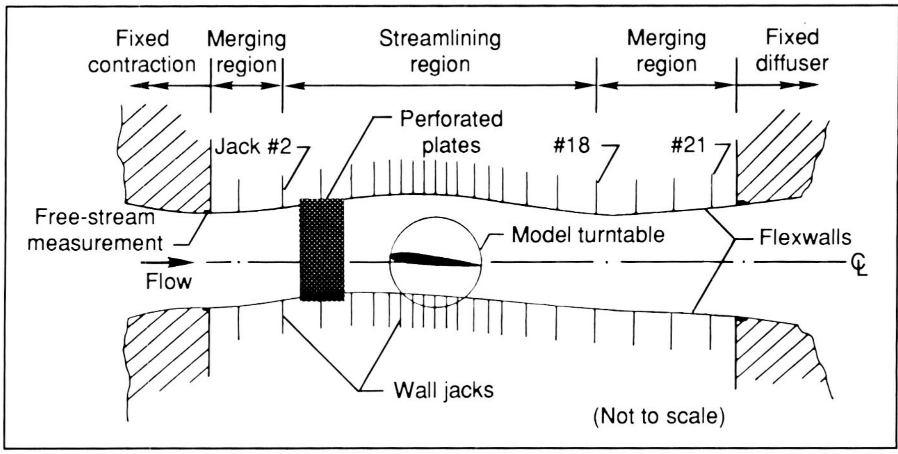

Schematic diagram of flexible-walled AWTS.

Wall Interference Studies With CAST 10-2/DOA-2 Airfoil

Wall interference studies are part of cooperative agreements among NASA, NAE (National Aeronautical Establishment) of Canada, ONERA (Office National d'Etudes et de Recherches Aérospatiales), and DLR (Deutsche Forschungsanstalt für Luft- und Raumfahrt). Researchers have chosen the CAST 10 section because it is a cambered supercritical airfoil that has been tested worldwide. This data base offers a unique opportunity to assess the quality of different wall interference correction techniques.

Two CAST 10 models were built, one in France with a 7.09-in. chord and the other in Canada with a 9-in. chord. Data on both models from facilities other than the 0.3-Meter TCT are presented. These facilities include the ONERA/CERT (Centre d'Etudes et de Recherches de Toulouse) T2 tunnel that has a two-dimensional flexible walled AWTS (for tests of the smaller model), and the larger model in the NAE 5-ft by 5-ft Blowdown Wind Tunnel fitted with a deep 15-in. wide two-dimensional test section with perforated top and bottom walls (for tests of the larger model).

The smaller French model was tested in the 0.3-Meter TCT over the Mach number range 0.7 to 0.8 with chord Reynolds numbers from 4×10^6 to 45×10^6. A comparison of lift data from the T2 and the 0.3-Meter TCT for the design Mach number of 0.765 at 4×10^6 Reynolds numbers with transition fixed and free is shown in the first figure. The comparisons are good, particularly in the matching of $C_{n_{max}}$. The severe effect of transition fixing at low Reynolds number is perfectly matched in both data sets, which is quite remarkable.

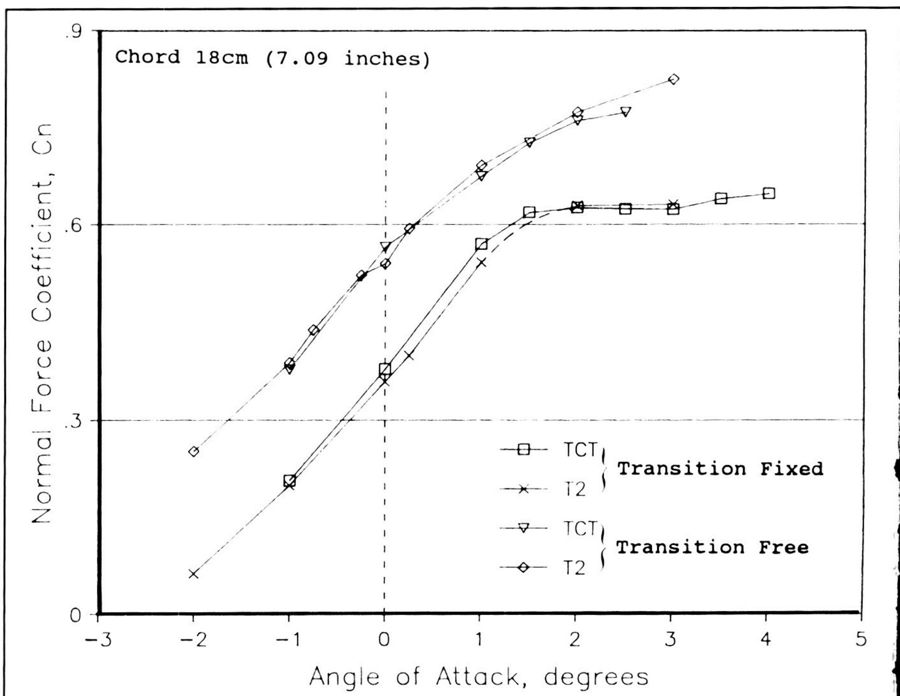

Comparison of lift data from the 0.3-Meter TCT and T2 tests at Mach 0.765 and 4×10^6 chord Reynolds number.

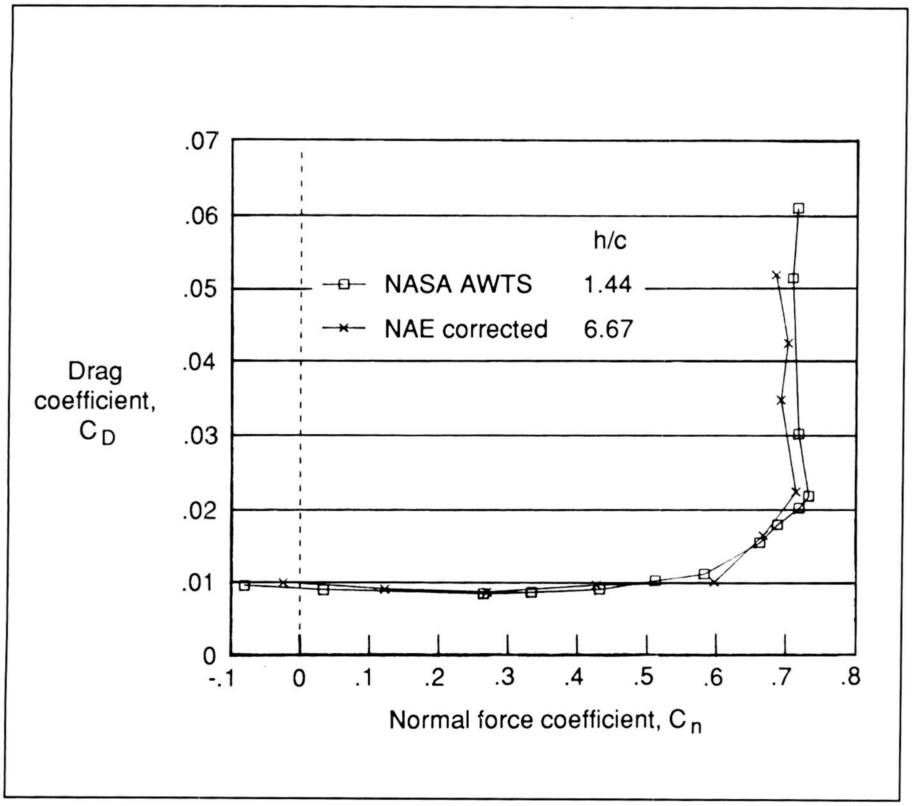

Comparison of NAE and NASA data from same model at Mach 0.765 and 20 × 10^6 chord Reynolds number.

These studies are very encouraging and indicate that comparisons can be made from one tunnel to another provided it is possible to properly account for wall interferences.

(S. W. D. Wolf, 45008)

NAE of Canada tested their large CAST 10 model with sidewall boundary-layer treatment. Posttest perforated wall interference corrections were then applied to the real-time data using the subsonic method of Mokry and Ohman. The NAE tests had a test section height-to-chord ratio of 6.67 (which is very large compared with a ratio of 1.44 in the 0.3-Meter TCT). These corrected two-dimensional data are probably the best available from a ventilated transonic test section. A typical comparison of real-time NASA data with corrected NAE data is shown in the second figure.

Transition was fixed to minimize the effects of tunnel turbulence on both data sets. The comparison is very good, except for a small uncertainty in $C_{n_{max}}$.

Minimization of Wall Interferences in Three-Dimensional Testing

Tests were conducted on a semispan wing in the 0.3-Meter TCT as part of the validation process for Langley Research Center wall adaptation schemes for three-dimensional testing. A simple unswept wing was mounted on the right sidewall of the AWTS. This force model, which has an aspect ratio of 4.0 with a mean aerodynamic chord of 3.41 in., was chosen because

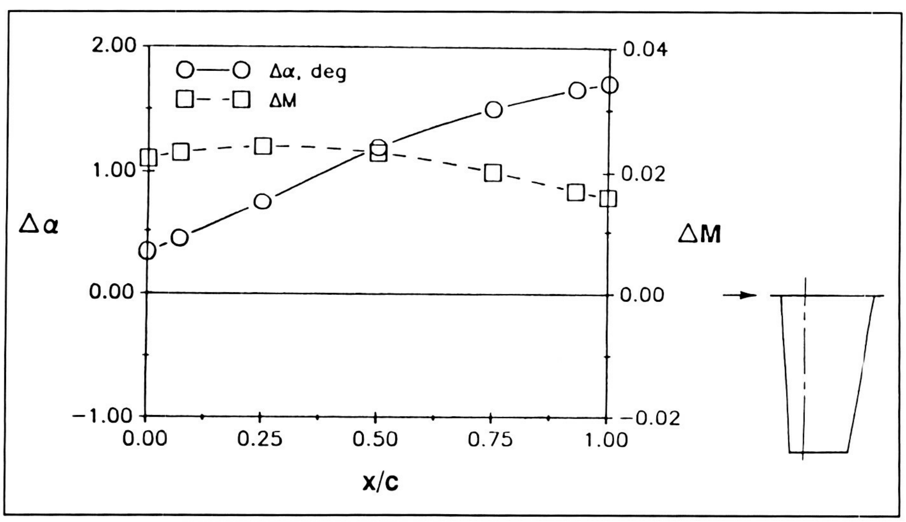

Chordwise variation of wall interference at wing root of semispan wing with walls straight ($M_\infty = 0.7$, $\alpha = 7°$, wing high).

A good agreement in the pressure distributions and drag measurements has also been seen.

it has an "interference free" data base. The model is small compared to the AWTS. The

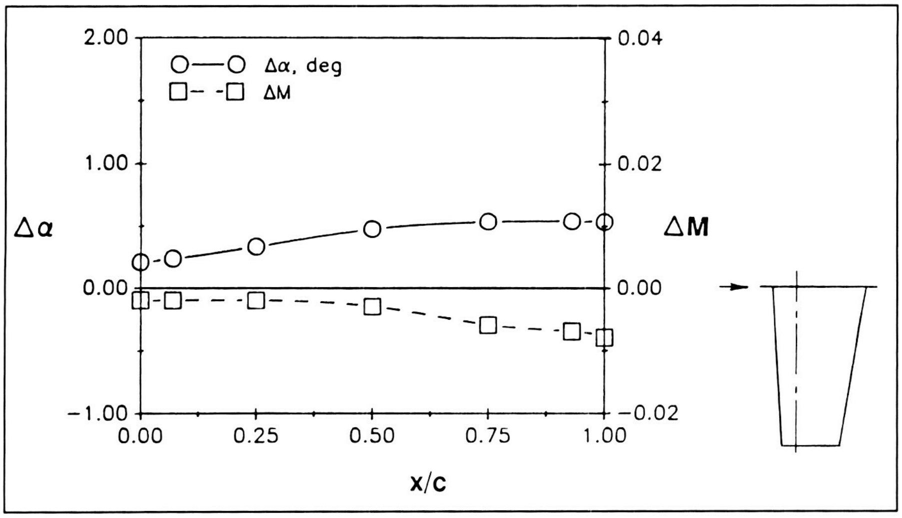

Chordwise variation of wall interference at wing root of semispan wing with shaped walls after one iteration of the wall adaption process ($M_\infty = 0.7$, $\alpha = 7°$, wing high).

solid blockage is 0.79 percent, and the semispan/tunnel width ratio is 0.51.

The model was tested at low Reynolds numbers and noncryogenic temperatures over the Mach number range 0.7 to 0.9 and an angle-of-attack α range from 0° to +7° (as limited by balance loads). With the wing mounted above the tunnel centerline (high position), some significant wall interferences were encountered at the highest angle of attack.

The first figure shows the calculated lift and blockage interference at the wing root with the walls straight. The induced Mach number is small and almost constant over the chord. However, there is a significant gradient in the induced α of 1.35° over the chord. The wall interference at other spanwise locations is similar, although the upwash becomes more uniform toward the wing tip.

After one adaptive movement of the flexible walls, according to a three-dimensional adaptation scheme by Rebstock (International Council of Aeronautical Sciences Report Number 88-3.8.2), the wall interference at the wing root is reduced, as shown in the second figure.

The induced Mach number becomes negligible, and the upwash gradient is greatly reduced. A similar interference reduction occurs over the span of the wing.

These preliminary results give encouragement that wall interferences in three-dimensional tests can be minimized by simple wall adaptation in only two dimensions.
(S. W. D. Wolf, 45008)

High Reynolds Number Test of Thin Fighter Wing

A typical airfoil used in supersonic fighter aircraft has a lift coefficient of 0.1 and a thickness of 5 percent. Building such a thin airfoil model with pressure instrumentation for cryogenic testing is very difficult. However, a technique that uses chemically etched pressure channels in the bond planes between multiple sheets of metal offers promise. This technique is being developed at Langley Research Center. The canard of the X29A fighter aircraft was chosen as a proof-of-concept model to build. This configuration has a maximum thickness of 5 percent chord, and

L-88-3055

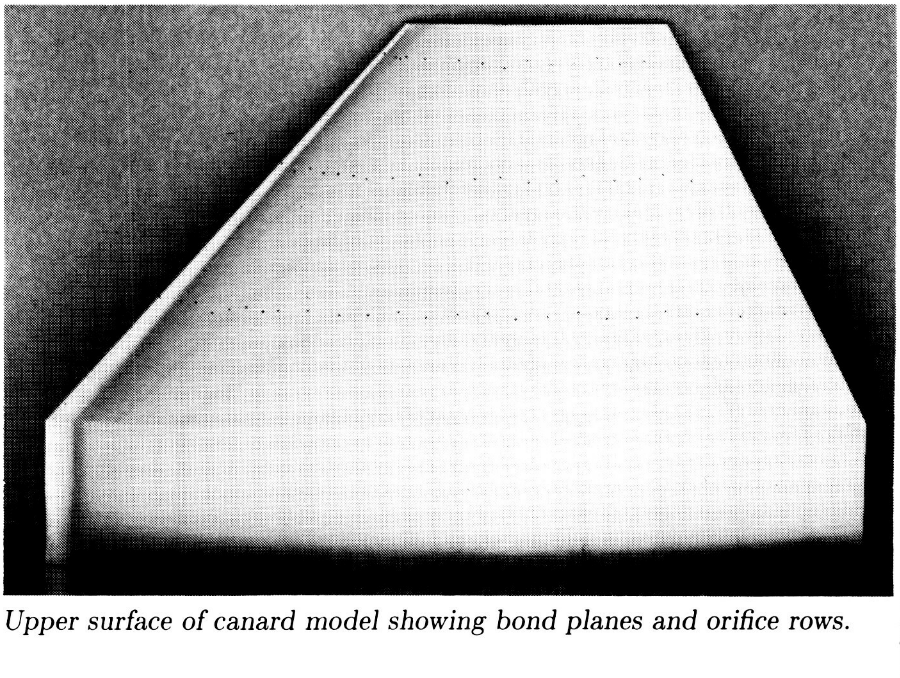

Upper surface of canard model showing bond planes and orifice rows.

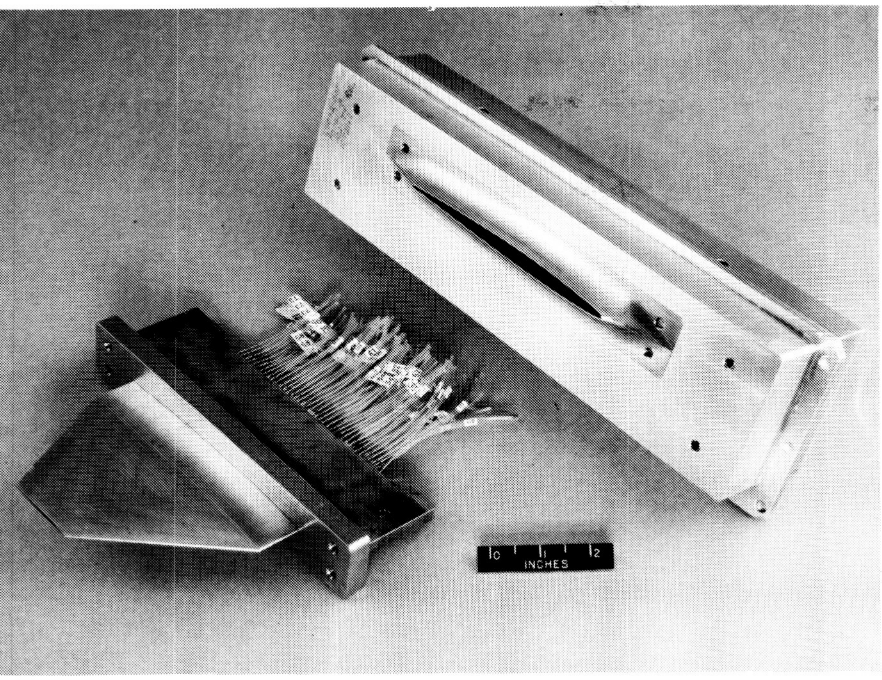

Canard model and mounting block to fit sidewall turntable. L-88-3052

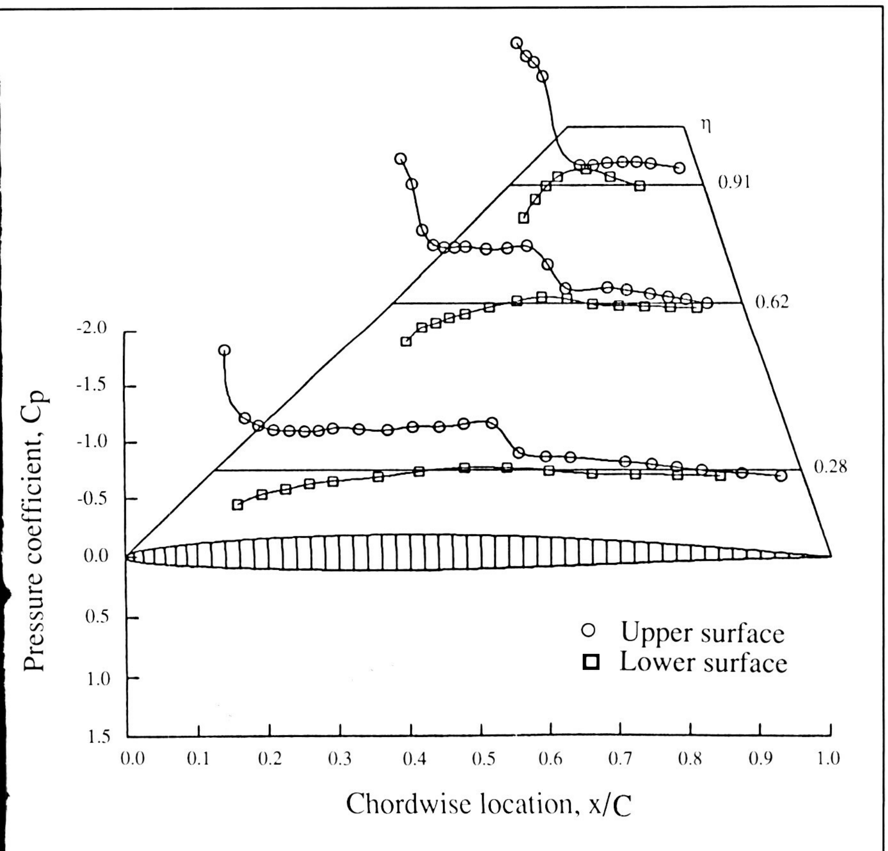

ample of pressure data on canard model for three spanwise rows.

it is highly tapered from root to tip, making pressure instrumentation even more challenging.

The first figure is a photograph of the X29A canard upper surface. There are three rows of orifices with a total of 56 orifices on the upper surface. Six thin plates form the upper surface of the airfoil. The outcrop of the five bond planes is clear in the figure. There are 37 additional orifices on the bottom surface. The orifices are deliberately staggered to minimize any buildup of boundary-layer instabilities. The choice of actual model size to test resulted in a root chord of 14.5 cm, a tip chord of 4.6 cm, and a semispan of 7.0 cm. This size gives a corresponding maximum thickness of only 0.725 cm (0.285 in.) at the root and 0.23 cm (0.091 in.) at the tip.

The model was mounted on the sidewall turntable in the Adaptive Wall Test Section of the 0.3-Meter TCT and was tested in May 1988. The second figure shows the model assembled with its fairing and mounting block ready for testing in the 0.3-Meter TCT. Testing was over nearly the full range of conditions available with the Adaptive Wall Test Section. This included both ambient and cryogenic operation at pressures to 6 bars at Mach numbers to 1.3. For testing this semispan three-dimensional model, the method of Rebstock was used to adapt the solid test section walls for minimum interference.

Aerodynamic data were taken for the airfoil (surface pressures and wake survey) at Mach numbers from 0.3 to 1.07. The tests covered angles of attack from $-4°$ to $+15°$. At most Mach numbers, a 10-to-1 range of

Reynolds numbers was covered, and flight values of Reynolds numbers were easily obtained. The third figure shows an example of the airfoil data at an angle of attack of 5.75°, a Mach number of 0.92, and a Reynolds number (based on mean aerodynamic chord) of 31.3×10^6.
(P. L. Lawing, 45137)

Unitary Plan Wind Tunnel

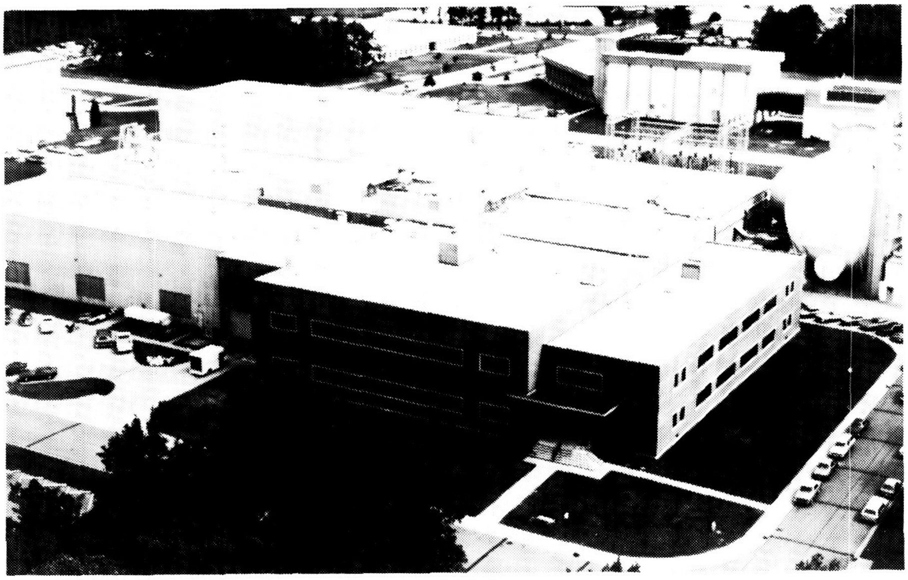

Immediately following World War II, the need for wind tunnel equipment to develop advanced airplanes and missiles was recognized. The military and the National Advisory Committee for Aeronautics (NACA) developed a plan for a series of facilities which was approved by the United States Congress in the Unitary Wind Tunnel Plan Act of 1949. This plan included five wind tunnel facilities, three at NACA laboratories and two at the Arnold Engineering Development Center. The Langley Unitary Plan Wind Tunnel (UPWT) was among the three built by NACA. The UPWT is a closed-circuit continuous-flow variable-density tunnel with two 4-ft by 4-ft by 7-ft test sections. The low-range test section has a design Mach number range of 1.5 to 2.9, and the high-range section Mach number varies from 2.3 to 4.6. The tunnel has sliding-block-type nozzles that allow continuous variation in Mach number while on-line. The maximum Reynolds number per foot varies from 6 $\times 10^6$ to 11 $\times 10^6$ depending on Mach number. The tunnel is used for force and moment, pressure distribution, jet effects, dynamic stability, and heat transfer studies. Flow visualization data, which are available in both test sections, include schlieren, oil flow, and vapor screen.

Laser Transit Anemometer Evaluation

A proof-of-concept test has been conducted to evaluate the capabilities of a laser transit anemometer (LTA) for use as a two-dimensional (2-D) velocity measurement technique in the UPWT. The LTA system utilizes a pair of 40-μm-diameter focused laser beams spaced 1230 μm apart to measure the transit times of individual seeding particles entrained in the flow. The 2-D flow direction is determined by the orientation of the two laser beam foci. The boundary-layer flow field on the cone forebody (5° half angle) of an axisymmetric model was seeded using kaolin particles (with a nominal size of 0.9 μm) injected through orifices located 3 in. from the apex. This method of seeding was performed to expedite the experiment because development of a tunnel seeding system was deemed unnecessary for this proof-of-concept test. The test was conducted in Test Section 2 of the UPWT. The test Mach numbers were 2.5 and 4.5 for Reynolds numbers of 1×10^6/ft and 2×10^6/ft.

Data were taken in a vertical plane that bisected the longitudinal centerline of the model at a location 25 in. from the apex. The LTA data were obtained from the outer edge of the boundary layer down to within 100 μm of the model surface. A typical LTA-measured boundary-layer velocity profile is shown in the figure along with a theoretical turbulent velocity profile. Although laminar velocity profiles were expected for the test conditions, schlieren photographs identified seed injection disturbances to the flow field, which probably induced premature boundary-layer transition. These results showed that the LTA or other Mie-scattering-based laser

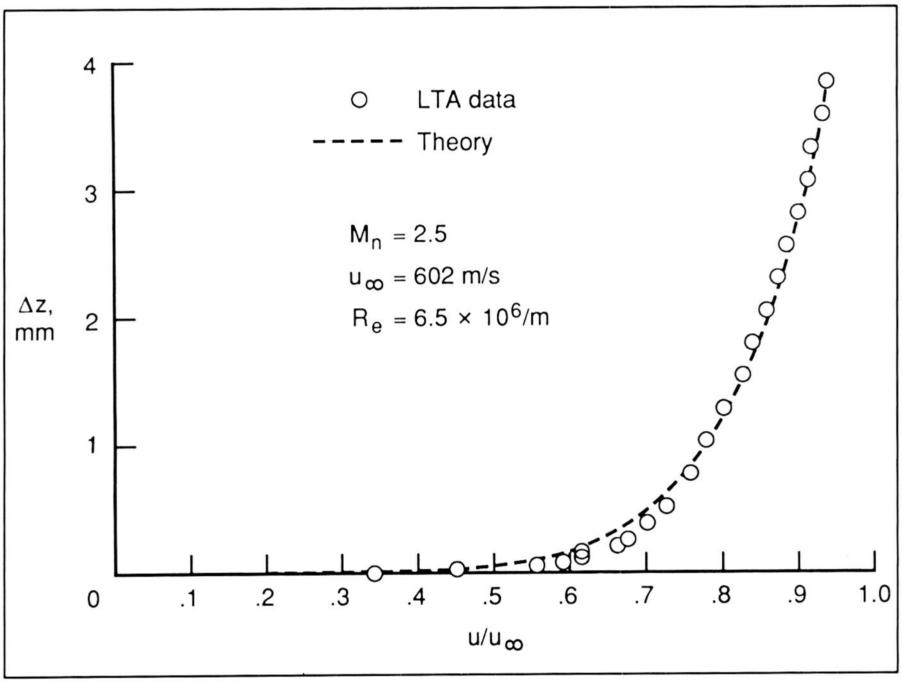

Typical turbulent boundary-layer profile measurement comparing LTA data with theory.

techniques such as laser Doppler anemometry (LDA) could be successfully utilized in the UPWT and that a tunnel seeding system should be developed for future testing.
(W. M. Humphreys, Jr., 44601, P. F. Covell, C. E. Nichols, Jr., and W. W. Hunter, Jr.)

Supersonic Aerodynamic Characteristics of Generic Accelerator Model

In support of the National Aero-Space Plane (NASP) Program, tests were conducted on a generic accelerator model in Test Section 1 of the UPWT in order to define the aerodynamic characteristics of the vehicle. The test Mach numbers were 1.5 and 2 for Reynolds numbers of 1 × 10^6/ft, 2 × 10^6/ft, and 4 × 10^6/ft. Angles of attack were varied from −4° to 27° and sideslip angles were varied from −8° to 8°. A parametric study was performed by adding different model components to the baseline configuration in order to determine their individual interference effects. Configuration variables included a delta canard and a trapezoidal canard; large and small centerline-mounted vertical tails, along with a set of wing-mounted verticals; and a set of model noses of varying bluntness. Wing position was varied by changing the longitudinal location and the degree of wing incidence. The vehicle was characterized by measuring the force and moment coefficients and by taking vapor screen and schlieren photographs of selected model configurations and test flow conditions.

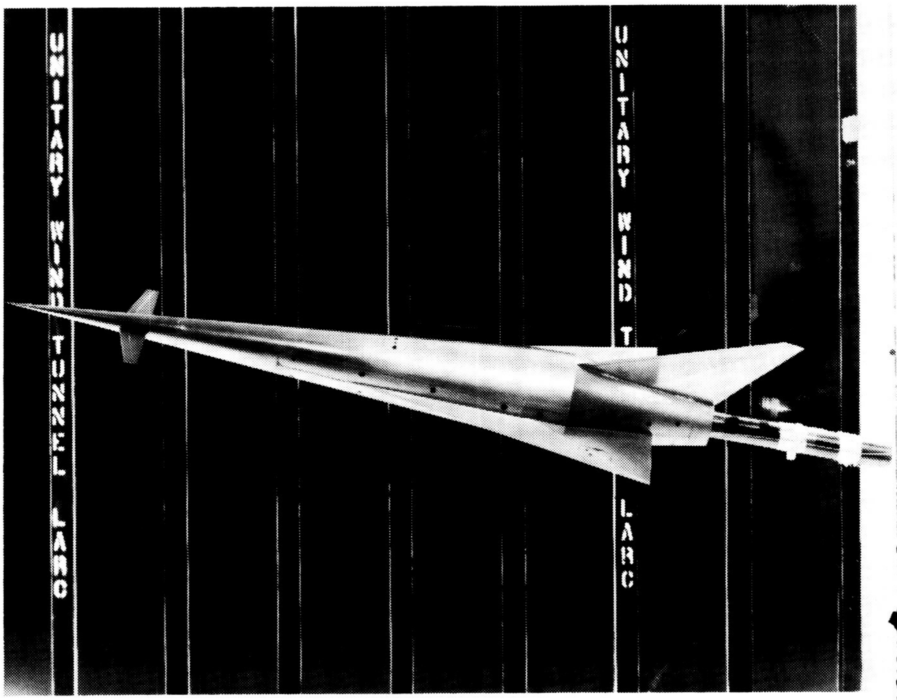

Generic accelerator model mounted in UPWT. L-88-6244

Preliminary analyses of the test results indicate that there are no Reynolds number effects. A slight increase in lift-to-drag ratio was effected by translating the wing to the aft position. As expected, a decrease in stability was observed with the addition of the canards; however, the trapezoidal canard showed a pitch-up tendency at high angles of attack.
(I. J. Walker, 45957, and P. F. Covell)

Supersonic Boundary-Layer Transition Detection Using Liquid Crystals

The location of boundary-layer transition can significantly impact aircraft performance at supersonic speeds. Generally, most transition detection techniques are impractical on standard wind tunnel models; hence, transition studies have been extremely limited. In a recent wind tunnel investigation, the liquid-crystal technique was shown to be both practical and applicable in detecting natural and grit-induced transition.

Natural transition studies using liquid crystals were conducted on a flat-plate model in the UPWT at Mach numbers from 1.5 to 2.5. The results are comparable to flat-plate results obtained in other large tunnels using pitot and temperature-sensitive paint techniques. The frequency response of the liquid

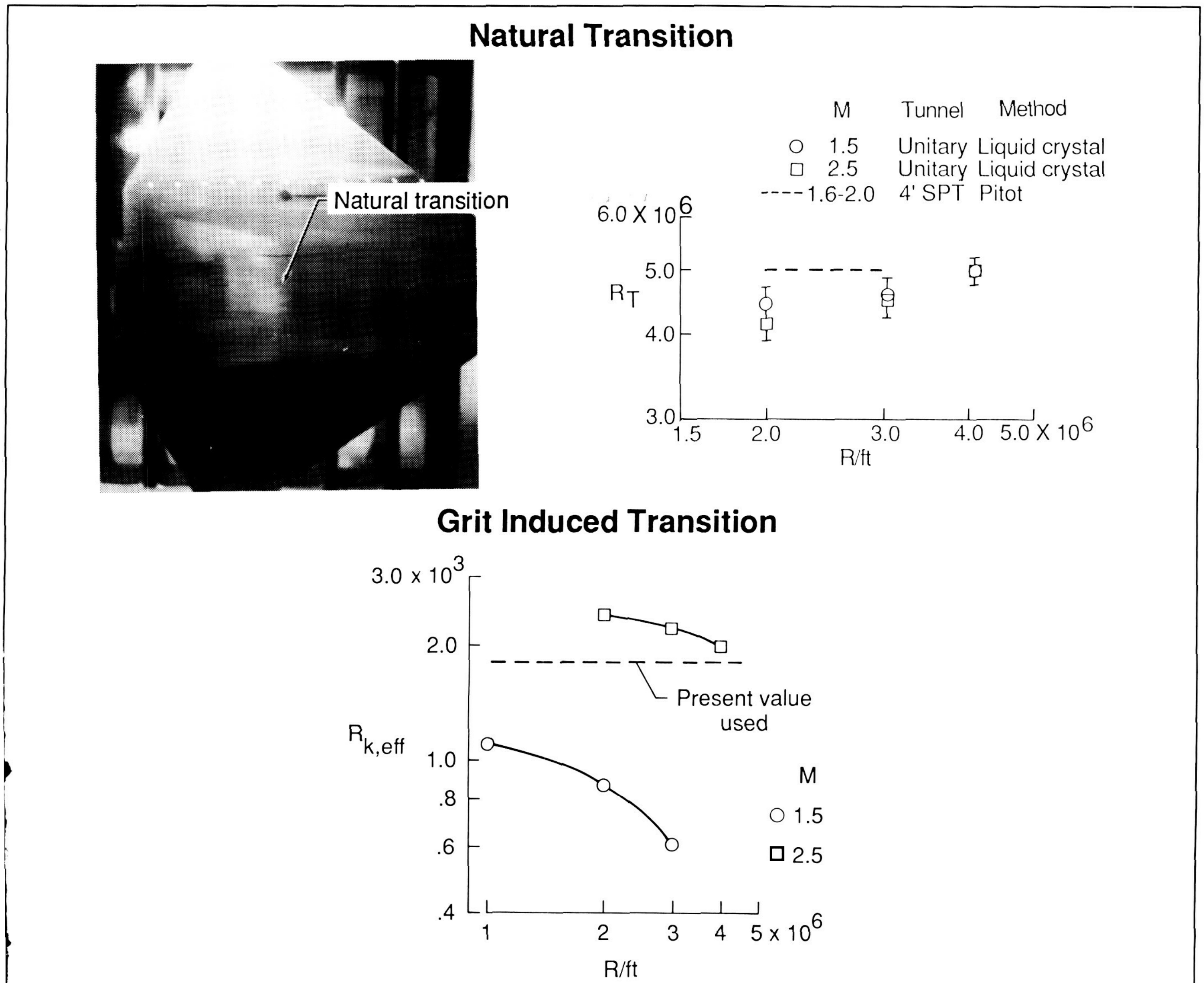

Natural and grit-induced boundary-layer transition.

crystals was sufficient to indicate the dynamic nature of the transition front.

Grit-induced transition was investigated by placing strips of various grit size near the flat-plate leading edge. The effective roughness Reynolds number $R_{K,\text{eff}}$ required for transition to occur near the grit strip is a strong function of both unit Reynolds and Mach numbers. These results illustrate the capabilities of the liquid-crystal technique for assuring that the appropriate transition grit size is employed in tests of planar aircraft surfaces.
(P. F. Covell, 45936, C. J. Obara, and R. M. Hall)

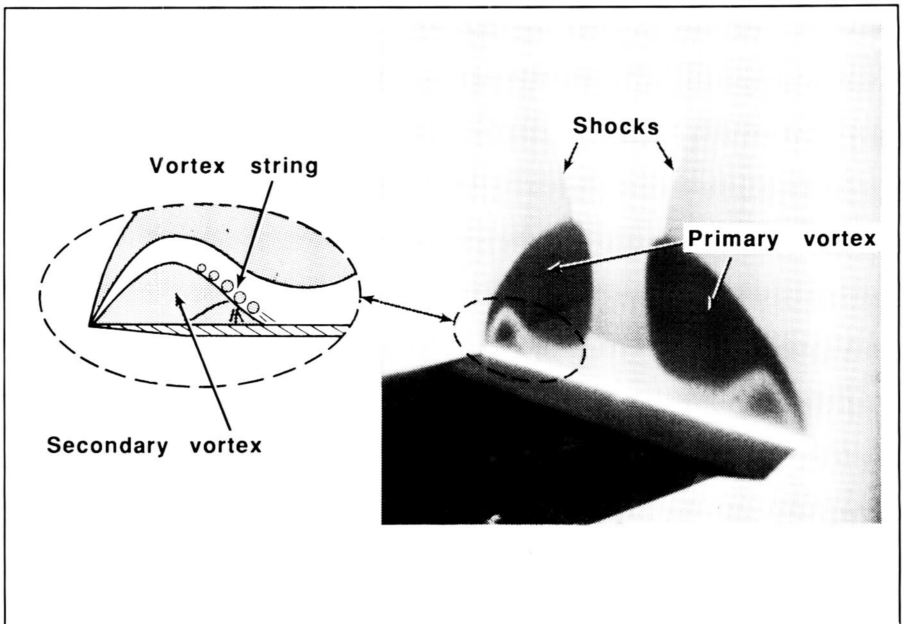

Laser vapor screen visualization of delta wing lee-side flow field.

Improved Vapor Screen Technique for Vortex Flow Field Research

Previous experimental studies have been performed to identify and classify the types of lee-side flow characteristics that occur on uncambered delta wings at supersonic speeds. These studies have utilized the vapor screen flow-visualization technique to obtain photographs of the model flow field. This technique is capable of identifying primary and secondary vortex systems, shocks, and separation regions. The standard vapor screen technique employs a mercury arc lamp/slit arrangement to create the light sheet.

Recently, tests were conducted using a laser to create the light sheet. The highly collimated nature of the laser light permitted a light sheet thickness of approximately 1/8 in. as opposed to a sheet thickness of nearly 1/2 in. for the mercury lamp system. Due to the difference in light sheet thickness, the observed flow field images were much sharper for the laser light sheet. Moreover, additional flow field features that had not been observed for the mercury lamp light sheet were revealed by the laser light sheet.

Results from a 75° sweep delta wing at Mach 2.4 for an angle of attack of 24° indicated a previously unseen string of small vortices located in the shear layer between the primary and secondary vortex. Also, higher order flow structures were observed within the secondary vortex. The additional understanding of the flow field gained through the use of this improved vapor screen technique will prove beneficial in future design and code validation studies.
(P. F. Covell, 45936, W. B. Krieger, D. B. Rhodes, and S. B. Jones)

Evaluation of Leading- and Trailing-Edge Flaps on Flat and Cambered Delta Wings at Supersonic Speeds

An experimental investigation has been conducted to evaluate the effectiveness of leading- and trailing-edge flaps on a flat and cambered wing of identical planform at supersonic speeds. The tests were conducted in Test Section 1 of the UPWT at Mach numbers of 1.6, 1.8, 2.0, and 2.16. The study geometry consisted of a clipped delta planform with an inboard and an outboard leading edge swept back 65° and 50°, respectively, and a trailing edge swept forward 25°. Both wings were configured with identical leading- and trailing-edge flaps and were attached to a generic fuselage.

The experimental results showed that highly complex and three-dimensional flows

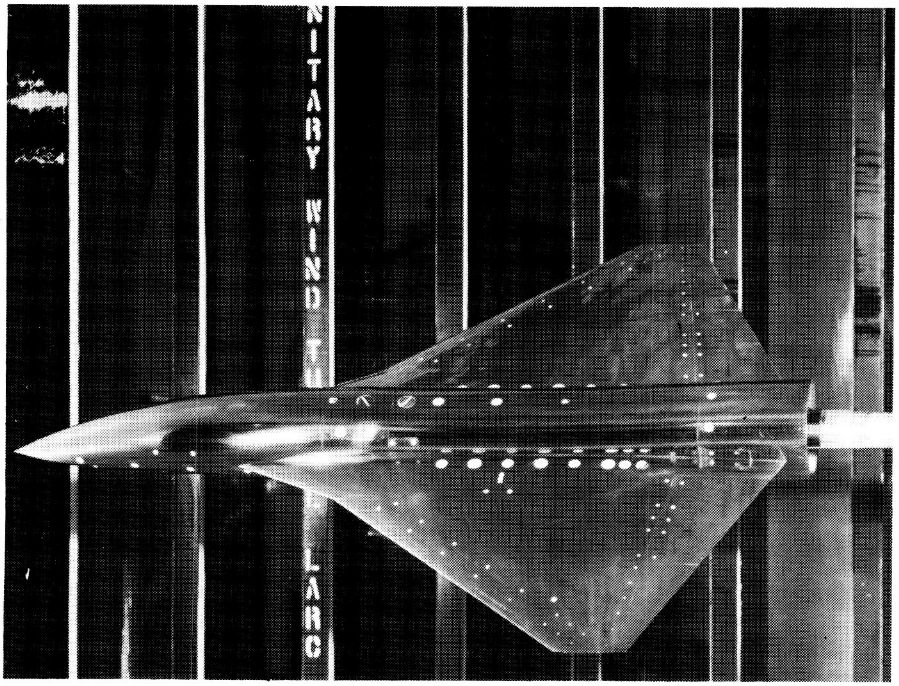

Generic fighter model installed in UPWT. L-88-3629

can occur over the wings with leading- and/or trailing-edge flaps deflected and that flap effectiveness varies significantly between a cambered and flat wing of identical planform and flap geometry. The data also showed that flap effectiveness per degree of flap deflection is highly nonlinear and that the variation in flap effectiveness parameters with Mach number is similar for the flat and the cambered wing.
(G. Hernandez, 45572, R. M. Wood, and R. E. Collins)

Aerodynamic Characteristics of Supersonic Fighter Interceptor Configuration

Tests were conducted on a supersonic fighter/interceptor model, developed by The Boeing Company and the United States Air Force, in Test Section 1 of the UPWT in order to define the aerodynamic characteristics of the vehicle and to validate the various linear and nonlinear theoretical prediction codes. The test Mach numbers were 1.5, 1.75, 2.0, 2.16, 2.36, 2.5, and 2.75 for Reynolds numbers of 1×10^6/ft, 2×10^6/ft, 3×10^6/ft, and 4×10^6/ft. Angles of attack were varied from $-2°$ to $12°$, and sideslip angles were varied from $-5°$ to $5°$. The baseline configuration consisted of a blended wing/body that was designed using a supersonic linear theory code. Surface pressure data were taken to compare with linear and nonlinear theoretical codes. Horizontal and vertical tails and nacelles were also tested on the baseline configuration. Tail and aileron deflections were studied to determine trim conditions of the configuration.

A mass-flow rake was placed at the nacelle exit to determine the mass-flow ratio and the internal drag. Shadowgraph and schlieren photographs were taken to confirm that the inlets were started. Oil-flow visualization photographs were obtained

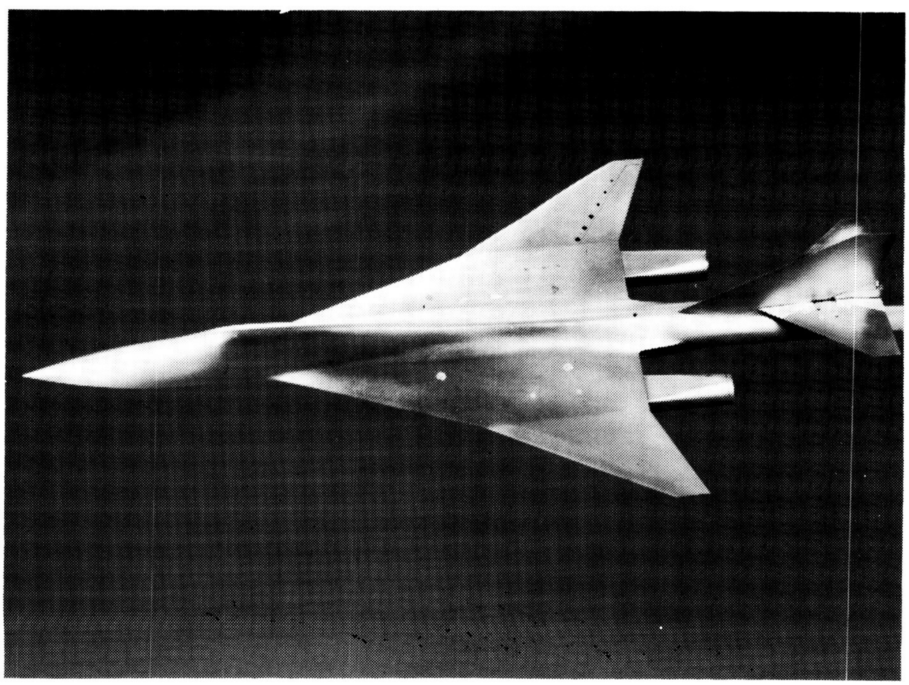

Advanced, blended wing/body configuration. L-88-6091

which showed that the blended wing/body intersection maintained attached flow until high angles of attack were reached. Vapor-screen photographs showed that the canopy on the fuselage shed a vortex that impinged upon the vertical tail at high angles of attack and caused asymmetric loading and directional instabilities of the configuration.
(S. X. S. Bauer, 45946)

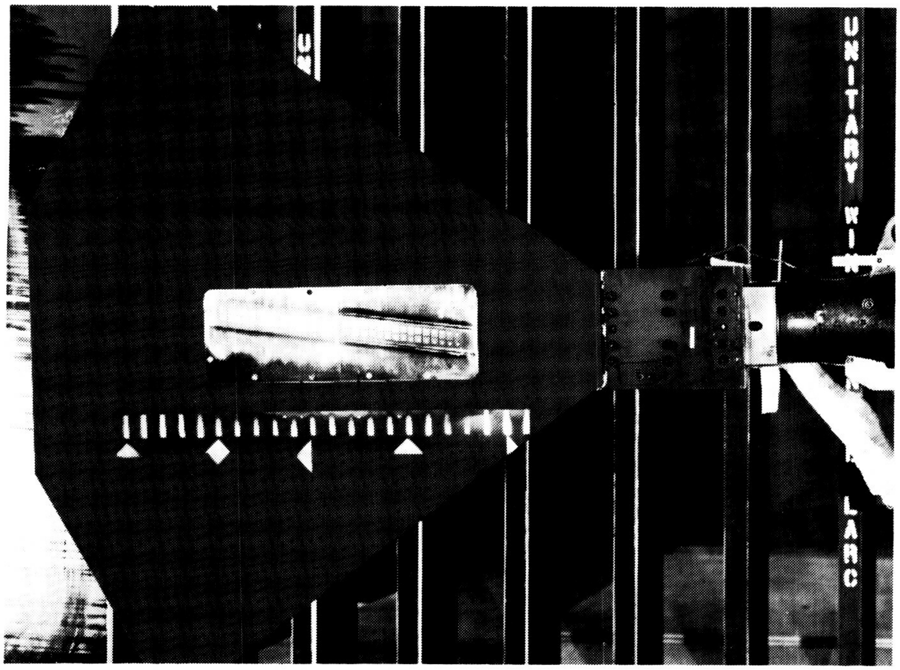

Flat-plate model used for boundary-layer transition studies. L-88-7192

Assessment of Boundary-Layer Transition Measurement Techniques

An experiment that assessed boundary-layer transition detection techniques has been conducted for Mach numbers of 1.5, 2.0, and 2.5 over a range of Reynolds numbers from 1.0×10^6/ft to 4.0×10^6/ft. This assessment was to compare, for the same test model and conditions, the sensitivity and ease of use of liquid crystals, passive infrared video photography, and vapor-deposited thin films. The model used for the experiment was a spatula-shaped flat plate at 0° incidence.

Because the three measurement techniques use different flow properties to detect transition, criteria were established to determine the location of transition. For liquid crystals, the midpoints of the region of fluctuating shear stress were used; for infrared photographs, the locations where the temperature of the insulated plate had increased by 0.1 K were used; and for the thin films, the locations where the intermittency factor reached 0.5 (that is, where the transitioning flow is turbulent 50 percent of the time and laminar 50 percent of the time) were used. Comparisons of the respective transition distances from the leading edge of the plate revealed that the liquid crystals in shear-sensitive mode and the infrared photography both detected transition at locations ahead of those corresponding to the 50 percent intermittency points for all Mach numbers, and that the crystals were more sensitive at the lower Mach numbers. These comparisons also showed that the infrared photography was more sensitive at the high Mach numbers and that the thin films worked well at all Mach numbers and served as the standard with which to compare the other techniques. For ease of use, the liquid crystals ranked first, followed by the infrared photography, and then the thin films.
**(R. M. Hall, 42883,
P. F. Covell, D. L. Carraway,
C. B. Johnson, C. J. Obara,
and R. E. Wright, Jr.)**

Hypersonic Facilities Complex

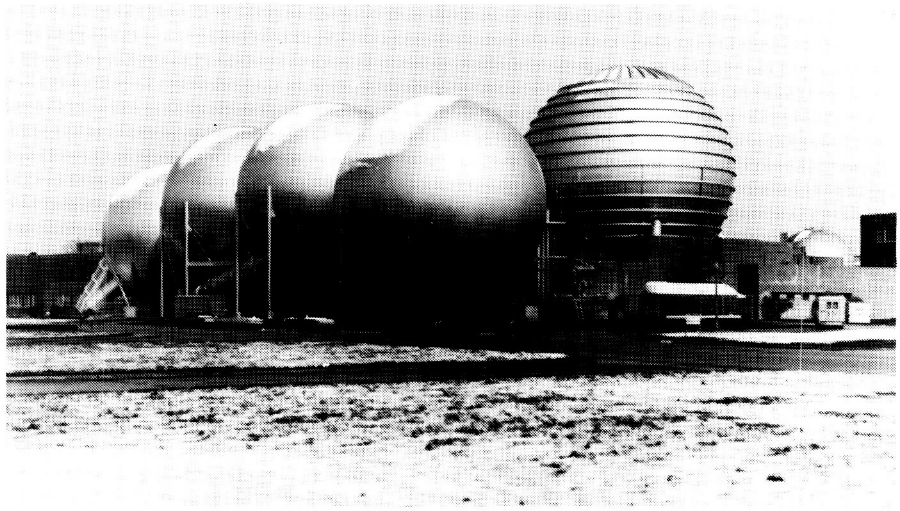

The Hypersonic Facilities Complex consists of several hypersonic wind tunnels located at four Langley Research Center sites. They are considered as a complex because together these facilities represent a major unique national resource for wind tunnel testing. The complex currently includes the Hypersonic CF_4 (tetrafluoromethane) Tunnel ($M = 6$), the Mach 6 High Reynolds Number Tunnel, the 20-Inch Mach 6 Tunnel, the Mach 8 Variable-Density Tunnel, the 31-Inch Mach 10 Tunnel, the Hypersonic Nitrogen Tunnel ($M = 17$), and the Hypersonic Helium Tunnel and its open jet leg ($M = 20$). These facilities are used to study the aerodynamic and aerothermodynamic phenomena associated with advanced space transportation systems, including future orbital-transfer and launch vehicles; to support the development of Aero-Space Plane technology, future planetary entry probes, and hypersonic missiles and transports; and to perform basic fluid mechanics studies, to establish data bases for verification of computer codes, and to develop measurement and testing techniques. A significant amount of the current testing in these facilities is classified, thus restricting the amount and content of test results that can be reported in the open literature.

CF_4 TUNNEL
$M_\infty = 6$ CF_4 $R_\infty = 0.25\text{-}0.55 \times 10^6$

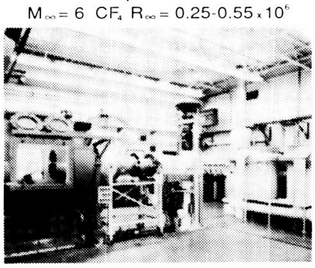

HIGH R_∞ M-6 TUNNEL
$M_\infty = 6$ AIR $R_\infty = 0.8\text{-}42.0 \times 10^6$

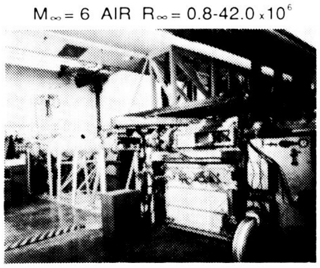

20-INCH M-6 TUNNEL
$M_\infty = 6$ AIR $R_\infty = 0.7\text{-}9.0 \times 10^6$

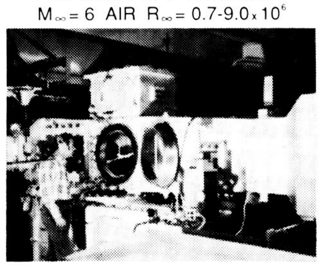

M-8 VAR.-DENS. TUNNEL
$M_\infty = 8$ AIR $R_\infty = 0.1\text{-}10.7 \times 10^6$

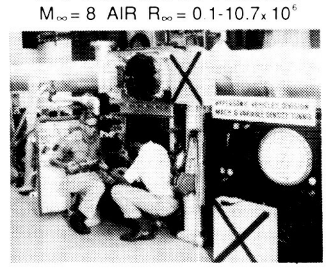

31-INCH M-10 TUNNEL
$M_\infty = 10$ AIR $R_\infty = 0.4\text{-}2.4 \times 10^6$

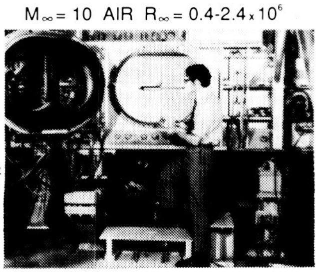

NITROGEN TUNNEL
$M_\infty = 17$ N_2 $R_\infty = 0.35 \times 10^6$

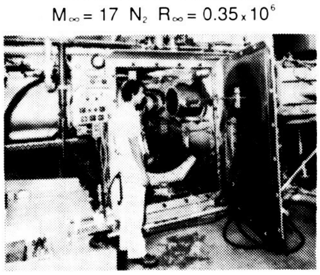

HELIUM TUNNEL
$M_\infty = 19\text{-}21.6$ He $R_\infty = 3.5\text{-}12.5 \times 10^6$

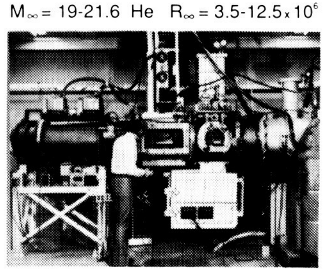

OPEN JET LEG-HE TUNNEL
$M_\infty = 20$ He $R_\infty = 6.0 \times 10^6$

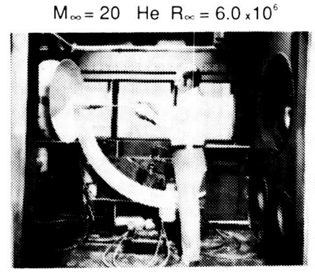

This complex of facilities provides an unparalleled capability at a single installation to study the effects of Mach number, Reynolds number, test gas, and viscous interactions on the hypersonic characteristics of aerospace vehicles. Several modifications are being made to the facilities to improve their reliability and flow quality.

Flow quality in 31-Inch Mach 10 Tunnel.

A recalibration of the 31-Inch Mach 10 Tunnel was necessary after extensive repair to the nozzle throat section. The approach was to use survey rakes to measure detailed lateral and longitudinal pitot pressure and total temperature profiles to determine free-stream flow uniformity and conditions over a range of reservoir pressures. A 4-in.-diameter hemispherical model was employed as a representative blunt model to explore potential blockage effects and to verify the calibration results for a blunt-body configuration. The inviscid test core increased in size from approximately 10 in. by 10 in. to 14 in. by 14 in. as Reynolds number increased from 0.25 × 10^6/ft to 2.5 × 10^6/ft. At a given axial station, the pitot pressure variation across the inviscid test core was less than 3.5 percent. Within ±3 in. of the nozzle centerline (6-in. core), where most models are tested, the pitot pressure variation was less than 1.5 percent. The smallest variations were observed at a reservoir pressure of 350 psia, where pitot pressure variation was less than 2 percent across a 12-in. by 12-in. test core and less than 1 percent in the center 6 in. of the test core.

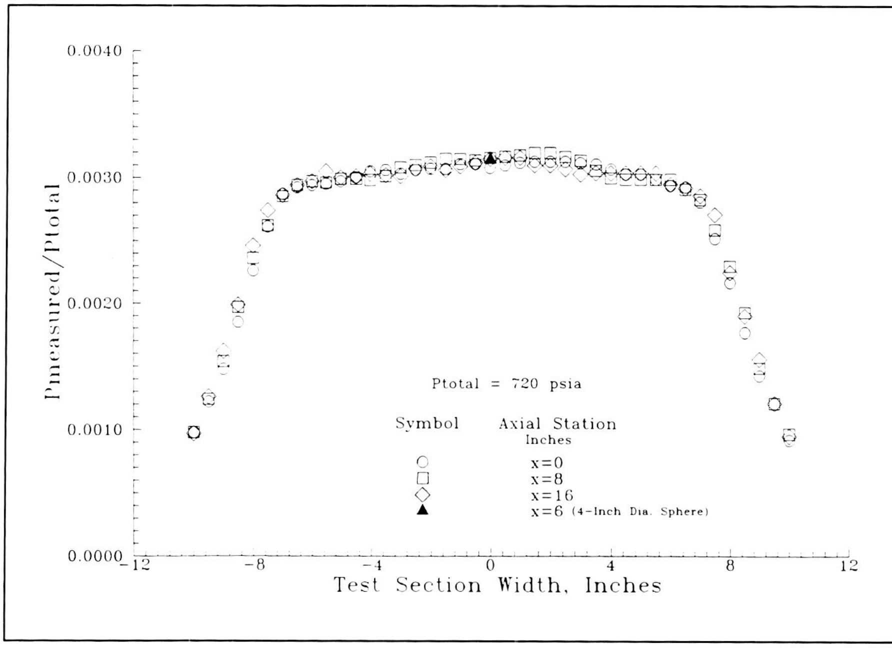

Pitot pressure profile across width of test section.

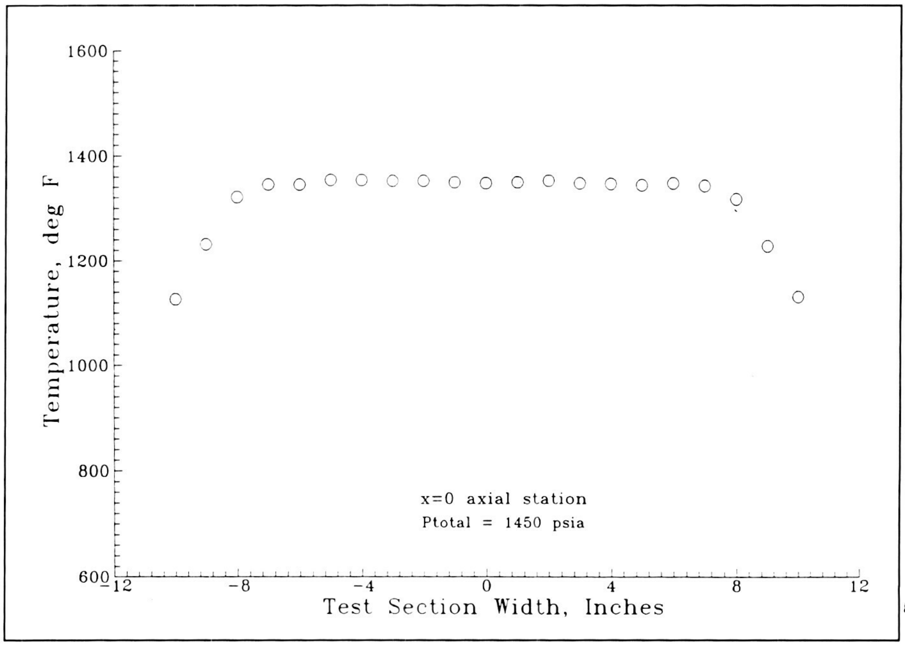

Total temperature profile across width of test section.

Excellent axial flow uniformity is shown in the first figure where the longitudinal variation in pitot pressure (averaged over a 6-in. test core) was less than 2 percent for 16 in. of the test section. Stagnation pressure measurements for the hemispherical pressure model agreed to within ±0.5 percent of the center pitot probe on the rake. This agreement indicates an absence of model blockage effects and verifies the pitot pressure rake results. Total temperature profiles showed

that temperature variation was less than 0.5 percent in the test core for the range of reservoir pressure. These highly uniform total temperature profiles, shown in the second figure, indicate flow symmetry about the test section centerline and substantiate the test core size deduced from the pitot pressure measurements.
(W. F. Hinson, 45231, and T. P. Dye)

Confirmation of low-density flow environment in Hypersonic CF_4 Tunnel.

The Hypersonic CF_4 Tunnel uses tetrafluoromethane (CF_4) as a test gas, which allows a partial simulation of real-gas effects for hypersonic entry vehicle aerodynamic and aerothermodynamic research. The facility is usually operated with a reservoir pressure of approximately 1500 psia, which produces a postshock Reynolds number $R_{e_{2,D}}$ (based on a body diameter) of 33,000. Tests on vehicles that fly at high altitude require a lower density, lower Reynolds number test environment. (An example of a class of high-velocity, high-altitude flight vehicles with blunt configurations is the Aeroassisted Orbital Transfer Vehicle, AOTV.) Recently, the facility has been successfully operated at a reservoir pressure of only 110 psia and a corresponding postshock Reynolds number of 3,000. Computed free-stream quantities in the test section are based on measured temperature and pressure in the reservoir and pitot pressure in the test section.

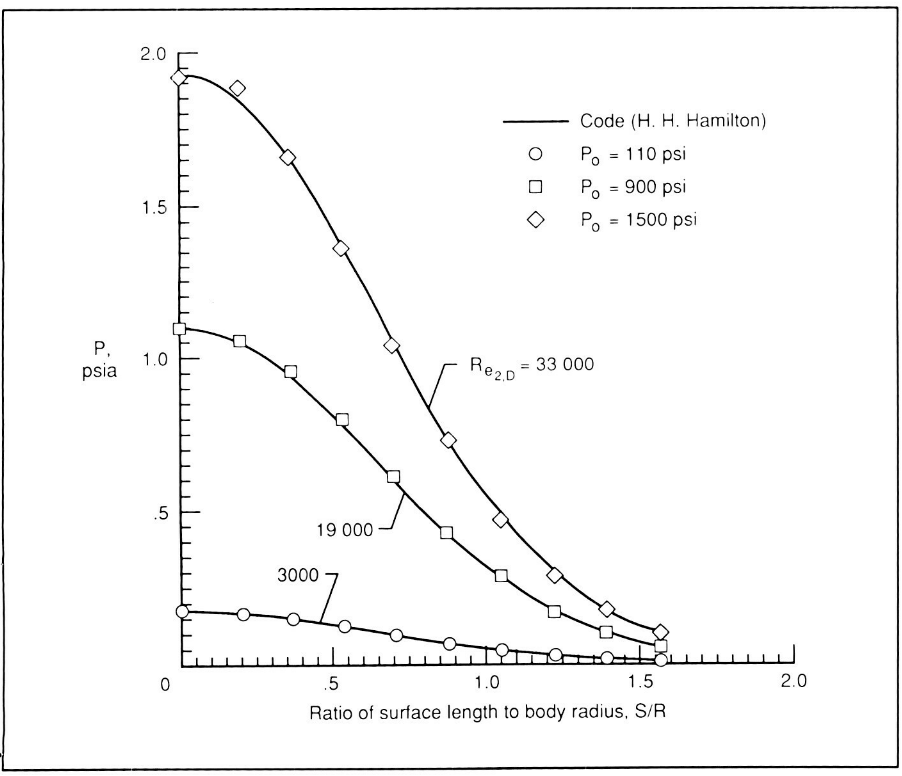

Measured and computed pressure distributions on hemisphere at three reservoir pressures P_o in Hypersonic CF_4 Tunnel. Hemisphere stagnation point is at $S/R = 0$.

As a first step in verifying that equations used to describe the expansion of flow through the nozzle with a reservoir pressure of 1500 psia were still valid at 110 psia, the distribution of pressure over the face of a 1.77-in.-diameter hemisphere was computed with a computer code that utilized CF_4 properties and input quantities that were previously computed (with a different code) for the free stream at both pressures. Pressure distributions over an identical body were measured in the tunnel with operation at both reservoir pressures and compared to the computed distributions. (Measurements and computations were also made at an intermediate reservoir pressure of 900 psia.) Agreement between the computed and measured pressure distributions over the hemisphere indicates that computed test section free-stream quantities are valid in the low-density, low-Reynolds-number environment. Testing of an AOTV configuration in this environment has been scheduled.
(W. L. Wells, 45237, R. E. Midden, and H. H. Senter)

Experimental Investigation of Proposed Lifting-Body Assured Crew Return Capability Vehicle

For the permanently manned Space Station *Freedom*, NASA is considering the use of one or more crew return vehicles docked at the structure. These vehicles must provide speedy, dependable return of the astronauts to Earth in the event of an accident or crew emergency and will be a safeguard to the assured crew

return capability (ACRC). The detailed mission requirements of such a vehicle have not yet been finalized, but configurations varying from ballistic shapes to winged reentry vehicles are under study. One of the concepts proposed by Langley Research Center is a lifting-body shape that produces moderate lift-to-drag values over the speed range; this concept provides some crossrange performance and offers the possibility of a conventional landing.

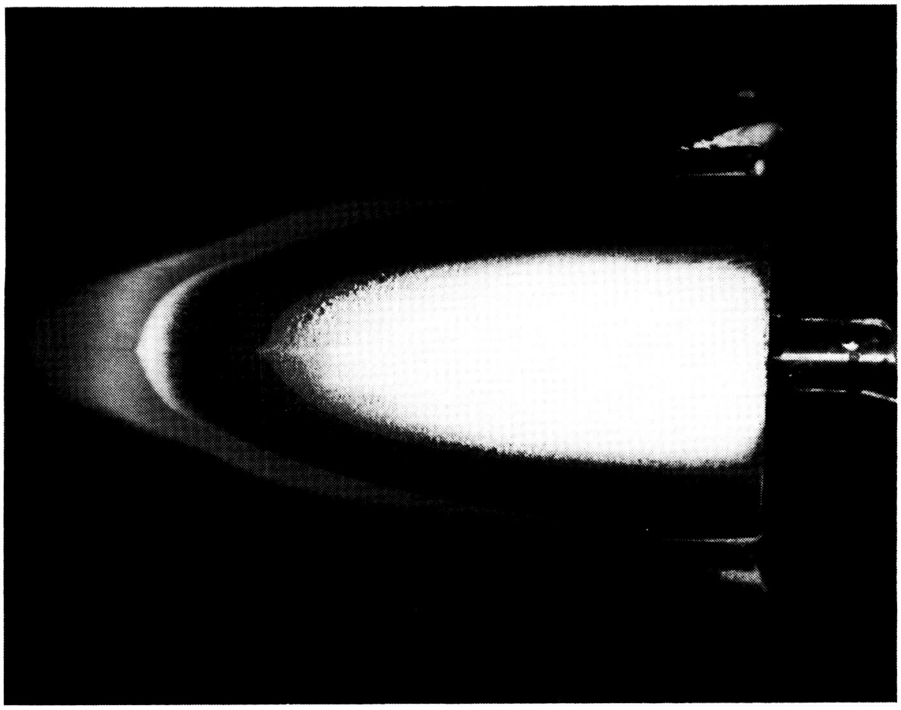

Thermal mapping pattern on ACRC lifting-body concept with unit Reynolds number of 0.5 × 10^6/ft, Mach number of 10, and angle of attack of 20°.

Development of an aerodynamic and aerothermodynamic data base for the lifting-body concept has been initiated at Langley Research Center. This data base will provide a better understanding of the vehicle performance across the speed range and will identify areas of high heating on the vehicle. The data base includes forces and moments, surface thermal mapping patterns, and surface streamline patterns.

Tests have been performed in the 31-Inch Mach 10 Tunnel using the phase-change paint technique to identify areas of concentrated heating. The lifting-body concept was tested over an angle-of-attack range from 0° to 45° and unit Reynolds numbers of 0.5 × 10^6/ft and 2.0 × 10^6/ft. The effects of angle of attack and Reynolds number on thermal mapping patterns were examined. Preliminary results indicate significant leeward heating over the canopy and streak heating on the fuselage sides. As expected, heating over the canopy decreases with increasing angle of attack or effective leeward shadowing; however, fuselage streak heating remains for all angles of attack. For this factor-of-4 increase in unit Reynolds number, no Reynolds number effect on thermal mapping patterns was noted.

(J. R. Micol, 45250, and T. Horvath)

Measured Heating Rates in Wake of AOTV

Flow in the near wake of an aeroassisted orbital transfer vehicle (AOTV) drag brake configuration is of interest because it converges in the potential location of a payload. The chief concern is that heating of the payload could result from impingement of the high-temperature shear layer that separates off the shoulder around the entire periphery of the aerobrake and tends to converge in the near wake. The magnitude and distribution of this impingement heating on a simulated payload (a cylinder) were recently measured in the 31-Inch Mach 10 Tunnel. The measurements were made with thin-film heat-transfer gauges in the wake of the Aeroassist Flight Experiment (AFE) drag brake configuration. Measurements were made along the length of the cylinder in four different planes with 45° separation. The tests were conducted at angles of attack from −10° to +5°.

Heating was greatest at the shear-layer impingement point in the aerobrake upper symmetry plane, decreased rapidly forward of that point (toward the aerobrake base), but remained relatively high downstream of that point. For example, at an angle of attack of 0° (the AFE nominal flight value), the heating at the impingement point was approximately 35 percent of the aero-

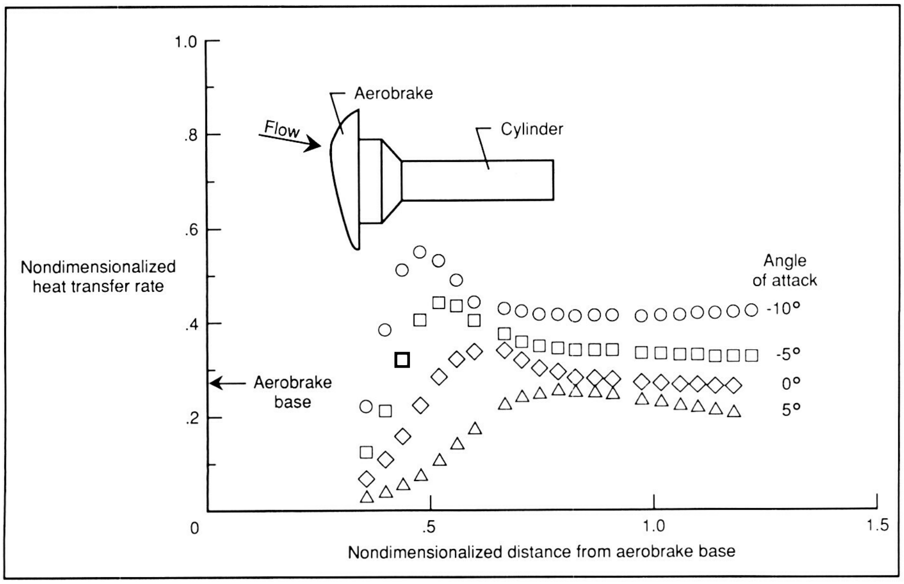

Measured heating distributions on cylinder in wake of AFE aerobrake in air at M_∞ of 10 and unit R_e of 0.25×10^6.

brake stagnation point heating; this heating decreased to approximately 25 percent toward the downstream end.

(W. L. Wells, 45237)

NASA/ONERA Cooperative Study: Aerodynamic Tests at Mach 6

Aerodynamic tests at Mach 6 were completed in support of an agreement with the French Aerospace Research Organization ONERA (Office National d'Etudes et de Recherches Aerospatiales) to test the same model in NASA and ONERA hypersonic wind tunnels. The purpose has been to compare the data and test techniques used by both organizations for aerodynamic and aerothermodynamic testing. The configuration used was a generic, winged reentry vehicle consisting of a nose section faired into a flat-sided fuselage, wings of a similar airfoil section as those on the United States Space Shuttle, and wedge-shaped tip fins. Tests were required to include Mach numbers of 6 and 10 in air and Reynolds numbers from 0.5×10^6/ft to 7.6×10^6/ft.

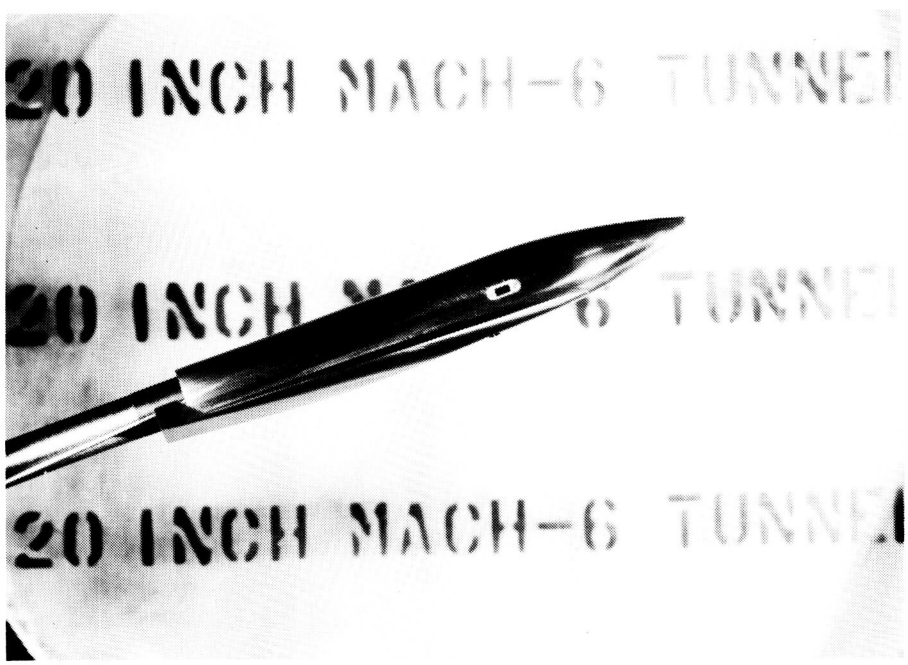

Winged reentry configuration installed in 20-Inch Mach 6 Tunnel.

L-88-12817

Force and moment tests were made in the 20-Inch Mach 6 Tunnel. Data were taken through an angle-of-attack range from −2° to 45° and at Reynolds numbers of 0.5×10^6/ft and 7.6×10^6/ft. No effects of control surface deflections were studied. A maximum lift-to-drag ratio of 3.2 was achieved at an angle of attack of 10°. The vehicle was trimmed at an angle of attack of 18° with no control surface deflections and with a lift-to-drag ratio of 2.5. No significant effects due to Reynolds number were seen other than an increase in drag.

(G. J. Brauckmann, 45234)

Comparisons of Measured and Predicted Pressure and Heat Transfer Distributions for AFE Vehicle

An extensive hypersonic aerodynamic/aerothermodynamic data base for the Aeroassist Flight Experiment (AFE) vehicle has been initiated at Langley Research Center. This data base will be used to calibrate computational fluid dynamics codes over a wide range of hypersonic continuum-flow conditions and will include forces and moments, pressures, and heating distributions measured over the forebody and in the wake region of the AFE. The experimental results and comparisons with predictions are expected to be of great interest to the designers of the AFE aeroshell and to the principal investigators of the various onboard experiments.

Tests were recently performed in the 31-Inch Mach 10 Tunnel to measure pressure distributions and heat-transfer rates over the forebody of 2.2-percent scale (3.67-in.-diameter) models of the AFE vehicle over an angle-of-attack α range from −10° to 10°. The effects of angle of attack and Reynolds number were examined on these measured quantities, and comparisons were made with modified Newtonian theory, an inviscid flow field code known as HALIS (High Alpha Inviscid Solution), and a Navier-Stokes solver referred to as LAURA (Langley Aerothermodynamic Upwind Relaxation Algorithm).

Results indicate a negligible effect of Reynolds number on forebody pressures and heating rates. The effect of angle of attack on pressure distributions indicated a slight overexpansion of the flow from the ellipsoid nose onto the cone at the lowest angle. Varying angle of attack over the range from 10° to −10° produced a movement of the stagnation region up and around the nose and onto the skirt; this movement resulted in an increase in heat-transfer rate at the corner. Pressure distributions predicted with HALIS and LAURA were in good agreement with measurements, whereas those predicted with the modified Newtonian theory (from which the original parametrics of the configuration were designed) were in good agreement over the vehicle nose, but in poor agreement over the cone section. Heat transfer rates predicted with the LAURA code were slightly lower than measured values in the stagnation region but showed better agreement over the cone section.

(J. R. Micol, 45250)

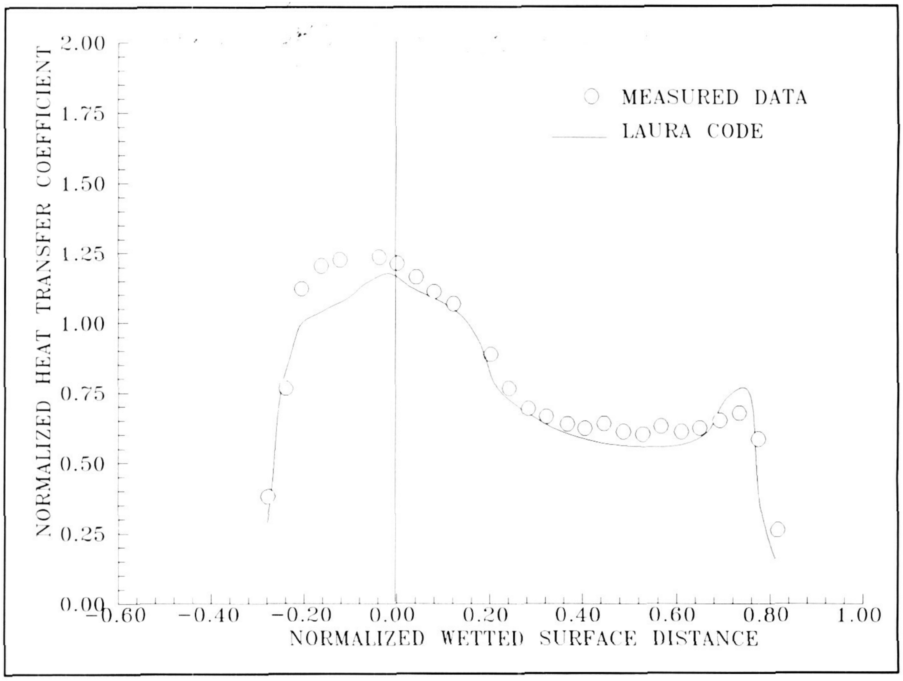

Comparison of experimental and predicted heat transfer distributions in air at Mach number of 10, unit R_e of 0.5 × 10^6/ft, and α of 0°.

Aerodynamic Characteristics of Systematic Series of Irregular Planform Wings at M = 10

Tests have been made in the 31-Inch Mach 10 Tunnel on a systematic series of irregular planform wings. For this study, the planforms were referred to as wing-fillet combinations with the inboard, more highly swept portion of the planform being defined as a fillet. The early phase of the study was directed toward improving the aerodynamics of the Space Shuttle orbiter, although the general long-range goals are applicable toward improved design of aircraft as well as certain advanced aerospace vehicles.

ORIGINAL PAGE
BLACK AND WHITE PHOTOGRAPH

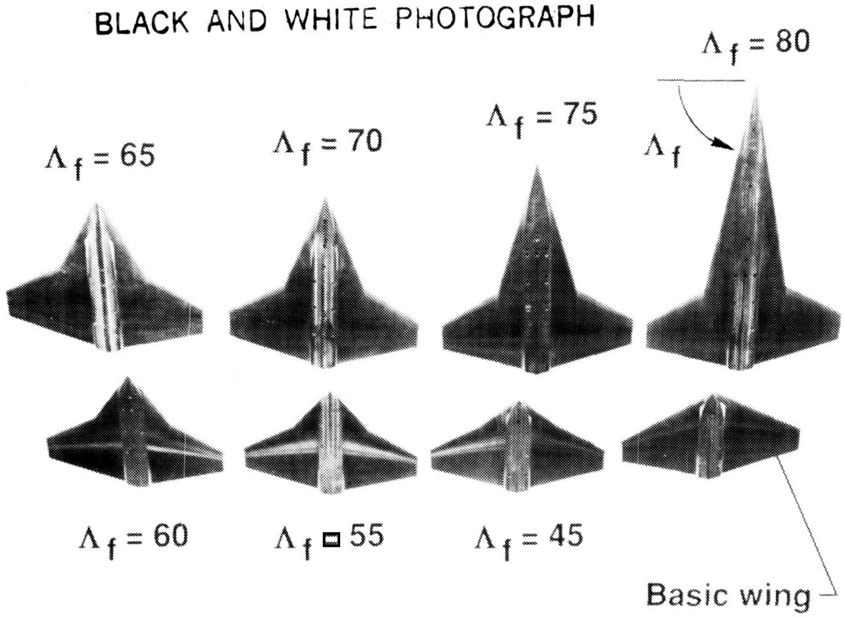

Basic 35° swept wing in combination with various fillets Λ_f. L-89-2137

The present series consisted of five basic planform shapes of constant area and aspect ratio; the variables included leading- and trailing-edge sweep. The basic wings had leading-edge sweeps of 25°, 35°, 45°, 53°, and 60°. The irregular planforms were formed by extensions to the basic wings in 5° or 10° increments up to a maximum of 80°. Also included for the 45° wing series were the effects of wing thickness ratio. The angles of attack ranged from approximately −4° to 56°; this range was sufficient to cover the angles for maximum lift-to-drag ratio L/D_{max} (for maximum glide crossrange) and maximum lift coefficient $C_{L,max}$ (for minimized aero-heating) at 0° of sideslip. Results of this investigation indicate that the addition of fillets resulted in increases in L/D_{max} primarily by reducing the minimum drag coefficient $C_{D,min}$ with large increases in $C_{L,max}$ for each wing. Increasing the wing thickness ratio resulted in large reductions in L/D_{max}, a small reduction in the value of $C_{L,max}$, and little or no effect on the center of pressure location as a function of angle of attack, for a given wing.

(B. Spencer, Jr., 45245)

Hypersonic Investigation of 5° Winged-Cone Configuration

One proposed generic transatmospheric vehicle (TAV) concept will utilize a large number of annularly arranged airbreathing engines to accelerate the vehicle into low-Earth orbit. The present configuration, which represents this vehicle type without

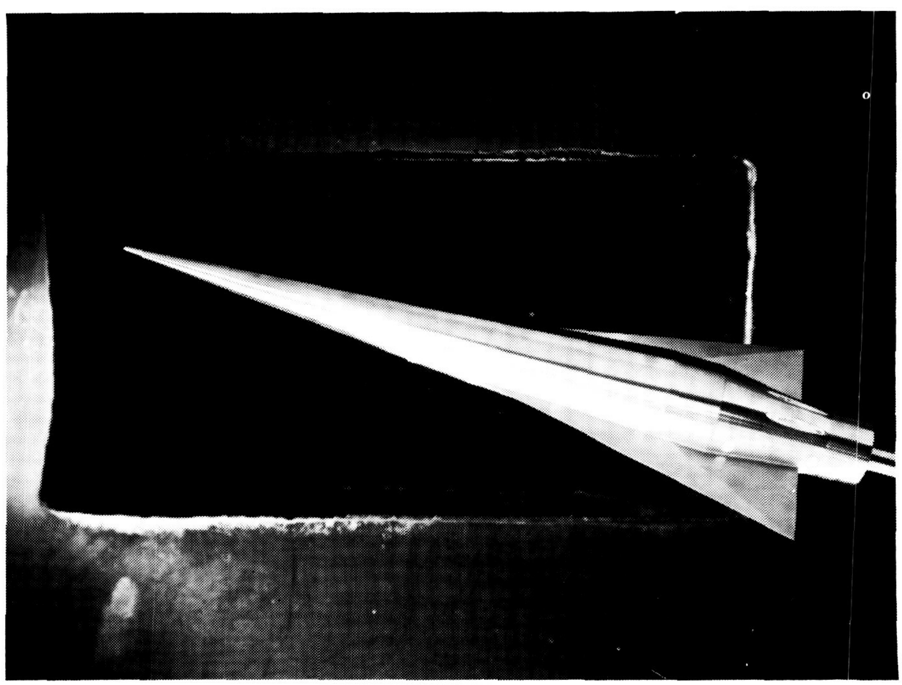

5° winged-cone model mounted in Hypersonic Helium Tunnel. L-88-8646

engines, was tested to provide data to validate computational fluid dynamic codes that will be required for predictive aerodynamic analyses of TAV concepts. The configuration incorporates a 5° conical fuselage forebody, a wing with an aspect ratio of 1.0, and a truncated cone/cylinder afterbody. Longitudinal aerodynamic investigations were made in the 20-Inch Mach 6 Tunnel and the Hypersonic Helium Tunnel (Mach 20) at angles of attack from −4° to 20°.

Test Reynolds numbers based on fuselage length ranged from 3.5×10^6 to 5.0×10^6 in the 20-Inch Mach 6 Tunnel and from 3.1×10^6 to 23.0×10^6 in the Hypersonic Helium Tunnel. Aerodynamic effects of nose bluntness, wing longitudinal position, and wing incidence were determined during these studies. These data obtained for the 5° winged-cone configuration provide the experimental hypersonic aerodynamic characteristics for Langley Research Center studies of the accelerator TAV concept that will encompass the flight Mach number range.
(W. P. Phillips, 45239)

ORIGINAL PAGE
BLACK AND WHITE PHOTOGRAPH

Scramjet Test Complex

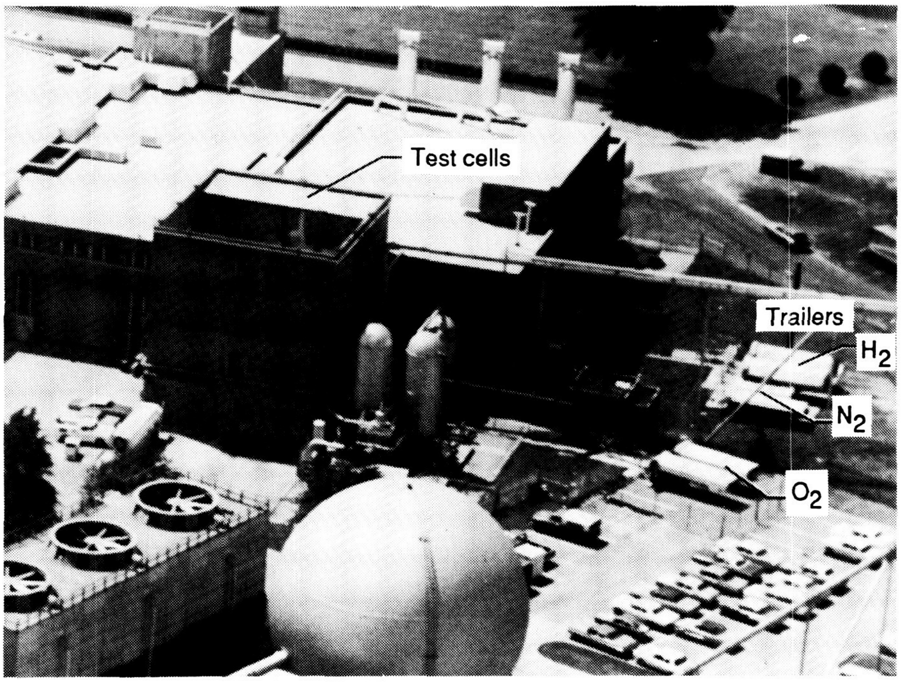

After an almost 15-year lull in interest for hypersonic flight, there is again a strong emphasis on the potential for a number of applications. These applications include an Aero-Space Plane or transatmospheric vehicle, which would be able to take off from a conventional runway and fly to orbit, as well as a variety of hypersonic airplane concepts for military reconnaissance, strike, or semiglobal transports. Langley Research Center has maintained a research team that has been working on basic hypersonics continuously throughout the last several decades. Facilities that played a key role at Langley in developing the present Space Shuttle configuration have been applied to a wide variety of other aerospace vehicles. Langley, the lead Center in defining Shuttle II, has been the only research organization in the Nation to continuously maintain a viable effort in hydrogen-fueled supersonic combustion ramjet propulsion since the 1960's. Ground tests of subscale engines conducted in the Scramjet Test Complex have demonstrated levels of net thrust sufficient to accelerate at Mach 4 and to cruise an airplane at speeds up to Mach 8 and beyond. These results are entirely consistent with the projection of attractive performance up to much higher speeds, even approaching orbital velocity.

A research program to develop technology for a hydrogen-burning airframe-integrated supersonic combustion ramjet (scramjet) propulsion system has been under way for several years at Langley. The experimental portion of this research consists of tests of engine components (inlets, combustors, and nozzles) and complete, component integration engine models.

Small-scale inlet tests for "screening" potential inlet designs are performed in a 9-in. by 9-in. Mach 4 blowdown tunnel. Larger scale inlet tests are performed in various other Langley aerodynamic wind tunnels. Small-scale direct-connect combustor tests that simulate a portion of the engine combustor are conducted in Test Cell #2 to provide basic research data on supersonic mixing, ignition, and combustion processes. The hot test gas is supplied to the combustor models by a hydrogen-air-oxygen combustion heater, which maintains 21-percent free oxygen by volume to simulate air with enthalpy levels ranging up to Mach 8 flight speeds. Various facility nozzles produce the desired combustor entrance flow conditions.

Designs from the individual component tests are assembled to form component integration engines so that tests can be conducted to understand any interactions between the various engine components and to determine the overall engine performance. These component integration tests are conducted in engine test facilities. The feature that separates these propulsion facilities from aerodynamic wind tunnels is their capability

Small-Scale Inlet Tests

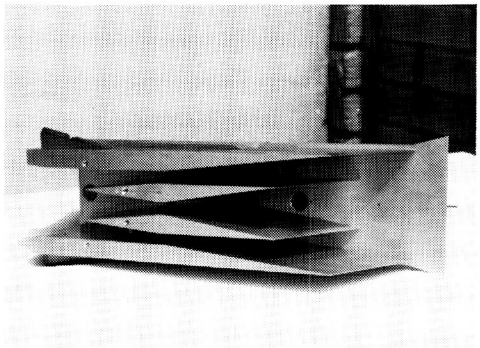

Inlet Model

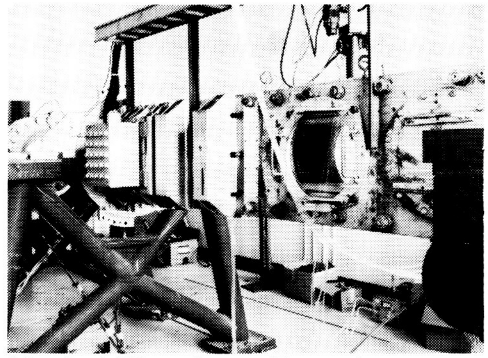

Mach 4 Blowdown Tunnel

Small-Scale Combustor Tests

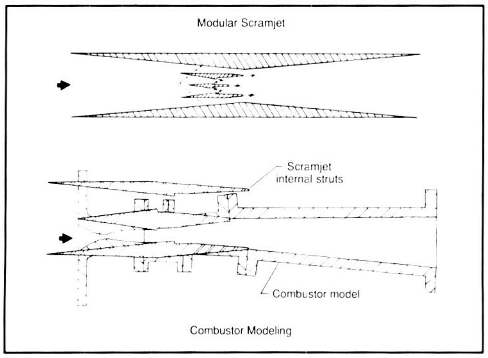

Combustor Modeling

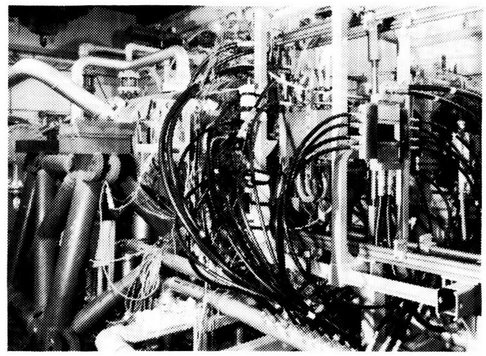

Test Cell #2

Engine Model Tests

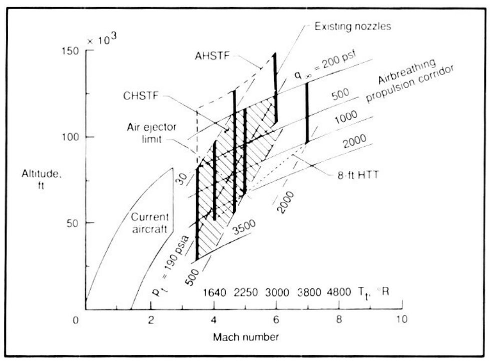

Potential Test Capability

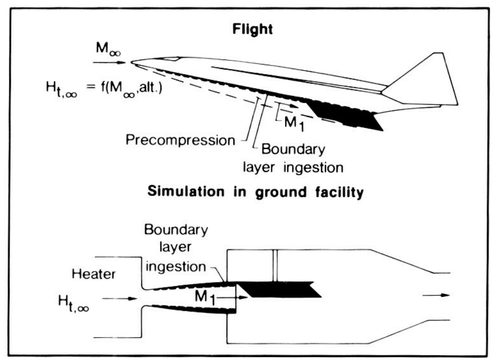

Flight Condition Simulation

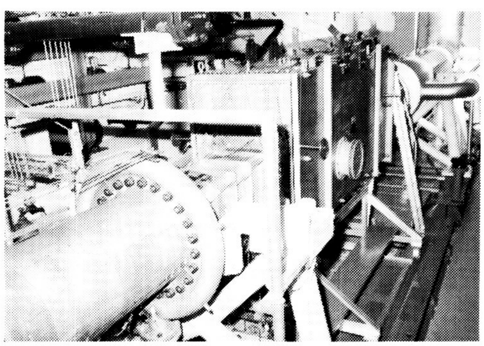

CHSTF; Test Cell #1

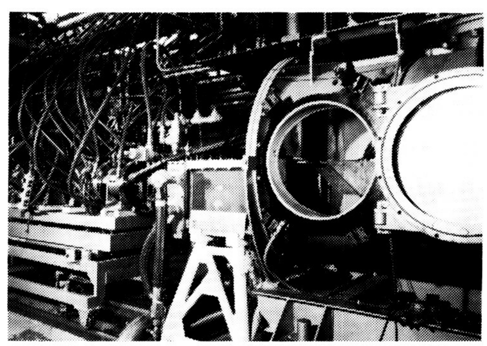

AHSTF

to produce true-velocity, true-temperature, and true-pressure flow for flight simulation.

The Combustion-Heated Scramjet Test Facility (CHSTF, Test Cell #1) uses a hydrogen-air-oxygen combustion heater to duplicate Mach 4 flight enthalpy. The test gas is exhausted to the atmosphere with the aid of an air ejector. A Mach 3.5 contoured nozzle with a 13-in.-square exit is presently attached to the heater to yield a free-jet tunnel flow (simulating Mach 4 flight conditions) for subscale engine tests. The Arc-Heated Scramjet Test Facility (AHSTF, Test Cell #2) uses an electric-arc heater to produce enthalpy levels corresponding to flight speeds up to Mach 8. The tunnel exhausts into a 100-ft-diameter vacuum sphere. Eleven-in.-square exit nozzles (Mach 4.7 and 6) are used to deliver a free-jet tunnel flow for scramjet engine tests. The same size models (frontal view approximately 6 in. by 8 in.) are tested in both these facilities.

In 1989, an oxygen replenishment system and new facility nozzles will be added to the 8-Foot High-Temperature Tunnel (8-Foot HTT), which is presently part of the Aerothermal Loads Complex. This tunnel will then be capable of testing large-scale engines (about 20 in. by 28 in.), multiple engines, or engines that have full nozzle expansion surfaces at Mach numbers of 4, 5, and 7. In addition, the operational capability of the Combustion-Heated Scramjet Test Facility is being enhanced by a new test gas heater, a new Mach 4.7 nozzle, and a new vacuum sphere/steam ejector system. Upon completion of these modifications, the 8-Foot HTT, together with the smaller scale facilities described, will comprise a Scramjet Test Complex at Langley unequaled in the Western World. The potential operational envelope of this complex would extend over a flight Mach number range from 3.5 up to 7. Some of the current testing in these facilities is classified, thus restricting the amount and content of test results that can be reported in the open literature.

CARS optical system in NDL facility. L-85-5639

Considered part of the Scramjet Test Complex is a Nonintrusive Diagnostics Laboratory (NDL), which contains the Coherent Antistokes Raman Spectroscopy (CARS) optical system and laboratory scale combustion devices used for fundamental combustion studies. Four devices that include an electronically heated furnace and three hydrogen-air combustion devices (a subsonic diffusion burner, a supersonic diffusion burner, and a premixed flat flame burner) provide an air temperature range from 300 K to 2200 K and a velocity range from air at rest to Mach 2 for study. Nonintrusive simultaneous measurements of temperature, nitrogen, and oxygen density have been made with the CARS system. The laboratory facility, shown in the figure above, provides space for the various development versions of the CARS optical system and facilities for handling air, hydrogen, and oxygen at high pressure as well as an exhaust duct for the burner products. Computer facilities are adjacent to the laboratory for burner control and data collection and processing. A new CARS system, configured to endure the harsh environment (>150 acoustic dB), is being assembled for use in Test Cell #2.

Measurements of Temperature and Density in Supersonic Reacting Flow for CFD Code Validation

To validate computational fluid dynamics (CFD) codes for supersonic reacting flows, a laboratory scale supersonic burner (SSB) has been constructed and installed in the CARS Laboratory at Langley Research Center. The SSB is an axisymmetric device (shown in the first figure) which produces a hot, Mach 2 flow of vitiated air with centerline injection of hydrogen at the exit plane. Measurements of temperature and nitrogen density have been made in the supersonic exhaust of the SSB using the laser system. These data have been collected to provide a data base for comparison with the results of CFD calculations for the supersonic reacting flow.

In the second figure, temperature and nitrogen density data are compared to CFD results. The lines represent the CFD calculations in the top four plots; in the bottom plot for the exit plane, the lines represent the CFD starting conditions. The circles are the average of 100 laser samples collected at each point. Good agreement is observed between CARS and CFD results.

(O. Jarrett, Jr., 46320, A. D. Cutler, R. R. Antcliff, and T. Chitsomboon)

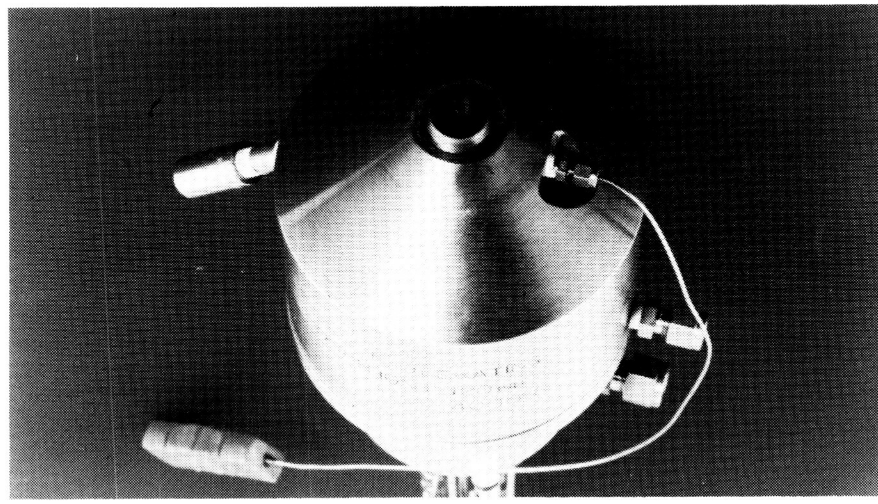

Supersonic combustor. L-85-11189

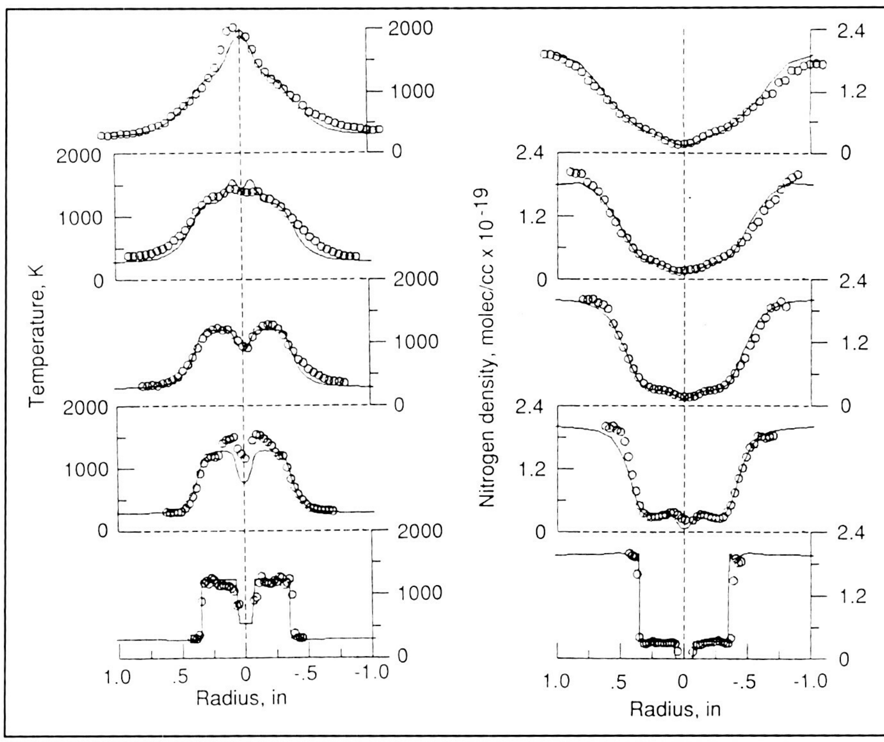

CARS temperature and nitrogen measurements compared to CFD results (bottom plot is exit plane and CFD starting conditions of supersonic burner flow; top four plots are at 1-in. increments from exit).

ORIGINAL PAGE
BLACK AND WHITE PHOTOGRAPH

Aerothermal Loads Complex

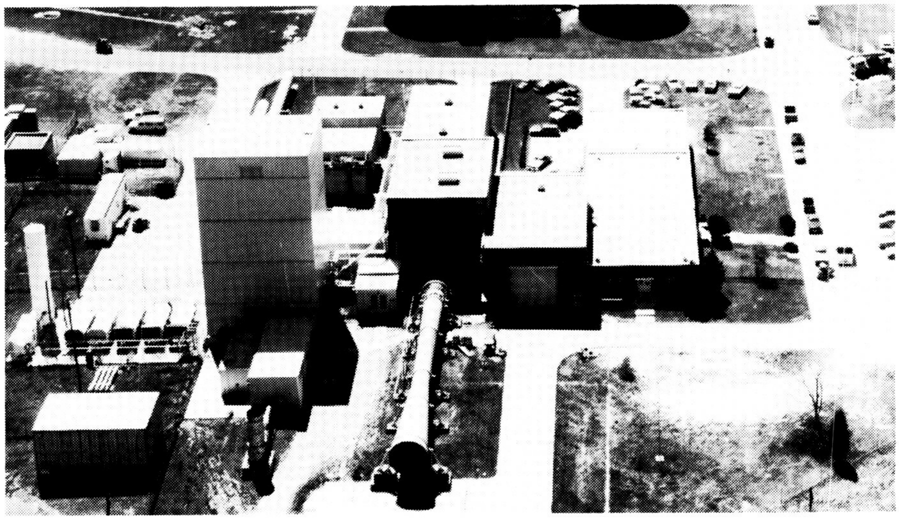

The Aerothermal Loads Complex consists of four facilities that are used to carry out research in aerothermal loads and high-temperature structures and thermal protection systems. The 8-Foot High-Temperature Tunnel (8-Foot HTT) is a Mach 7 blowdown-type facility in which methane is burned in air under pressure and the resulting combustion products are used as the test medium with a maximum stagnation temperature near 3800° R in order to reach the required energy level for flight simulation. The nozzle is an axisymmetrical conical contoured design with an exit diameter of 8 ft. Model mounting is semispan or sting with insertion after the tunnel is started. A single-stage air ejector is used as a downstream pump to permit low-pressure (high-altitude) simulation. The Reynolds number ranges from 0.3 to 2.2 × 10^6/ft with a nominal Mach number of 7, and the run time ranges from 20 s to 180 s. The tunnel is used

8-FOOT HIGH-TEMPERATURE TUNNEL
M = 7 R = 0.3 - 2.2 x 10^6
H = 700 - 1000 BTU/lb

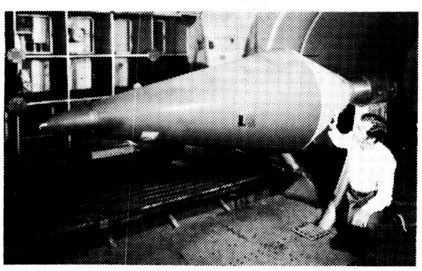

7-INCH HIGH-TEMPERATURE TUNNEL
M = 7 R = 0.3 - 2.2 x 10^6
H = 700 - 1000 BTU/lb

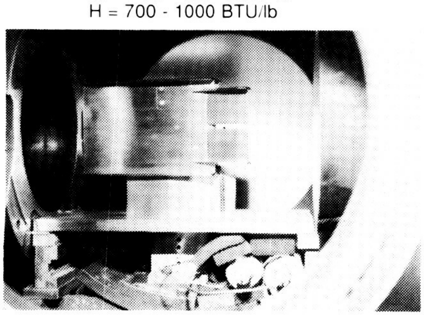

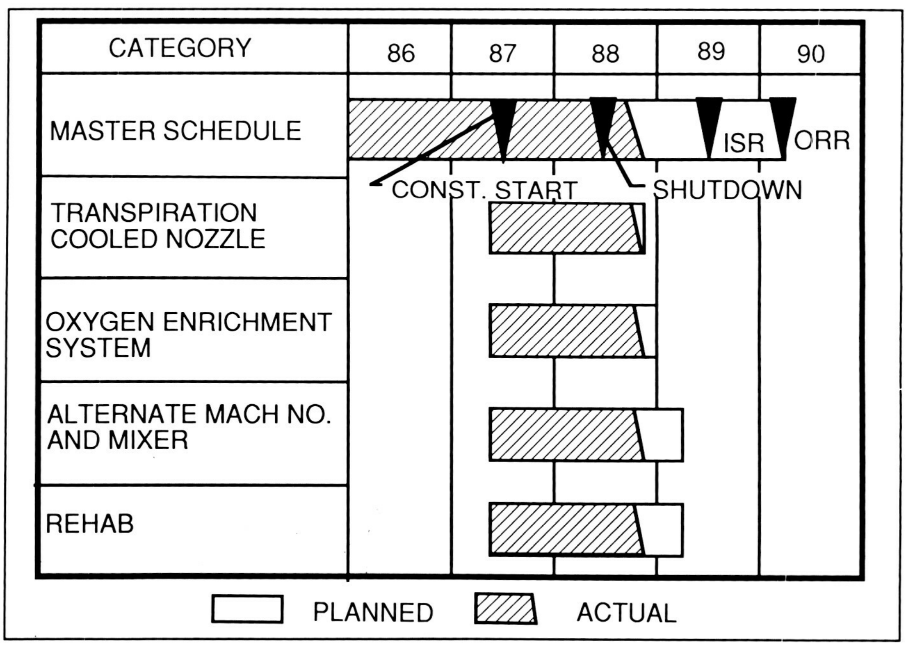

8-Foot HTT modification project schedule; ISR is integrated systems review; ORR is operational readiness review.

for studying detailed thermal-loads flow phenomena as well as for evaluating the performance of high-speed and entry vehicle structural components. A major effort is under way to provide alternate Mach number capability as well as O_2 enrichment for the test medium. This is being done primarily to allow models that have hypersonic airbreathing propulsion applications to be tested.

The 7-Inch High-Temperature Tunnel (7-Inch HTT) is a 1/12-scale version of the 8-Foot HTT with basically the same capabilities as the larger tunnel. It is used primarily as an aid in the design of larger models for the 8-Foot HTT and for aerothermal loads tests on subscale models. The 7-Inch HTT is currently being used to evaluate various new systems for the planned modifications of the 8-Foot HTT.

The 20-MW and 5-MW Aerothermal Arc Tunnels are used to test models in an environment that simulates the flight reentry envelope for high-speed vehicles such as the Space Shuttle. The amount of energy available to the test medium in these facilities is 9 MW and 2 MW, respectively. The 5-MW is a three-phase ac arc heater and the 20-MW is a dc arc heater. Test conditions such as temperature, flow rate, and enthalpy vary greatly because a variety of nozzles and throats are available and model sizes can range from 3 in. in diameter to 1-ft by 2-ft panels. These facilities are currently on standby status.

Fluctuating pressure loads under hypersonic boundary layer.

High-frequency fluctuating pressure loads are an important consideration on supersonic and hypersonic flight vehicles. These loads must be ascertained experimentally with instrumentation capable of withstanding the adverse environment associated with such flows. To aid in this measurement technology development, an experiment was conducted on a flat-plate, boundary-layer survey model in the 8-Foot HTT to measure surface pressure fluctuations underneath a hypersonic boundary-layer flow. A 6-in.-square, water-cooled insert was instrumented with an array of piezoresistive sensors (0.093 in. diameter) and installed in a 107-in. by 51-in. boundary-layer survey model shown in the figure. The model was then inserted into a Mach 4.6, 2840°F total-temperature flow. Data were taken for 4 s at a sampling rate of 125 kHz and stored on a hard disk for posttest analysis.

Power spectrum levels of the fluctuating pressures over the frequency range from 100 Hz to 40 kHz varied from approximately 128 dB at the low frequencies down to 100 dB at the high frequencies for the test conditions stated. Except for the low-frequency range up to approximately 3 kHz, the spectrum falls off exponentially with frequency. The total spectrum level, obtained by integrating under the spectrum curve, is approximately 147 dB. The completion of this experiment demonstrates the ability to measure high-frequency loads in a high-temperature, high-speed flow environment. Particular elements of concern were sensor installation, data acquisition, and calibration. This measurement capability is essential in defining fluctuating pressure loads on high-speed vehicles.

(T. L. Parrott, 45273, and C. W. Albertson)

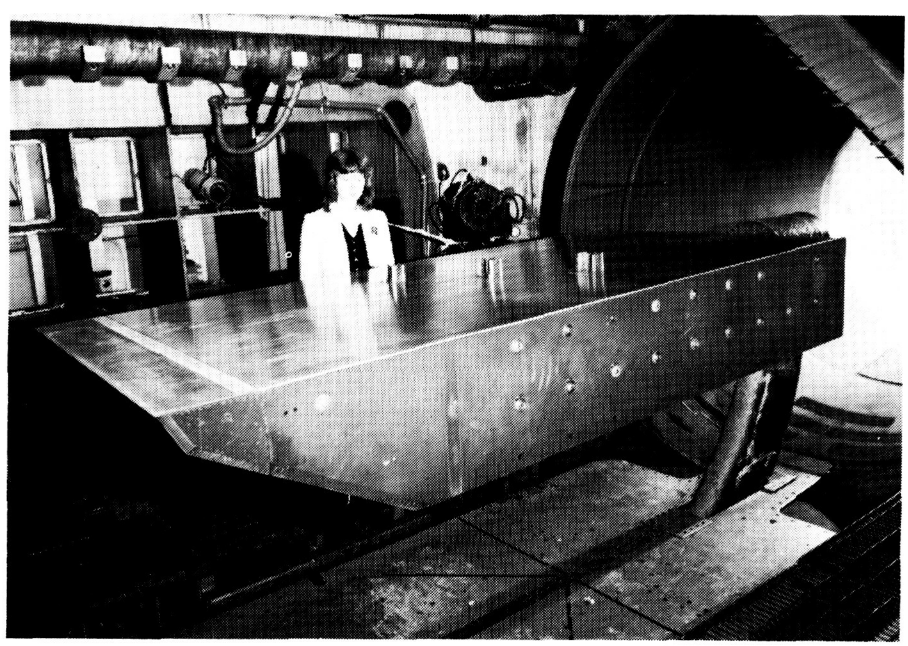

Model used in investigation of hypersonic fluctuating loads. L-88-3992

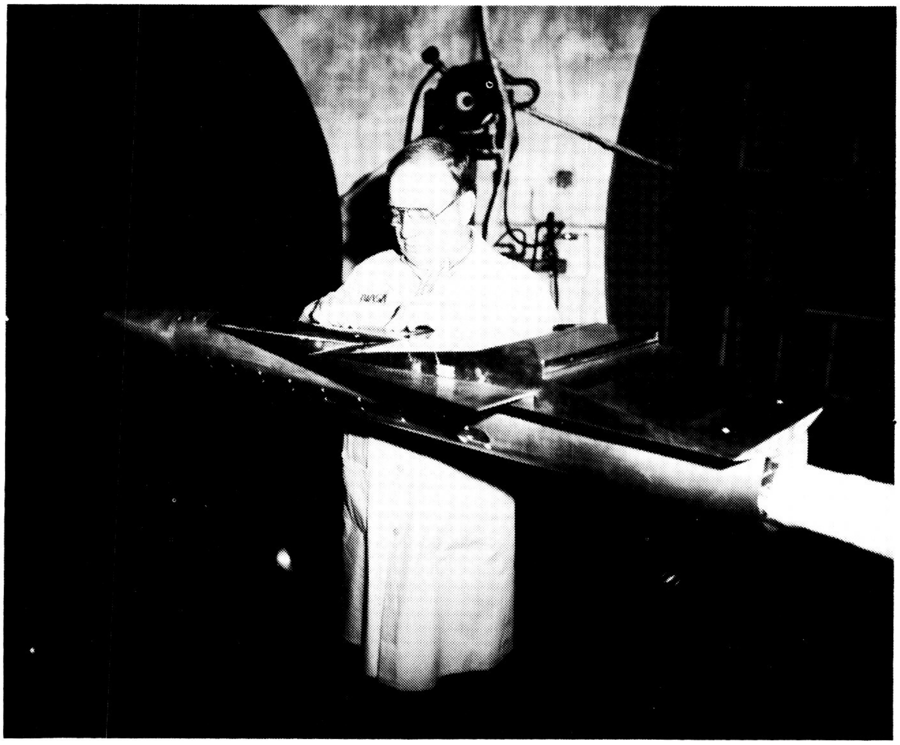

Modified NASP baseline configuration installed in 8-Foot HTT.

L-88-03440

Heat Transfer and Pressure Investigation of Modified NASP Baseline Configuration

The goal of the National Aero-Space Plane (NASP) project is to develop a research vehicle that will be able to take off from a conventional runway, fly with a single stage to orbit, and return. In order to achieve this goal, significant advances must be achieved in a number of disciplines, not the least of which is the development of accurate computational techniques for the prediction of the heat and pressure loads that the vehicle will be subjected to during the portions of the flight trajectory which cannot be duplicated in ground-based facilities. As a part of the NASP technology efforts, a cooperative Langley Research Center and Boeing Advanced Systems Company investigation of a modified version of the configuration (known as the "Government Baseline") was conducted in the 8-Foot HTT. This configuration was chosen because Boeing had an existing model that could be modified for the tests at substantially lower cost than constructing a new model and because the baseline configuration, which is now unclassified, would allow easier dissemination of the data to those developing computational techniques. The purpose of the test series was to obtain pressure and heat transfer data on a realistic, large-scale (1/20), NASP-like configuration for both laminar and turbulent boundary-layer conditions. In particular, the distribution of the pressure and heat transfer instrumentation was biased toward the upper surface or lee side of the vehicle (for positive angles of attack) because the prediction of lee-side characteristics is significantly more difficult than that for the windward side and existing lee-side data for small-scale models were more in question.

The tests were conducted in the Langley 8-Foot HTT at a nominal Mach number of 6. Unit Reynolds number was varied from approximately 0.6×10^6/ft to approximately 1.6×10^6/ft. The model was tested at angles of attack from approximately 0° to approximately 15°. Results from this investigation indicate that the expected increases in windward side heat transfer and pressure coefficients with angle of attack were obtained; the lee-side heat transfer distribution remained relatively constant at approximately the same level obtained at an angle of attack of 0° for all angles of attack investigated; and the lee-side pressure coefficient distribution showed a trend toward more negative values with increasing angle of attack.

(D. E. Reubush, 46002)

Acoustics Research Laboratory

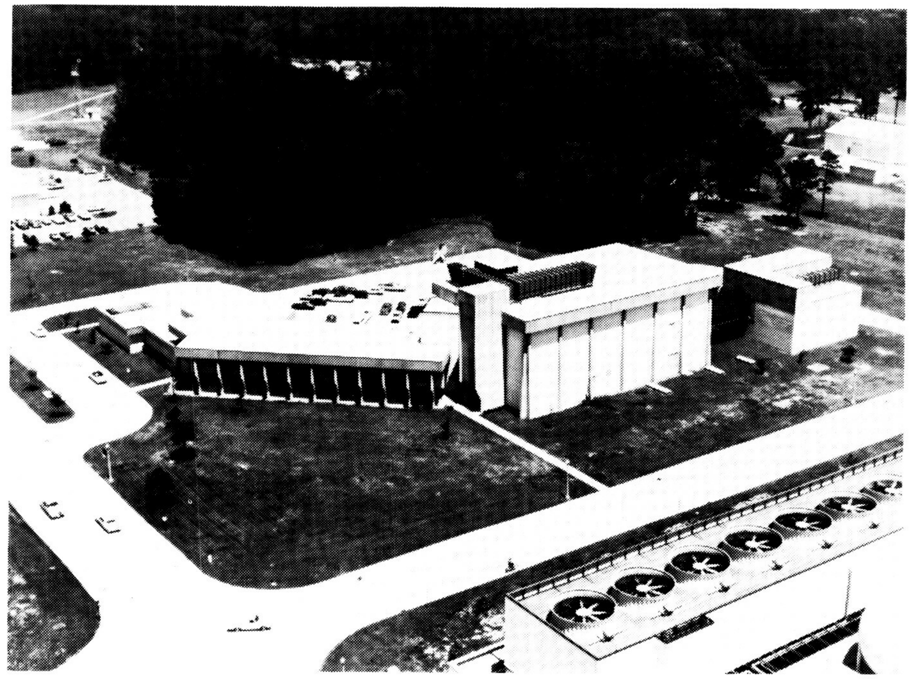

The Langley Acoustics Research Laboratory (ARL) provides the principal focus for acoustics research at Langley Research Center. The ARL consists of the anechoic quiet flow facility, the reverberation chamber, the transmission loss apparatus, and the human-response-to-noise laboratories. The anechoic quiet flow facility has a test chamber treated with sound-absorbing wedges and is equipped with a low-turbulence, low-noise test flow to allow aeroacoustic studies of aircraft components and models. The test flow, which is provided by either horizontal high-pressure or vertical low-pressure air systems, varies in Mach number up to 0.5. The reverberation chamber, which is used to diffuse the sound generated by a noise source, provides a means to measure the total acoustic power spectrum of the source. The transmission loss apparatus has a source and a receiving room, which are joined by a connecting wall. A test specimen such as an aircraft fuselage panel is mounted in the connecting wall for sound transmission loss studies. The human-response laboratories consist of the exterior effects room, the anechoic listening room, and the Freedom space station/aircraft acoustic simulator.

Three laboratory companions of the ARL are the Anechoic Noise Facility, the Jet Noise Laboratory, and the Thermal Acoustic Fatigue Apparatus (TAFA). The Anechoic Noise Facility is equipped with a very-high-pressure air supply used primarily for simulating nozzle exhaust flow. The Jet Noise Laboratory has two coannular supersonic jets for studying turbulence evolution in the two interacting shear flows that are typical of high-speed aircraft engines. Hot supersonic jets with temperatures corresponding to those associated with afterburners can also be simulated in the Jet Noise Laboratory. The TAFA provides the capability to subject flat structural panels to high-level acoustic pressures and high-temperature radiant heating to 1200°F.

Noise Control in Composite Model Fuselage

With the advent of composites as the primary fuselage structural material, a great deal of effort has gone into defining their static and dynamic load-carrying abilities. However, due primarily to their lighter weight, the noise transmission characteristics have been shown to suffer. Without a thorough understanding of the noise transmission mechanisms for realistic built-up composite structures, effective advantage may not be taken of innovative solutions such as passive and active damping and active noise and vibration control. A comprehensive test on a realistic composite structure under carefully controlled conditions

ORIGINAL PAGE
BLACK AND WHITE PHOTOGRAPH

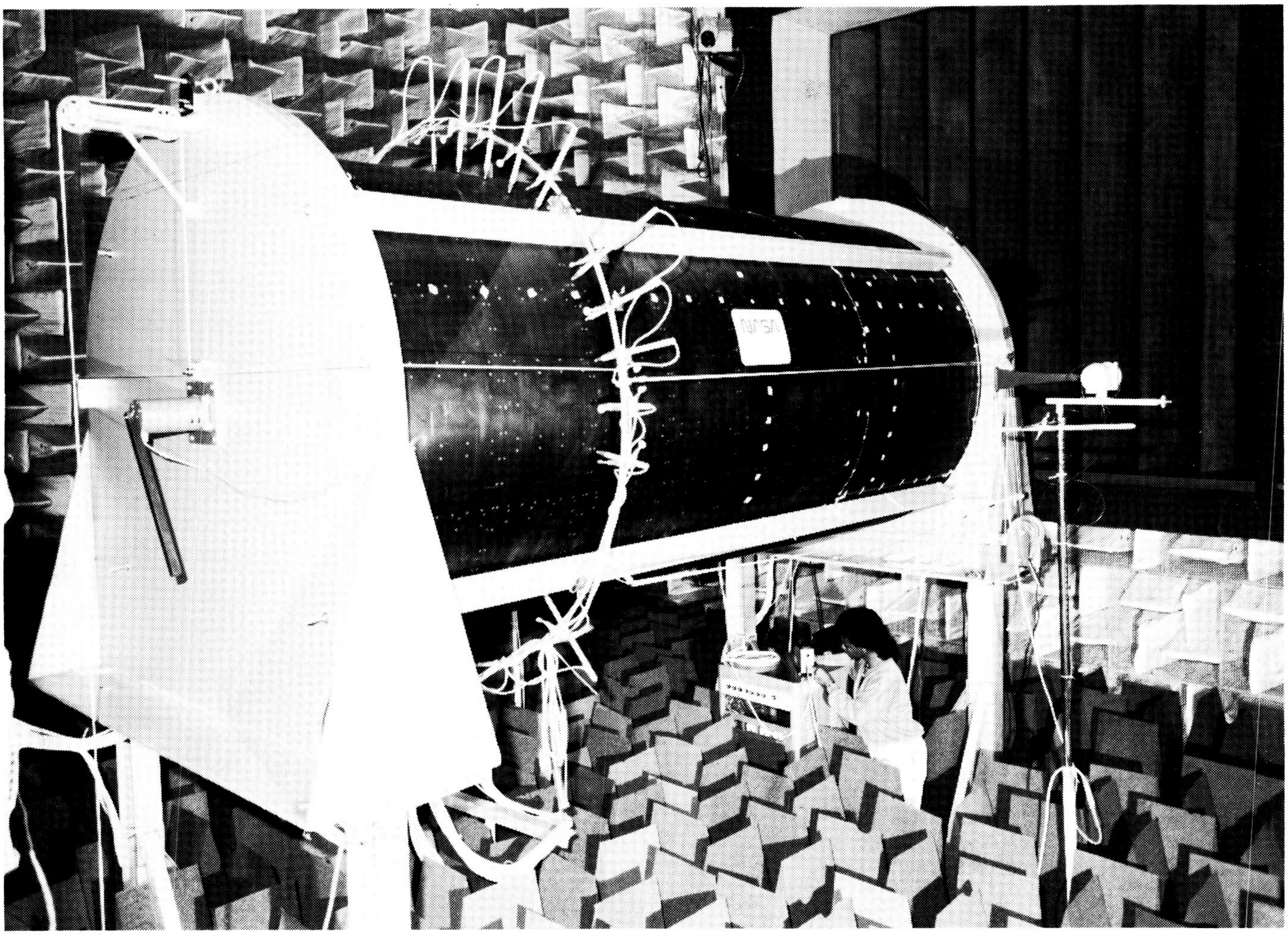

Composite fuselage model in anechoic quiet flow facility. L-89-00352

has been performed to address these issues as well as the effect of source structure on noise transmission.

The cylinder structure shown in the anechoic quiet flow facility of the Acoustics Research Laboratory consists of a continuously wound graphite-filament cylinder of nine plies laid at five different angles giving a total shell thickness of 0.067 in. Continuously bonded rings spaced every 15 in. and 22 equally spaced stringers make the 12-ft long, 5.5-ft-diameter structure representative of an aircraft fuselage. A floor is installed in the interior of the cylinder. Tests were completed both with and without acoustic foam damping installed on the interior walls.

A data base has been generated which consists of measurements of the exterior pressure distribution over the cylinder surface, 22 accelerometer measurements on a circumference in a fixed source plane, and an extensive mapping of the interior three-dimensional pressure field. Exterior sound fields over a range of frequencies from 50 Hz to 900 Hz were provided by a single acoustic point source, by two point sources on opposite sides in a single cross section that operated both in phase and out of phase, and finally by a phased array of point sources which provided the trace velocity of a propeller. In addition, source spacing effects were investigated.

These data, in combination with several analytical models, are providing insight into the forced response of complex structures both composite and conventional and should provide a solid basis upon which to provide effective and lightweight noise and vibration isolation.
(R. J. Silcox, 43590)

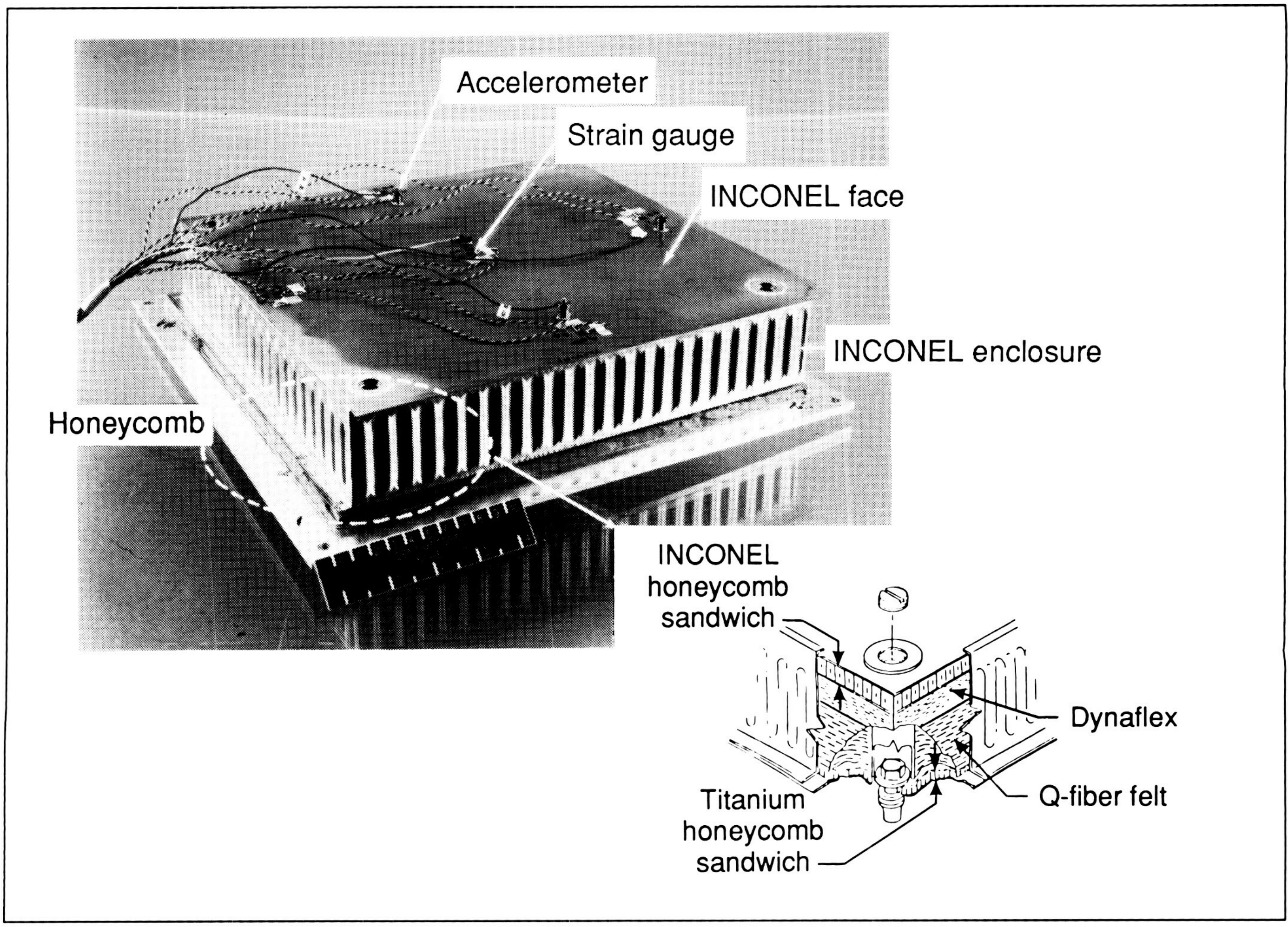

Honeycomb TPS panel. L-88-8491

Acoustic Response of TPS Panels

Fatigue life estimation of complex aircraft structures requires detailed knowledge of how these structures respond to the loads they experience in flight; this is especially true of the structures that will be used on advanced aircraft such as the National Aero-Space Plane. Structural panels located at critical areas on such an aircraft may experience very intense acoustic loads combined with very high temperatures. Measurement of the stresses produced by such loads on hot structures and determination of the effect of these stresses on fatigue life represent a major challenge to the technical community.

To investigate experimental methodology for obtaining measurements for combined acoustic and thermal loads, a study was conducted to measure the strain response of three superalloy honeycomb thermal protection system (TPS) panels at both ambient and elevated temperatures. The TPS panels (shown in the figure) consisted of an outer Inconel sandwich panel, a central layer of insulation, and an inner titanium sandwich panel. Through-panel fasteners at each corner were used to attach the panels to an aluminum plate that simulated the primary structure. Detailed strain measurements were obtained at ambient temperature and acoustic noise levels up to 160 dB. Results indicated that the measured strains were relatively low and varied linearly with noise level. Comparable measurements of strain response (using special high-temperature strain gauges) at temperatures up to 1000°F are under way. **(J. D. Leatherwood, 43597)**

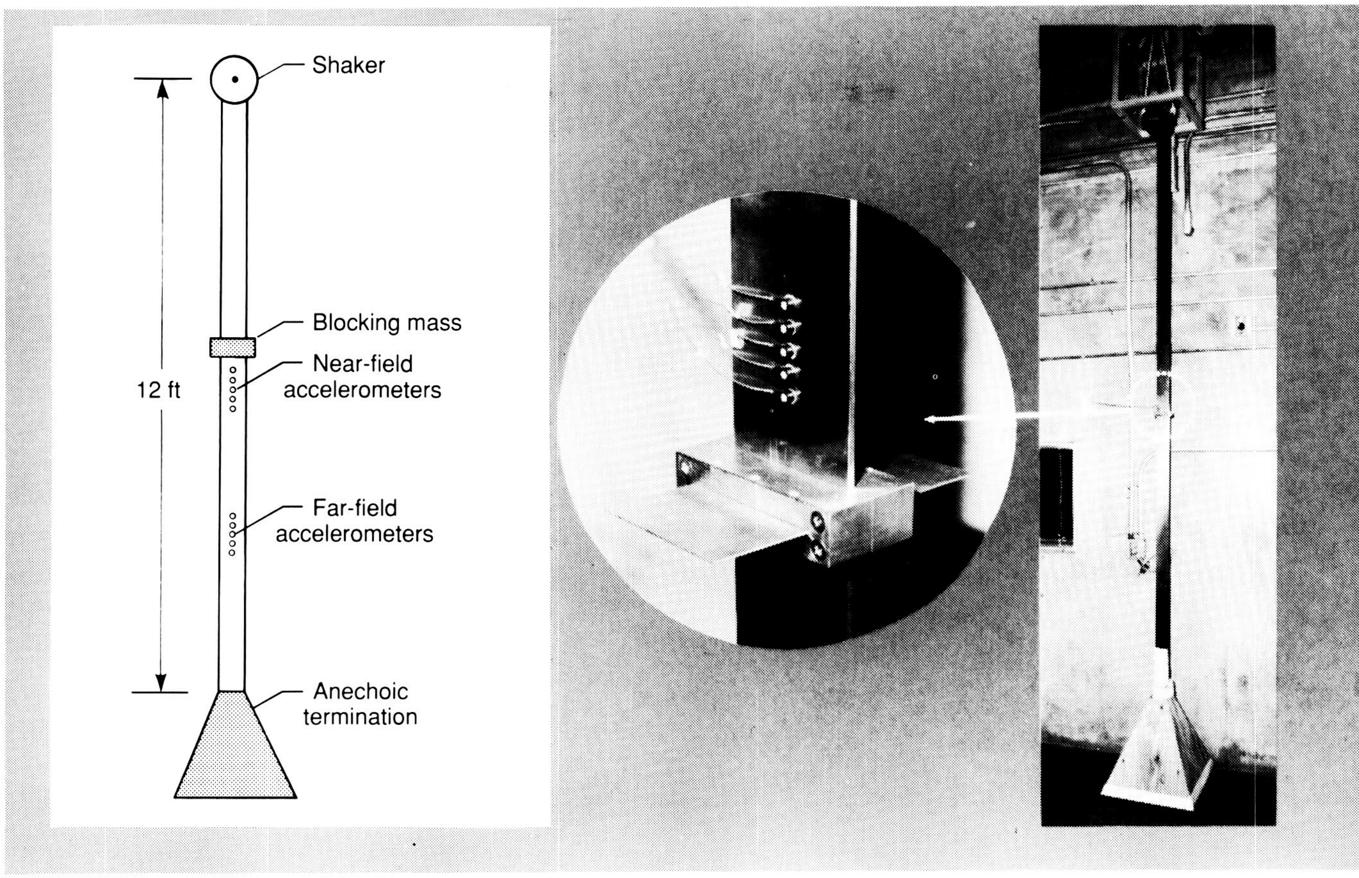

Test apparatus for structureborne power flow measurement. L-88-5011

Structureborne Power Flow Measurement

Aircraft interior noise may arise from a combination of airborne acoustic transmission and structureborne vibration. To aid in the identification of structureborne noise paths and the optimized application of noise and vibration control treatments, methods to measure structureborne power flow are needed. Previous research on experimental methods for measuring structureborne power flow has centered on a technique that uses two closely spaced accelerometers. Valid results can be achieved with this method if measurements are confined to "free field" conditions, with no power sources or boundaries in the vicinity of the transducers. A revised method has been proposed which requires the use of five accelerometers for a one-dimensional problem. The primary advantage of this method is that its results should remain accurate near sources and boundaries. An experimental study to compare the two methods was performed using a 12-ft beam with a shaker attached to one end and a sandbox termination at the other end to approximate semi-infinite behavior. As indicated in the figure, the blocking mass clamped to the beam served as a boundary, and the shaker provided the input power.

Measurements were made at a location far from the source and the blocking mass (far field), and, as expected, the two methods provided similar estimates of power flow. In the near field of the blocking mass, however, estimates of power flow for the two methods diverge, particularly at lower frequencies. Comparisons of power flow estimates in the near and far fields indicated that the five-accelerometer method remains accurate under near-field conditions. It is anticipated that the use of this method will be extended to more complex structures.

(K. P. Shepherd, 43583)

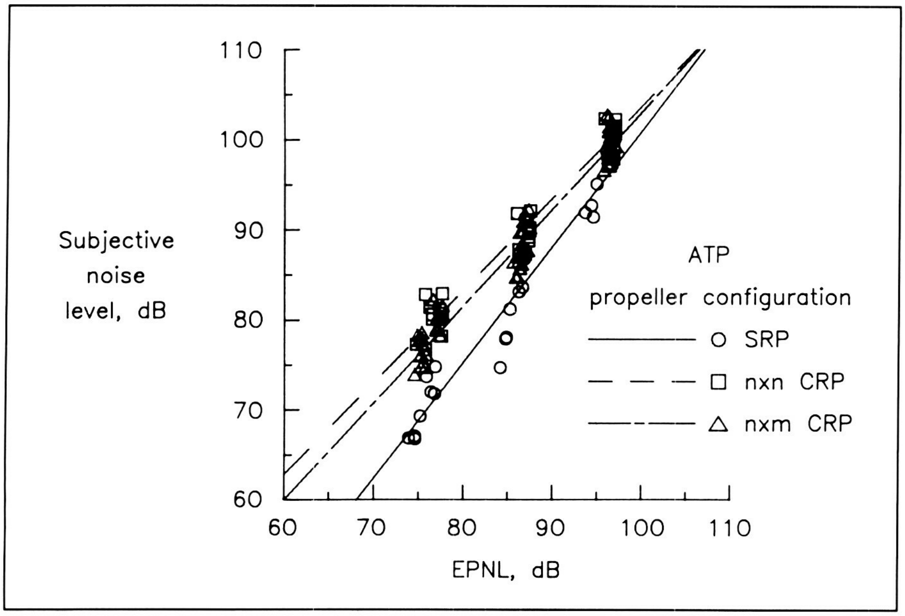

Comparison of annoyance responses using effective perceived noise level (EPNL).

Community Noise Annoyance to Advanced Turboprop Aircraft With Different Propeller Configurations

Advanced turboprop (ATP) aircraft are expected to have one of three propeller configurations that include a single-rotating propeller (SRP), counterrotating propellers with an equal number of blades on each rotor (n×n CRP), or counter-rotating propellers with an unequal number of blades on each rotor (n×m CRP). The harmonic tonal content of ATP noise occurs at frequencies higher than those generated by conventional propeller aircraft but lower than those generated by conventional jet aircraft. Each propeller configuration also has unique noise characteristics due to differences in harmonic content and tonal directivity patterns. The ATP aircraft will come into general usage only if their noise meets standards of community acceptability currently applied to conventional aircraft. An experiment has been conducted in the anechoic listening room (a human-response-to-noise laboratory) of the Acoustics Research Laboratory to compare the annoyance of flyover noise from ATP aircraft having different propeller configurations with the annoyance of flyover noise from conventional turboprop and jet aircraft.

The Aircraft Noise Synthesis System was used to generate 40 realistic, time-varying simulations of ATP takeoff noise. Of the 40 noises, 8 represented SRP configurations, 12 represented n×n CRP configurations, and 20 represented n×m CRP configurations. In the experiment, 64 subjects judged the annoyance of the synthesized ATP takeoffs along with recordings of five conventional turboprop takeoffs and five conventional jet takeoffs. Each of the noises was presented at three sound pressure levels to the subjects in the anechoic listening room.

Analyses of the judgments examined the effects on annoyance of blade passage frequency, tone-to-broadband noise ratio, propeller configuration, and aircraft type. For example, the figure compares the annoyance responses to ATP aircraft with different propeller configurations. The annoyance prediction ability of current noise measurement and correction procedures was also examined. The addition of duration corrections and corrections for tones above 500 Hz to the noise measurement procedures improved prediction ability.
(D. A. McCurdy, 43596)

XV-15 Tiltrotor Far-Field Acoustics Flight Test

A flight test to collect a far-field acoustics data base from an XV-15 Tiltrotor aircraft (Tail Number 702) was performed in September 1988. The resulting data base will be used to validate the capability of the ROTONET prediction code to correctly predict the noise spectra and the tone-corrected perceived noise level (PNLT) and effective perceived noise level (EPNL) noise metrics. The test, which was a joint venture between Langley Research Center and Bell Helicopter Textron, was performed in a quiet, countryside environment near Maypearl, Texas. The flight test consisted of repeated Tiltrotor aircraft flyovers of a rectangular microphone array that consisted of five linear microphone arrays with four microphones in each row. Flight paths directly over the center linear microphone array at two altitudes yield high-confidence, highly accurate ensembled-averaged acoustics measurements directly be-

ORIGINAL PAGE IS
OF POOR QUALITY

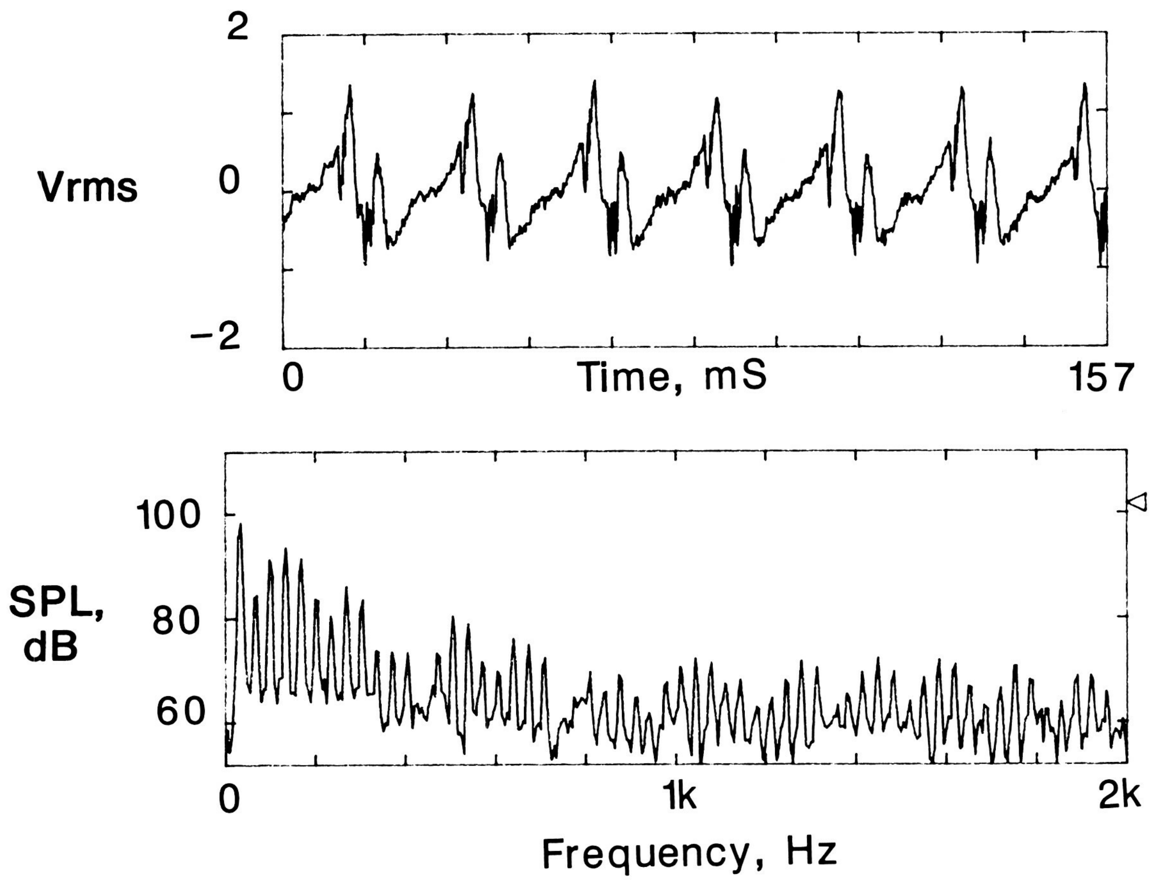

Preliminary acoustic time history and narrowband spectra for XV-15 Tiltrotor aircraft with observation angle of 30° below aircraft horizon, velocity of 90 knots, and nacelle tilt of 85°.

neath and at four sideline angles on each side of the Tiltrotor aircraft. Variation of the aircraft forward speed and the nacelle tilt angles permitted additional acoustics measurements resulting in a data base that characterized the lower hemisphere acoustics signature of the Tiltrotor aircraft throughout its operational envelope.

Preliminary analysis of some of the data has shown some particularly interesting and unexpected results. The results for the 0° nacelle tilt case (tiltrotor airplane mode for enroute flight) indicate that the acoustic signature is that of a typical quiet propeller aircraft. In the figure, however, the time history and narrowband spectra for a flyover at 90 knots forward speed with a nacelle tilt angle of 85° are shown. This particular flight condition (tiltrotor helicopter mode for landing and takeoff) shows the presence of a blade vortex interaction noise that appears to be worse than that encountered by a typical noisy helicopter during landing and takeoff. While further detailed analysis must be performed for validation of the ROTONET prediction code, preliminary data analyses have shown that a community noise problem may exist during the landing and takeoff maneuvers for the present tiltrotor aircraft design.

(R. A. Golub, 45281)

Active Control of Vibration in Beams

Transmission of vibration within aerospace structures has been a particularly troublesome problem for propeller-driven aircraft and helicopters. The frequencies of vibration typically range from 100 Hz to 1000 Hz and are quite often difficult to

reduce by conventional means without an unacceptable weight penalty. One innovative concept that may prove viable is active control using vibrational inputs to the structure either to reduce its overall response or to constrain the vibration to isolated areas of the structure where it is not objectionable to the passengers.

In order to investigate this technology, a simple aluminum beam was assembled with well-defined boundary conditions as shown in the figure. The beam was excited by an attached shaker at one end, and various blocking masses provided a variety of termination conditions. A control shaker was actuated at a midway point of the beam as shown in the figure. An adaptive feedback control scheme provided the necessary excitation to this shaker in order to minimize the response output from an accelerometer placed as shown. The control scheme utilized a fast least mean squares algorithm to converge the parameters of the controller to minimize the accelerometer output and maintain control under changing conditions.

Results obtained to date with the single controller setup shown provided 25 dB to 40 dB of vibration reduction over the various subregions of the beam. The experiment demonstrated two different mechanisms of control. The first was a reduction in the input power from the excitation shakers due to a change in the source loading. The second was a blocking effect implemented at the control shaker effectively reflecting the vibrational energy back to the primary shaker. The results are providing validation to a parallel analytical program that is itself yielding additional insight into the control mechanisms.
(R. J. Silcox, 43590)

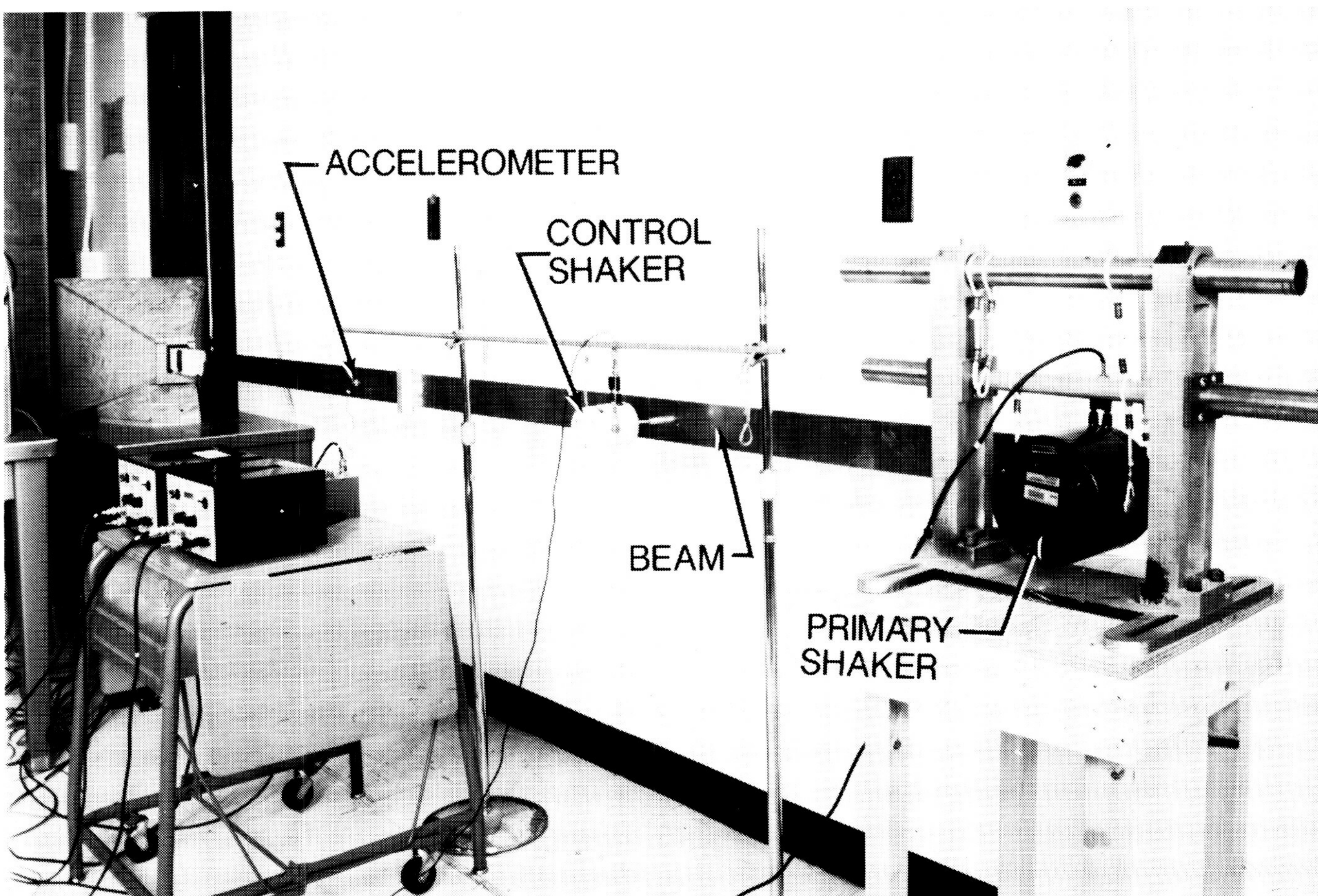

Beam test setup showing transducer configuration.

L-88,1107

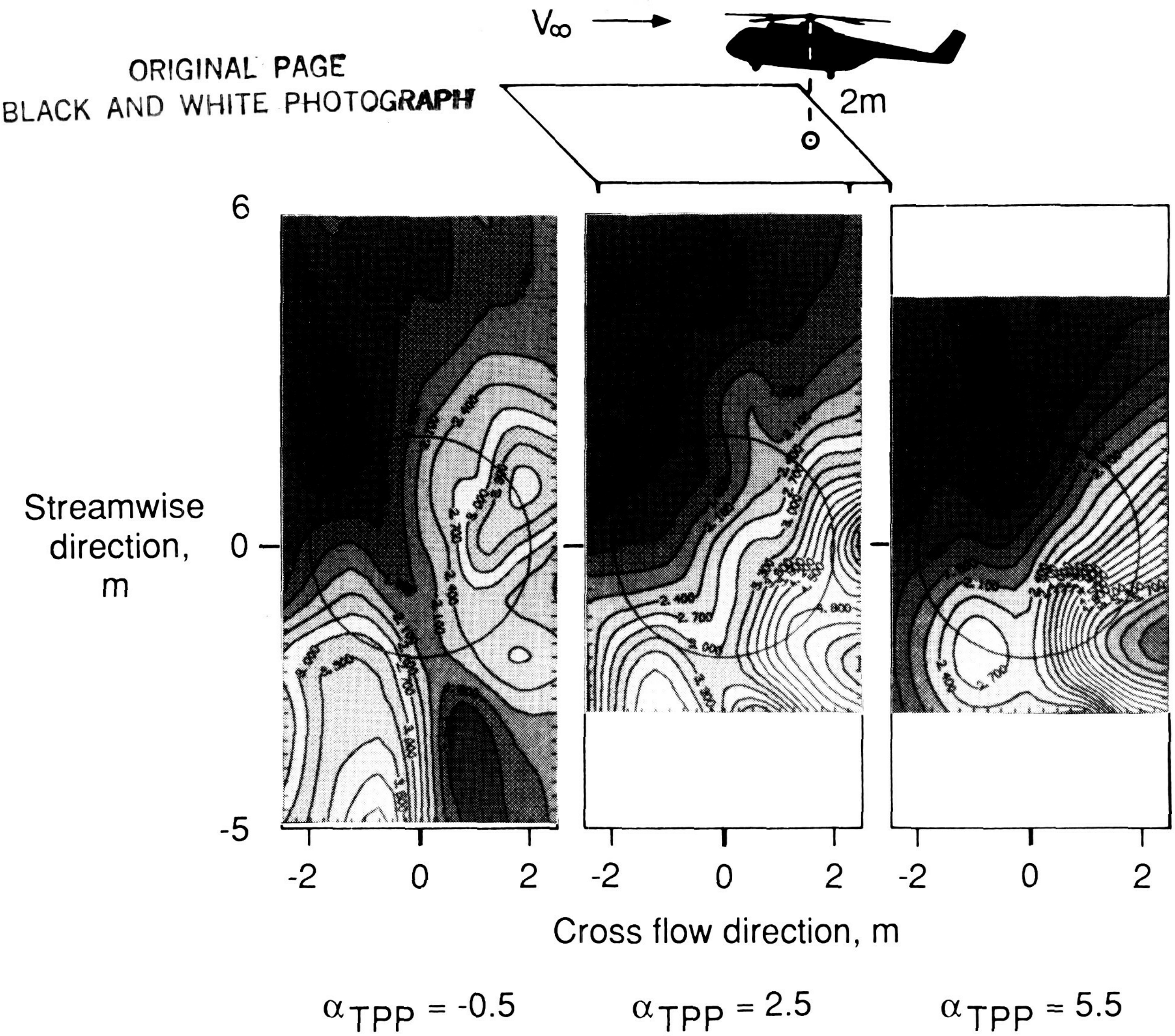

Variation of rotor impulsive noise directivity with flight angle.

Directionality of Helicopter Impulsive Noise

High levels of helicopter impulsive noise occur when helicopter rotor blades meet the tip vortices previously shed into the rotor's wake. This interaction noise, called blade-vortex interaction (BVI) noise, is a major cause of community noise problems and an important factor in helicopter noise certification procedures.

The strongly directional radiation of this noise source and its dependence on the helicopter flight condition were studied during a recent rotor noise experiment in the German/Dutch Acoustic Wind Tunnel (DNW, Duits-Nederlandse Windtunnel/ Deutsch Niederlandischer Windkanal). The experiment was performed and funded by the German Aerospace Research Establishment, the Deutsche Forschungsanstalt für Luft- und Raumfahrt (DLR). NASA participated as part of a NASA-DLR Letter of Agreement on rotor acoustics research. Although the work was not performed in a Langley Research Center facility, it is included here because of its international interest.

The noise radiation pattern of this impulsive noise source was measured in a large plane under (both upstream and downstream of) the rotor in the open jet test section of the DNW facility. A

large matrix of test conditions was measured to define the changing directionality with helicopter flight speed and flight mode (ascent, descent, or level flight). Noise level contours for an 80-knot condition are shown in the figure for three different rotor flight angles (tip-path-plane angle α_{TPP}). The changing directionality of the highest noise levels with the flight angle is clearly evident by the different patterns.

These results show the strong sensitivity of blade-vortex interaction noise to flight condition and provide the technical basis for the refinement of noise certification procedures.
**(R. M. Martin, 43631,
R. E. Grandle, and
M. A. Marcolini)**

Avionics Integration Research Laboratory—AIRLAB

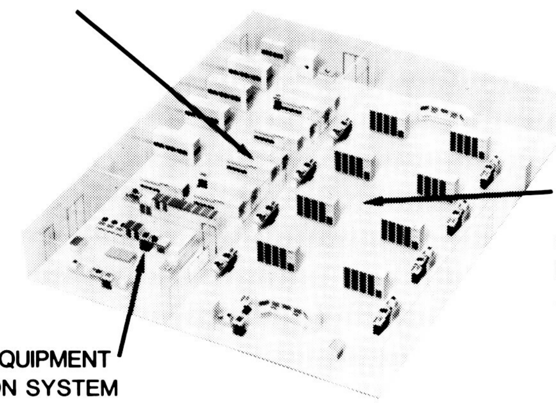

The United States leads the world in the development, design, and production of commercial and military aerospace vehicles. To maintain this leadership role throughout the 1990's and beyond will require the incorporation of the latest advances of digital systems theory and electronics technology into fully integrated aerospace electronic systems. Such efforts will entail the discovery, design, and assessment of systems that can dramatically improve performance, lower production and maintenance costs, and at the same time provide a high, measurable level of safety for passengers and flight crews.

AIRLAB has been established at Langley Research Center to address these issues and to serve as a focal point for United States government, industry, and university research personnel to identify and develop methods for systematically validating and evaluating highly reliable, fully integrated digital control and guidance systems for aerospace vehicles.

The increasing complexity of electronic systems entails multiple processors and dynamic configurations. These developments allow for greater operational flexibility for both normal and faulty conditions, thus impacting and compounding the validation process. Whereas a typical reliability requirement for current electronics systems is a probability of failure of less than 10^{-6} at 60 minutes, the requirement for flight-critical electronic controls is for a probability of failure of less than 10^{-9} at 10 hours. Obviously, a new validation process is essential if this significant increase in reliability (four orders of magnitude) is to be achieved and believed.

Validation research in AIRLAB encompasses analytical methods, simulations, and emulations. Analytical studies are conducted to improve the utility and accuracy of advanced reliability models and to evaluate new modeling concepts. Simulation and emulation methods are used to determine latent fault contributions to electronic system reliability and hence aircraft safety. Experimental testing of physical systems is conducted to uncover the latent interface problems of new technologies and to verify analytical methods.

AIRLAB is a 7600-ft^2 environmentally controlled structure located in the high-bay area of Building 1220. AIRLAB houses a number of microcomputer and minicomputer resources and several special fault-tolerant research hardware test specimens dedicated to the support of validation research. The minicomputer resources consist of eight Digital Equipment Corporation VAX 11/750 computers, one VAX 11/780 computer, four MicroVAX II computers, one GKS (Graphical Kernel System) VAXstation II, one VAXstation 3200, two Sun workstations, and four IBM-PC compatibles. These resources are used to control experiments (such as fault insertions and performance monitoring); retrieve, reduce, and display engineering data; develop and validate simulations; and develop and validate analytical reliability and performance estimation tools. Also included in AIRLAB are three advanced fault-tolerant computer systems,

fault-tolerant multiprocessor (FTMP), fault-tolerant processor (FTP), and verifiable integrated processor for enhanced reliability (VIPER), which are designed to explore fault-tolerant techniques for future flight-critical aerospace applications and to serve as research test beds for validation studies in AIRLAB.

High-speed data acquisition system for fault-tolerant computer characterization.

Fault injection and fault-free validation experiments were previously performed in AIRLAB on the fault-tolerant multiprocessor to characterize system behavior and baseline performance using a software-driven data acquisition system. With the low data rate available using this data acquisition system, only data on system-wide or global behavior could be acquired. Deviations from normal system behavior had been noticed, but nothing could be determined concerning its cause. The data acquisition rate of the experiment overloaded the old data acquisition system capabilities, thus affecting the results.

A nonintrusive Data Acquisition System (DAS) was designed, and a prototype was built and tested. The system was interfaced to a minicomputer, and control software was developed to automate experiments. The new high-speed DAS was designed to monitor the fault-tolerant multiprocessor buses and download the acquired data to a VAX minicomputer for analysis. The data read from the fault-tolerant multiprocessor system bus (at 8 Mb/s) is stored in a random access memory (RAM) buffer (128 Kb) and then downloaded to the VAX through a direct memory access (DMA) channel (at 6.4 Mb/s). The DAS monitors the system bus until a user-selected word is detected; this event triggers the DAS to start acquiring data into the buffer.

The data acquisition length is determined by the user. The VAX host has access to status and control bits that can be used to synchronize the DAS operation with other hardware (e.g., fault injector) during experiments. The DAS provides a three-orders-of-magnitude increase in the data acquisition rate, compared with the previous system, and allows real-time acquisition of the system state during experiments without affecting or requiring changes to the system under test. The DAS provides the capability to uncover and characterize specification, design, and implementation errors by opening a clear window into the operation of the system under test.

(P. A. Padilla, 46187)

Testing Semi-Markov Unreliability Range Evaluator (SURE) Tool

The complexity of current fault-tolerant computer systems makes computation of system reliability extremely difficult. Exact analytical computation of reliability is virtually impossible except for the simplest systems, and even manual derivation of an approximation is impractical for complicated systems. The Semi-Markov Unreliability Range Evaluator (SURE) program has been developed as a reliability analysis tool to compute unreliability bounds for complex systems.

Although no formal methodology exists for establishing 100-percent confidence in a reliability analysis tool, performing a series of well-documented formal test cases can help establish a sense of validity. To examine the accuracy of the SURE program, three stages of testing were conducted. First, SURE's bounds were compared to exact analytic solutions for simple reliability models. For more complex models in which derivation of the exact solution is infeasible, comparisons were made with existing tools such as ARIES (Automated Reliability

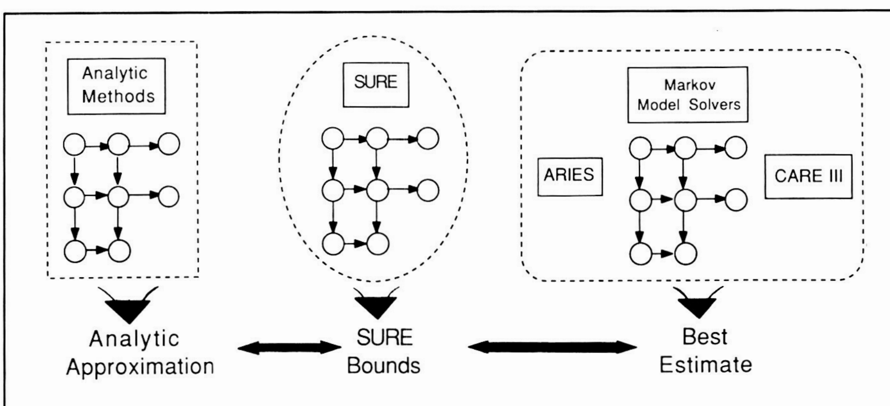

Comparison of SURE to existing reliability assessment techniques.

Interactive Estimation System), CARE III (Computer-Aided Reliability Estimation, version 3), and two Markov model solvers. Finally, the underlying mathematics were reviewed, and relative error estimates were derived for the reliability estimate.

This testing represented the first independent, comprehensive evaluation of the SURE tool. Over 35 models and 250 test cases were used to test SURE. No cases were found in which SURE's bounds did not envelop the exact unreliability or the best estimate of unreliability for any model tested. In general, the bounds were very tight, and the upper bound provided a particularly good estimate of system unreliability. These results concurred with the findings from the analytical study of the bounding theory and relative error estimates. Overall, the results of this testing give the users of the SURE program confidence in the accuracy of the SURE bounds.

(K. J. Hayhurst, 46215)

Performance Modeling of Aircraft Systems

Performance modeling has become an important tool in validating aircraft system behavior. Timing parameters, which are part of reliability models (such as recovery times), can be studied and measured with performance modeling tools. The use of performance tools enables system designers to become more familiar with system behavior earlier in the design cycle. In this way, costly, conceptual designer errors can be uncovered before designs are committed to production.

Performance modeling tools have been used extensively by the Boeing Advanced Systems Company in the Integrated Airframe Propulsion/Control System Architecture Program (IAPSA). The IAPSA system design is based on Advanced Information Processing System (AIPS) building blocks. Quad, triplex, and dual fault-tolerant computers and repairable I/O (input/output) mesh networks can be constructed from the AIPS building blocks. Given the hundreds of sensors and actuators that must be connected to the system processors, many configurations are possible. The performance tools give

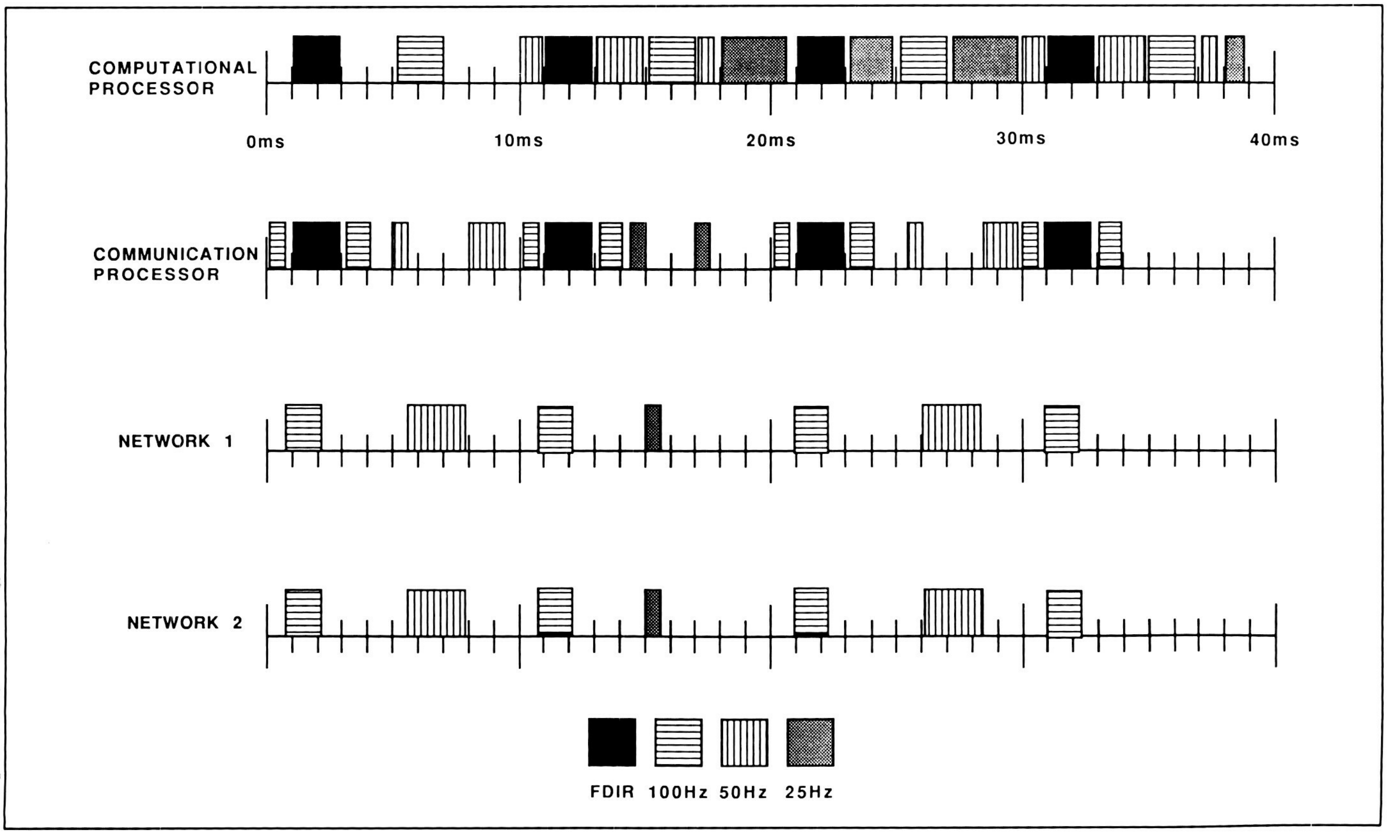

Aircraft system performance monitoring.

the system designer a way to evaluate each candidate system's performance characteristics.

The timing diagrams shown in the figure were derived from the output of a performance model of the IAPSA/AIPS system. A single AIPS channel contains two processors, a computational processor, and an I/O processor. Both processors execute priority-based preemptive schedulers. This particular system also had two mesh networks. The first and second lines of the timing diagram are the task loads on the computational and I/O processor, respectively. The second and third lines are the communication loads on the two mesh networks. The processing and communication times for three multirate task groups plus the fault-tolerant executive (fault-detection isolation and recovery or FDIR) are displayed as pulses on the time line. Clear space signifies auxiliary processing time that could be used for additional tasks. A requirement of the IAPSA system is that it must have a 100-percent processing growth margin. As can be seen from the processor time lines, this requirement has not been met for this particular configuration.
(D. L. Palumbo, 46185)

Aerospace Controls Research Laboratory

The purpose of the Aerospace Controls Research Laboratory (ACRL) is to conduct research and testing of spacecraft control systems. The ACRL is equipped with modern microcomputer facilities for simulations, data acquisition, and real-time control system testing. Both control law testing using structural test articles and advanced control system component development are supported by the laboratory. The ACRL provides the controls community with facilities on which the performance of competing control laws may be compared.

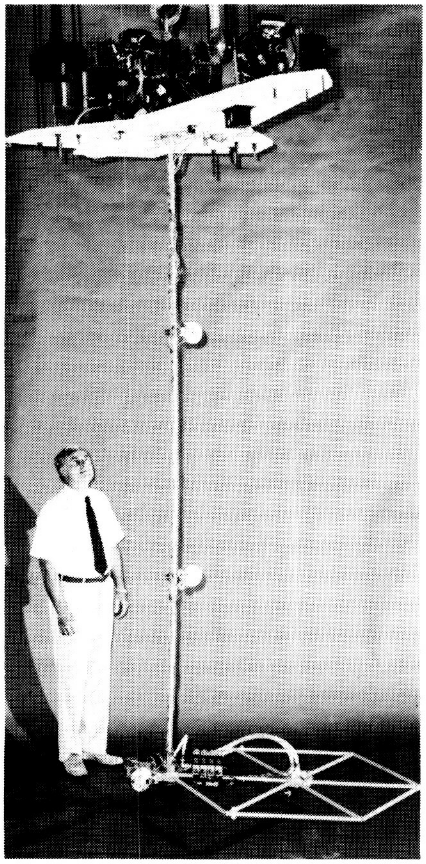

Spacecraft Control Laboratory Experiment (SCOLE). L-87-7321

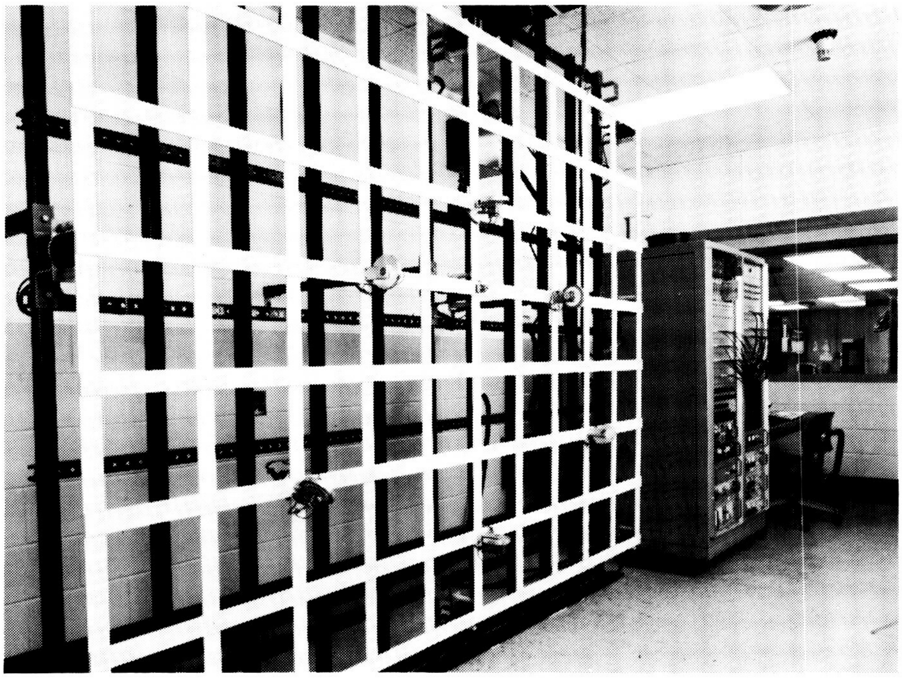

Grid experiment. L-84-10319

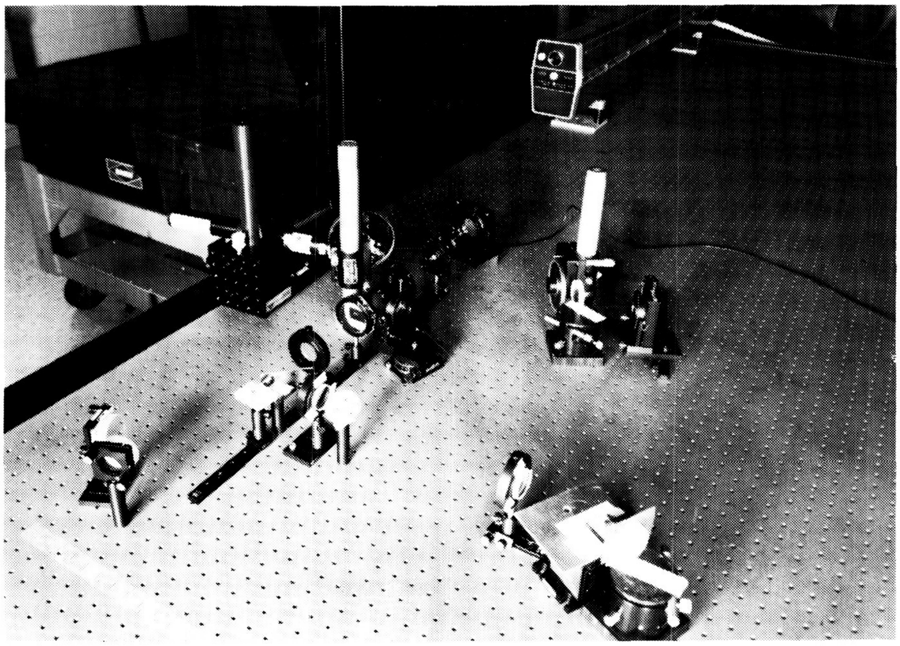

Advanced sensor and actuator facility. L-89-325

Two structural test articles are currently available. One, the Spacecraft Control Laboratory Experiment or SCOLE, allows testing of control laws for a complete spacecraft. The test article mimics the Space Shuttle with a large flexible offset-feed antenna attached to the payload bay. Reaction jets, control moment gyros, and torque wheels, along with accelerometers and rate sensors permit real-time control law implementation on SCOLE (see the first figure). The other test article is the Grid experiment. This facility is designed to support research in the control of flexible area structures. The grid, which is made of 2-in. by 1/8-in. cross-section aluminum bars bonded at 12-in. intervals to form a 7-ft by 10-ft lattice, is suspended vertically by two 2-ft-long cables and has appreciable low-frequency structural dynamics, inertial sensors and torque wheels, and microprocessor-based distributed computing components (see the second figure).

The advanced sensor and actuator facility supports research in control system components for space systems. Component development currently focuses on optical sensing and computing devices. Two different photogrammetric position tracking systems and an optical holographic image storage device are being developed. The facility (shown in the third figure) includes equipment for performing experiments in optics, two stable tables, optical mounts, lenses, mirrors, polarizers, beam splitters, photomultiplier tubes, a 5-mW HeNe laser and a 35-mW HeNe laser, a precision rotary stage, and laser beam steering systems.

SCOLE optical attitude measurement system test.

A test was performed on the SCOLE optical position attitude measurement system. This system consists of two position-sensitive detector cameras po-

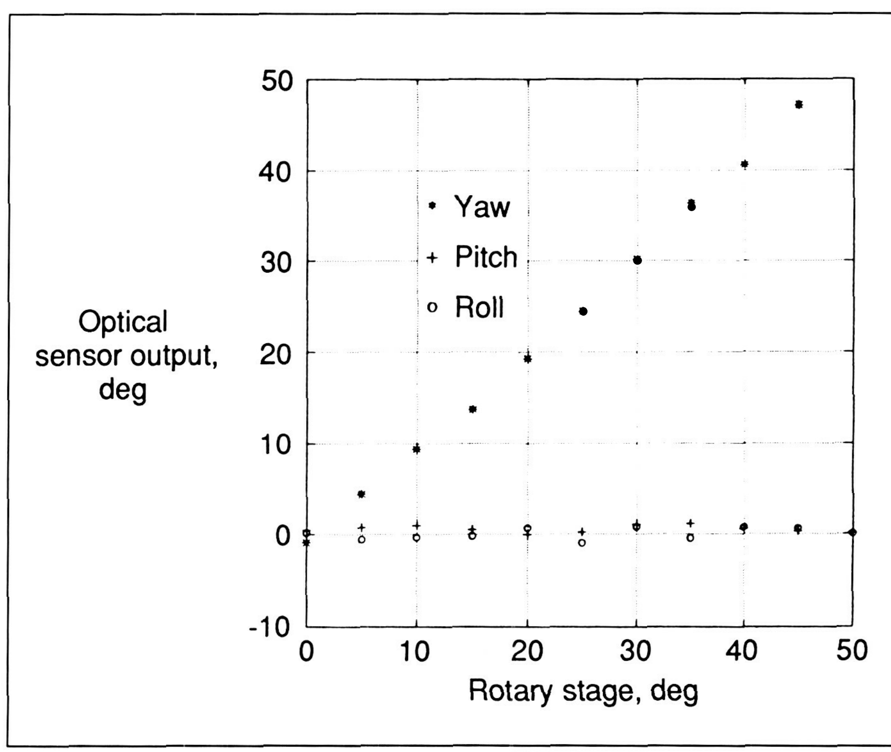

Rotary stage test in yaw for optical measurement system.

sitioned above SCOLE and at 45° with respect to the vertical. The cameras point to the center of the SCOLE platform. Small infrared diodes fixed on the platform are imaged by the two cameras. The positions of the diodes in the cameras are used to determine the location of the rigid-body platform. The test of the optical system was performed in the laboratory using a scale model of the SCOLE. The model was mounted on a computer-controlled precision rotary stage that varied the yaw attitude of the model. As the yaw attitude of the model was varied, the optical system measured the position and attitude of the model. Calibration and tracking techniques were developed to improve the performance of the system prior to installing it on the SCOLE. Further tests of the optical attitude measurement system in the SCOLE environment are planned.*
(S. S. Welch, 46611)

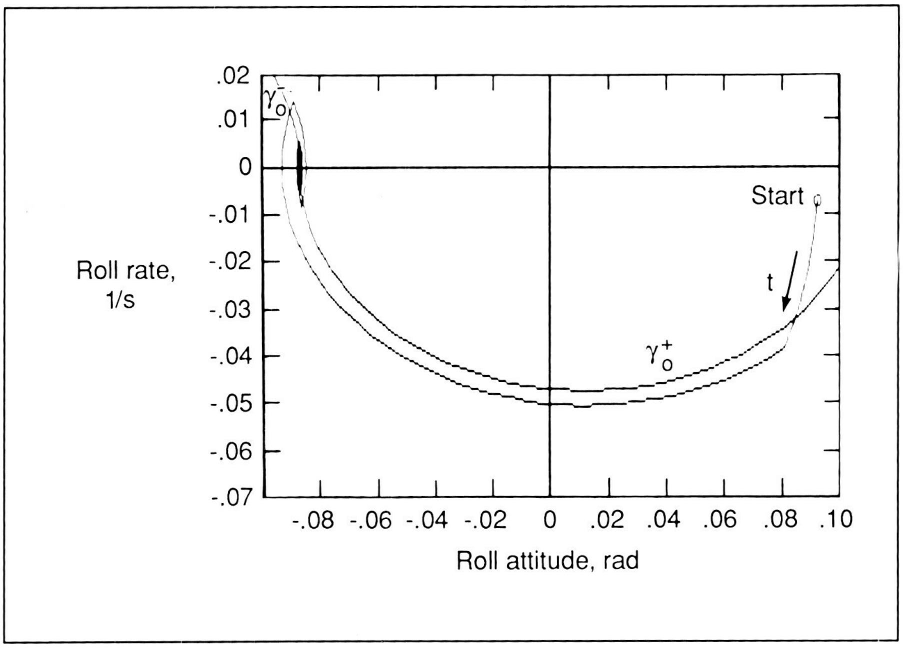

Simulation of minimum-time slew maneuver.

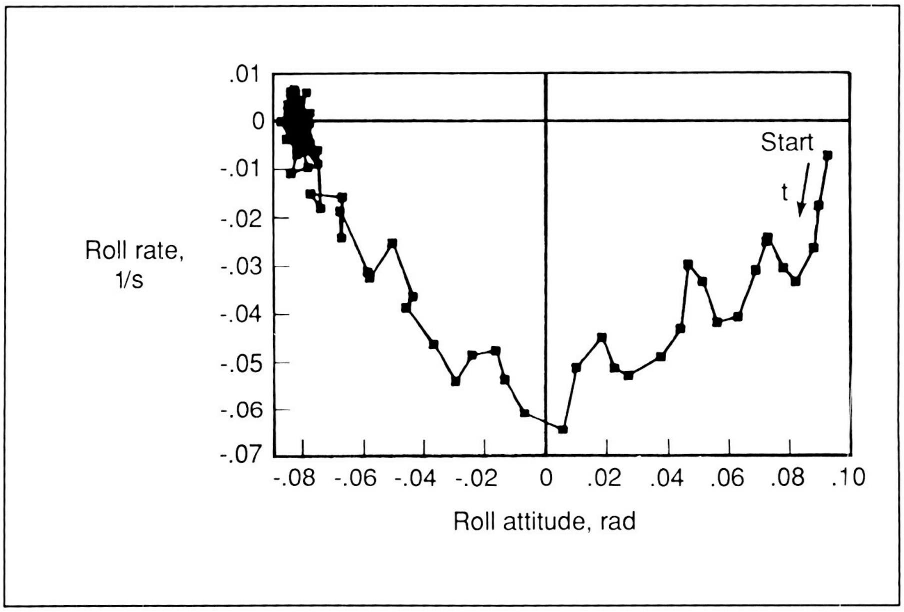

Test result of minimum-time slew maneuver experiment.

Initial Attitude Control Test on SCOLE

Future spacecraft are expected to be inherently flexible because of their large size and low weight. Maneuvering is expected to involve complex interactions between the structural dynamics and the control system. This research has been conducted to develop and validate a control law for attitude maneuvers of highly flexible spacecraft. An initial attitude control test was made on SCOLE in which the platform was constrained to move only in rotation. The goal of this test was to perform a rigid-body minimum-time slew maneuver. Cables were installed between the reflector and the platform to suppress flexibility of the mast and reflector and to make the system rigid. Comparison between simulation and test results of phase-plane trajectories (as shown in the figures) revealed small differences in attitude and in time-to-target of 2 percent. Further testing with the cables removed is planned to validate control laws specifically designed to handle flexibility.
(J. Shenhar and R. Montgomery, 46615)

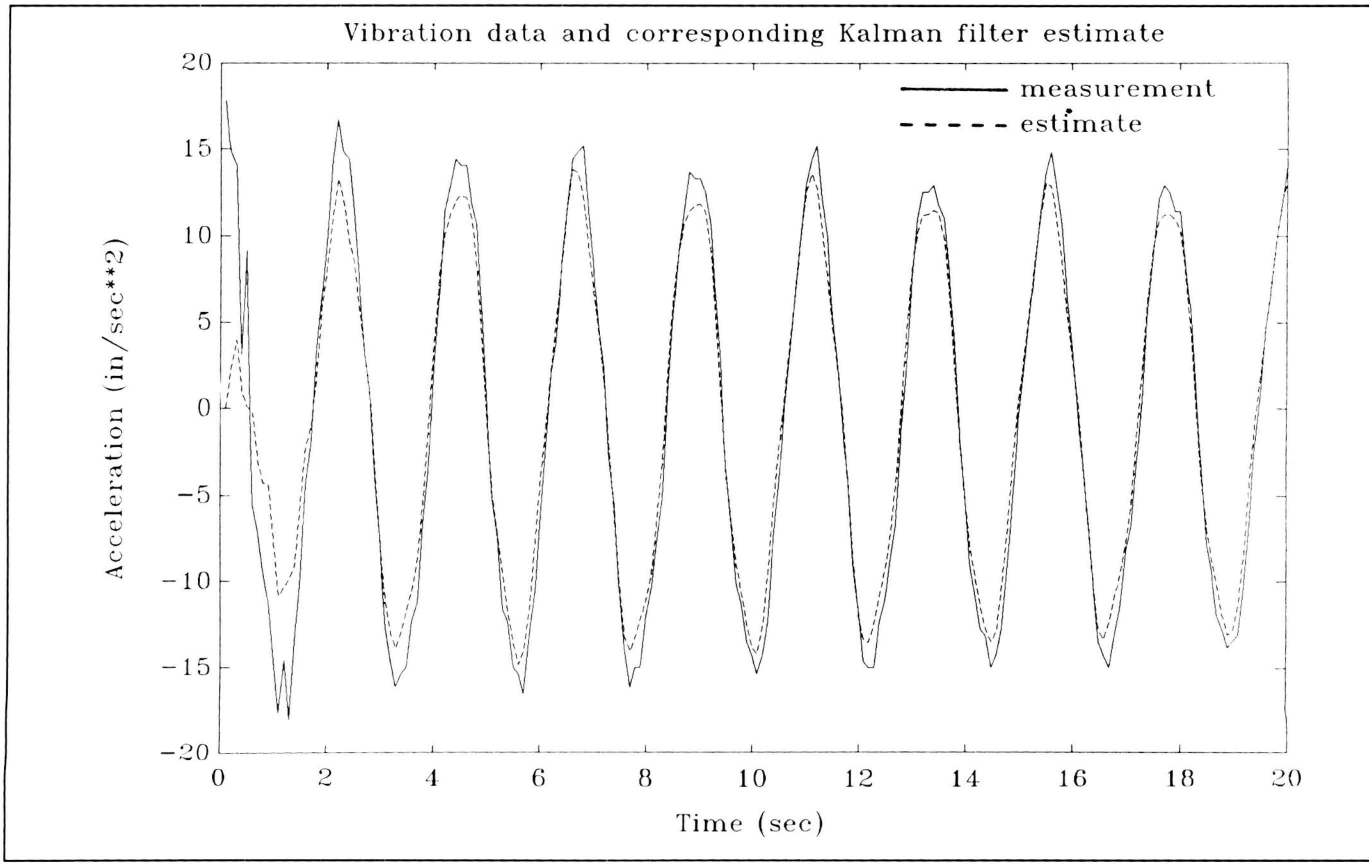

Comparison of actual and estimated accelerometer data.

Kalman Filter Performance Test on SCOLE

Structural dynamics of spacecraft are inherently infinite dimensional whereas the control laws used for maneuvering and vibration suppression are necessarily finite dimensional. Several algorithms have been proposed to take into account the existence of the modes not considered in the control law. SCOLE provides an excellent facility on which the performance of these algorithms can be compared. A test of a Kalman-filter-based algorithm was made with the SCOLE mast in a cantilevered configuration in which the platform rigid-body motion is constrained. The purpose of the test is to examine the performance of a finite-state Kalman filter in a system that possesses an infinite number of modes. Initial results demonstrate close agreement between the Kalman estimate and accelerometer data when only one of the modes that the filter was designed for was excited. These results show that the filtered estimate is adequate when the mode is accounted for in the filter design. Further testing is planned for high-order systems in which multiple modes are excited. Investigations will be conducted to study the effect of a reduced-order filter based on a selected number of modes which may not necessarily be among the group of excited modes.

(D. Ghosh and R. Montgomery, 46615)

Transport Systems Research Vehicle (TSRV) and TSRV Simulator

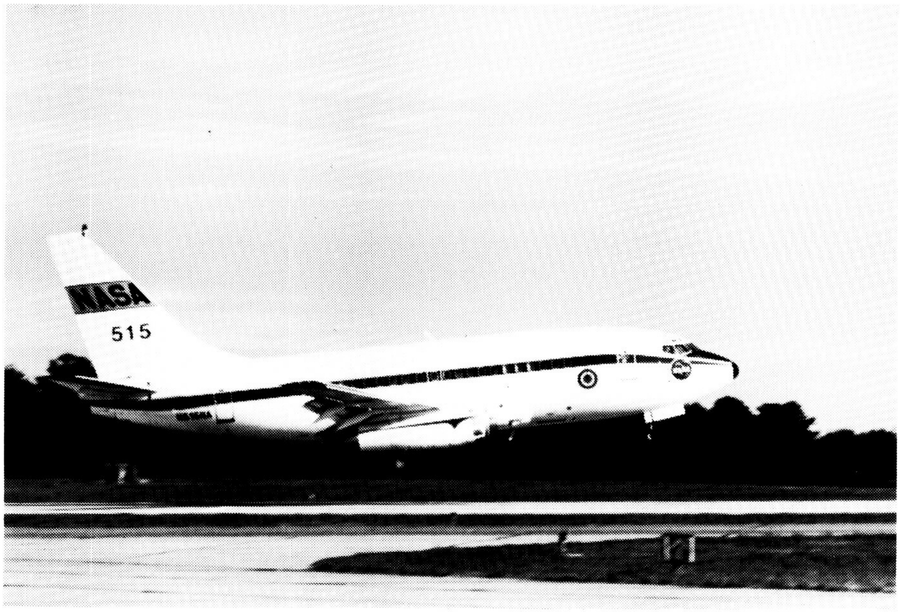

The Transport Systems Research Vehicle (TSRV) and TSRV Simulator are primary research tools used by the Advanced Transport Operating Systems (ATOPS) Program. The goal of the ATOPS Program is to increase the operational capability of modern aircraft and foster their integration into the evolving National Airspace System.

A comprehensive upgrade has been completed on the TSRV, a specially instrumented Boeing 737 airplane. New capabilities include color cockpit displays and advanced experimental avionics.

The TSRV has two flight decks: a conventional Boeing 737 flight deck provides operational support and safety backup, and the fully operational research flight deck, positioned in the aircraft cabin, provides the capability to explore innovations in display formats, contents, and in-aircraft operations.

The "all-glass" research flight deck presents information to the crew via eight newly installed 8-in.-square electronic displays representative of the technology to become available in commercial transports in the 1990's. The state-of-the-art color displays are driven by new, onboard computers and, most importantly, specially developed computer

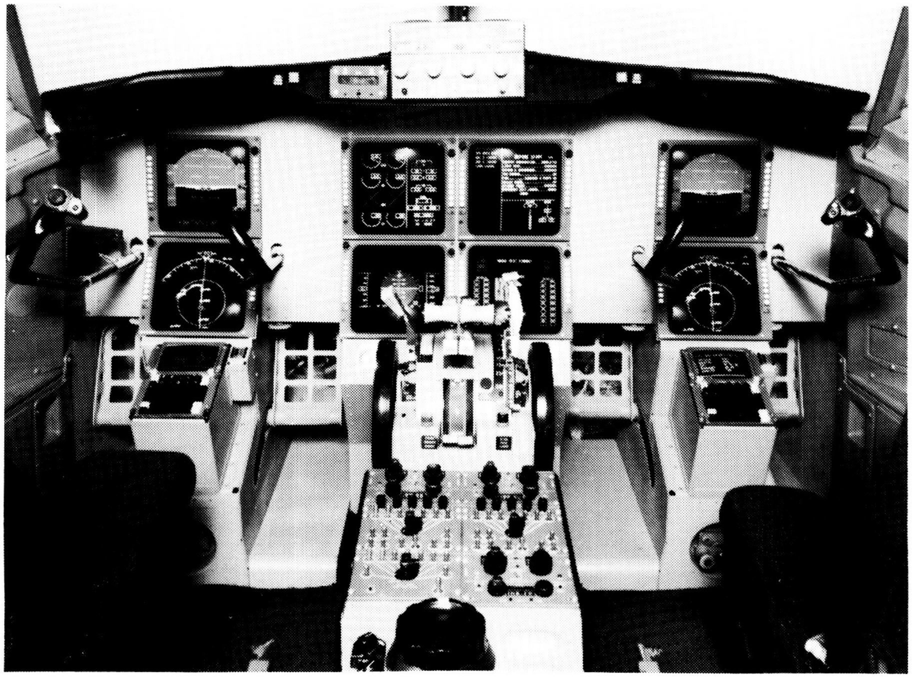

New TSRV aft cockpit configuration. L-87-3645

software. These new technologies make it possible to more clearly display information presented only partially or in scattered locations on existing electromechanical and first-generation electronic displays in today's aircraft.

In addition to video concepts for primary flight and navigation displays in front of both pilot and copilot, center panel displays provide the capability to monitor engine and system status and to manage aircraft systems operation. The center panel displays will permit research on how additional information can be displayed and used to improve situational awareness, air traffic control communications, flight management options, and traffic awareness.

The TSRV Simulator provides the means for ground-based simulation in support of the ATOPS research program. The Simulator, which is also being modified to duplicate the upgraded aft flight deck located in the TSRV, allows proposed concepts in such areas as guidance and control algorithms, new display techniques, operational procedures, and man/machine interfaces to be thoroughly evaluated. Promising simulation research results become the subjects of actual flight test research.

Development of Revised Lateral Control Wheel Steering Algorithm for ATOPS/Boeing 737 Airplane

The purpose of this research was to improve the performance of a baseline lateral control wheel steering (LCWS) algorithm for the ATOPS/Boeing 737 research airplane. The initial task was to use the ATOPS TSRV Simulator package (including the baseline bank-angle-capture LCWS algorithm) and to incorporate three candidate replacement algorithms for comparative analysis with the baseline LCWS. The three candidate algorithms included a modified version of the rate-command/attitude-hold algorithm (with a washed-out bank-angle command feedforward signal to the aileron) developed by Youngstown University; a rate-command/attitude-hold system with a proportional feedforward bank angle signal to the aileron (PFFBA) which was test flown on the ATOPS airplane last year; and a modified version of PFFBA which differs from the second algorithm by the addition of a constant-radius turn and true track-hold capabilities.

The baseline and each of the three revised LCWS algorithms were evaluated on the TSRV Simulator. The third algorithm was subsequently selected for further refinement and detailed pilot evaluation due to its superior

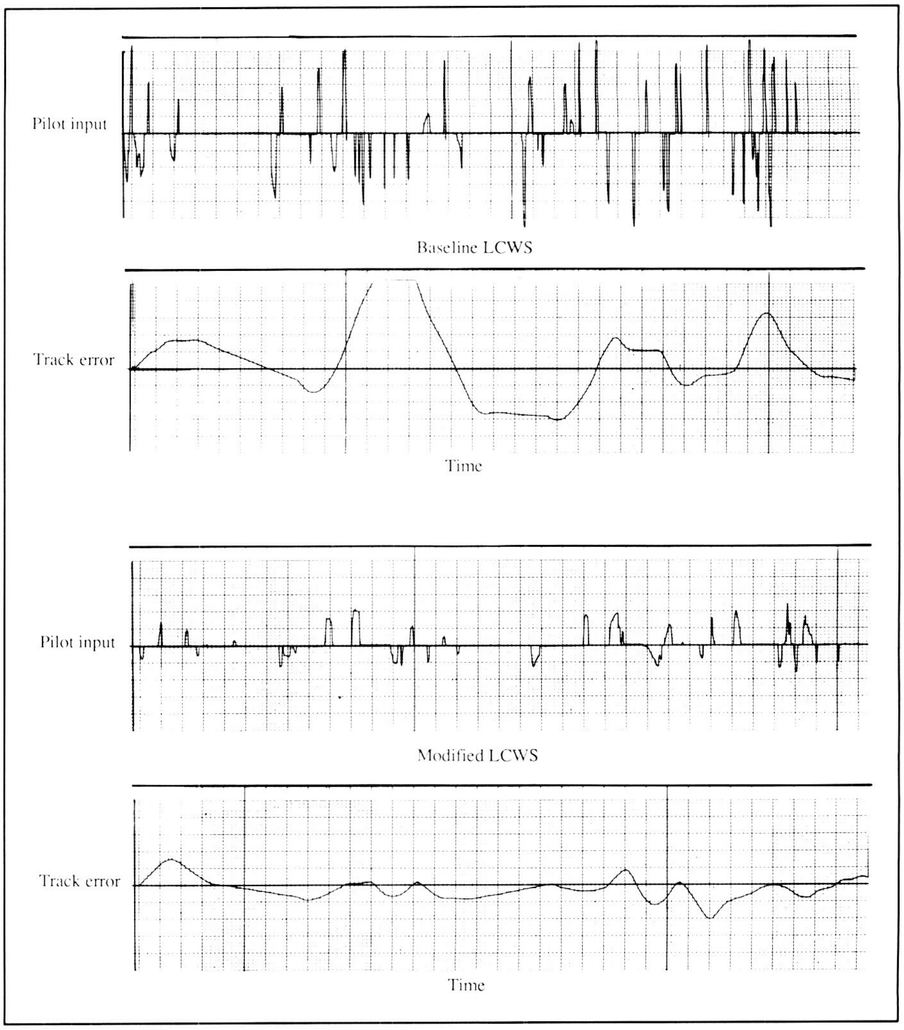

Comparison of pilot work load and performance between baseline and modified LCWS.

performance. These additional refinements included the addition of an improved turn-coordination scheduling algorithm; a revision of the track-hold entry logic (which reduced the wings-level engagement window from 2.5° to 1° and added logic to engage the wings-level mode as a function of roll rate as well as roll angle); and extensive experimentation with inner-loop gains, time constants, side-stick forces and gains, and cockpit display options.

The modified PFFBA LCWS algorithm was evaluated by several pilots. Each pilot suggested modifications that were incorporated and resulted in additional performance improvements. The general consensus is that the present performance of the modified LCWS is, in pilot rating language, very "satisfactory," whereas the performance of the baseline LCWS was very "unsatisfactory." One factor that illustrates this is that the most recent pilot comments are no longer concerned with the control algorithm but rather with how high and low the stick forces should be and what information should be presented on the flight displays.

The example data in the figure compare lateral control inputs and aircraft ground track error between the baseline LCWS and the improved LCWS algorithm for a decelerating, curved approach and landing piloting task. Note that the improved LCWS significantly reduces pilot work load and achieves improved performance.
(W. D. Grantham, 44012)

Flight Test of AI-Based Control Mode Panel Logic

Flight-crucial software for the control mode panel (CMP) of the ATOPS TSRV has been developed with artificial intelli-

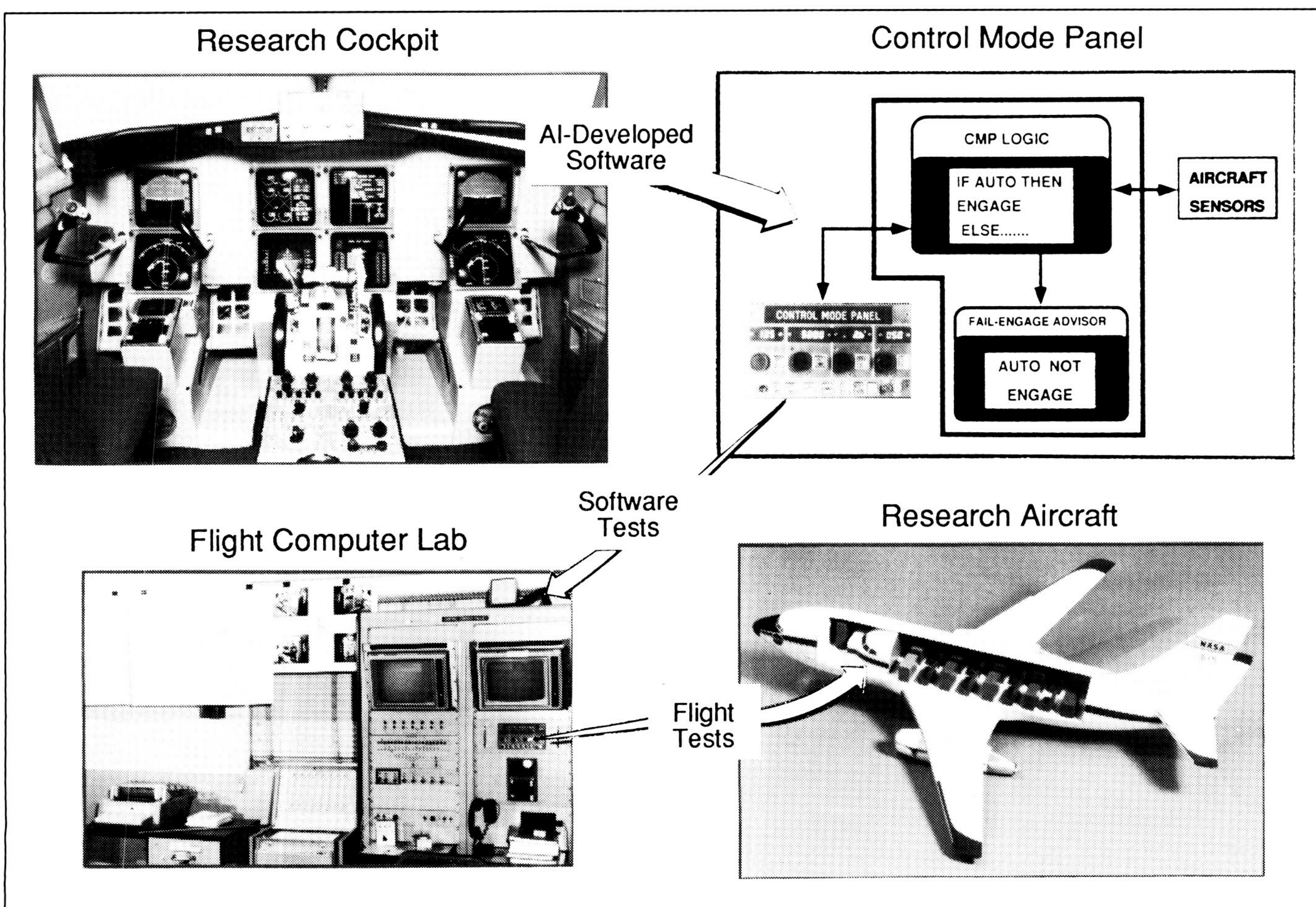

Flight demonstration of artificial intelligence use for aircraft flight systems. L-89-593

gence (AI) programming tools and methods and successfully flight-tested on the TSRV. This software is a complex set of logic which was integrated into the fly-by-wire control system software of the TSRV and interfaced with the CMP, which is mounted in the center of the glare shield of the research cockpit (as shown in the figure). This software receives inputs from the CMP when the pilot pushes buttons and turns knobs on the CMP to select various control modes and to set desired flight parameters of the fly-by-wire control system. In turn, the CMP receives data from the software logic to turn on/off lights within the CMP buttons to provide control system status information for the pilot.

The AI-based CMP logic software was developed on a computer workstation, using the symbolic processing language LISP. This software originated from flow chart documents of the baseline logic, which had originally been developed using conventional programming techniques. The LISP code was subsequently translated to C code for real-time operation and flight testing on the TSRV. A new feature called a Fail-Engage Advisor (FEA), which was also developed with AI methods, generates cathode-ray tube (CRT) messages for the pilot; these messages describe why a mode fails to engage. This feature was recognized as being highly valuable cockpit information and was easily added as a result of the AI-based software structure. This AI implementation effort has shown that AI programming tools have the potential to reduce programming time for logic-intensive functions by an order of magnitude.

Prior to the flight test, the AI-based software was tested in a ground-based flight computer laboratory in the TSRV flight computer to ensure its proper operation (see the figure). The flight test exercised all 11 control modes of the fly-by-wire control system including their submodes of preselect and arming. In the autoland mode, seven submodes were tested; these include the localizer capture and track, glideslope capture and track, decrab, flare, and auto rollout. The FEA was tested for more than a dozen fail-engagement conditions, and proper messages were generated for each condition. In one case of confusion in the research cockpit, the FEA was used to confirm that the localizer was engaged for the autoland control mode by pushing the "Land" button on the CMP and noting the FEA messages (if the localizer had not been engaged, a message "Localizer not engaged" would have been displayed). Being aware that the localizer was engaged permitted continuation of the tasks at hand. No anomalies were observed during the 5 hours of testing.

(R. M. Hueschen, 44036, and J. W. McManus)

Takeoff Performance Monitoring System Flight Tests

The Langley Research Center Takeoff Performance Monitoring System (TOPMS) provides pilots with graphic and numeric information pertinent to their decision to continue or abort a takeoff. This information is conveyed to the pilots by means of electronic screens on the instrument panel. The TOPMS

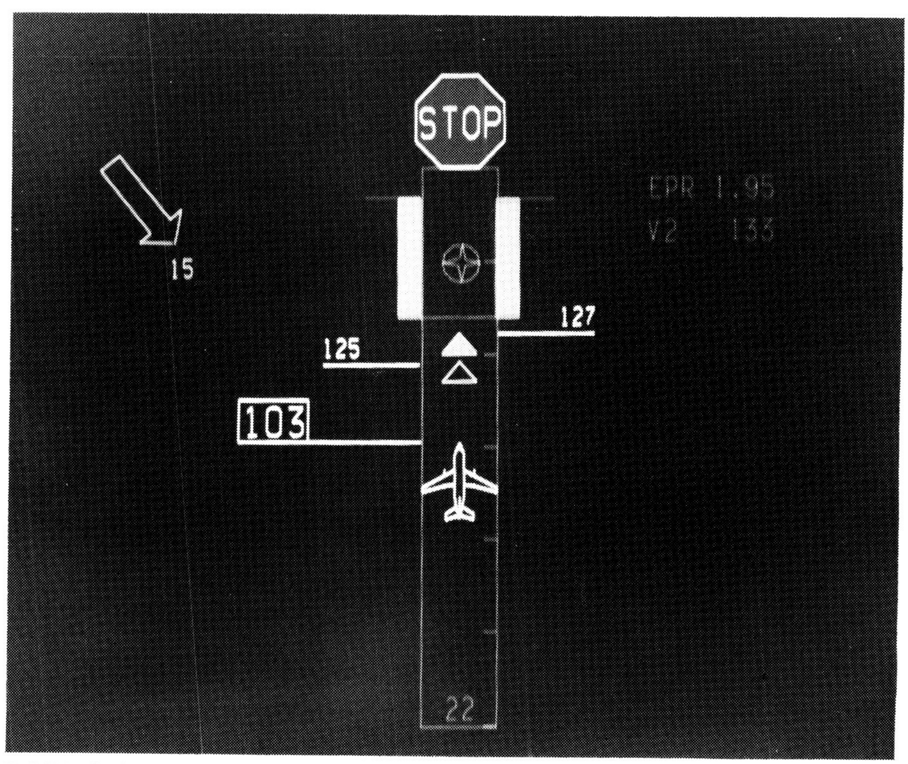

TOPMS flight test display. L-88-07913

has been evaluated on the TSRV Simulator by 41 pilots and was flight-tested during 1988 on the TSRV itself. Basic flight testing was done at the Wallops Flight Facility, high-speed aborts were made at the Space Shuttle landing strip at Kennedy Space Center, and several high-altitude takeoffs were made at the Asheville, North Carolina, airport. The TOPMS performed satisfactorily in all situations.

The figure shows the TOPMS flight test display where the airplane has reached 103 knots; unsatisfactory along-track acceleration has shifted the predicted rotation point (solid triangle) down the runway (the open triangle shows initial prediction). A "Stop" sign has also appeared and has advised an abort. The circled star shows where the airplane can be stopped with maximum braking. The vertical bars indicate that both engine EPR's (engine-pressure-ratios) are at the correct level (1.95); therefore, the problem is apparently drag related (in this flight, fully deployed spoilers during the takeoff roll were used to create this abort condition).

Five different pilots monitored the TOPMS display during the flight tests; all thought it provided useful and credible information. One patent has been issued for the TOPMS; another is pending.
(D. B. Middleton, 44034)

TIMER Simulation and Flight Evaluations to Improve Airport IFR Capacity

The objectives of this research are to define, develop, and evaluate evolutionary ATC (air traffic control) concepts that employ automation aids which would improve the capacity, reliability, and economy of extended terminal flow operations (en route approach, transition, and terminal flight to the runway) when used with projected ground and avionic hardware. The evolutionary system must accommodate current and future advanced-technology aircraft. A time-based concept called TIMER (Traffic Intelligence for the Management of Efficient Runway-scheduling) has been developed which integrates en route flow control, runway scheduling, and spacing, together with fuel saving flight-idle descents to both fully utilize instrument flight rules (IFR) runway capacity and improve fleet efficiency. TIMER was designed for evolutionary integration into today's manual, voiced-linked ATC system by generating suggested speed and vector instructions to assist the controller in delivering non-four-dimensional aircraft at their scheduled times. TIMER was incorporated into the Terminal Area Air Traffic Model (TAATM) for fast-time evaluation. A real-time version was developed and linked with a transport cockpit simulation for crew-in-the-loop, conventional aircraft performance measurement. Verification flight tests were conducted with the ATOPS Boeing 737 flying under TIMER control at Wallops Flight Facility.

Based on results from a fast-time parametric sensitivity evaluation of the TIMER concept to determine the effects of key system variables, real-time simulation tests, using airline crews, were conducted with the full work load DC-9 cockpit simu-

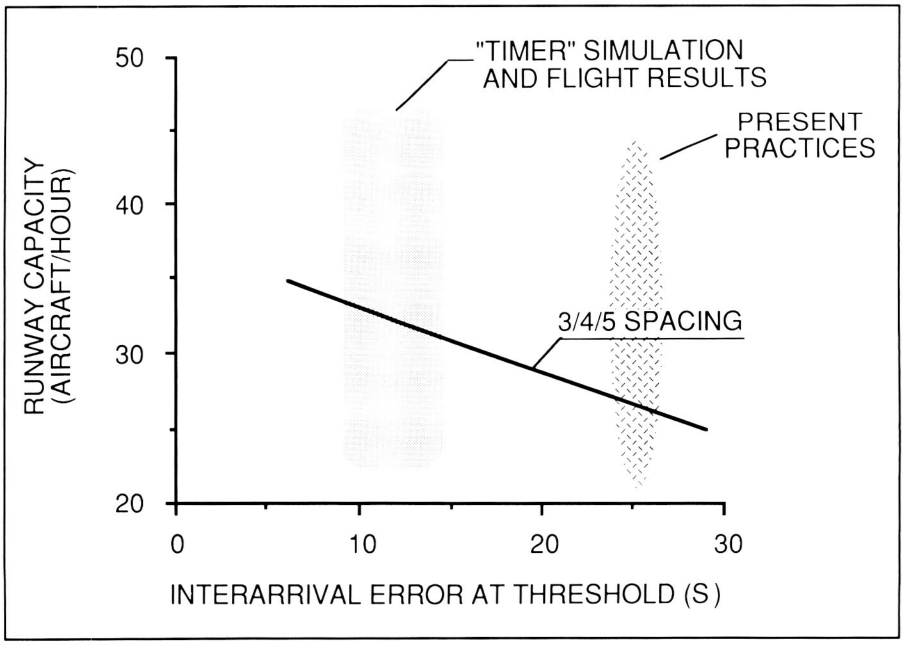

Effect of interarrival error on runway capacity (IFR).

lator and a certified ATC controller. Test results have demonstrated that conventional non-four-dimensional aircraft can be delivered to the runway with an interarrival error standard deviation in the region of 10 s to 15 s. As the figure shows, this translates to approximately an 18-percent arrival capacity improvement over the 26 s achieved in present practice. Flight tests, performed at Wallops Flight Facility, verified these findings by using the forward cockpit of the ATOPS Boeing 737 flying under real-time TIMER control. The simulator and flight test results demonstrate that a significant part of the capacity benefits possible from an extended-terminal time-based ATC flow-control system can be realized before the airline fleet is equipped with four-dimensional flight management systems.
(L. Credeur, 42041)

Requirements for Flying Complex Approach Paths With Advanced Jet-Transport Airplanes Using MLS

As part of the joint Federal Aviation Administration/NASA Microwave Landing System (MLS) Advanced Applications Program, one research objective has been to determine guidance requirements for flying jet-transport-type airplanes equipped with electronic flight displays and advanced flight control systems for manually controlled flight along complex, curved paths. A study has been conducted to determine flight director requirements, electronic map versus standard horizontal situation indicator (HSI) displays, and effects of various path geometries, including length of the final approach segment and consecutive turns.

A real-time piloted simulation was used to evaluate three different guidance display options including flight director (FD) and map display, FD and HSI display, and map display with no FD. Test runs were made along six complex, curved paths with final approach segments between 1.25 nmi and 0.25 nmi. Runs were also made along a standard instrument landing system (ILS) approach so that work load and tracking accuracies between flying complex and conventional straight-in paths could be compared. Airplane state, navigation, control activity data, pilot comments, and pilot instrument scan data were collected. Eight subject pilots (six airline pilots and two NASA pilots) each flew approximately 78 data runs with various wind and moderate turbulence conditions.

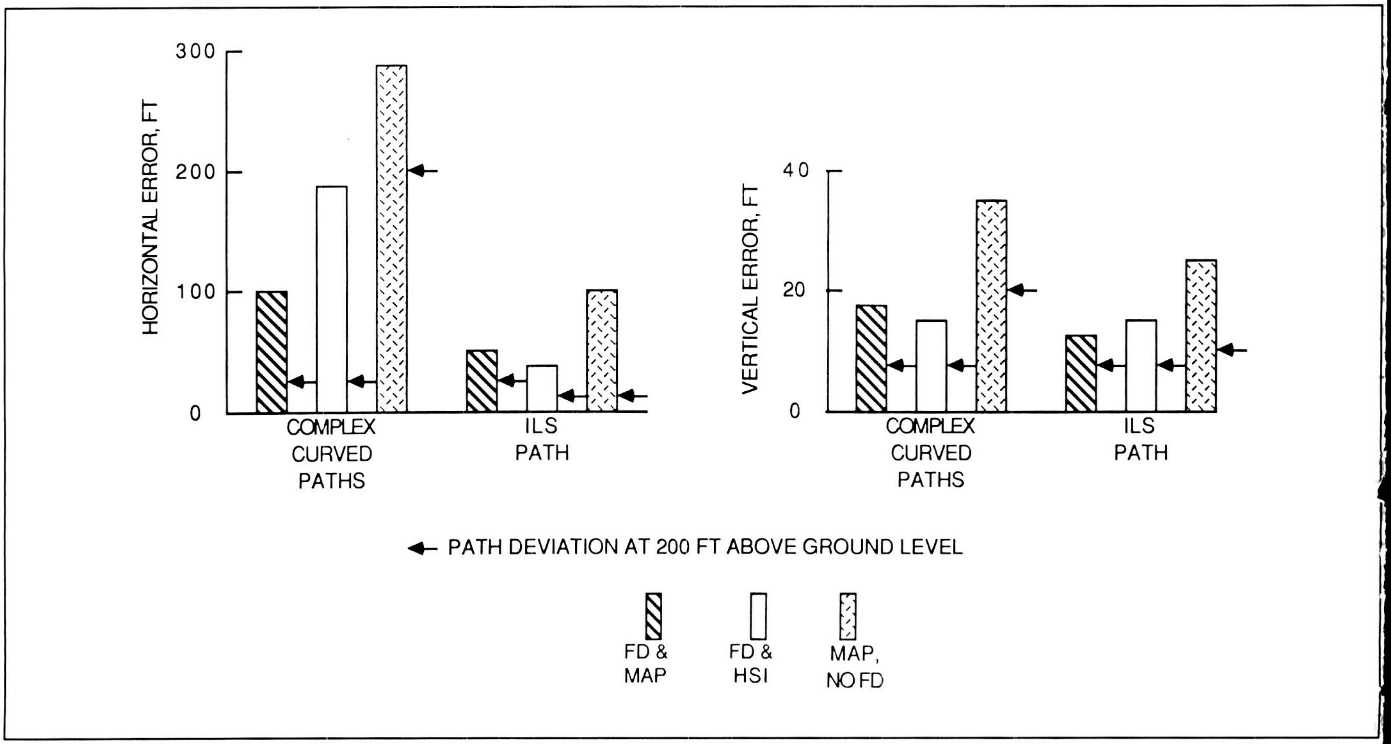

Guidance comparison, path tracking errors (root mean square).

Analysis of the path tracking data (see the figure) along the complex paths indicates that lateral path-tracking performance is slightly improved with the map display versus the HSI display (both using the FD), although tracking accuracy at the decision height (200 ft above the ground where the pilot must land the airplane by looking out the window) is approximately the same. Vertical tracking accuracy was unaffected by the HSI and map display options. Tracking data indicate that the FD is required for precision complex approach paths with low decision heights. While the tasks were more demanding to fly, even the shortest final approach paths were judged, by the subjects, to be acceptable with FD guidance. In addition, although pilot work load is slightly higher for the curved paths as compared to the ILS path, the data and pilot comments indicate these operations are acceptable for normal airline operations. The results of these tests show that airplanes equipped with the proper guidance may be flown on highly complex, curved paths within the MLS signal coverage. This will result in more airplanes attaining the benefits of curved paths including increased airport capacity, safety, and noise abatement capabilities.
(C. E. Knox, 42038)

Documentation of Flow Properties on Fuselage of Transport Airplane

The documentation of flow properties on the fuselage of transport aircraft is important for several reasons. In connection with the drag reduction work at Langley Research Center, extensive information on the fuselage boundary layer has been obtained to help design turbulence manipulators, the so-called large-eddy breakup (LEBU) devices. The upper part of the fuselage of the Boeing 737 (operated under the ATOPS Program) was instrumented, and data were gathered through the entire flight envelope of the aircraft. The data were monitored in a real-time situation through use of the onboard computer systems, thus allowing the implementation of several extra flight conditions when unexpected results were observed.

In the figure, a sample comparison of measured and computed pressure distributions is shown. In general, good agreement was obtained. The measured boundary layer was appreciably thicker than predicted. Spanwise variations of local skin friction indicate that flow disturbances originating in the cockpit window region cause excessive boundary-layer growth downstream along the fuselage. In-flight oil-flow visualization with a video camera mounted in the vertical tail allowed documentation of wall streamlines for a variety of conditions. Cross flow and lateral divergence were monitored.
(A. Bertelrud and R. D. Watson, 45723)

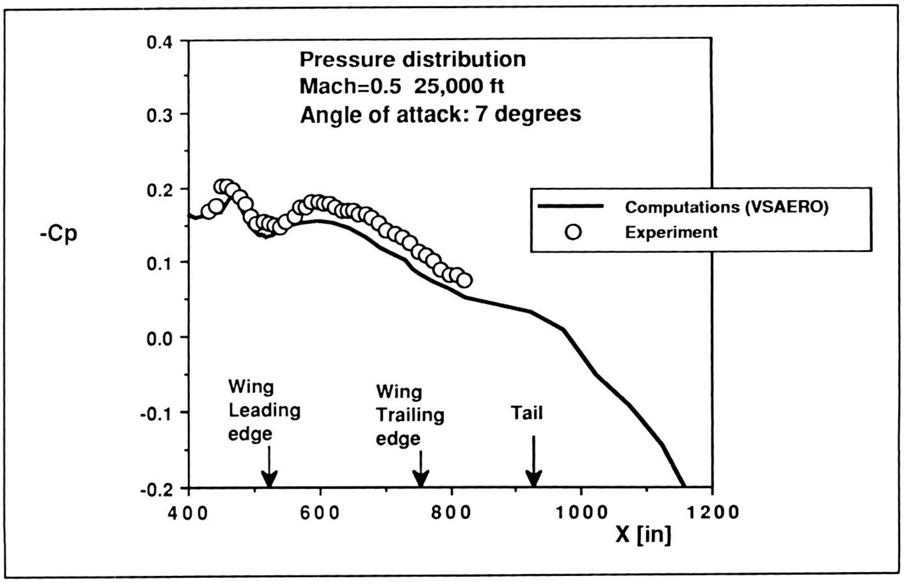

Comparison of measured and computed pressure distributions.

Crew Station Systems Research Laboratory

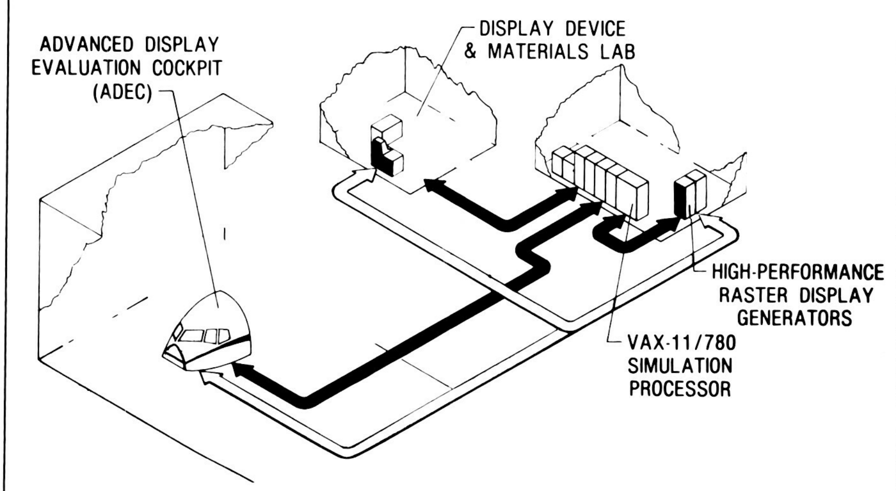

The trend in modern cockpits has been to replace electromechanical instruments with electronic control and display devices. The NASA Crew Station Electronics Technology research program is at the forefront of this trend with research and development activities in the areas of advanced display media, display generation, and cockpit controls/displays/flight subsystems integration. Specific areas of current interest are high-performance stereo pictorial primary flight display graphics; information management techniques; large-screen full-color display media; wide-screen, panoramic display concepts; virtual, panoramic, real-world displays; and image sensor fusion techniques.

The Crew Station Systems Research Laboratory (CSSRL) serves as a primary testing facility for the concepts and devices emerging from this research program. The laboratory provides a unique civil capability to conduct iterative development and pilot/vehicle experimental evaluation research for advanced cockpit technologies in a highly realistic flight simulation environment. The CSSRL also provides a lighting research facility that represents the full range of ambient and solar lighting conditions to be encountered by an aircraft cockpit and allows for the determination of not only the lighting characterizations of cockpit displays but also the determination of pilot/vehicle performance effects under realistic lighting conditions.

Major elements of the CSSRL are the Advanced Display Evaluation Cockpit (ADEC), which is a reconfigurable research cab; the Aircraft Cockpit Ambient Lighting and Solar Simulator (ACALSS), which provides real-world ambient and solar lighting conditions to the ADEC cockpit; and two separate general-purpose digital processors, one of which handles system input/output and vehicle math model simulation, while the other acts as host processor and preprocessor for two graphics generators. Other major elements include three high-performance raster graphics display generators (one of which has its own host co-processor), which provide sophisticated graphics formats to the display devices (cathode-ray tubes, flat panels, helmet-mounted displays); a fiber optic link to the central computing facility, which can provide high-fidelity simulation math models for research requiring more complex vehicles; and a Display Device and Materials Laboratory, which provides facilities for flat-panel materials/device technology developments and photometric bench evaluations.

Evaluation of I/O Devices for Management of Large-Screen Displays

The rapidly expanding application of digital systems to avionic functions provides more operational capability to the transport aircraft crew. This added capability, however, also provides more information to be displayed and managed within the limited confines of the cockpit environment. An approach to displaying and managing this information is being investigated at Langley Research Center. This approach involves a large-screen, multiwindow, whole-flight-deck display concept. To efficiently interact with such a display concept, user-friendly interface methods must be utilized. The goal of this effort has been to compare three different input/output (I/O) technologies as interface methods to a whole-flight-deck display by collecting objective and subjective data in a simulator.

Three I/O technologies that were utilized include a multifunction control throttle and stick (MCTAS) concept, a thumb-ball concept, and a touch-screen concept (shown in the first figure). The MCTAS concept incorporated a throttle switch and hand-controller buttons. The switch located in the throttle handle was used for cursor movement and numerical changes. The thumb-ball concept was similar to the MCTAS system, except cursor movements and numerical changes were made through a miniature trackball embedded in the hand controller. The touch-screen concept utilized a capacitive screen for pilot inputs.

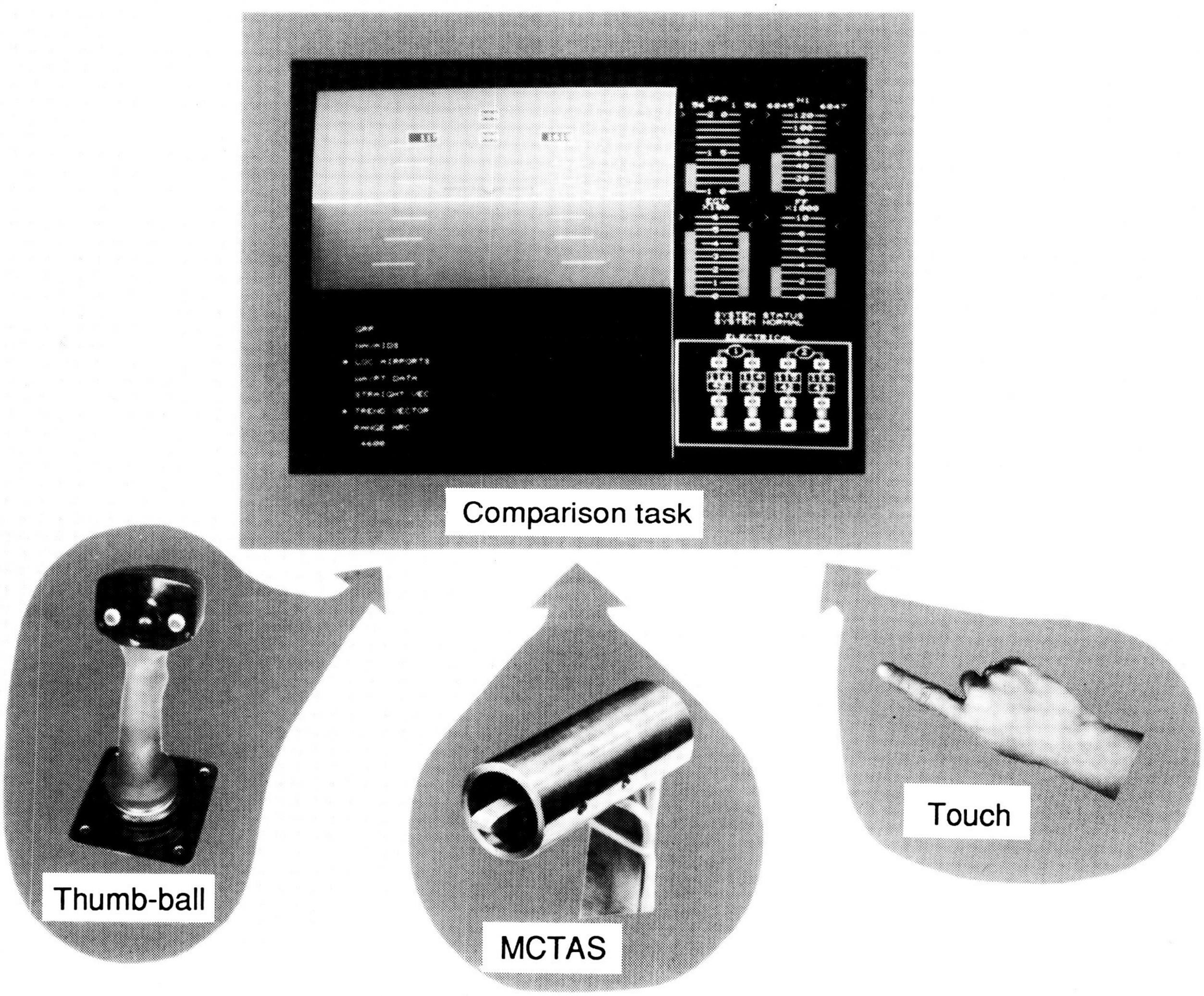

I/O devices evaluated in study on interactive management of large-screen display concept. L-88-7172

Completion times for five pilots for various tasks were collected in a simulated transport environment for each concept.

Objective and subjective results indicated the thumb-ball concept was the most efficient and user-friendly interface for the present implementations. Pilots noted it was desirable to operate all aspects of the pilot interface from the hand controller by using one hand. This action freed the second hand for other tasks and helped reduce pilot work load. Favorable reactions to all three I/O devices, with suggestions for improved implementations, were expressed. In general, the large-screen whole-flight-deck display concept, interfaced with an effective multifunction control concept, was seen as a promising method for managing aircraft systems. Not unexpectedly, the completion time differences between the three interfaces varied with the task being performed, although the thumb-ball implementation consistently performed better than the other two concepts (as shown in the second figure).

(D. R. Jones, 42006, and R. V. Parrish)

Effectiveness of Stereo and Pathway Cues in 3-D Primary Flight Display

Recent advances in liquid-crystal shuttered stereo viewing systems, coupled with high-performance computer graphics, have made possible the generation of integrated, three-dimensional (3-D) pictorial flight displays having a unique depth cue, called stereopsis. Exploitation of that technology provided the basis for this research in the form of a stereo 3-D real-world flight display having, as primary features, curved "pathway-in-the-sky" and "follow-me" aircraft symbols designed for curved approach-to-landing piloting tasks. The overall goal of this research was to achieve situation-at-a-glance pilot awareness; the specific goals were to determine the value of stereopsis and pathway cues for flight control.

Control reaction times provided a primary assessment criterion in an eight-pilot simulation study. The use of stereo 3-D capability was hypothesized to de-

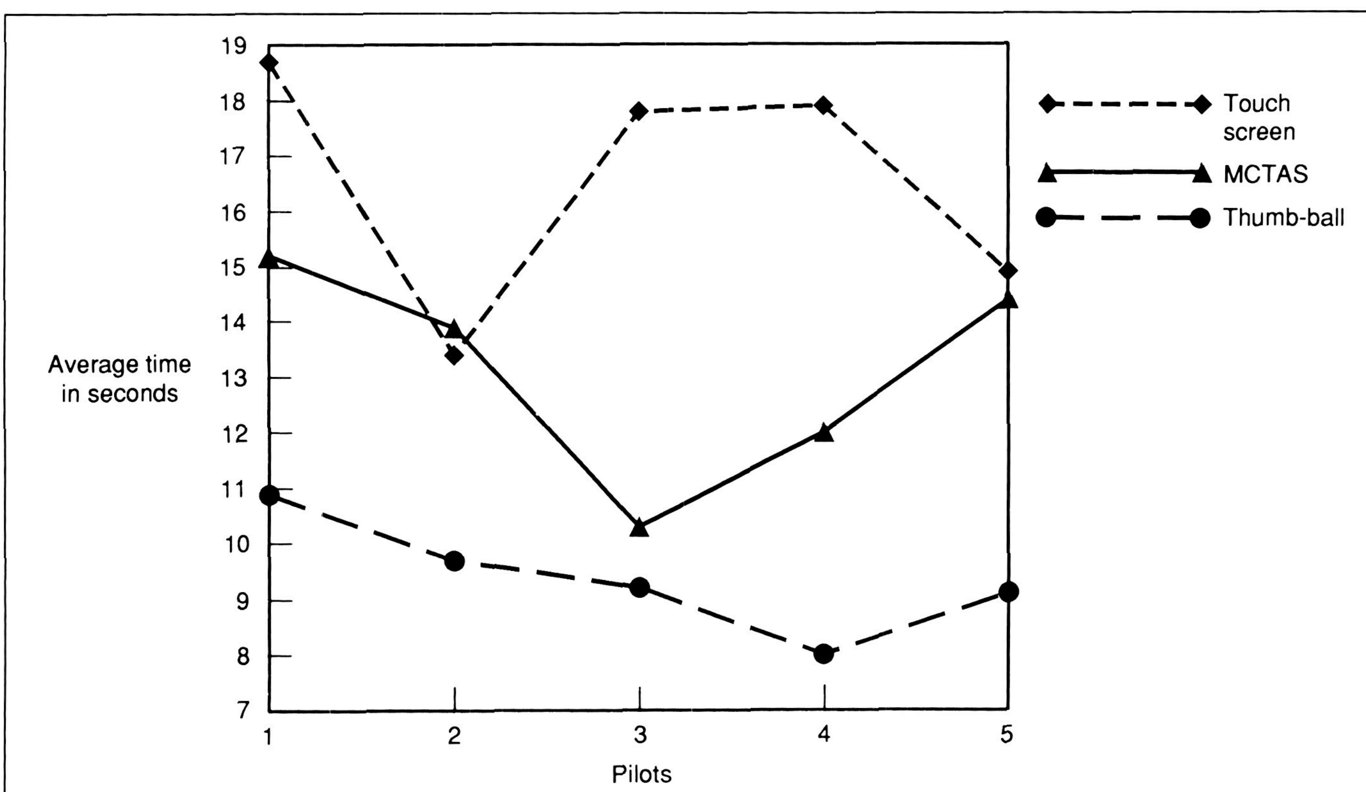

Completion times of various tasks for three I/O devices for each pilot.

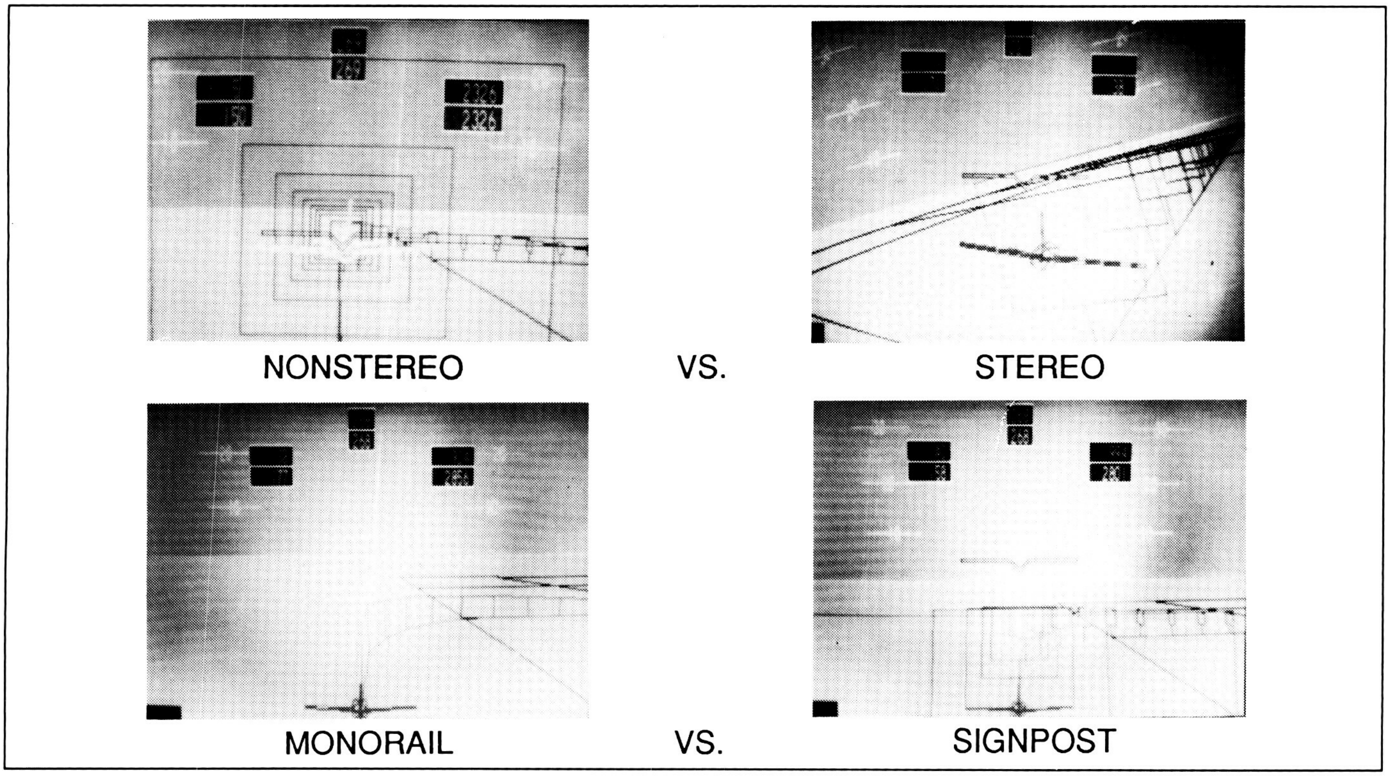

Stereo 3-D pictorial flight display study: recovery from flight path offset. L-88-12124

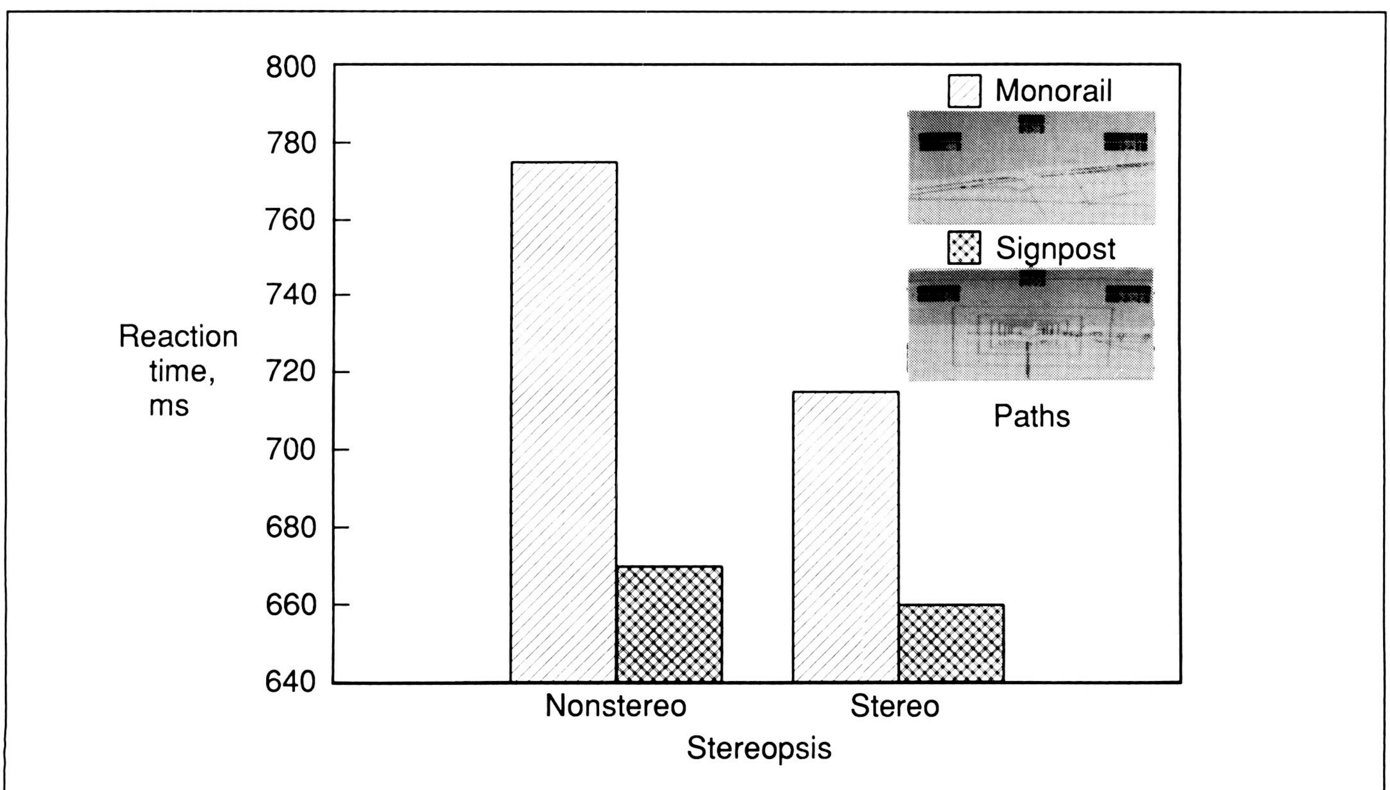

Effect of stereopsis and pathway type on pilot reaction time.

crease reaction time in correcting a flight path offset. Two pathways, a monorail and a signpost (as shown in the first figure) were used. At the start of each trial, the pilots were initiated on the nominal flight path. After 2 s, the pilots were offset to one of eight positions. As soon as the pilots detected an offset, they were required to make the initial stick input to fly toward the nominal flight path. After their initial input, the trial was ended.

Pilots responded more quickly when the display was presented in stereo 3-D than when a monocular (i.e., nonstereo) display was presented (as shown in the second figure), indicating improved situational awareness with stereo. The average reaction time was 690 ms for stereo display versus 725 ms for the nonstereo display. The responses to the signpost pathway were significantly faster than were the responses to the monorail pathway (665 ms versus 750 ms, respectively). The second figure shows that the difference in reaction times between the signpost and monorail pathways was much greater when the nonstereo display was used instead of stereo 3-D. This means that it is potentially more critical for designers of nonstereo pictorial displays to carefully evaluate the effectiveness of their pathway cues. Further, the pilots were able to respond faster when the "follow-me" aircraft was displayed than when it was not (695 ms versus 720 ms).
(M. Nataupsky, 42001)

Human Engineering Methods Laboratory

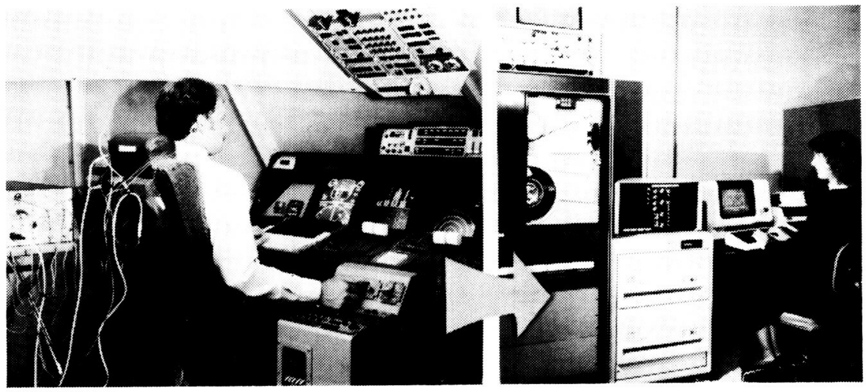

Simulator with Bioinstrumentation   Data Acquisition & Analysis

The Human Engineering Methods (HEM) Laboratory has been established to develop measurement technology to assess the effects of advanced crew station concepts on the crew's ability to function without mental overload, excessive stress, or fatigue. The laboratory provides the capability for measurement of behavioral and psychophysiological response of the flight deck crew.

The facility comprises state-of-the-art bioinstrumentation as well as computer-based physiological data acquisition, analysis and display, and experiment control capability. Software has been developed which enables the demonstration of work load effects on the steady-state evoked brain response and transient evoked response signals as well as the monitoring of electrocardiographic (EKG), electromyographic (EMG), skin temperature, respiration, and electrodermal activity.

The Langley Research Center-developed oculometer capability has been integrated with the other physiological measurement techniques. Subjective rating and secondary task methods for assessing mental work load have also been implemented. A computer-based criterion task battery is available for preliminary testing (with human subjects) of work load techniques that are being validated prior to evaluation and application in the simulators. Satellite physiological signal conditioning and behavioral response capture stations are located at the simulator sites to provide human response measurement support for flight management and operations research.

Indication of Operator Boredom Mental State by Physiological Measures

The safety of crew/vehicle systems may be threatened as increased automation changes the role of the pilot from controller to monitor, producing a mental state such as boredom. This state can be exacerbated by long-duration missions such as transoceanic flights. The goal of this research is to detect the mental state of the pilot which may lead to performance degradation and, then, to intervene to restore acceptable performance. The first step was to establish the sensitivity of physiological measures to serve as parameters of a boredom detection model.

The study was designed to establish the sensitivity of electrocardiogram, electroencephalogram (EEG), and pupil diameter (PD) measures to operator mental state. An underload condition was created by having subjects perform a fault-acknowledgment task having repetitive responses with minimal novelty, complexity, and uncertainty. This task consisted of monitoring faults presented on a jet engine pictorial and acknowledging the fault with minimal response time. Performance parameters included response time and response accuracy. Physiological measures were monitored over a 1-hour test session for each of 11 subjects.

C-2

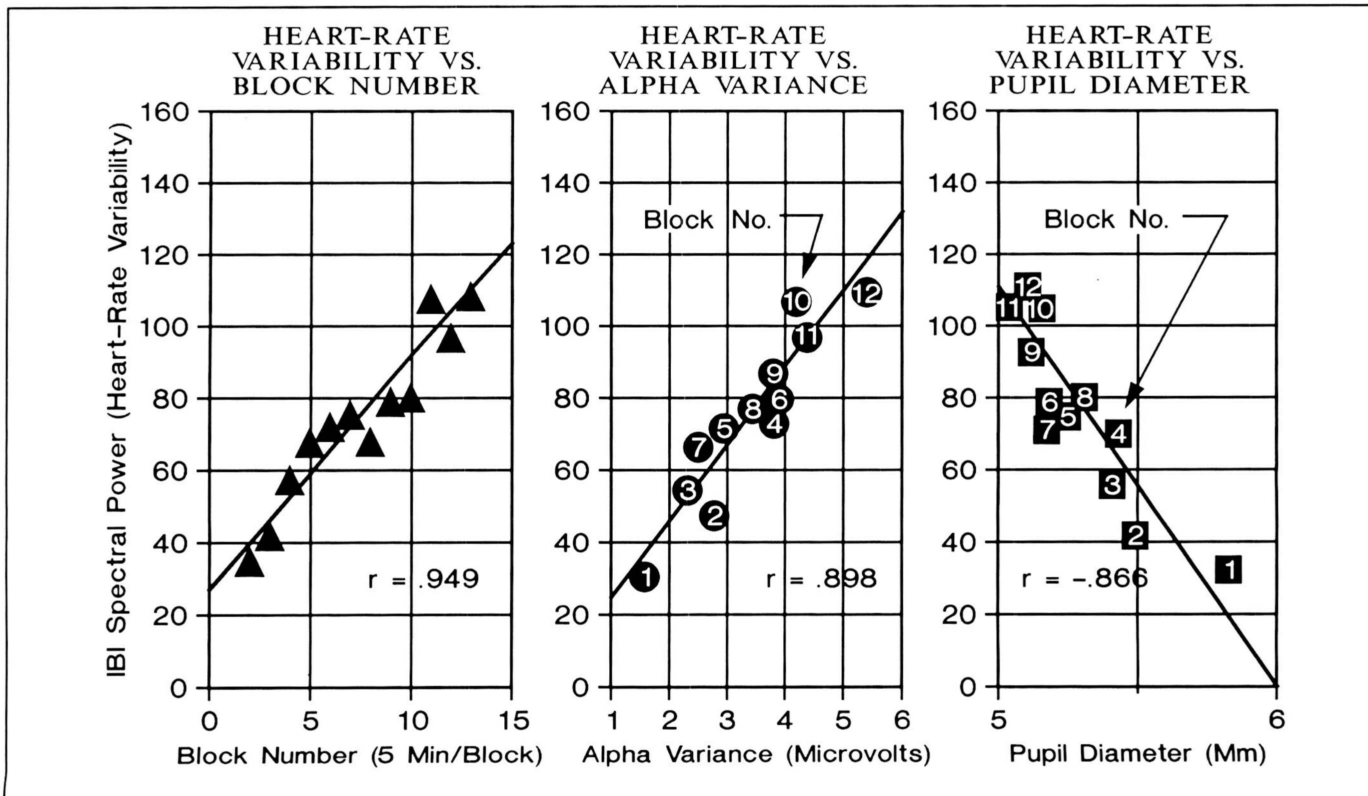

Averaged data (from 11 subjects) which show correlation of three physiological measures.

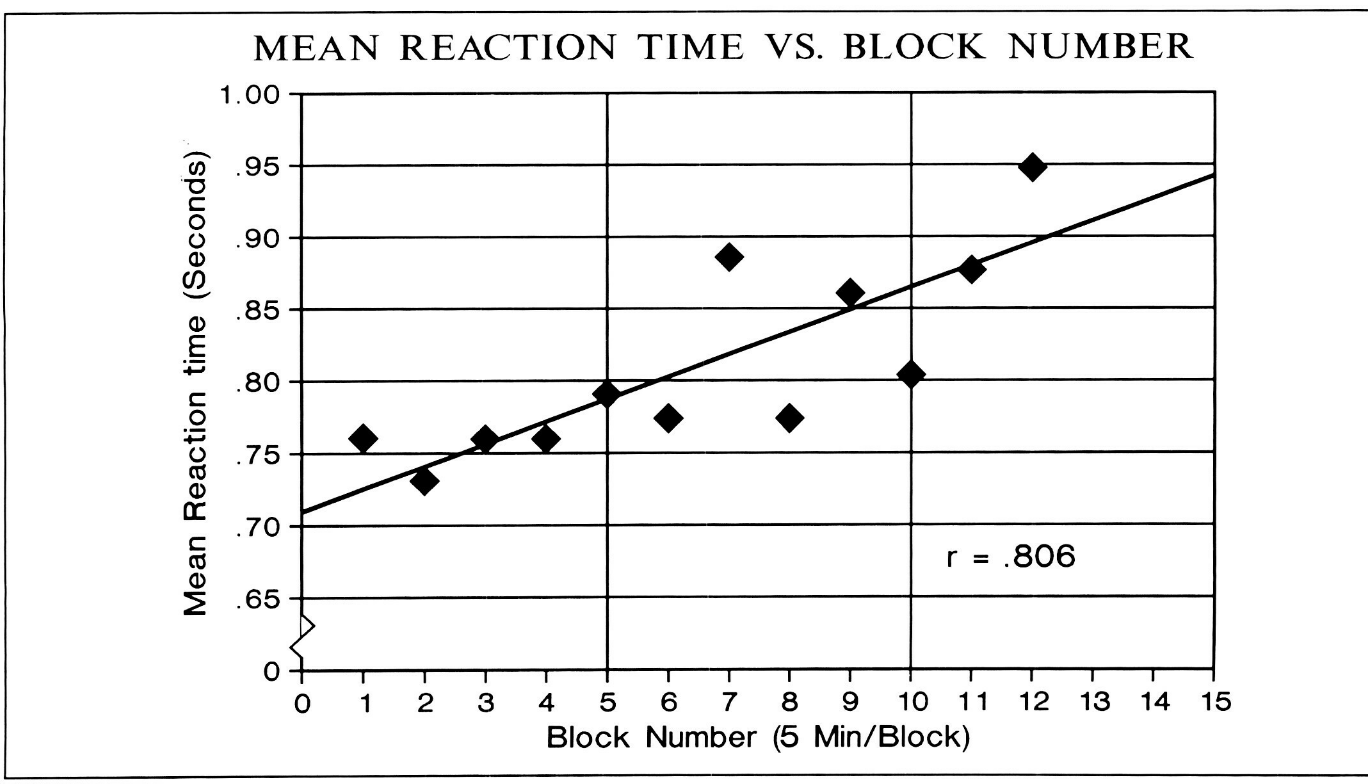

Averaged data (from 11 subjects) which show decrement in underload task performance.

Heart rate variability (HRV), alpha variance (EEG component), and PD exhibited changes indicative of boredom (see the first figure). This figure shows HRV versus test session block number. Correlations among heart rate variability, alpha variance, and pupil diameter, with block number, were high (0.949, 0.855, and −0.864, respectively). The figure also shows high correlations between heart rate variability and alpha variance (r = 0.898) and heart rate variability and pupil diameter ($r = -0.866$). The results demonstrate high sensitivity of physiological measures to a laboratory underload situation and provide parameters for a boredom detection model. A surprising result (shown in the second figure) was the deterioration of subject performance (increased reaction time) with block number ($r = 0.806$). The correlation of reaction time with heart rate variability, alpha variance, and PD was 0.675, 0.613, and −0.638, respectively, which provides encouragement that the boredom detection model could detect the onset of boredom and, thereby, predict a consequent deterioration in human performance.
(J. R. Comstock, Jr., 46643, R. L. Harris, and A. T. Pope)

General Aviation Simulator

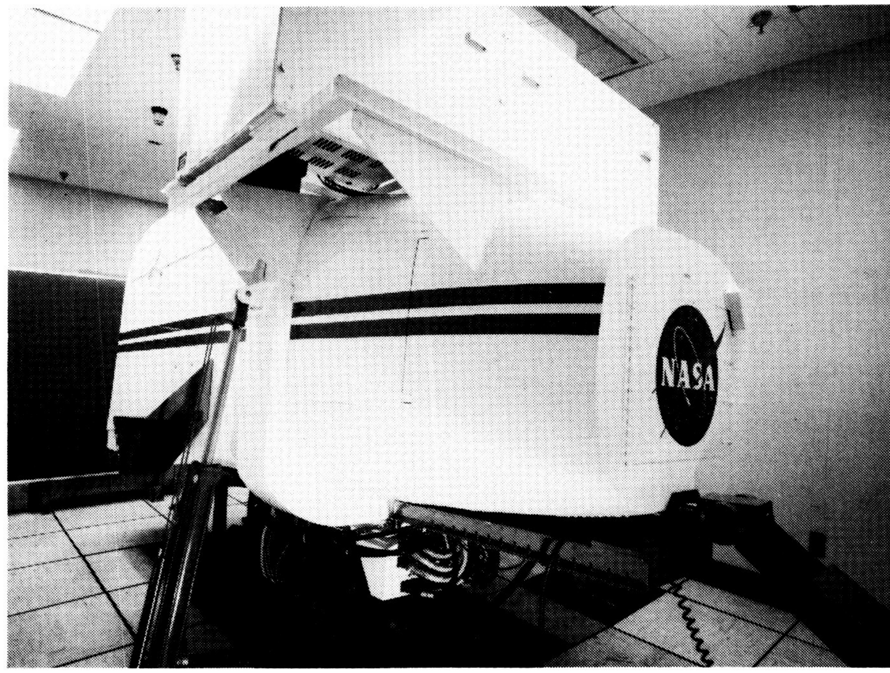

The General Aviation Simulator (GAS) consists of a general-aviation aircraft cockpit mounted on a three-degree-of-freedom motion platform. The cockpit is a reproduction of a twin-engine propeller-driven general-aviation aircraft with a full complement of instruments, controls, and switches, including radio navigation equipment. Programmable control force feel is provided by a "through-the-panel" two-axis controller that can be removed and replaced with a two-axis side-stick controller that can be mounted in the pilot's left-hand, center, or right-hand position. A variable-force-feel system is also provided for the rudder pedals. The pilot's instrument panel can be configured with various combinations of cathode-ray tube (CRT) displays and conventional instruments to represent aircraft such as the Cessna 172, Cherokee 180, and Cessna 402B. A collimated-image visual system provides a 60° field-of-view out-the-window color display. The visual system can accept inputs from a terrain model board system and a computer-generated graphics system. The simulator is flown in real time with a CDC CYBER 175 computer to simulate aircraft dynamics.

Research conducted in the GAS on the single-pilot instrument flight rules (SPIFR) has identified the pilot interface with cockpit controls and displays as a critical factor in reducing pilot work load and blunders. A research program was conducted to evaluate the impact of various levels of data link capability on general-aviation (GA) SPIFR operations. The levels tested varied from uplink only of short air traffic control (ATC) messages to uplink and downlink of complex messages. Another research application using the GAS has been the investigation of flight control problems encountered in recovering a twin-engine GA aircraft to normal flight after one engine fails.

Research has been conducted to improve the ride quality of GA aircraft by developing gust alleviation control laws to reduce the aircraft response to turbulence while still maintaining generally good flying characteristics. A research study under way is the GA Easy Fly, a program to investigate ways of making general-aviation airplanes easier to fly, especially for low-time or nonpilots.

Easy-to-fly general-aviation airplanes.

New control and display concepts are being developed and tested for the nonprofessional general-aviation pilot. A variety of control systems were tested using the General Aviation Simulator, but the most promising system employed a decoupled flight vector control system. This system combined the features

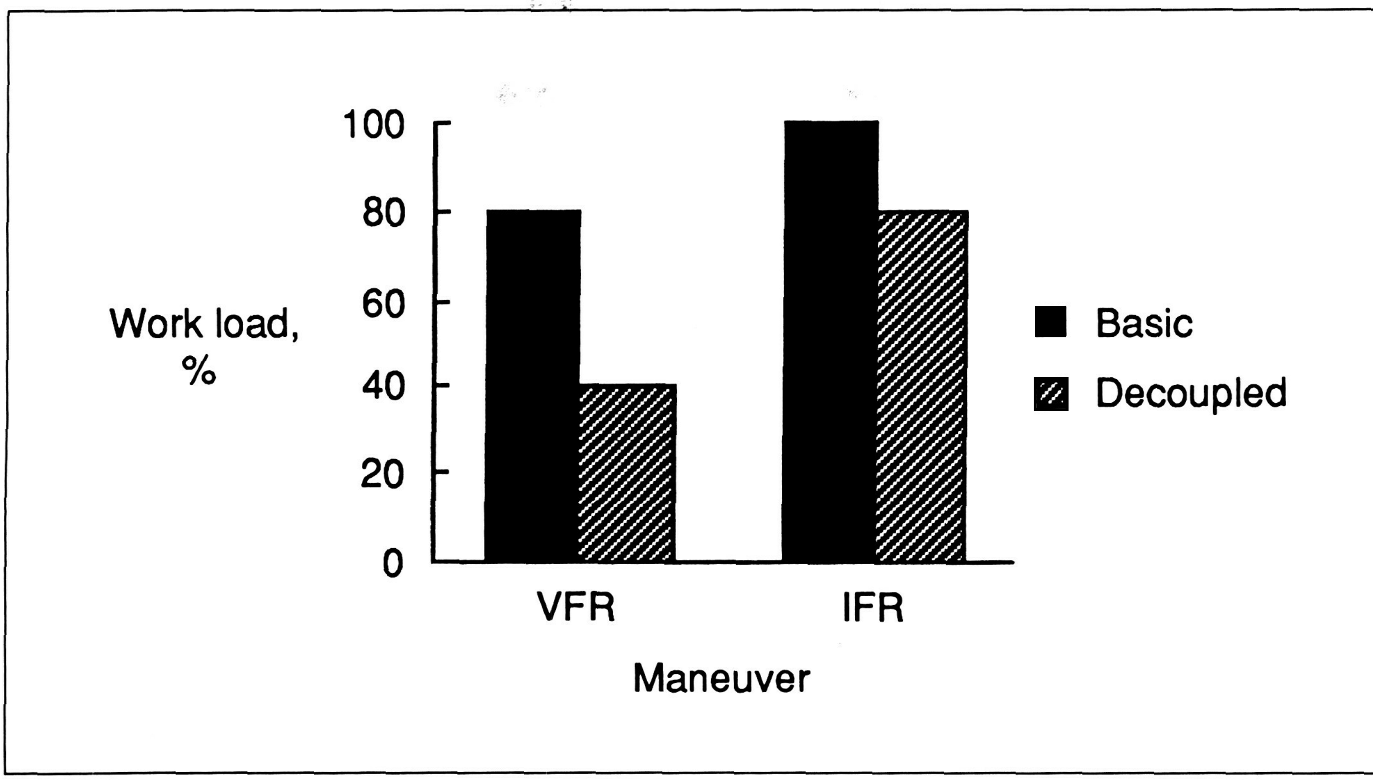

Reduction of pilot work load with decoupled flight vector control system.

found in existing general-aviation autopilot and autothrottle technology in an easy-to-use configuration. The throttle levers commanded the airspeed, the longitudinal wheel commanded the vertical speed, and the lateral wheel commanded the direction of flight. This system was highly beneficial for both nonprofessional and professional pilots and reduced the pilot work load significantly in both good-visibility visual flight rules (VFR) operations, and poor-visibility instrument flight rules (IFR) operations, as shown in the figure. Full-mission flight maneuvers including takeoffs and landings were not only easier to fly but also safer to fly because of the automatic stall deterrence capabilities of the decoupled flight vector control system.

Preliminary tests of an advanced display for use with the decoupled flight vector control system are presently under way. This head-up display uses a computer-generated pictorial view of a "highway in the sky," which the pilot can easily follow with the decoupled control system. The display and control system are designed to maximize the transfer of ordinary driving skills to the operation of a small airplane with the ultimate goal of reducing initial training and proficiency requirements. Except for following the altitude changes of the "highway in the sky," the pilot's simulation task in flight is similar to driving a car with a cruise control.

(E. C. Stewart, 43939)

Differential Maneuvering Simulator

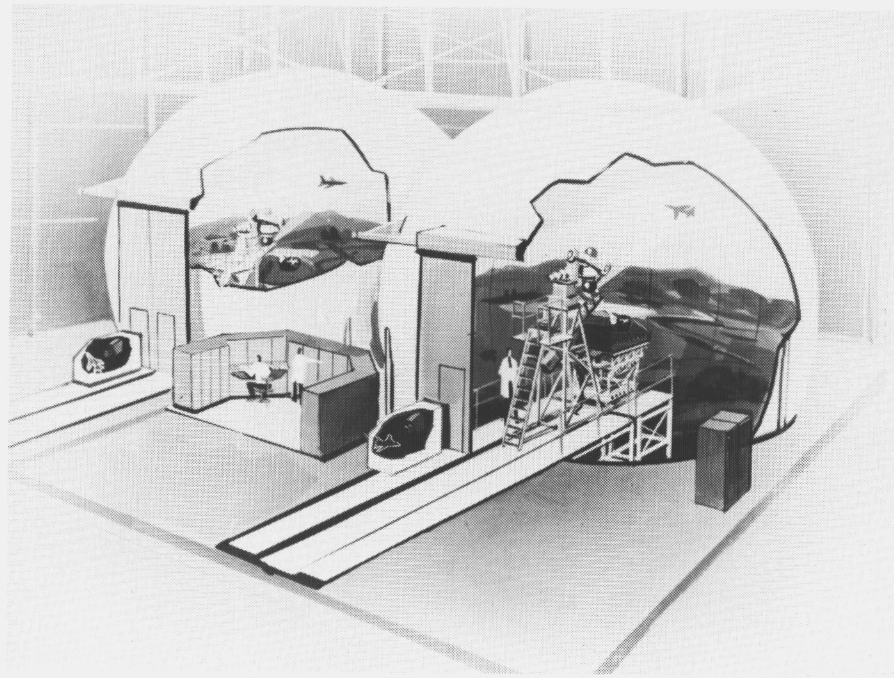

The Langley Differential Maneuvering Simulator (DMS) provides a means of simulating two piloted aircraft operating in a differential mode with a realistic cockpit environment and a wide-angle external visual scene for each of the two pilots. The system consists of two identical fixed-based cockpits and projection systems, each based in a 12.2-m-diameter (40-ft) projection sphere. Each projection system consists of a sky/Earth projector to provide a horizon reference and a system for target image generation and projection. The internal sky/Earth scene provides reference in all three rotational degrees of freedom in a manner that allows unrestricted aircraft motions. The present sky/Earth scene has no translational motion. The internal visual scene also provides continuous rotational and bounded (300 ft to 45,000 ft) translational reference to a second (target) vehicle in six degrees of freedom. The target image presented to each pilot represents the aircraft being flown by the other pilot in this dual simulator. Each cockpit provides three color displays with a 6.5-in. square viewing area and a wide-angle head-up display. Kinesthetic cues in the form of a g-suit pressurization system, helmet loader system, g-seat system, cockpit buffet, and programmable control forces are provided to the

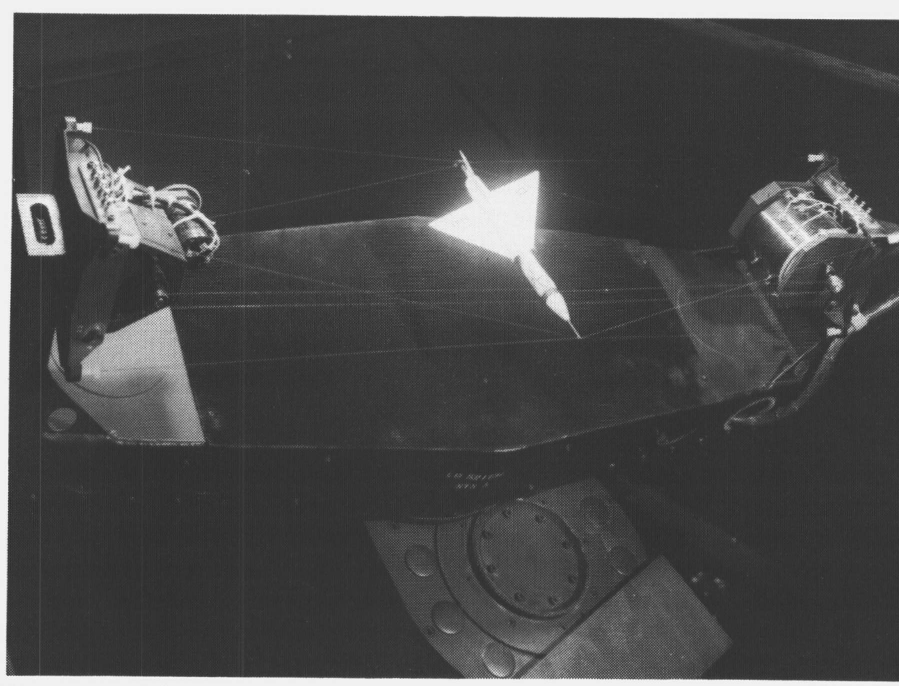

Target model. L-71-2579

pilots consistent with the motions of their aircraft. Other controls include a side arm controller, dual throttles, and a rotorcraft collective. Research applications include studies of high-angle-of-attack flight control laws, evaluation of evasive maneuvers for various aircraft and rotorcraft, and evaluations of the effect of parameter changes on the performance of several baseline aircraft.

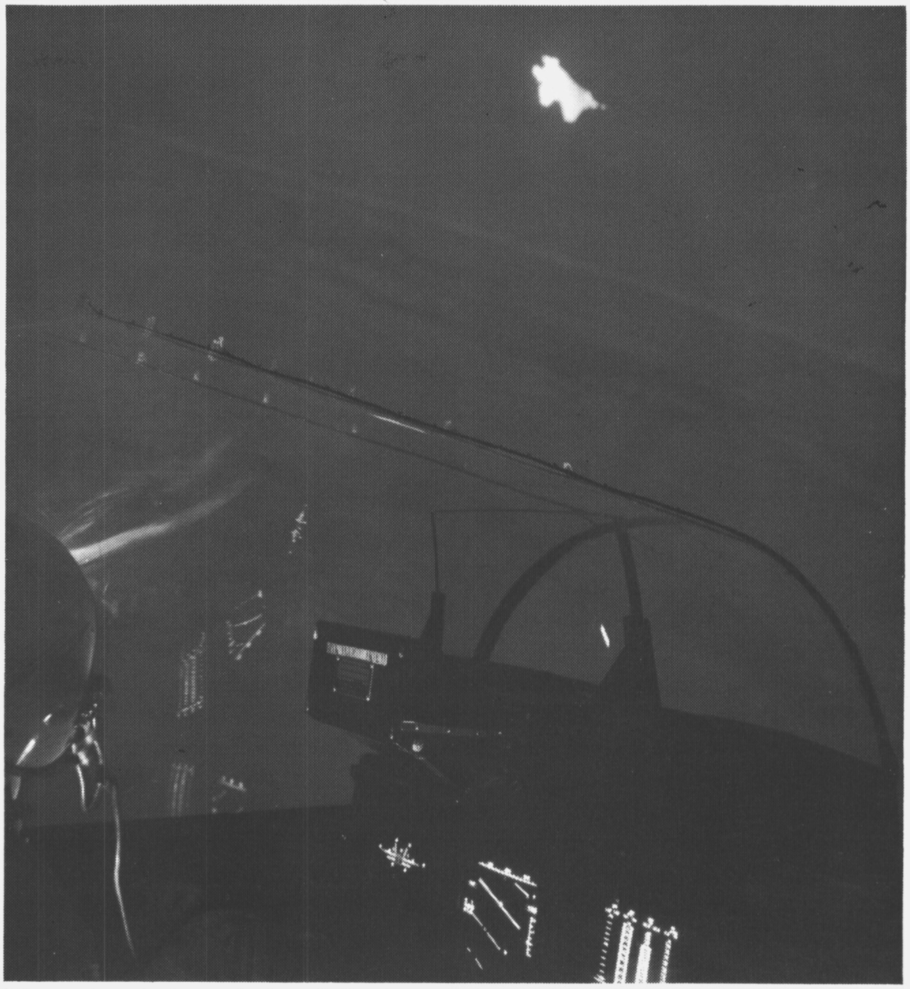

View of cockpit and visual display. L-87-8822

Advanced Aerodynamic Controls Research

The importance of providing future fighter aircraft with the ability to rapidly maneuver throughout their flight envelope has been shown in numerous air combat studies. A maneuvering limitation that is typical of current combat aircraft is the inability to produce rapid coordinated roll motions at high angles of attack. This capability can be achieved through the use of advanced control concepts that provide significant improvements in yaw control effectiveness. One such concept is deflectable forebody strakes. By manipulating the strong forebody vortical flows, these devices can produce effective yaw control at high angles of attack where conventional rudders offer little or no effectiveness.

Piloted simulator studies on the DMS are being conducted to investigate the benefits of this concept in a realistic combat maneuvering environment. The primary objectives of these simulation studies are to evaluate the enhancements in maneuvering capability provided by the deflectable strakes and to define the flight-control-law requirements to maximize these benefits. A full-envelope simulation model of the F-18 airplane is being used in these investigations. Using wind tunnel data, the aerodynamic effects of the deflectable forebody strakes were added to this baseline simulation model, and the control laws were tailored to take into account the specific aerodynamic characteristics of these devices. The results show that these devices can provide significant roll rate improvements, particularly at higher speed and angle-of-attack conditions at which rapid roll capability is especially advantageous in air combat. The results of these simulation studies combined with those from other ground-based tests will lead ultimately to a full-scale flight test of this concept on the NASA F-18 High-Angle-of-Attack Research Vehicle.

(M. E. Ogburn, 41175, and K. D. Hoffler)

Visual/Motion Simulator

ORIGINAL PAGE
BLACK AND WHITE PHOTOGRAPH

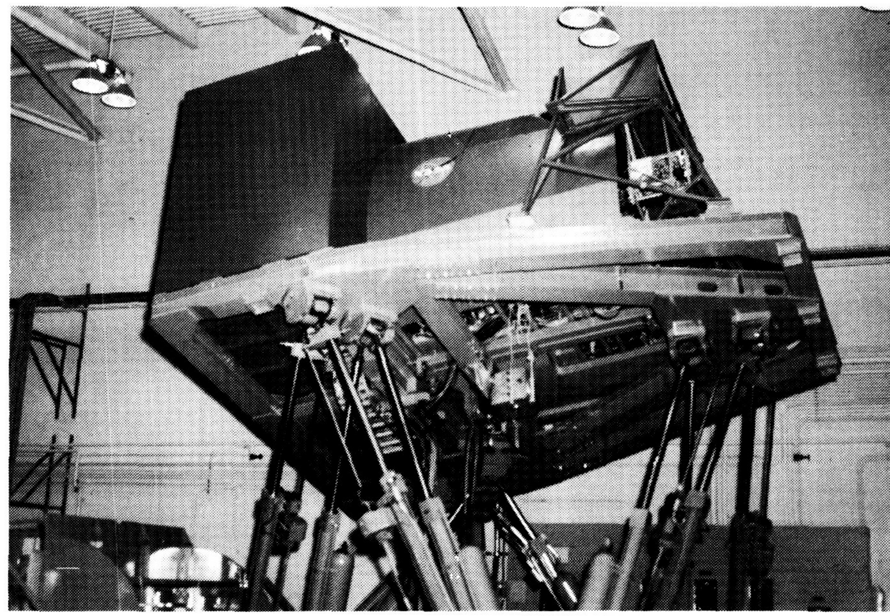

The Visual/Motion Simulator (VMS) is a general-purpose simulator consisting of a two-man cockpit mounted on a six-degree-of-freedom synergistic motion base. A collimated visual display provides a 60° out-the-window color display for both left and right seats. The visual display can accept inputs from several sources of image generation. A programmable hydraulic-control loading system is provided for column, wheel, and rudder in the left seat. A second programmable hydraulic-control loading system for the right seat provides roll and pitch controls for either a fighter-type control stick or a helicopter cyclic controller. Right-side rudder control is an extension of the left-side rudder control system. A friction-type collective control is provided for both the left and the right seats. An observer's seat was installed in 1986 to allow a third person to be in the cockpit during motion operation.

A realistic center control stand was installed in 1983 which, in addition to providing transport-type control features, provides auto-throttle capability for both the forward and reverse thrust modes. Motion cues are provided in the simulator by the relative extension or retraction of the six hydraulic actuators of the motion base. Washout techniques are used to return the motion base to the neutral point once the onset motion cues have been commanded. In addition, a g-seat is provided which can be interchanged between the left and right seats to augment the motion cues from the base.

Research applications have included studies for transport, fighter, and helicopter aircraft. These studies addressed phenomena associated with wake vortices, high-speed turnoffs, microwave landing systems, energy management, multibody transports, maneuvering stability flight characteristics, wind shear recovery guidance, vortex flaps and stereographic displays. Numerous simulation technology studies have also been conducted to evaluate the generation and usefulness of motion cues.

Completed Simulation Study of Airplane Trajectory Guidance During Wind Shear Encounters

Microbursts and low-level wind shear pose a significant threat to transport-category airplanes during takeoff and landing. A critical issue is how best to manage available airplane performance during inadvertent encounters with microburst winds for the case when the wind field ahead of the airplane is not known. The objective of this effort was to evaluate the piloting factors and performance of a candidate set of wind shear recovery techniques in a piloted simulation environment. Batch simulations of wind shear encounters, using a simple point-mass airplane model, and results from research in optimal recovery trajectories were

used to develop recovery techniques and estimate sensitivity to variations in the shear. Three recovery techniques were then implemented as flight director guidance algorithms in the VMS, programmed with the math model of a Boeing 737-100 airplane. These techniques include pitch, in which constant pitch attitude in the shear is maintained; acceleration, in which airspeed deceleration is used to recover lost climb capability; and flight path angle, in which the trajectory is controlled to avoid obstacles and unnecessary climb. The pitch technique requires only the existing attitude instrument, and the acceleration technique can be implemented on all existing transports. The flight path angle implementation requires inertial systems. A total of 252 data runs were flown by three research pilots; each run consisted of a wind shear encounter shortly after takeoff.

The batch and simulator results indicate that the characteristics of a recovery procedure that maximizes airplane performance, in a takeoff wind shear encounter, include an initial reduction in pitch attitude to reduce the climb rate, the use of the smallest acceptable climb angle, and, late in the encounter, an increase in pitch up to the stick shaker angle of attack. Stick shaker activation must be delayed as long as possible. Flight-path-angle-based guidance was less sensitive to variations in the wind shear and had better overall performance, when compared to constant pitch and acceleration-based guidance. The figure shows a comparison of the three techniques in a batch simulation. The results of the batch and piloted simulations generally agreed, but the difference in performance between the recovery techniques was less in the piloted simulation than was predicted by the batch simulation. The experimental variation in performance between piloted runs was generally greater than the difference in performance between recovery techniques.

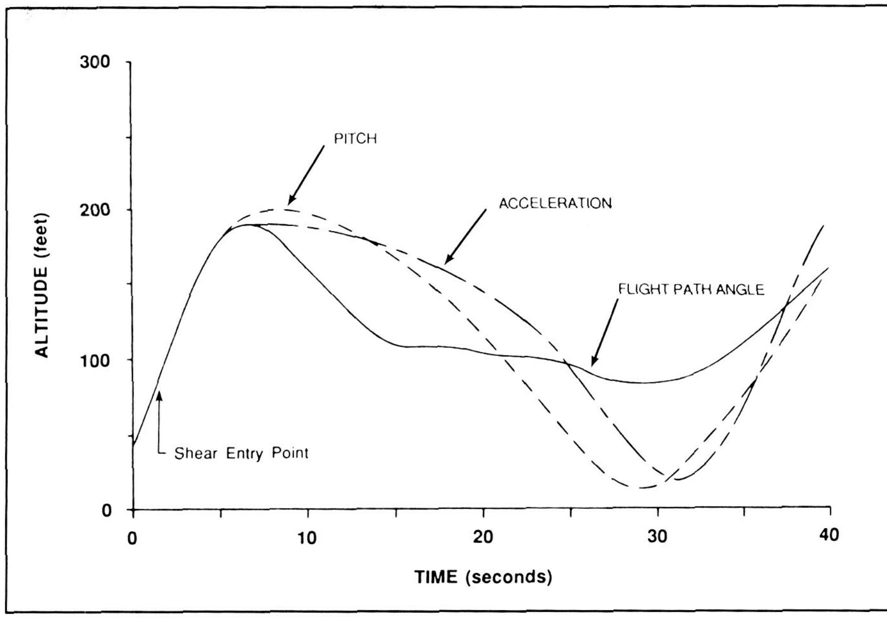

Effect of guidance strategies on recovery performance (batch simulation).

The results indicate that the performance increases of advanced recovery techniques predicted by batch simulations will not always be realized in a piloted environment. The results suggest, furthermore, that the recovery techniques (recommended by the current Federal Aviation Administration wind shear training program) for takeoff wind shear encounters cannot be improved without significantly improved guidance algorithms and displays. Flight-path-angle-based guidance shows the most promise for further development.

(D. A. Hinton, 42040)

Stereopsis Cueing in Display Enhancements for Simulated Rotorcraft Precision Hover Tasks

Advanced flight display concepts that embody true three-dimensional (3-D) images were conceived and evaluated at Langley Research Center in order to assess the supposition that stereopsis cues could be used in 3-D pictorial displays to enhance the situational awareness of pilots conducting precision tasks in a simulator.

The efficacy of stereopsis cueing in 3-D pictorial displays was assessed in a real-time piloted simulation experiment of a rotorcraft precision "hover-in-turbulence" task. The experiment utilized the VMS in a fixed-base mode. In a full factorial experimental design, seven pilots endeavored to fly to and maintain a hover by visually aligning inner and outer wickets (see the first figure), thus attaining the desired hover po-

ORIGINAL PAGE
BLACK AND WHITE PHOTOGRAPH

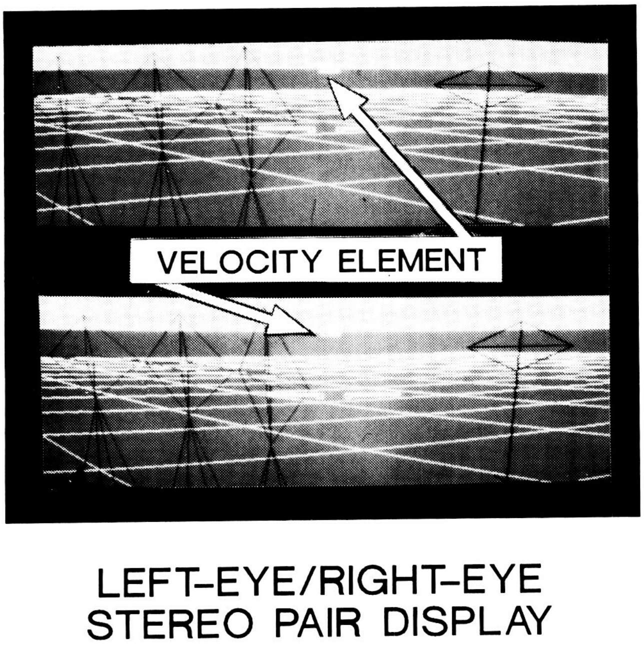

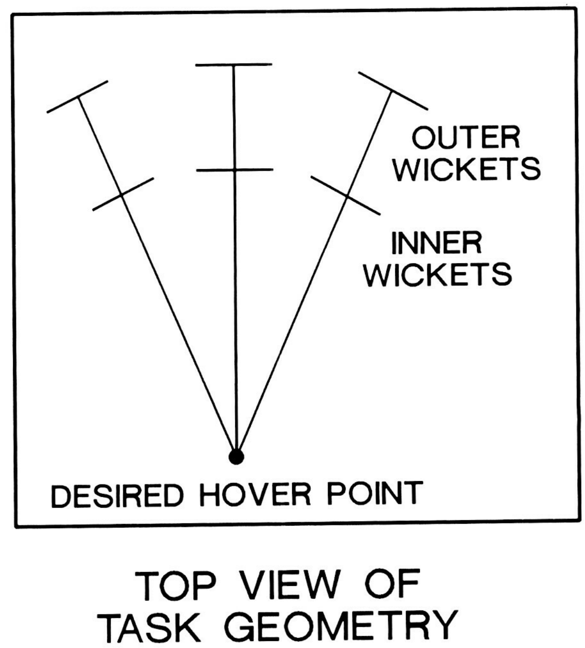

Rotorcraft precision hover task.

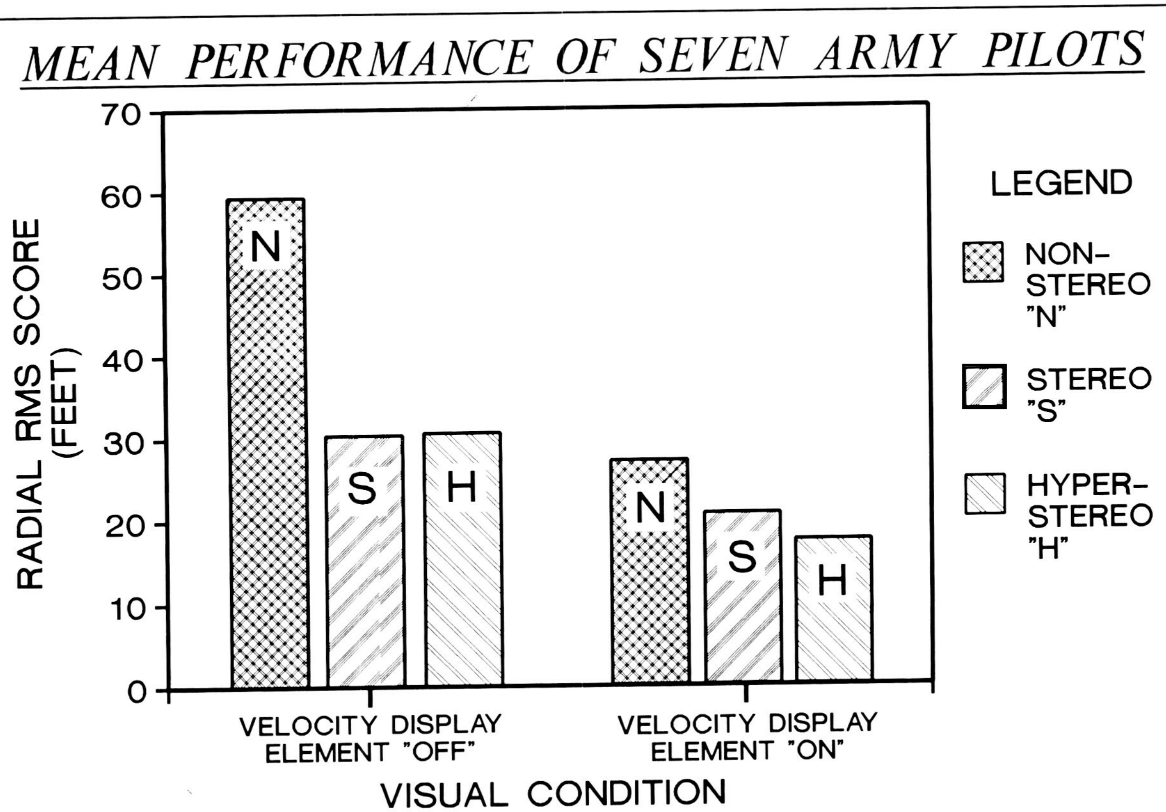

Effectiveness of stereopsis cueing in rotorcraft precision hover task.

sition. The display conditions examined included the presence or absence of a velocity display element (as shown in the figure), as well as the stereopsis cueing conditions of nonstereo (no stereopsis depth cues), stereo 3-D, and hyperstereo. The latter condition represented the case of the pilot's eyes (image sources) being located 6 ft apart (as might be encountered with forward looking infrared (FLIR) cameras mounted on each side of a cockpit for a binocular display), rather than the usual 2 in.; this hyperstereo condition provided exaggerated depth cues in the display. The performance metrics for the study included root mean square (RMS) values of the displacement from the desired hover point, the pilot control inputs, and subjective pilot comments.

Both the objective and subjective results overwhelmingly indicated that the depth cues provided by the stereo displays enhanced the situation awareness of the pilot. The enhancement was particularly effective when the velocity information element was absent from the display (see the second figure), implying that velocity information, as well as positional information, can be more readily extracted from the stereo presentation. Pilot control input data revealed that 12 to 21 percent less control action was required to attain the superior hover performance using the stereo displays. Stereopsis cueing appears to offer a means of displaying complex information in a natural way to enhance situation awareness and provide improved pilot/vehicle performance, without accompanying increases in control activity.
(S. P. Williams, 46650, and R. V. Parrish)

Space Simulation and Environmental Test Complex

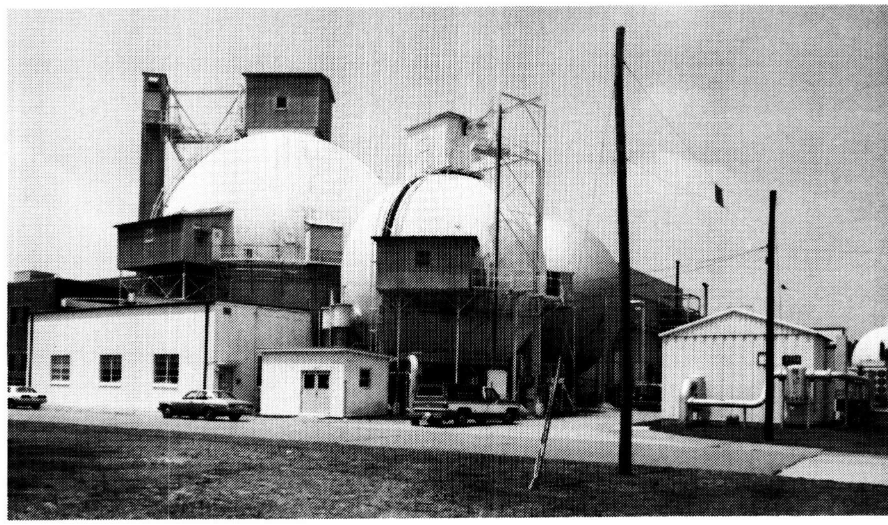

60-ft-diameter Space Simulation Sphere.

The 60-ft-diameter Space Simulation Sphere (Building 1295) can simulate an altitude of 320,000 ft (2×10^{-4} mm Hg). This vacuum level is attainable in 7 hours with a three-stage pumping system. The carbon steel sphere is accessible through a personnel door, a 12-ft-diameter specimen door, and a 4-ft maintenance door at the top. A 2-ton hoist located at the top enhances specimen handling inside the sphere. Sight ports are located both at the top and at the equator. Two closed-circuit television cameras, a videocassette recorder, and an oscillograph are available. Firing circuitry and a programmer are available for the use of pyrotechnics, and a system of flood lights is installed in the sphere to facilitate high-speed photography. The sphere is used primarily for dynamic testing of aerospace components and models at a near-space environment.

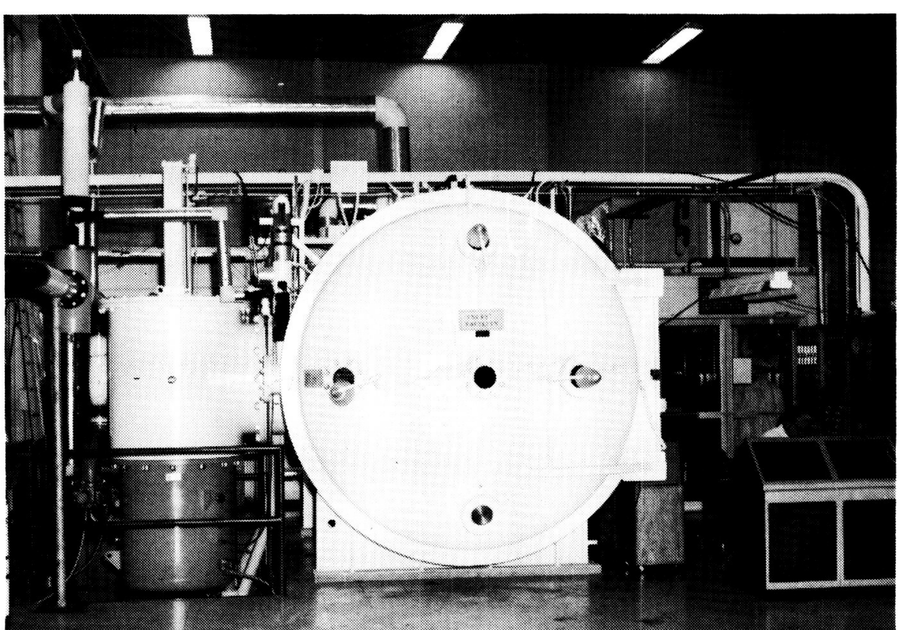

8- by 15-Foot Thermal-Vacuum Chamber. L-82-9672

Thermal-vacuum testing has long been a prerequisite to the active deployment of space experiments. A series of experiments that optically sense characteristics of the Earth's atmosphere from outer space necessitated the creation of an ultrahigh-cleanliness thermal facility. The optical components of these experiments would be severely degraded by contamination by oils or other vaporous materials commonly found in thermal chambers and vacuum pumping systems. Langley Research Center upgraded the 8- by 15-Foot Thermal-Vacuum Chamber (in Building 1250) by repeated vacuum bakeout and solvent wipedown. Two 35-in. cryogenic pumps were installed, and cold traps were inserted in the rough-

ORIGINAL PAGE
BLACK AND WHITE PHOTOGRAPH

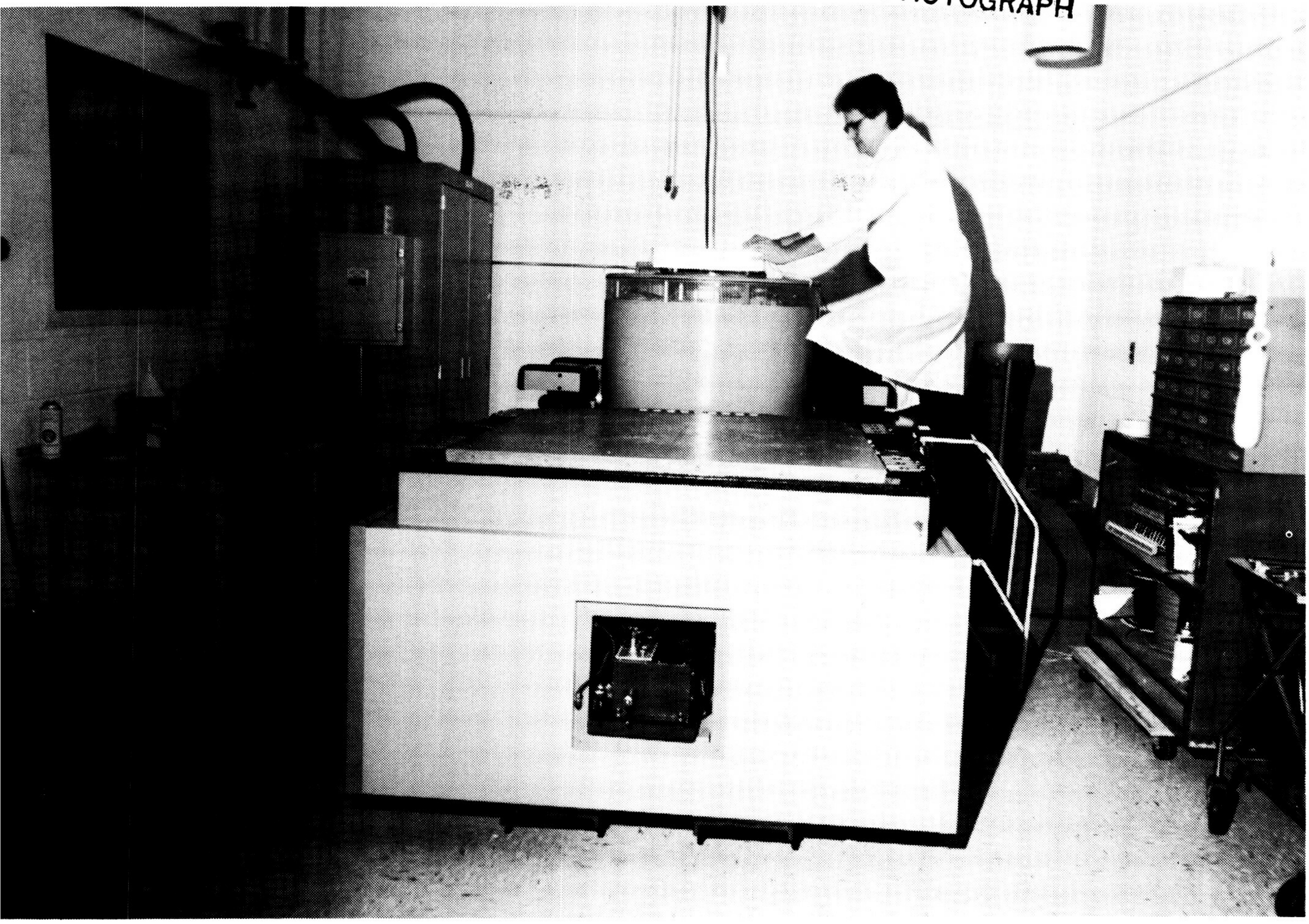

Unholtz-Dickie T-1000 shaker. L-85-10833

ing pump lines to eliminate back contamination from the pumps. The chamber is capable of −300°F to +1000°F temperatures and has glass ports for solar illumination simulation.

A 5- by 5-Foot Thermal-Vacuum Chamber (also in Building 1250) augments the thermal testing capability. The smaller stainless-steel chamber is used for subsystem and component testing. A completely enclosed liquid nitrogen cryopanel with eight ports that have externally adjustable irises can cool the ambient temperature to −300°F. Removable heater banks are used for precise temperature control and high ambient temperature applications. The chamber uses a 570 ft^3/min roughing pump and a 32-in. diffusion pump to reach its capacity of 1×10^{-7} torr. The pumping capability is high relative to the chamber volume; therefore, the 1×10^{-7} torr level can be attained in 1.5 hours.

Structural integrity of aerospace hardware is essential for both performance and safety. The Engineering Vibration Test Facility in Building 1250 is used to perform environmental vibration tests on aerospace flight systems and components to demonstrate that the flight equipment will maintain structural integrity when exposed to a mission environment. The facility includes two shaker units and centralized equipment for control, data acquisition, and signal processing. One unit is an Unholtz-Dickie T-1000 shaker with a 24,000-lbf peak force and a 1-in. armature stroke. The second shaker, a recent addition, is an Unholtz-Dickie T-4000 unit with a 40,000-lbf peak force and a 1-in. stroke (1.75-in. stroke for shock testing). The vibration control room houses a GenRad 2514 vibration control system for shaker control and signal processing plus signal conditioning and analog data recording equipment for 12 channels of data. Through auxiliary equipment, the data capacity can be expanded. Tests are con-

ducted with great care given to equipment, test article, and personnel safety. Closed-circuit television coverage is used to safely monitor the test article during all tests.

Army Helicopter-1 Rotor Test

Tests of a 13-ft-diameter composite helicopter rotary blade were conducted in collaboration with the Army Rotary Craft Aerodynamics (ARCA) Office. The tests were performed with two 4-lb, 6.5-ft-long blades that were attached to a rotor hub assembly. This assembly was attached to a spin table mounted to the floor of the chamber. The composite blades were instrumented with strain gauges through a slip-ring assembly within the spin table. Rotary tests to measure lift loads were conducted at various vacuum levels from 1 atm to 5×10^{-3} mm of Hg. The rotors were rotated to a maximum of 120 r/min. Test events were recorded on a videocassette recorder, and test data were recorded on an FM analog recorder. The test objective was to measure the rotating blade stresses at a pitch angle of 0° with no aerodynamic loading. The low ambient pressure attainable in the 60-ft-diameter Space Simulation Sphere created the needed environment.

The test results were consistent with derived conclusions from air tests and gave the ARCA Office high confidence in the performance of the blades at low rotation levels. The figure shows the initial setup in a four-blade configuration; however, the actual tests were performed with only two blades.
(R. N. Messier, 45621)

L-87-10472

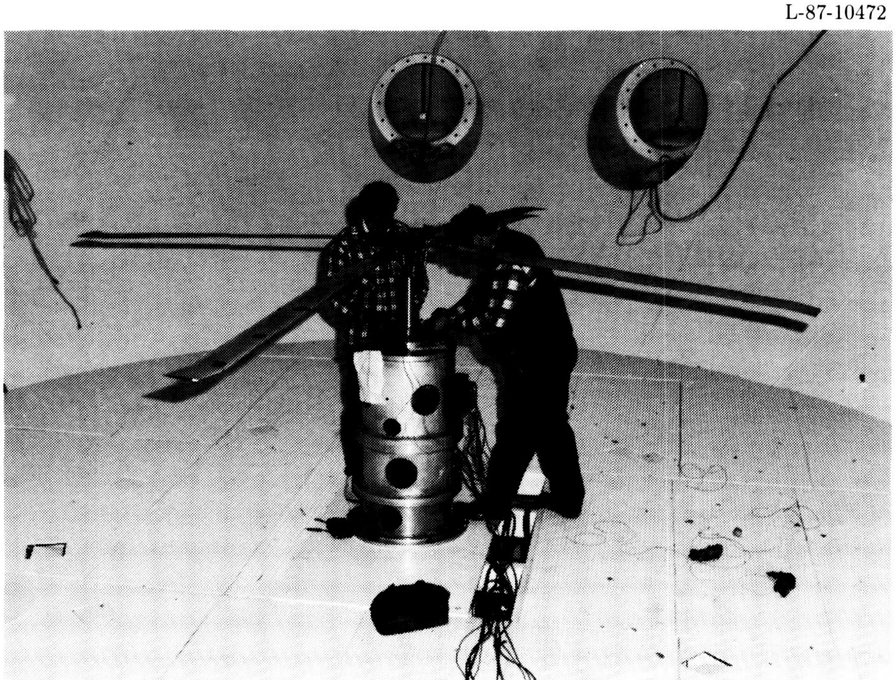

Helicopter blade test setup in 60-ft-diameter Space Simulation Sphere.

Thermal Cycling Test of LASE Flight Electronics

The LASE (Lidar Atmospheric Sensing Experiment) aircraft instrument will be flown on numerous missions on the Ames Research Center ER2 aircraft and will take measurements of water vapor. The flight hardware must be capable of obtaining accurate measurements over the broad inflight temperature extremes. The 5- by 5-Foot Thermal-Vacuum Chamber was used to expose the LASE power distribution box (equipment mounting deck) to the required vacuum and temperature extremes. The flight hardware was instrumented with thermocouples on the box exterior and on an interior relay heat sink. An ambient thermocouple was mounted near the LASE hardware and used for temperature control. An IBM personal computer and Keithley data acquisition and control system were used to generate the required continuous temperature ramp profile and record all test data. An error signal derived from the control thermocouple modulated two 2500-W heater banks to track the programmed temperature profile. For below-ambient temperatures, the cold shrouds were partially filled with LN_2 using a stand-alone set point controller whose feedback mechanism was a thermocouple attached to the shroud wall.

Ramp excursions were between +35°F and +135°F. The required pressure was one-half atmosphere; therefore, a circulation fan was operated throughout the test to ensure uniform ambient temperatures. Ramp rates and dwell times were program controlled. Termination limits were included in the software to prevent hardware damage from

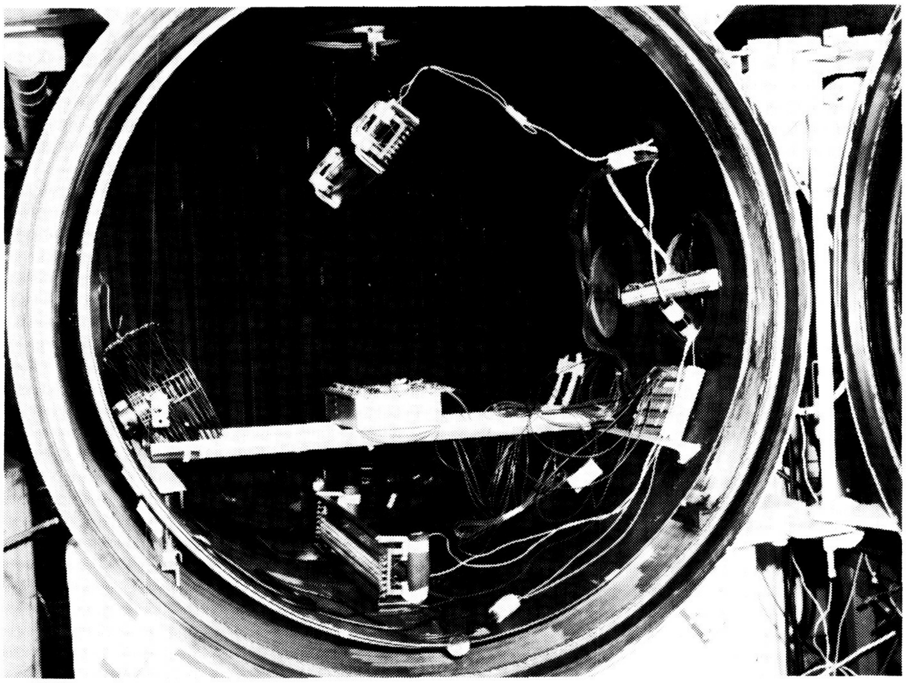

LASE flight electronics in 5- by 5-Foot Thermal-Vacuum Chamber.

L-88-03171

extreme temperature exposure. Ambient and relay heat sink temperatures were recorded continuously. All temperatures and ramp set points were displayed in real time as was the number of completed cycles. The test duration was 5 days of continuous operation for a total of 15 cycles. The flight hardware demonstrated no workmanship shortcomings. The figure shows the LASE hardware mounted in the 5- by 5-Foot Thermal-Vacuum Chamber.
(T. J. Lash, 45644)

HALOE Sun-Look Test

The Halogen Occultation Experiment (HALOE) is a multisolar sensor instrument that will collect global data concerning ozone chemistry while orbiting the Earth on the Upper Atmosphere Research Satellite. The instrument consists of a Cassegrain telescope with optics that relay solar radiance from 2 μm to 10 μm to an eight-channel sensor unit mounted on a mainframe. The pointing system consists of a Sun sensor attached to the mainframe telescope that is mounted on biaxial gimbals. The pointing system must both precisely point the telescope at the Sun and track the Sun during periods of data collection. The Sun sensor consists of one digital and two analog sensors that operate in the spectral range of 0.4 μm to 0.9 μm. Boresight alignment of the three Sun sensors to the science telescope was accomplished in the laboratory using solar simulators. However, verification of the alignment was only possible by direct viewing of the Sun.

Sun sensor and telescope data for alignment determination were obtained by multiple vertical scans across the Sun. By using a personal computer, near-real-time data analysis of the solar limb position measurements provided the reference for determining the relative position of the Sun

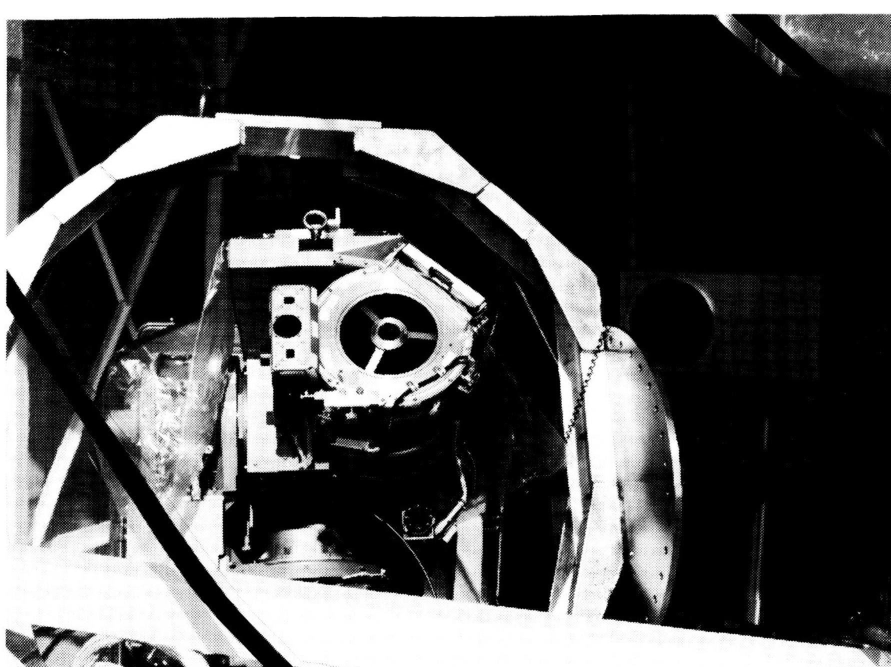

HALOE tracking Sun during alignment verification. L-88-5202

sensor and telescope. The test was performed in a class 100 portable clean room positioned at the roll door in Building 1250. Facility provisions and instrument ground support equipment (GSE) were tailored to acquire data at the optimum time of noon. The figure shows the HALOE, which is mounted in its unique cradle, tracking the Sun during the Sun sensor alignment verification test.
(A. S. Moore, 47094)

Vibration Testing of HALOE Instrument

HALOE flight instrument on Unholtz-Dickie T-1000 electromagnetic shaker.
L-88-09248

Concentrations of eight gases in the upper atmosphere will be measured by the HALOE. This instrument will be placed into orbit by the STS (Space Transportation System) in the early 1990's. As a part of the required structural validation for STS experiments, vibration tests were conducted to demonstrate good workmanship and to obtain vibration characteristics for use in structural analyses. Of particular interest was how the vibration characteristics might change with varying levels of vibration input. These tests were performed in the Engineering Vibration Test Facility in Building 1250.

The workmanship test was conducted by applying a random vibration environment through an electronically driven shaker to the base of the HALOE in each of three orthogonal axes. Data acquisition consisted of measuring and recording the vibration input as well as the output response at 27 locations on the HALOE.

The same instrumentation used in the workmanship test was used to determine the natural frequency, damping factor, and mode shape for all HALOE structural modes below 50 Hz. Narrowband random vibrations at several levels of power were used as inputs to obtain information on the variation of the HALOE dynamic characteristics with increases of vibration input. Swept sine vibration tests of constant amplitude were also used to confirm the results of the random input test. These sine tests were repeated with increased amplitude to study the nonlinear vibration response.

The HALOE instrument is shown in the picture on the Unholtz-Dickie T-1000 electromagnetic shaker. A contamination protective bag covers the instrument to maintain cleanliness during vibration testing. The HALOE instrument successfully passed all vibration tests and is totally compatible with the Upper Atmosphere Research Satellite mission.
(T. C. Jones, 47037)

HALOE Thermal-Vacuum Testing

The HALOE optical remote sensor will globally monitor the vertical distribution of key gases in the ozone chemistry by measuring the extinction of solar radiation (in the 2.5-μm to 10.0-μm range) which passes through the Earth's atmosphere during solar occultation. HALOE is one of 10 instruments on the Upper Atmosphere Research Satellite, which is a free-flying satellite scheduled for a late 1991 Space Shuttle launch. During 1988, the flight instrument has undergone extensive testing

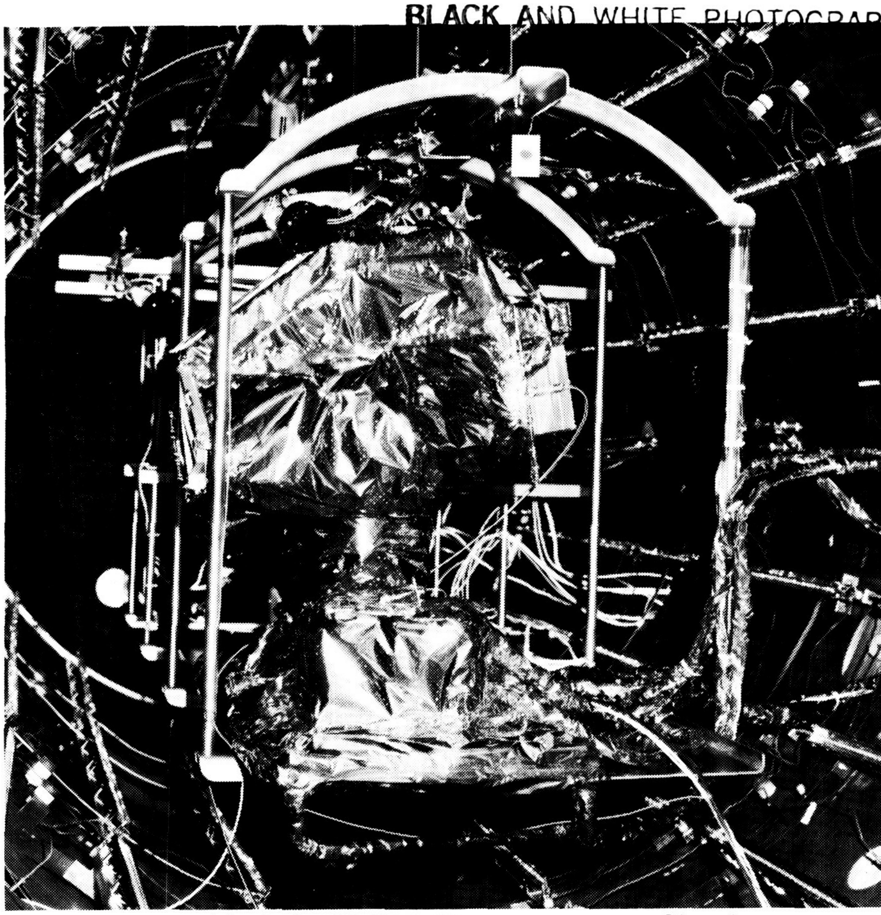

HALOE mounted in 8- by 15-Foot Thermal-Vacuum Chamber. L-86-8011

in the 8- by 15-Foot Thermal-Vacuum Chamber to demonstrate acceptable performance during repeated exposure to simulated flight thermal environmental extremes.

During September 1988, the flight acceptance test on the pyrotechnic pin pullers on the HALOE gimbal assemblies and the telescope door was performed. Successful firings under simulated temperature extremes were monitored with accelerometers and movie cameras. Pyrotechnic blowby was monitored using a modified temperature-controlled quartz-crystal microbalance contamination monitor (TCQCM), a mass spectrometer, and a witness plate. Upon completion of the pyrotechnic firings, a vacuum bakeout of the instrument at 127°F was performed to drive off and trap any contaminates that may have accumulated on the HALOE during this and previous testing.

In December 1988, HALOE underwent final thermal cycling between the predicted flight temperature extremes in the 8- by 15-Foot Thermal-Vacuum Chamber. Additional test objectives that were fulfilled included the evaluation of multilayered insulation efficiency, instrument crosstalk and gain calibration versus temperature, radiometric performance sensitivity to temperature, and instrument balance stability with time. The figure shows the HALOE instrument mounted in the 8- by 15-Foot Thermal-Vacuum Chamber prior to the start of the test.
(R. Foss, 47049)

Mass Properties Measurement of HALOE Instrument

Experiment weight, center of gravity (CG), and mass moment of inertia (MI) must be precisely known for HALOE in order to determine launch loads and meet spacecraft attitude control requirements while in

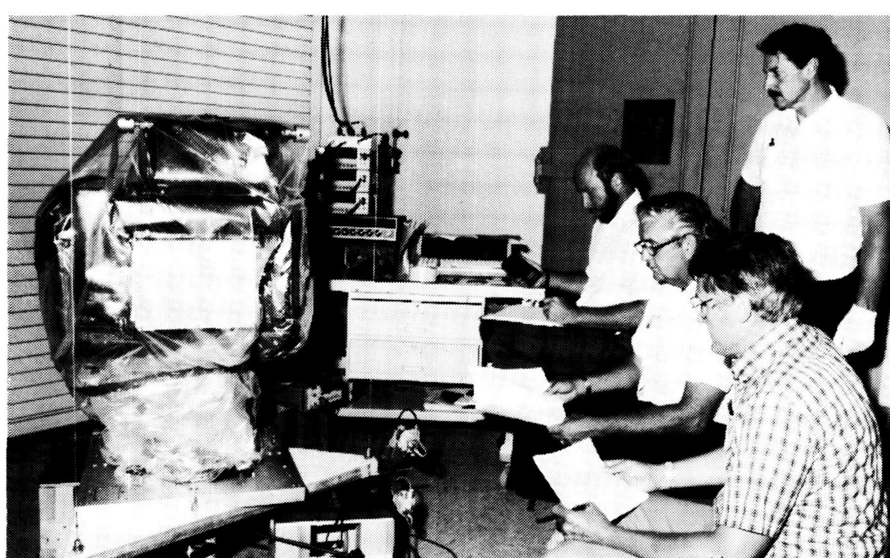

Trifilar Torsional Center of Gravity and Moment of Inertia System with HALOE instrument. L-88-8661

ORIGINAL PAGE
BLACK AND WHITE PHOTOGRAPH

orbit. The mass properties of the HALOE instrument were determined using the Trifilar Torsional Center of Gravity and Moment of Inertia System (TTCG&MIS) located in the Engineering Vibration Test Facility in Building 1250.

The TTCG&MIS utilizes three load cells, three analog-to-digital converters, a 10-V dc power supply, a suspended test platform, a Hewlett Packard computer, and a mass properties algorithm developed at the Engineering Vibration Test Facility. The CG about three orthogonal axes was determined by mounting the HALOE instrument onto the TTCG&MIS in the proper orientation. Load cell data from each suspension cable were monitored by the computer, and the CG of the instrument was determined automatically by the algorithm through a summation of moments. The mass moment of inertia for each axis was individually determined by locating the center of gravity of the HALOE instrument above the CG of the test platform, initiating a torsional oscillation, and measuring the time period of the oscillation. The length of suspension cables, the radius of rotation, and the suspension cable load cell data are used in the algorithm to calculate the MI about the given axis. The measurement system and platform mass properties are determined prior to the test. The algorithm automatically subtracts these tare values. The figure shows the HALOE instrument mounted on the test equipment.
(C. Jenkins, 47080)

Advanced Technology Research Laboratory

The Advanced Technology Research Laboratory was completed in late 1988 in support of the NASA Space Energy Conversion Research and Technology Program. The laboratory houses multidisciplinary research activities assessing the feasibility of spacecraft-to-spacecraft laser power transmission for propulsion and for electric power distribution, conducting theoretical studies on galactic and solar cosmic ray exposure and shielding, and developing ultra-high vacuum gas-surface interaction technology. Major facilities include three solar simulators that include a single-lamp unit of 50 kW input power, a dual-lamp unit of 100 kW input power, and a state-of-the-art single-lamp unit of 160 kW input power. These simulators provide a range of solar irradiance conditions for the multifaceted research into the direct conversion of solar energy to laser power. The research includes investigations using solid, liquid, and gas lasers powered by simulated sunlight; electrically driven diode lasers; and the conversion of laser power back into electricity. Theoretical research is supported by a computational capability that includes the latest computer technology. In addition, the facility is fully integrated into the Center's high-speed data network. A group of laboratories house ultra-high vacuum equipment that simulates the space environment and specialized conditions associated with advanced spacecraft. The laboratory also contains a large, multikilojoule capacitor bank that is the energy source for the development of technology for a multimega-ampere plasma switch and for research on laser-power beaming.

High-Power Laser Tests

Since 1980, the output power obtained from an iodine photodissociation laser excited by simulated solar energy has increased from less than 1 mW pulsed to more than 10 W continuous, the highest power ever obtained from this type of laser. The power from such an iodine photodissociation laser is limited by simulator power. A technique, called Q-switching, which stores and then releases energy in a pulse, was recently used on this laser to increase the peak output power by more than an order of magnitude. Q-switching by an electro-optic cell, often used with other lasers, was not possible because of the large absorption of the cell at the iodine laser wavelength of 1.3 nm. The Q-switching was achieved with a high-speed pneumatic chopper inserted in the oscillator cavity. A continuous succession of pulses of over 150 W was obtained from the laser, which was pumped by a continuous argon arc simulator.

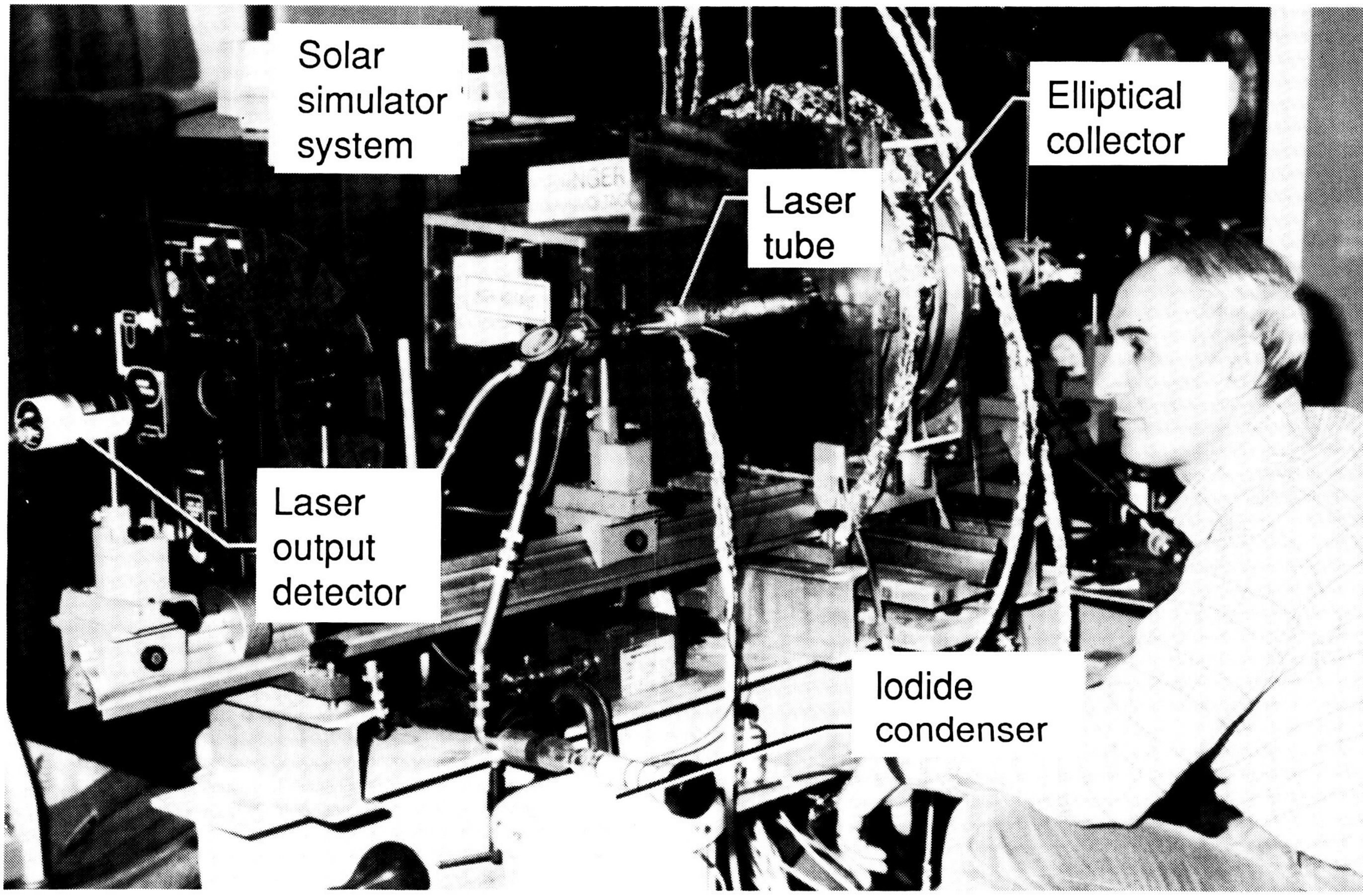

Experimental apparatus for iodine flow laser tests. L-89-743

This is the first Q-switching of a continuously excited iodine laser and is the highest peak power ever achieved with a simulator-pumped gas laser. The gas lasant n-C_3F_7I flowed longitudinally through the laser cavity by a pressure differential induced by an evaporation-condensation system. The variation of continuous or pulsed laser power with parameters, such as lasant pressure, lasant flow rate, and chopper speed, was measured and is being analyzed. **(W. E. Meador, 41434)**

Master-Oscillator Power-Amplifier Development for Space Laser Power Transmission

Space missions are demanding larger power requirements as payloads become heavier and more complex. A novel concept uses the Sun as the prime power source for a space-based laser power transmission station that beams power directly to vehicles for propulsion or to satellites, or platforms, for conversion into electricity. Transmitted powers may exceed 1 MW, and beam quality must be sufficiently high for transmission over distances in excess of 1000 km. Tests are progressing on a master-oscillator power-amplifier (MOPA) system that has potential advantages over a single laser oscillator scaled to multimegawatt power levels. The figure shows the primary components of a MOPA, a laser oscillator, and an amplifier. In this configuration, the laser oscillator needs only to provide a relatively low power beam; the amplifier preserves the beam quality and provides the increase in power for transmission. Initial tests determined that at a 1-Hz repetition rate, t-C_4F_9I was the most efficient laser medium and could provide amplification of at least a factor of 4. A xenon chloride laser was developed as the oscillator with a repetition rate of 5 Hz, which was amplified to produce multikilowatt pulses. It

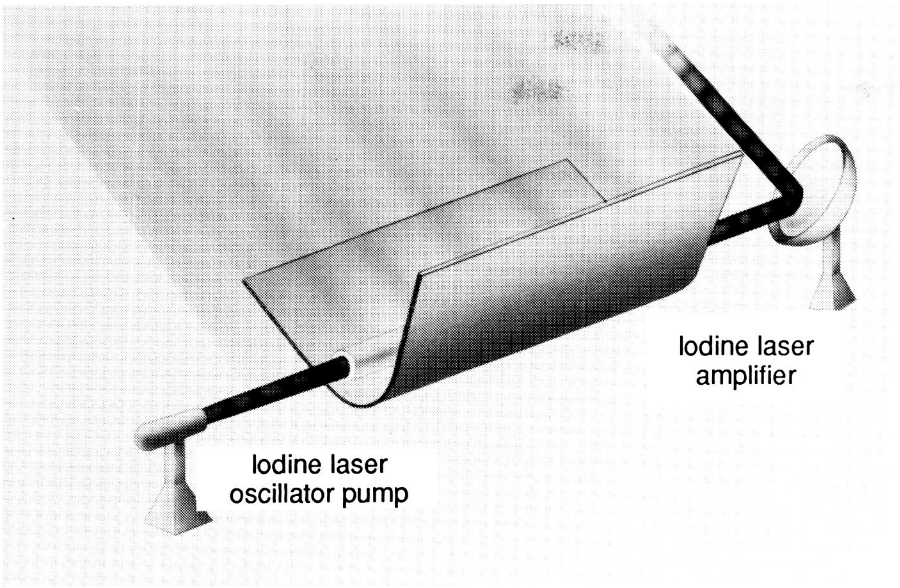

Basic MOPA system. L-89-1332

is necessary to push the repetition rate even higher to achieve the high average power necessary for laser power transmission.

A system is now being tested that uses a xenon chloride laser to excite an oscillator coupled to a solar-simulator-powered amplifier with C_3F_7I as the laser medium. The solar simulator uses an argon arc lamp to excite a 15-cm-long amplifier at a solar concentration of approximately 1700. The C_3F_7I gas flows through the amplifier driven by an evaporation-condensation cycle to produce a gas velocity of 20 m/s. A gain in excess of 1.5 was measured, and again, a multikilowatt pulse power was achieved. This is the first reported solar-pumped laser amplifier capable of a continuous output train of high-power laser pulses suitable for studies of far-field beam profiles and evaluation of long-distance transmission efficiency.
(J. H. Lee, 41473)

Atomic Oxygen Beam Generator

The composition of the atmosphere at a spacecraft's orbital altitude (200 km to 1000 km) combined with the spacecraft orbital velocity results in hyperthermal atomic oxygen impingement on spacecraft surfaces with a flux of 10^{15} cm^{-2}s^{-1} and a kinetic energy of approximately 5 eV. The high chemical reactivity of this atomic oxygen flux has caused substantial degradation of organic materials on the Space Shuttle and suggests that materials on Space Station *Freedom*, composites used in large space structures, exterior coatings on the optics of the Hubble Space Telescope, proposed ultraviolet telescopes, and future laser communications systems may have a substantially reduced lifetime. It is therefore essential to study the effects of atomic oxygen on materials in a ground-based laboratory.

An unusual approach to the development of a laboratory atomic oxygen gun is under way; this approach simulates the orbital conditions and involves the use of two unique phenomena,

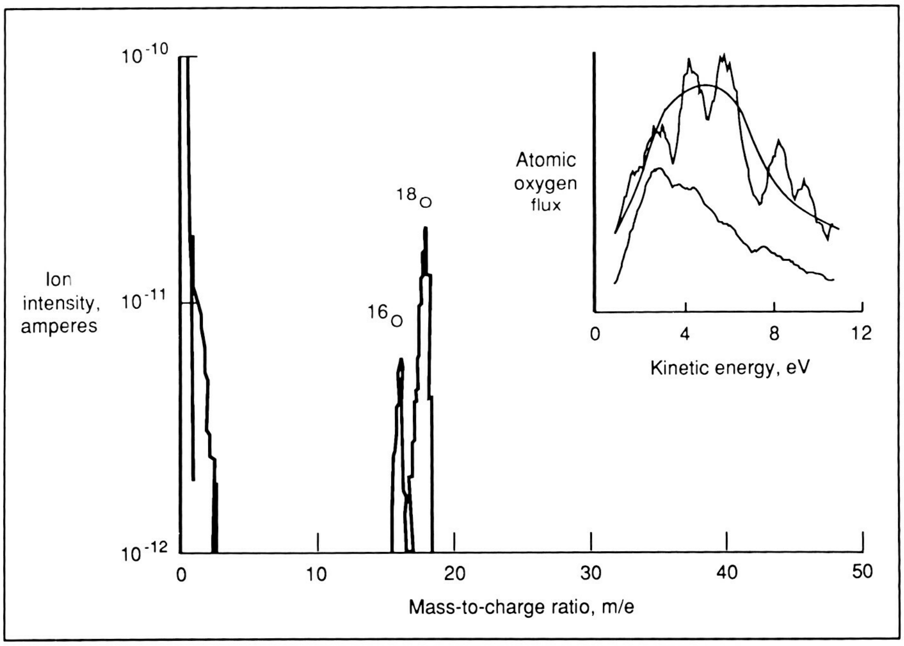

Intensity of atomic oxygen produced by electron-stimulated desorption from silver surface, with inset showing kinetic energy distribution of flux.

the unusually high permeability of oxygen through silver and electron-stimulated desorption of atoms or molecules from a surface. Normally, when the oxygen atoms diffusing through silver arrive at the vacuum interface, surface diffusion occurs that results in oxygen atom recombination and the subsequent desorption of oxygen molecules. By using an incident flux of low-energy electrons (100 eV to 500 eV) on this surface, the oxygen atoms are excited and desorb as hyperthermal atomic oxygen neutrals and oxygen ions with an energy of 1 eV to 10 eV. Laboratory experiments have demonstrated proof of this concept. High-purity atomic oxygen fluxes greater than 1×10^{12} $cm^{-2}s^{-1}$ and with kinetic energies between 2 eV and 6 eV have been measured and provide the basis for a laboratory instrument.
(R. A. Outlaw, 41433)

Structural Dynamics Research Laboratory

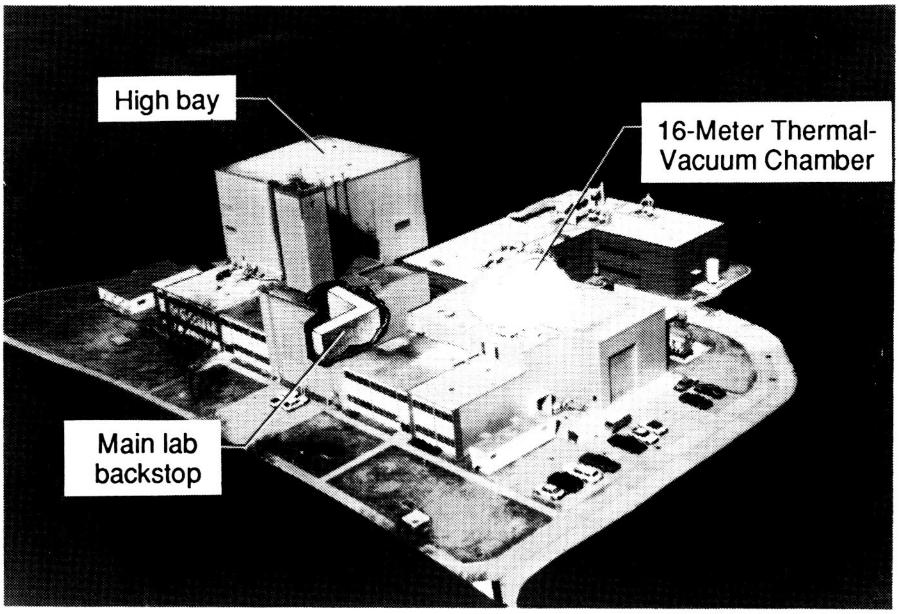

The Structural Dynamics Research Laboratory is designed to conduct research on the dynamic behavior of spacecraft and aircraft structures, equipment, and materials. It offers a variety of environmental simulation capabilities, including acceleration, vacuum, and thermal radiation. Improvements are under way which will benefit controls and structures interaction research.

The newest feature of the laboratory is the Large Component Test Laboratory, which is an open room with a full environmental control system and nominal dimensions of 75 ft by 84 ft by 79 ft high. The laboratory contains various sized hoists and accessible platforms for suspension systems, instrumentation, and viewing.

The dominant feature of the main laboratory is a 38-ft-high backstop of I-beam construction. Test areas available around this facility are 15 ft by 35 ft by 38 ft high and 12 ft by 12 ft by 95 ft high.

Another feature of the laboratory is the 16-Meter Thermal-Vacuum Chamber. It has a 55-ft-diameter hemispherical dome with a removable five-ton crane, a 64-ft-high dome peak, a flat floor, and an option for a large centrifuge or a rotating platform. Access is by an airlock door and an 18-ft-high by 20-ft-wide test specimen door. Ten 10-in.-diameter view ports are randomly spaced for visually monitoring tests. A vacuum level of 10 torr can be achieved within 120 minutes and, with diffusion pumps, 10^{-4} torr vacuum can be achieved in 160 min. The centrifuge attached to the floor of the chamber is rated to 100 g, with a 50,000-lbf capacity and a maximum allowable specimen weight of 2000-lb. Six-ft mounting faces for test articles are available at 16.5-ft and 20.5-ft radii. The tables can accommodate electromagnetic and hydraulic excitation devices. A temperature range of 100°F is obtained from 250 ft^2 of portable radiant heaters and liquid-nitrogen-cooled plates.

Available excitation equipment includes several types of small shakers. The largest is hydraulic with a maximum of 1200-lbf, 6-in. stroke, and 0-Hz to 170-Hz range. All areas are monitored by closed-circuit television cameras, connected by voice, and are hard-wire connected to a control data acquisition and processing room. State-of-the-art capability for up to 220 channels of data is available for signal conditioning and analog and digital data recording. Two GenRad 2515 digital signal processing systems are available along with a VAX 11-780/EAI 2000 hybrid computer system for simulation and on-line test control. A variety of mostly new auxiliary data logging and signal processing equipment is also available.

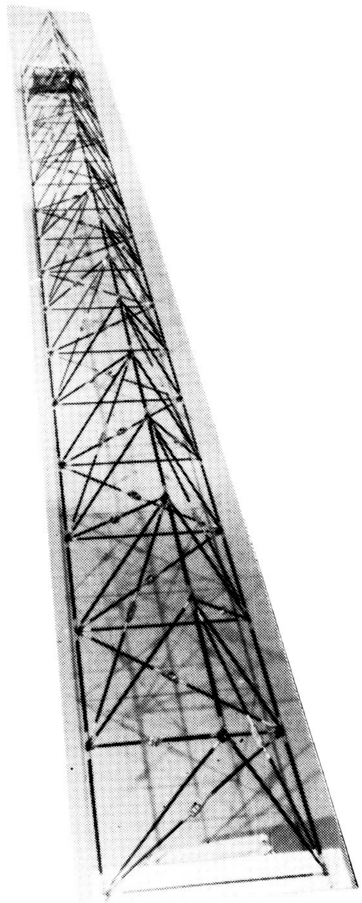

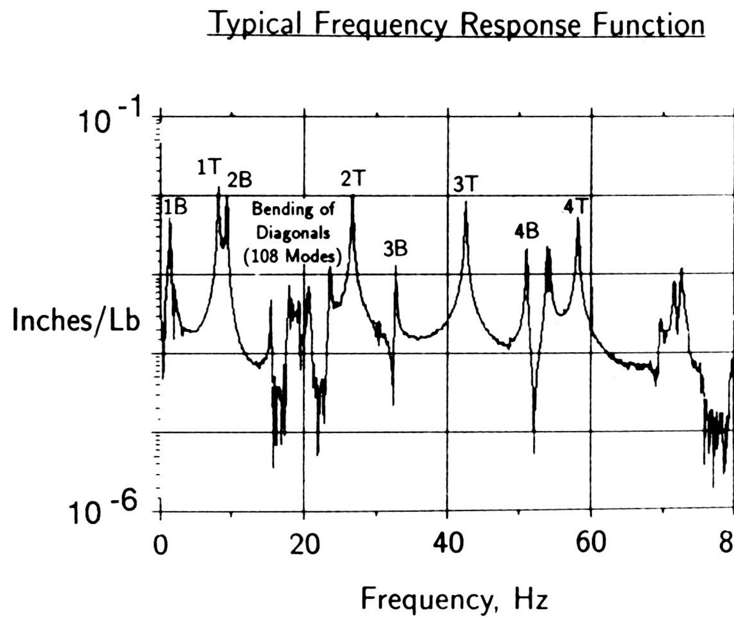

Mini-Mast 20-m ground test article.

L-88-12395

Mini-Mast Ground Test Program

Because of their high efficiency, truss beams will be used as the framework for many future large space structures, such as Space Station *Freedom*. Accurate analytical models of the truss-beam elements are required to ensure acceptable structural and dynamic characteristics of the overall system, including avoidance of adverse interaction with the spacecraft's control system. To examine potential problem areas in developing and verifying these models, an 18-bay, 20-m-long, deployable/retractable truss beam was designed and built and is being used at Langley Research Center as a ground test bed. The structure is referred to as the Mini-Mast. It was manufactured to flight-quality specifications by Astro Aerospace Corporation, Carpinteria, CA, using graphite/epoxy tubes for strut members and precision titanium parts. A statically determinant design (three longerons) with mid-diagonal hinges was selected.

Baseline static and dynamic tests of the Mini-Mast in its initial testing configuration (cantilevered vertically from the floor with a 70-lb tip plate) have been completed. Static tests were performed under both bending and torsional tip loads. Overall, the static bending results correlated well with analytical predictions. In torsion, however, significant friction and deadband were observed. These effects are attributed primarily to localized bending and sliding of the diagonal members at the end-fittings. Dynamic tests were conducted using two shakers. A typical frequency function measured in these tests is shown in the figure. The identified modes up to fourth bending, at approximately 50 Hz, agree well with predictions. The cluster of modes near 20 Hz, resulting from first bending of the diagonal members, is also predicted well by analysis. The precise mode shapes in this frequency range have not

yet been identified, however, because individual truss members were not instrumented. A second cluster of modes, near 70 Hz, is attributed to the second bending of the diagonal members, but this behavior is still unconfirmed. Consistent with the observed nonlinear static torsion results, the damping of the torsional modes increased significantly with increased dynamic force level. Modal damping of approximately 0.5 percent of the critical value at low force level increased to 3 percent to 5 percent at higher levels. Several test challenges were encountered, including the identification of repeated eigenvalues (all bending modes), high sensitivity of bending direction with slight asymmetries, and modal clustering due to diagonal-member bending.

This project is one of the first combined analytical/experimental programs conducted using a flight-quality, representative large space structure. In-house capabilities, both analytical and experimental, were exercised significantly and improved as a result of the work. These experiences will help ensure the development of accurate analytical models in future flight programs.
(R. S. Pappa, 44321)

Ground Testing Scale Models of Large Space Truss Structure

Verification of analyses for predicting the on-orbit dynamic response of large space truss structures is an important research challenge. In past programs, analysis verification has been ultimately accomplished through ground testing of space vehicles in a mated configuration. However, the increasing size and complexity of future space systems limit the capability to perform such tests. Thus, there will be an even greater reliance on analysis for preflight verification. Through the use of scale models, dynamic analyses can be verified on the ground and can be extended to on-orbit predictions of the full-scale space system.

Research methods for designing scale models of large space structures, such as Space Station *Freedom*, are currently receiving considerable attention. In addition, techniques for performing dynamic ground tests of these structures are being developed. There are three major focuses for this work; these include data acquisition and modal analysis, suspension systems, and model assembly and facility logistics. A variety of hardware is being used to examine these topics in preparation for tests of a fully configured dynamic scale model of Space Station *Freedom*. These test structures have a number of common characteristics including low frequency and closely spaced modes, low damping, and large concentrated masses on a relatively lightweight structure.

The figure shows a simulated scale-model truss suspended in the Large Component Test Laboratory. This model consists of 23 truss bays with payload mass simulators located in the middle and at each end. As shown in the figure, the truss is suspended by two steel cables that are approximately 75 ft long. Initially, a series of static tests were performed to characterize the system. The truss itself was statically tested at the component level (i.e., truss struts and joints) and at the substructure level (10-bay cantilevered segment). The suspension system was also tested to determine the linearity and stiffness of the cables over the expected operating load range. Finally, static tests of the combined truss/suspension assembly produced excellent agreement with analysis predictions.

Dynamic tests of the suspended truss system are currently under way, and the initial results are encouraging. Previously, modal tests of a 10-bay

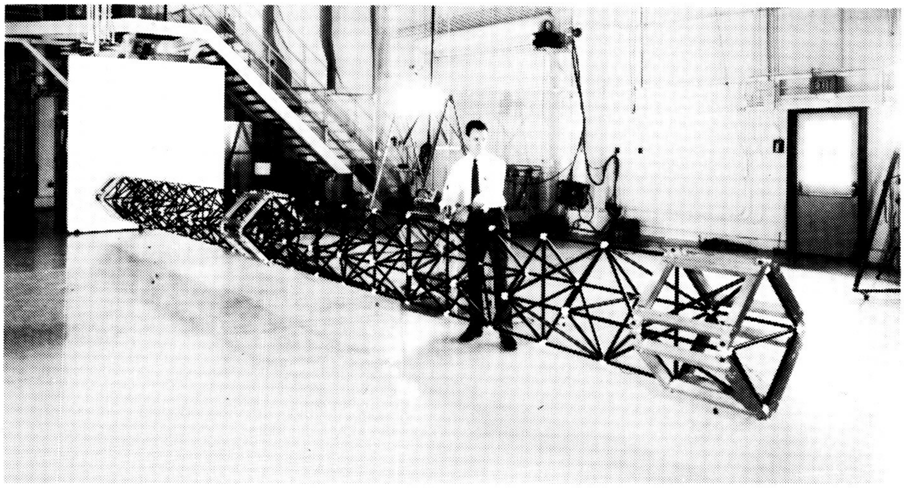

Simulated scale-model truss structure suspended for dynamic testing.
L-88-5127

cantilevered segment verified the analytical models for predicting the truss vibration frequencies and mode shapes. Tests performed to date on the suspended truss have produced results for the vibration modes of the suspension system and the first four global truss modes that are in good agreement with analysis predictions.
(P. E. McGowan, 44350)

Structures and Materials Research Laboratory

Built in 1939, this laboratory has been contributing significantly to the development of aircraft structural designs and validation since World War II. Work conducted in this laboratory includes the characterization and application of advanced materials and the development of novel structural concepts. Static testing, environmental testing, and material analysis are performed using the unique capabilities of this laboratory. Results of the testing and analysis are directly applicable to the structures and materials technologies development required for future advanced subsonic aircraft, high-speed transports, high-performance military aircraft, and large space systems. Research performed here focuses on the development of structural mechanics technology and advanced structural concepts required to enable the verified design of efficient, damage-tolerant advanced composite aircraft structural components subjected to complex loading and environmental conditions. This research also focuses on space-durable advanced materials and structural designs for future large space systems with significant improvements in performance and economy.

The main feature of the laboratory is its static testing equipment. A 1,200,000-lb-capacity testing machine is used for tensile and compressive tests of specimens up to 6 ft wide by 18 ft long. This machine has been used to test full-scale, compression-loaded cover panels for aircraft structures. Lower capacity testing machines of 300,000-, 120,000-, 100,000-, and 10,000-lb capacity also are used for smaller specimens. These machines have been used for a wide range of tests that examine both material properties and structural response. Capability exists for testing large structural specimens such as the trusses used for Space Station Freedom development and future large space structures. Test data are recorded using a high-speed automated data acquisition system, and these data are reduced and analyzed using on-site computers.

Environmental testing for materials is performed using inert atmosphere furnaces with temperature capabilities up to 4500°F. A 3200°F inert atmosphere dilatometer/thermogravimetric analyzer also is used. A hypersonic materials environmental system is capable of continuous operation at Mach 5 to 150,000-ft altitude to simulate operating conditions for future high-speed and hypersonic aircraft. The system is used to study the effects of environment on the materials used for future high-speed and hypersonic aircraft applications. Polymer films are studied using two 30-in.-diameter electron irradiation chambers capable of pressures to 10^{-8} torr and of energy levels to 100 keV.

Material analysis of fiber-reinforced composite materials and of new alloys is performed using a scanning electron microscope, an electron probe analyzer, X-ray equipment, and an electron microscope. This equipment is used for fundamental material science studies of emerging materials for aerospace applications.

Evaluation of Pultruded J-Stiffened Graphite/Epoxy Wing Panels

Structural concepts that exploit the structural efficiency of composite materials and are also suitable for cost-effective fabrication methods are being studied for primary structures applications for future aircraft. The stiffened panel shown in the figure has three J stiffeners and has been designed for a transport aircraft wing box with inplane loadings of $N_x = 22,000$ lb/in. in compression and $N_{xy} = 1,900$ lb/in. in shear. The panel was made by the pultrusion process in which graphite/epoxy materials for the appropriate laminate configurations were pulled through a heated die of the desired cross-sectional shape which cured the composite panel as it passed through the die. A 20-ft-long wing plank was made by this process and then cut into panels of the desired length for testing at Langley Research Center. Undamaged panels and panels with small holes exceeded the compression design ultimate load for this heavily loaded panel concept. Panels subjected to low-speed impact damage failed at approximately 78 percent of design ultimate load. These test results indicate that the pultrusion process can be used to fabricate usable heavily loaded graphite/epoxy-stiffened wing panels in high-production volumes for future aircraft wing applications.

(J. H. Starnes, Jr., 43168)

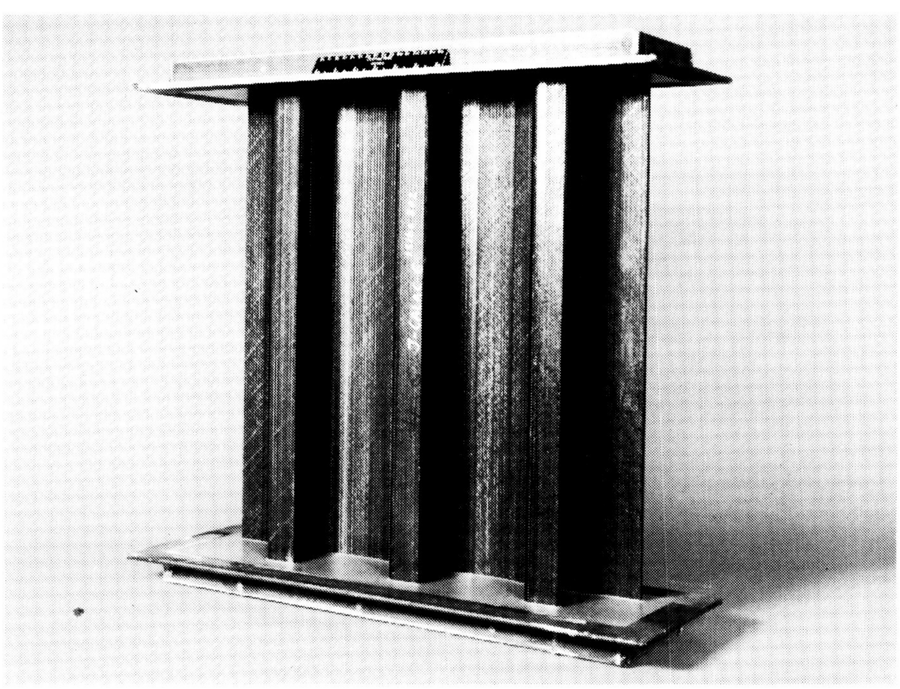

Pultruded graphite/epoxy J-stiffened wing plank. L-88-02189

Demonstration of Space Station Freedom Truss Assembly With Mobile Transporter

The primary structure for Space Station *Freedom* is an erectable truss beam that consists of a series of segments (21 for the initial configuration) called bays. Each bay is a 5-m cube constructed from long tubes (struts) which are connected at the corners (nodes) by quick-attachment joints. The on-orbit construction of the truss beam uses astronauts in extravehicular activity working from astronaut positioning devices on a Mobile Transporter (MT) to assemble the members of the truss beam.

A full-scale operational test article of the MT concept was designed and fabricated at Langley Research Center to demonstrate the procedures and assembly rates for the construction of the truss structure for Space Station *Freedom*. The MT test article consisted of an assembly platform, two astronaut positioning devices, and a drawbar system. A stationary tower was also fabricated to support the test article during subsequent testing. The assembly platform provided a stable base under which the truss was assembled. The astronaut positioning devices were used to move the astronauts to the appropriate work site during the assembly process. When a truss bay had been assembled, it was indexed out of the work area by

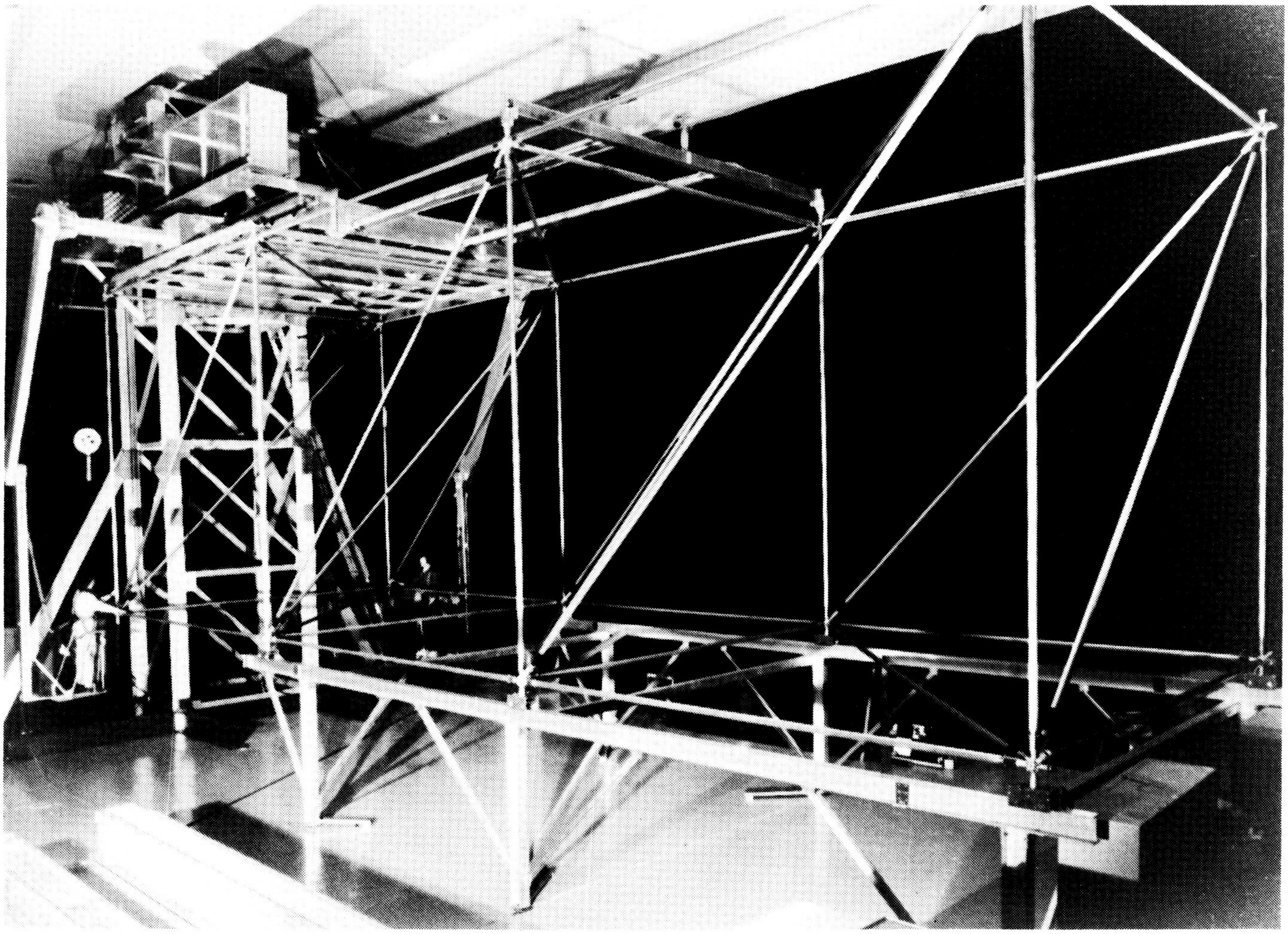

Three bays of Space Station Freedom truss structure assembled in 1 g using MT.

the drawbar system, thus producing the relative motion between the truss and MT simulating the on-orbit travel of the transporter along the completed truss structure. The astronaut positioning device system and the drawbar system were hydraulically powered in this ground test version. The controls for these systems were located at two remote consoles positioned on either side of the MT. Each console was operated by one test engineer who could view the activity for the tests and could communicate verbally over headsets with the test personnel.

Assembly tests were conducted both in 1 g in the Structures and Materials Research Laboratory and in 0-g simulation at the Marshall Space Flight Center Neutral Buoyancy Simulator (NBS). During the 1-g tests the operation of the MT was evaluated and the assembly procedures for the truss structure were developed. The test article was then sent to the NBS for simulated 0-g assembly tests; fourteen test runs were conducted using a total of eight subjects in astronaut extravehicular activity suits. During an assembly test, three bays of structure (44 struts) were assembled one bay at a time, under the transporter platform, by two test subjects. Results showed that astronaut assembly of a structure the size of Space Station *Freedom* can be rapid and efficient when using the MT. Three bays of truss structure can be assembled in 20.27 min (27.6 s/strut) using trained personnel. This is one-half the assembly rate used to determine truss assembly times in previous Space Station *Freedom* studies.

(J. J. Watson, 43116, H. G. Bush, W. L. Heard, Jr., and M. S. Lake)

NDE Research Laboratory

The reliability and safety of materials and structures are of paramount importance to NASA. The assurance of reliability must be based on a quantitative measurement science capability that is nondestructive. The Langley Research Center NDE Research Laboratory has as its prime focus the development of new measurement technologies that can be directly applied to ensuring material integrity. Furthermore, the laboratory activity is strongly directed toward developing physical properties required for structural performance.

A new facility has been constructed which added 16,000 ft^2 of laboratory space to the existing nondestructive evaluation (NDE) research area. This new facility was furnished and occupied in January 1989 and will allow for some expansion of NDE efforts over the coming years.

The NDE Research Laboratory is a combination of research facilities providing advanced NDE capabilities for NASA and is an important resource for government and industry technology transfer. The laboratory is the Agency's focal point for NDE and combines basic research with technology development and transfer. The activity concentrates on NDE materials measurement science for composites and metals with emphasis in materials characterization as well as impact damage, fatigue, applied and residual stress, and structural NDE with smart sensors/materials. A particular new focus highlights NDE requirements for Space Station Freedom on-orbit NDE and national problems of aging aircraft.

The facility is a state-of-the-science measurement laboratory linking 16 separate operations to a central computer consisting of a VAX-750 with 10 megabytes of internal memory and more than 500 megabytes of fast storage tied to staff desktop microcomputers. The system interfaces with a real-time video input-output so that NDE images can be obtained, processed, and analyzed on-line. The major laboratory operations include a 55-kip and a 100-kip load system for stress/fatigue NDE research, a magnetics laboratory for residual stress, three computer-controlled ultrasonic scanners for imaging material properties, a technology transfer laboratory, an electromagnetic impedance characterization laboratory for composite fiber integrity, and a composite cure monitoring laboratory for process control sensor development. Other major laboratory operations include a nonlinear acoustics laboratory for advanced NDE research, a laser modulation applications laboratory for remote sensing and smart materials, a pressure and temperature derivative laboratory for higher order elastic constant measurements, a thermal NDE laboratory, and a signal processing laboratory for improved image resolution and information transfer. An X-ray

tomography system is under construction to provide the first view of material or structural failure under load and will be on-line in 1990.

Thermal Diffusivity Measurements in Carbon-Carbon Composites for Porosity Evaluation

In recent years, carbon-carbon (C-C) composite materials have come into widespread use in aerospace industries. These materials are particularly attractive for high-temperature applications due to their thermal and mechanical behavior. Few quantitative measurements, however, have been made to characterize these materials. One problem encountered with C-C composites is porosity. Materials engineers have determined that the degree of porosity is correlated to interlaminar sheer strength in C-C composites. Since repetition of the C-C processing cycle reduces porosity, a technique for assessing porosity between processing cycles which is noncontacting and does not contaminate the material would be of value. A material property that is related to density and therefore to porosity is thermal diffusivity. Thermal diffusivity is easily measured remotely with infrared techniques and is therefore an attractive candidate measurement for assessing porosity between processing cycles of C-C composites.

A noncontacting technique for measuring thermal diffusivity which utilizes an Nd-YAG laser as a thermal wave source and an infrared camera detector has been developed at the NDE Research Laboratory. Thermal diffusivity is extracted from the phase delay between the thermal wave source and a spatially offset detection region. Diffusivity can be determined for three orthogonal directions to indicate the variation of diffusivity with structural anisotropy of the material or to account for effects of local variations in the fiber direction due to fiber weave in the composite lay-up. In the figure, results are given for diffusivity measurements of a series of samples which have undergone varying numbers of repetitions of the processing cycle, thus producing a range of porosity levels. A strong correlation of diffusivity in the through-ply direction with the bulk density, and therefore with the level of porosity of the composite material, is shown. **(D. M. Heath, 44963, and W. P. Winfree)**

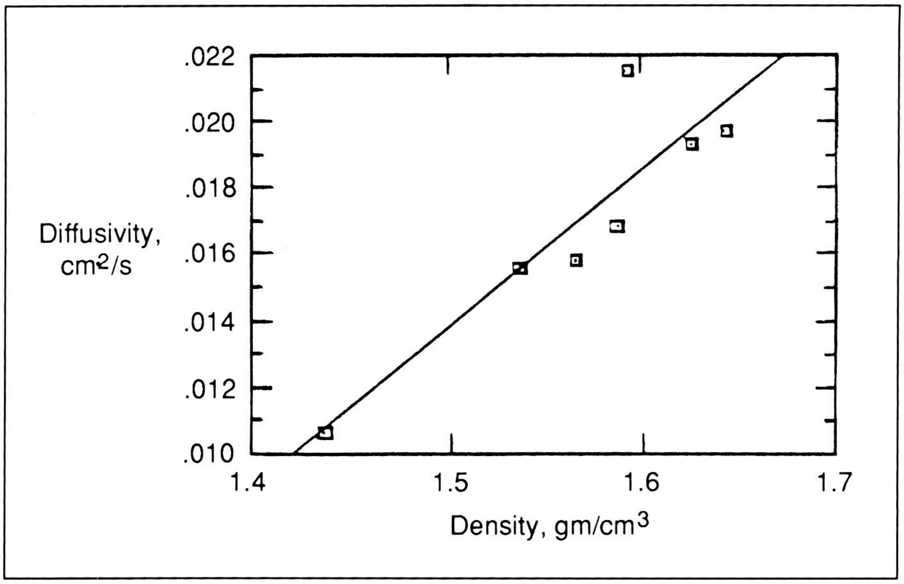

Thermal diffusivity versus density of C-C composite material.

Ultrasonic Imaging of Stiffness Coefficients in Composites

The stiffness of materials is one of the design characteristics used by engineers. In the past, one method of measuring the stiffness coefficients of a material was to perform an ultrasonic measurement on specially designed samples that were cut with specific angles. This allowed for a single measurement of the different coefficients. In the NDE Research Laboratory, a novel ultrasonic technique for measuring location by location the stiffness coefficients in actual composite parts is being developed. This technique will provide the ability to nondestructively detect weaknesses in materials; this information can also be used to input data into finite-element codes. The actual linear behavior of a part can be predicted under various load conditions.

This measurement technique has been applied to actual Space Shuttle carbon-carbon brake

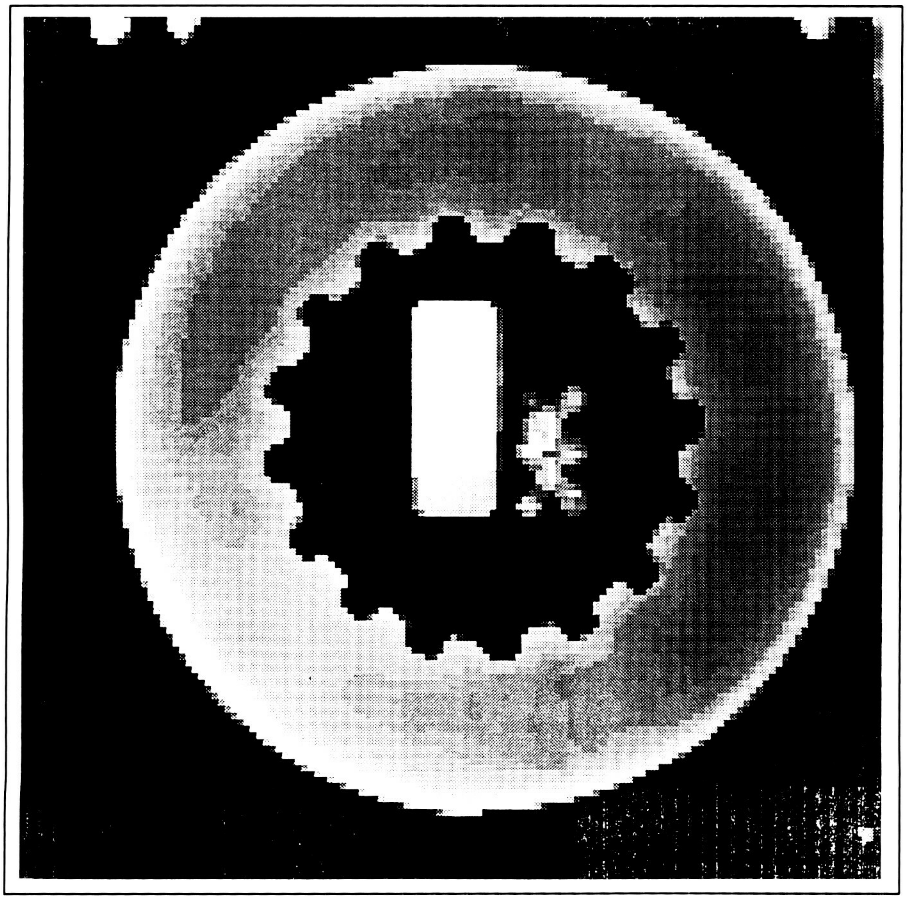

X-ray image of carbon-carbon brake stator component.

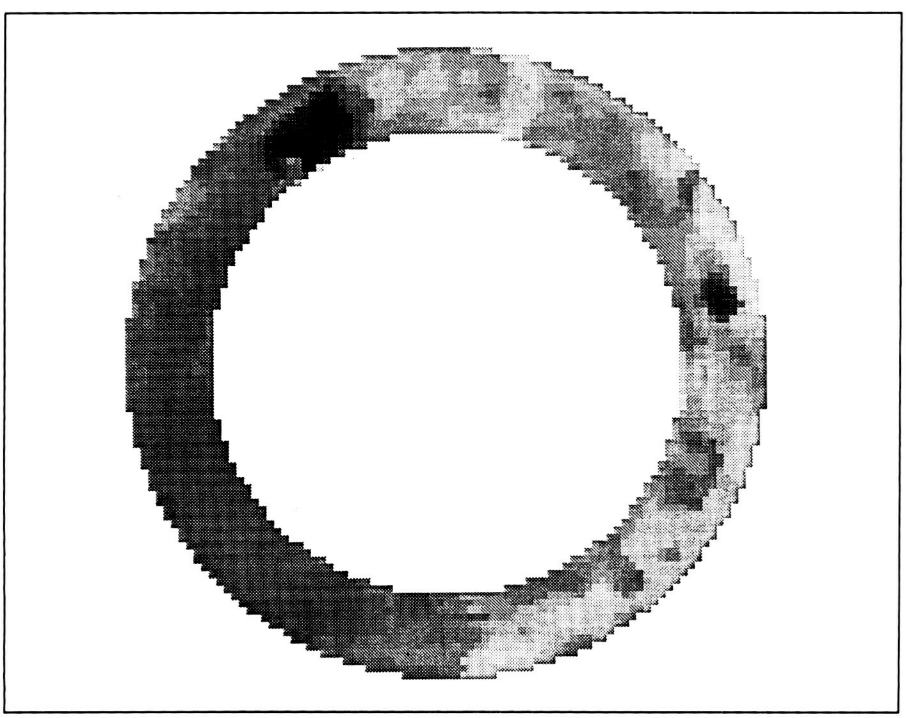

One ultrasonic stiffness image of same carbon-carbon stator component.

shoes in response to a request by the Lyndon B. Johnson Space Center to assist in the NDE of their carbon-carbon brake shoe program. Because of the ultrasonic attenuating and scattering nature of this material, testing for acceptance and recertification has been very troublesome. The first figure ws a conventional X-ray image of the whole brake stator disk which shows only small variations in density. Based on the symmetry of this material, nine stiffness coefficients for each location in the stator were measured with this technique to produce a stiffness image. The second figure shows one of the stiffness coefficient images. For scanning simplicity, the areas of the brake stator disk away from its edges were measured; this resulted in the simple ring-shaped image shown. A dark area is evident on the image of this brake shoe; this area represents an approximately 15-percent loss in stiffness. Since X-ray images are related to material density, the first figure does not indicate the significant loss in stiffness that occurred.
(E. I. Madaras, 44993)

Ultrasonic Technique to Determine Fatigue States of Structurally Significant Aluminum Alloys

In the field of metals, aluminum alloys are the mainstay of the aircraft industry because of their strength-to-weight ratio and other useful properties. Unlike many steels, however, aluminum alloys will fail under low-level cyclic stress loads. As the number of fatigue cycles on an aluminum structure increases, so

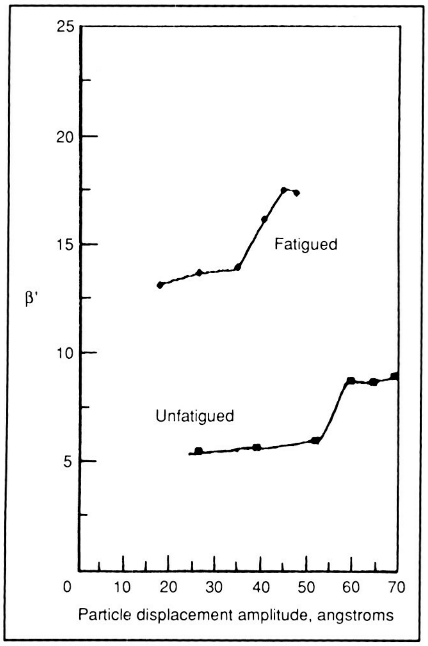

β' versus amplitude for unfatigued and fatigued Aluminum-2024.

does the probability for failure. Hence, the fatigue properties of aluminum are particularly significant in determining the remaining useful life of an aircraft in an air fleet, especially in an aging aircraft.

The feasibility of an ultrasonic technique as a nondestructive method of evaluating the state of fatigue in Aluminum-2024 has been investigated. Specifically, the acoustic nonlinearity parameter β' was determined for both fatigued and unfatigued samples (from the same lot) from measurements of absolute amplitudes of fundamental and harmonic ultrasonic waves by the capacitive detector technique. As found in the figure, a 100-percent increase in the nonlinearity for the fatigued samples is shown.

Insight into the mechanism for this increase is also contained in the plots. A precipitous rise in the nonlinearity parameter occurs as a function of fundamental amplitude. This result is consistent with the predictions of a theory developed for interfaces that are caused to separate under the action of large-amplitude ultrasonic waves. A further investigation into the effect is presently under way.

(W. T. Yost, 44991)

Smart Structures

Fiber optic sensors provide the opportunity to fabricate materials with internal sensors that can serve as lifetime health monitors, analogous to a central nervous system. The embedded fiber optic sensors can be interrogated by various techniques to measure internal strain, temperature, pressure, acoustic waves, and other parameters indicative of structural integrity.

Experiments have been conducted on composite samples with embedded sensors to measure strain using an optical phase-locked loop; this loop measures changes in the optical phase by producing changes in the modulation frequency of an optical phase by causing changes in the modulation frequency of an optical source (such as a laser).

Optical fibers were embedded in a graphite/epoxy composite filament wound tube. Resistance strain gauges were mounted externally to the tube to provide a reference strain measurement. The tube was subjected to bending stress and, simultaneously, strain and optical phase measurements were obtained. The figure indicates the excellent correlation obtained between the measured strain and the frequency (phase) change of the optical phase-locked loop that was used to interrogate the embedded optical fiber.

Embedded fiber optic sensors can be used to measure dynamic and static strain in large flexible structures such as Space Station

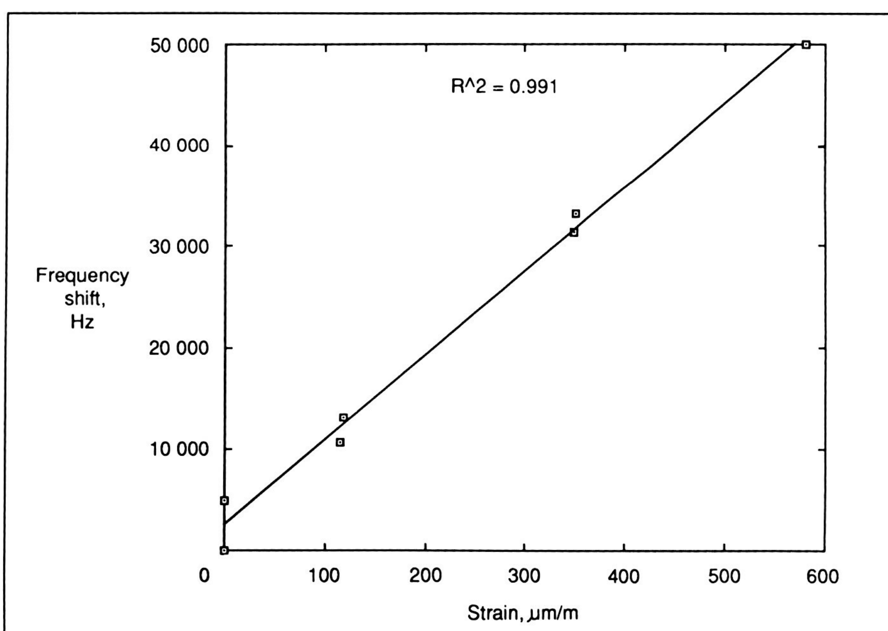

Correlation of fiber and strain gauge.

Freedom and can provide data on structural integrity and feedback for structural control. In addition, a single, multiplexed fiber will serve several sensor functions and can be a communication link. These sensors have the potential for lifetime monitoring of aircraft and spacecraft for real-time nondestructive evaluation. **(R. S. Rogowski, 44990)**

ORIGINAL PAGE
BLACK AND WHITE PHOTOGRAPH

Vehicle Antenna Test Facility

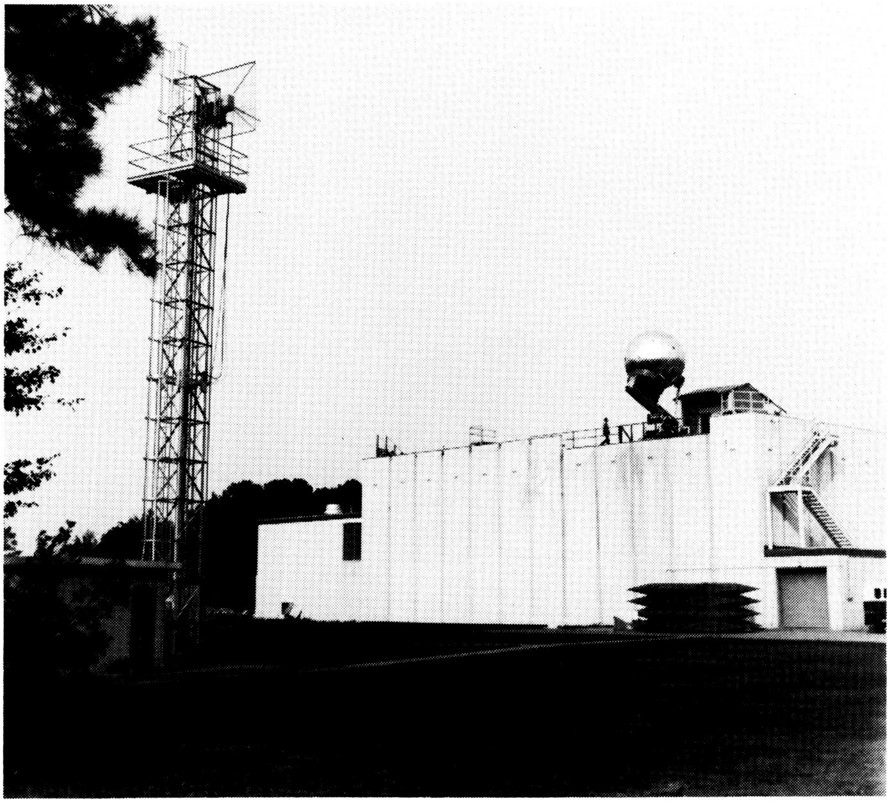

The Vehicle Antenna Test Facility (VATF) is a research facility used to obtain data for new antenna performance and electromagnetic scattering data in support of various research programs. The VATF consists of two indoor radio frequency anechoic test chambers and an outdoor antenna range system. The anechoic chambers provide simulated free-space conditions for measurements from 100 MHz to >40 GHz. The anechoic chambers, which are shaped like pyramidal horns to reduce specular reflections of the walls, are over 100 ft long and have test area cross sections approximately 30 ft by 30 ft.

A spherical near-field (SNF) measurement capability was added to the low-frequency anechoic chamber. A precision antenna positioning system, antenna source tower, and optical alignment system designed for SNF measurements were installed in the low-frequency anechoic chamber, and the capability now exists for automatic performance of precision SNF measurements up to at least 18 GHz. Antennas with diameters up to 12 ft can be measured if their electrical size is no greater than 100 wavelengths (i.e., diameter/wavelength ≤100). This limitation is imposed by the SNF system software, which transforms the near-field data to

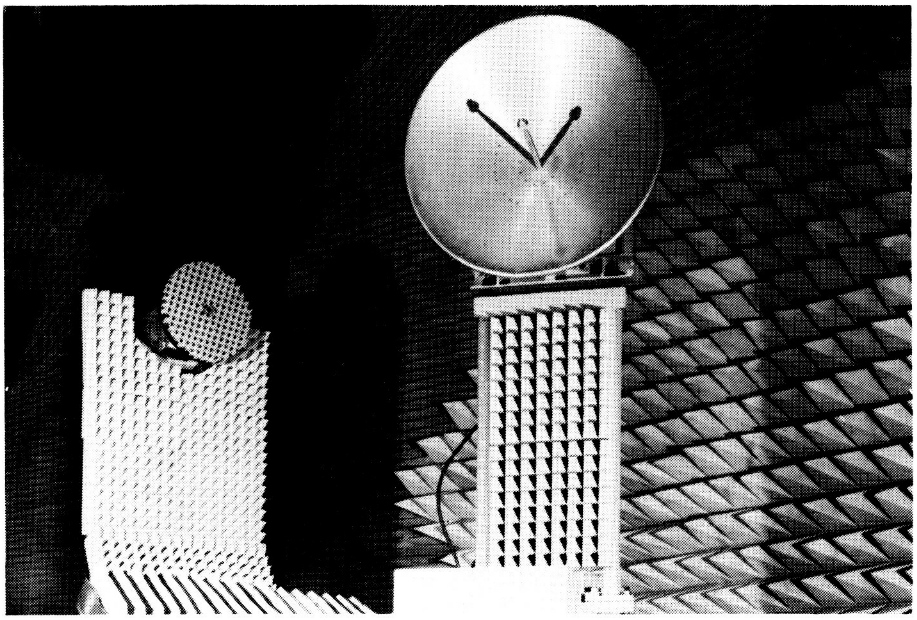

Spherical near-field equipment. L-85-2143

obtain the desired far-field data. Measured data stored on disk can be processed to provide antenna directivity, polar or rectangular plots of the radiation patterns, and three-dimensional contour plots of the antenna radiation characteristics.

The high-frequency anechoic chamber was used to establish a Compact Range Facility. The compact range is an electromagnetic measurement system used to simulate a plane wave illuminating an antenna or scattering body. The plane wave is necessary to represent the actual use of the antenna or scattering from a target in a real-world situation. The compact range utilizes an offset-fed parabolic reflector to create the simulated plane wave test conditions. The standard commercially available compact range is limited to the measurement of antennas or models with maximum dimensions of 4 ft over the frequency range of 4 GHz to 100 GHz.

The outdoor antenna range system is available for use when the antenna or test model size or frequency precludes the use of the anechoic chambers. The outdoor range consists of two remote transmitting towers that are spaced 150 ft and 350 ft from the test positioner mounted on the VATF roof. The VATF has several electronic laboratories with the extensive measurement capability needed to support the design of unique antennas prior to their evaluation in the antenna chambers or on the outdoor antenna range system.

Antenna Pattern Measurements for Helicopter Applications

Scale-model measurement of vehicle antenna radiation patterns is an important step in the development of accurate antenna pattern prediction codes. This fact is particularly true for antennas mounted on complex structures such as helicopters. Depending upon the operating frequency and location, aircraft structure can have a significant effect on antenna performance.

A 1/10-scale, advanced attack helicopter model (shown in the first figure) has been developed and tested for antenna radiation pattern verification in the low-frequency anechoic chamber. Aircraft azimuth, elevation, and roll plane antenna patterns were measured for a monopole antenna located on the underside of the fuselage. Initial baseline tests were conducted with the rotor blades removed from the model and then repeated with the rotor blade assembly fixed at a 45° angle to the aircraft longitudinal axis. Measurement data collected during these verification tests confirmed the basic accuracy of the Electromagnetic Surface Patch (ESP) code for a typical helicopter geometry. The ESP code combines the moment method (MM) of electromagnetic analysis with a computationally efficient geometric modeling technique. Comparison of a predicted roll plane pattern (solid line) with the measured pattern (dashed line) for a monopole antenna operating at 200 MHz is shown in the second figure.

After full verification of the code at all frequencies of interest, ESP pattern predictions will guide selected antenna tests for specific United States Army helicopter configurations. Both static interactive effects of aircraft structure and dynamic effects of rotating blades on antenna

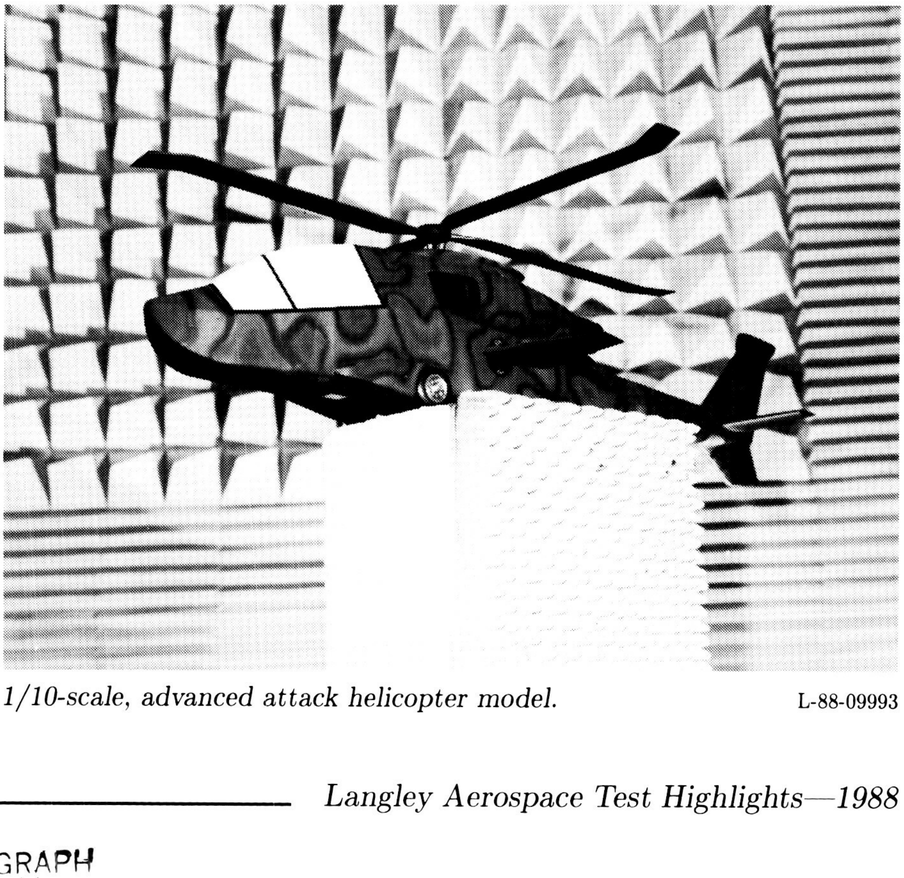

1/10-scale, advanced attack helicopter model. L-88-09993

ORIGINAL PAGE
BLACK AND WHITE PHOTOGRAPH

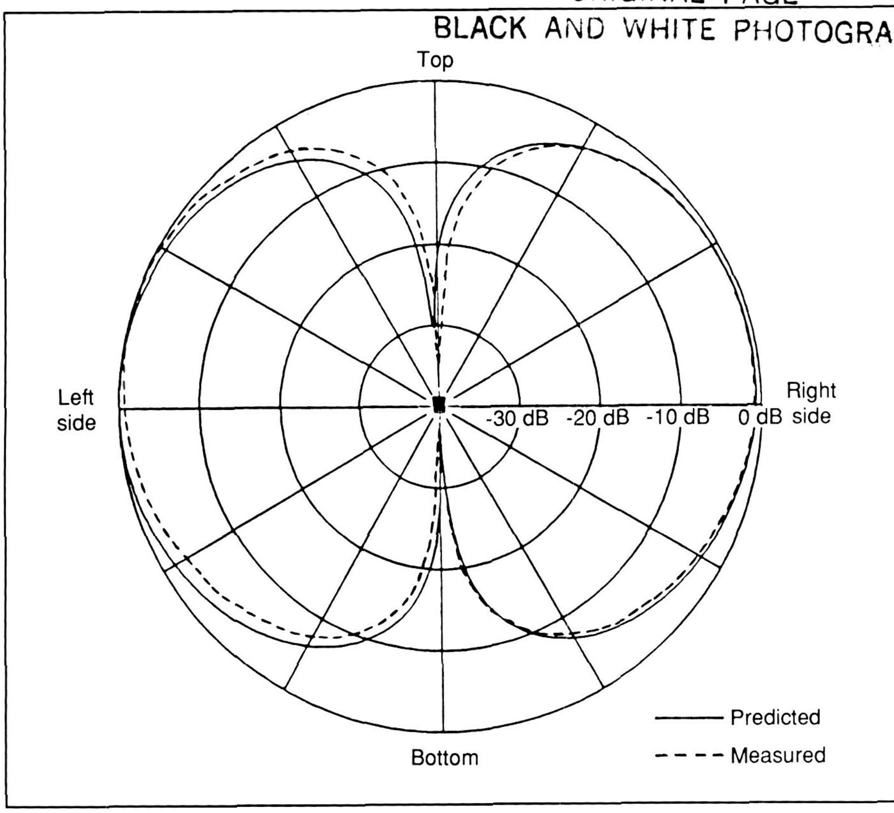

Predicted and measured roll plane antenna patterns for 1/10-scale, advanced attack helicopter with rotor blades removed.

radiation characteristics have become increasingly important to the performance of advanced helicopter avionics systems. Application of electromagnetic analysis codes and comprehensive scale-model testing can assure optimum aircraft antenna location, and, additionally, reduce costly field modification and full-scale testing for both existing and future Army helicopters.
(G. C. Barber, 41818)

Antenna Tests on Aeroassist Flight Experiment (AFE) Model

During 1988, the 4/10-scale model of the Aeroassist Flight Experiment (AFE) spacecraft was tested in the low-frequency anechoic chamber. These tests were performed in order to evaluate various antenna configurations that could be used on the actual spacecraft. The test frequency was 5.266 GHz, which was scaled to the size of the spacecraft so that it remained the same size in wavelengths as that of the full-size spacecraft. The antennas used were helixes in quartz dielectric cavities.

The antenna testing consisted of measuring single antenna elements as well as various array configurations. Preliminary radiation patterns were measured at 11 antenna locations on the front and sides of the spacecraft. Eight-element and four-element array configurations were tested in accordance with the baseline configuration proposed by the Marshall Space Flight Center.

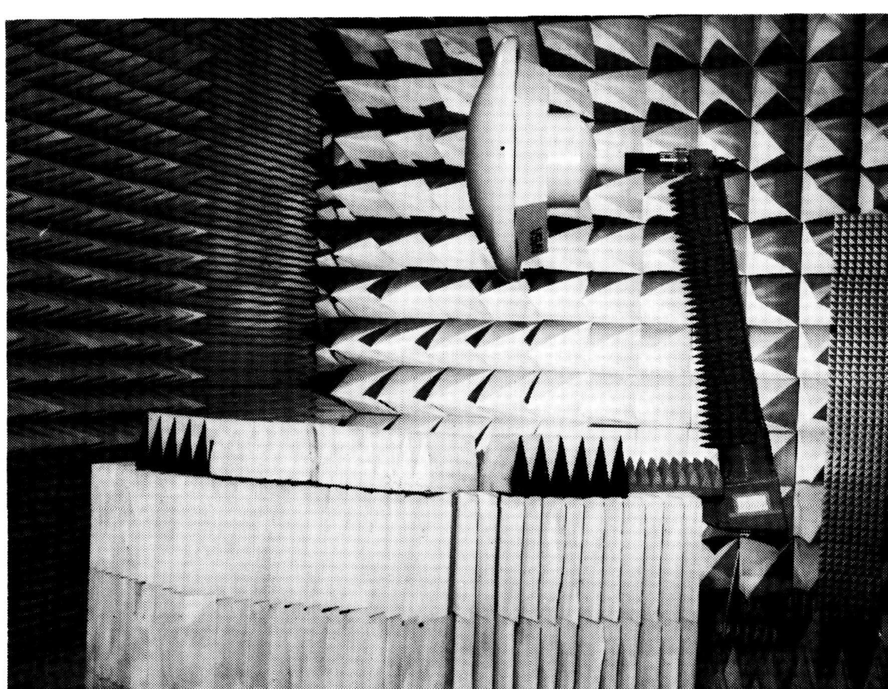

AFE model being tested in low-frequency anechoic chamber. L-88-6477

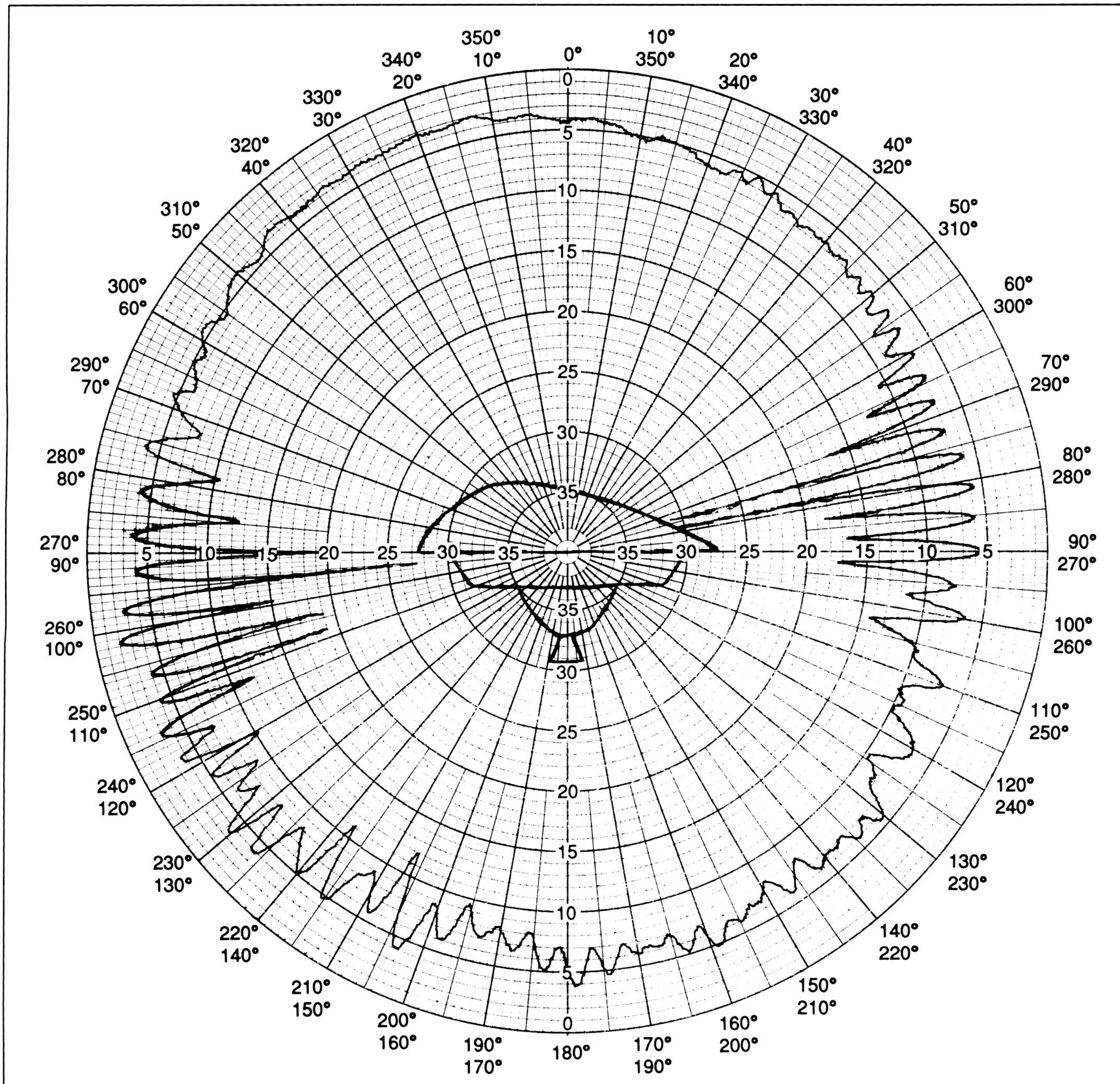

Measured radiation pattern of two-element antenna array at 5.266 GHz.

Due to spacecraft-to-satellite tracking problems that may be encountered using array configurations, a two-element array consisting of one antenna on the front of the model and one antenna on the back of the model was tested. This design approach will provide a minimum of pattern ripple along the sides of the model and drastically reduce the communications problems with the tracking satellite during the aeropass data period. Additional tests are planned to further refine this antenna design approach for potential applications.

(D. Shively, 41816)

Advanced Compact Range Measurement System

Langley Research Center is involved in the development of advanced, indoor measurement systems suitable for performing antenna and scattering measurements. A new dual-chamber concept using a Gregorian subreflector system, as shown in the first figure, is being proposed for compact range applications. This concept places the feed and subreflector in a small chamber adjacent to the measurement range that contains the main reflector and target. These two chambers are connected by a small coupling aperture that is located at the focus of the main reflector. This system can potentially provide improved taper, ripple, and polarization performance in the target zone. Because the main reflector uses a subreflector, its focal length can be decreased without a loss in performance. This, in turn, reduces the minimum length requirement for the main chamber.

The most serious potential errors associated with this dual-chamber concept are related to the scattered fields emanating from the coupling aperture. Even though the reflected field from the subreflector focuses to a small region that is on the order of a few wavelengths in diameter, there are diffracted fields from the subreflector and feed spillover fields that are not focused and tend to illuminate the aperture edges. As a result, the coupling aperture edges must be treated with a radio frequency absorber to reduce these scattering terms.

The Gregorian subreflector has been constructed at Langley. The radiation pattern performance of the system was evaluated by placing the feed chamber onto the antenna positioner in the low-frequency anechoic chamber as shown in the second figure. Radiation patterns mea-

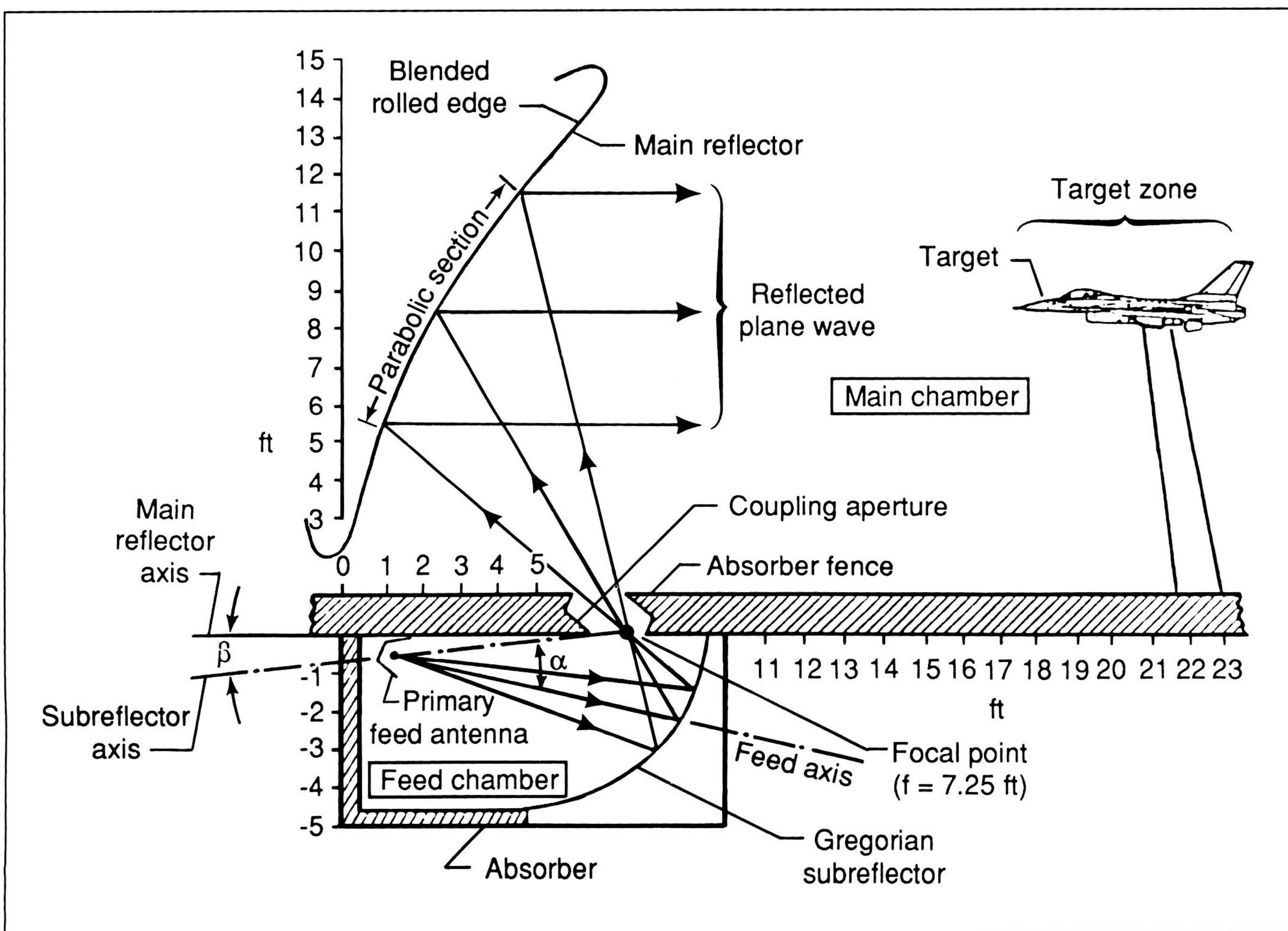

Dual-chamber compact range configuration.

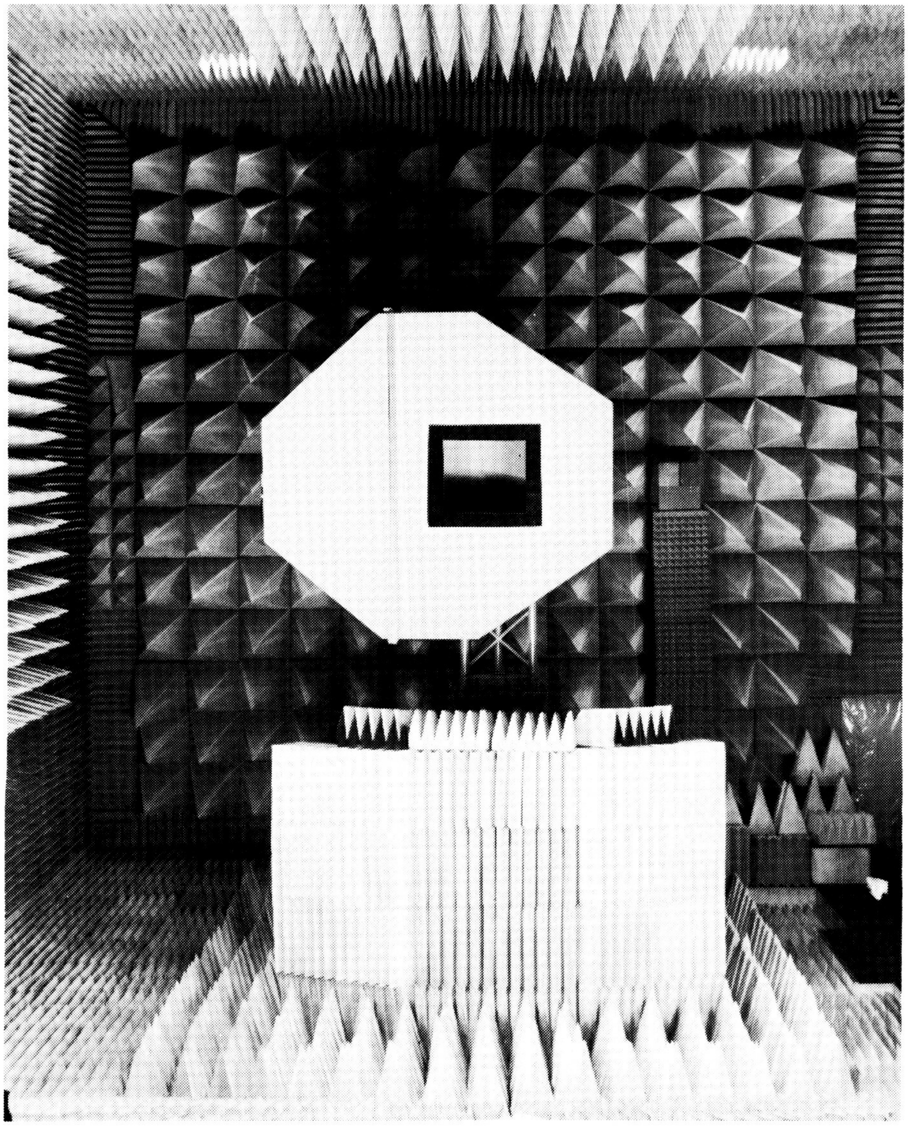

Feed chamber in low-frequency anechoic chamber. L-87-8938

sured at 10 GHz for two different absorber treatments of the coupling aperture are shown in the third figure. These measurements show the improvement in performance as the absorber is added to all aperture edges. These measurements have shown that the Gregorian subreflector system is capable of providing the required performance needed for an advanced compact range measurement system.
(M. C. Gilreath, 41817)

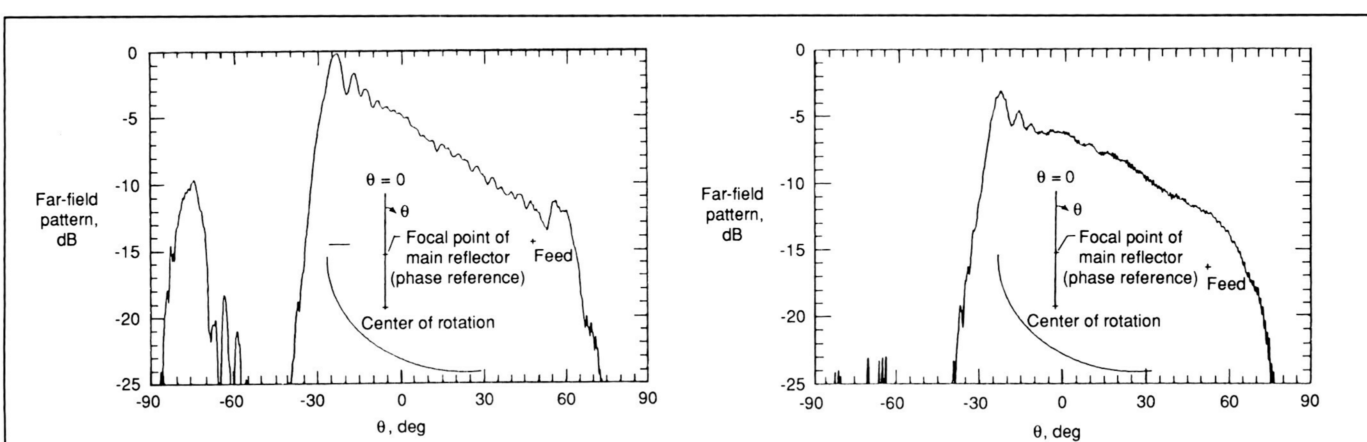

Principal plane patterns of feed chamber (absorber on one edge of aperture (left); absorber on all edges of aperture (right)).

Impact Dynamics Research Facility

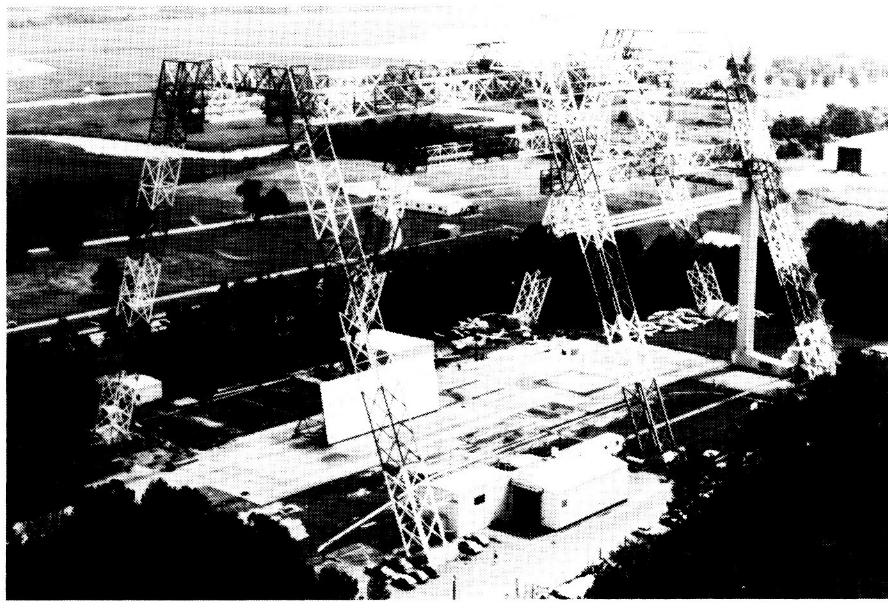

This facility, which was originally used by the astronauts during the Apollo Program for simulation of lunar landings, has been modified to simulate crashes of full-scale aircraft under controlled conditions. The aircraft are swung by cables, pendulum-style, into the concrete impact runway from an A-frame structure approximately 400 ft long and 230 ft high. The impact runway can be modified to simulate other ground crash environments, such as packed dirt, to meet a specific test requirement.

The aircraft is suspended by swing cables from two pivot points 217 ft off the ground. It is then pulled back along an arc to a predetermined height by a pullback cable from a movable bridge on top of the A-frame, released from the pullback cable, and allowed to swing, pendulum-style, into the ground. An instant before impact, the swing cables are separated from the aircraft by pyrotechnics. The length of the swing cables regulates the aircraft impact angle from 0° (level) to approximately 60°. Impact velocity can be varied up to approximately 65 mph (governed by the pullback height) and to 90 mph with rocket assist. Variations of aircraft pitch, roll, and yaw can be obtained by changes in the aircraft suspension harness attached to the swing cables. Onboard instrumentation data are obtained through an umbilical cable attached to the top of the A-frame. Data are transmitted by hard wire to the control room at the base of the A-frame. Photographic data are obtained by onboard cameras, ground-mounted cameras, and cameras mounted on top of the A-frame. Maximum allowable weight of the aircraft is 30,000 lb.

Static Response of Composite Fuselage Floor Sections

Composite materials are presently being investigated as the primary structural material for the next generation of aircraft. To determine the behavior of composite aircraft structure under crash conditions, detailed experimental and analytical studies of structural subcomponents are being conducted. Two circular 6-ft-diameter graphite/epoxy fuselage floor sections with the identical skeletal framework of 3 graphite/epoxy 6-ft-diameter semicircular Z cross-section frames (Z-frames), 3 aluminum floor beams, and 15 graphite/epoxy stringers were statically tested as an initial step in assessing the response of such structural subcomponents to vertical impacts. One specimen (skinned specimen) had a graphite/epoxy skin that was bonded and riveted to the frames and stringers, whereas the other specimen was without skin (skeleton specimen). The load-deflection response for the skeleton floor section shown in the figure was reduced by one-third to allow comparison with data

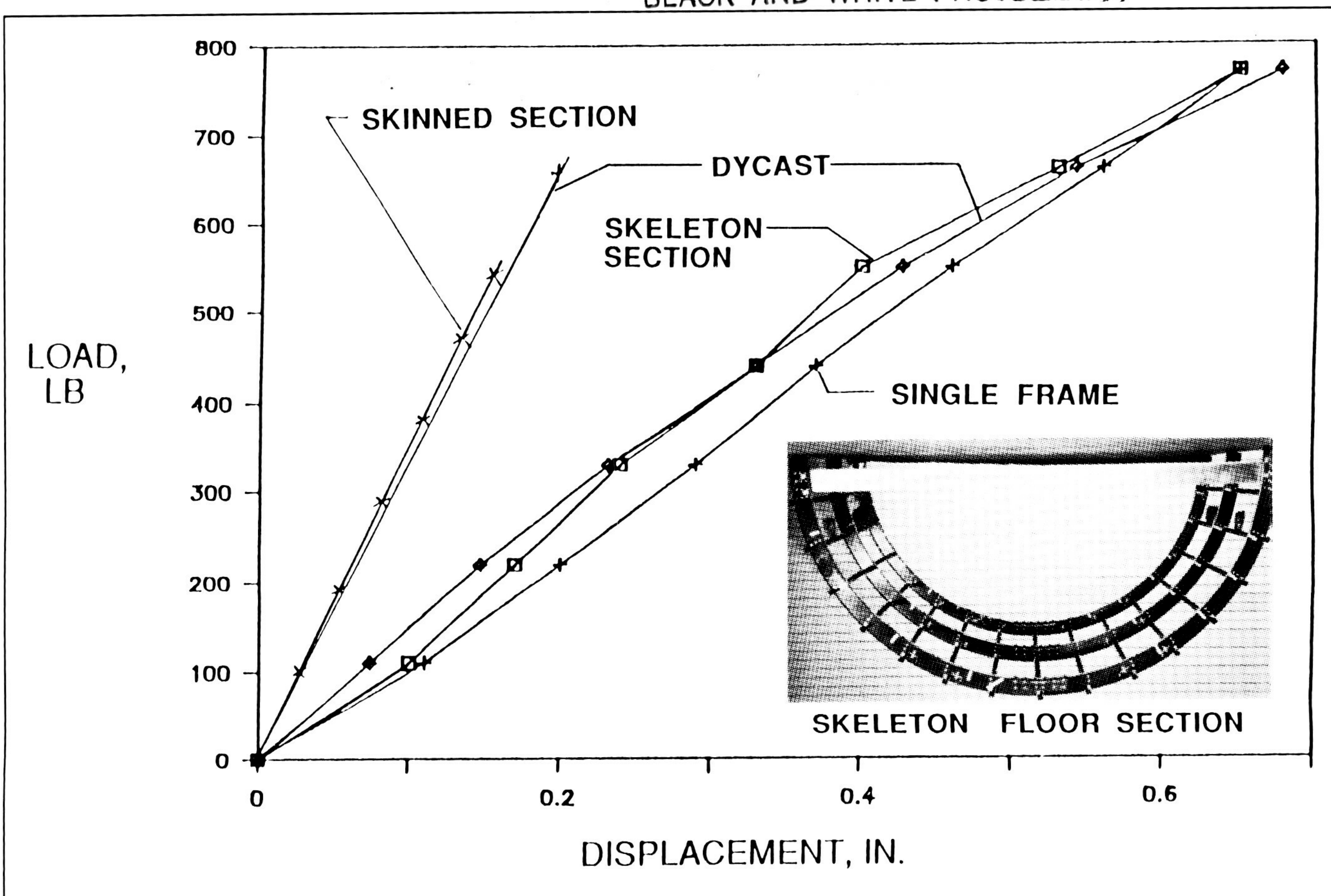

Experimental and analytical load-displacement behavior of composite subfloor sections.

from a single frame. The floor section load for one frame agrees very well with the single frame data. For the skinned specimen, the load-deflection stiffness was approximately four times larger than the stiffness of the skeleton specimen.

DYCAST (Dynamic Crash Analysis of Structures) finite-element computer models were used to predict the load-deflection response with different boundary conditions on the out-of-plane and twisting deformation of the specimen. The best analytical/experimental correlation was obtained for boundary conditions that allowed the frame to bend out of plane but not to twist. These assumptions agreed with experimental observations. The best correlation for the skinned section was obtained by constraining the out-of-plane and twist displacements. Tests of such specimens provide a data base and understanding of the crash behavior of composite structures and will allow development of innovative concepts to improve energy absorption characteristics.

(R. L. Boitnott, 44151, E. L. Fasanella, and H. D. Carden)

Interim Transportation Overpack Container Experiments and Analysis

An experimental and analytical program has been conducted at the Impact Dynamics Research Facility on the Interim Transportation Overpack Container (ITOC) system being developed by the United States Army Armament Research, Development, and Engineering Center (ARDEC). The ITOC is a steel vault-like structure (6 ft long, 4 ft wide, and 3 ft high) designed to house three artillery projectiles for security and protection in the event of a helicopter crash and postcrash fire. Dynamic Crash

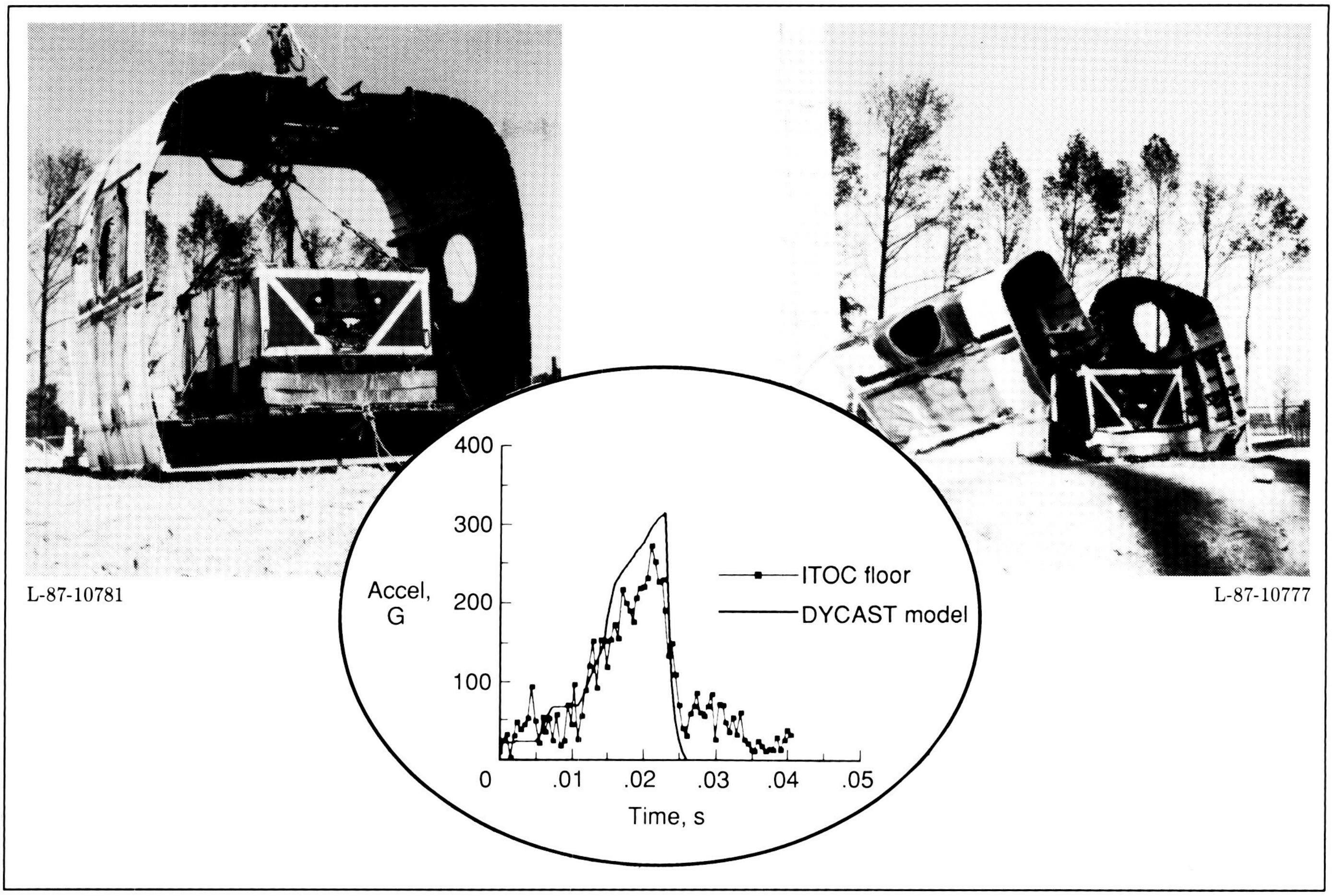

Pretest and posttest photographs of ITOC in helicopter section and experimental/analytical acceleration comparison.

Analysis of Structures analytical models were constructed prior to the test to predict responses of the ITOC. Tests of fully instrumented ITOC packages mounted inside a CH-47 helicopter section shown in the figure were performed at 100 ft/s (197-ft drop height) onto a 5-ft depth of soil over a concrete impact surface to test the integrity of the ITOC. To limit loads on the ITOC and the interior projectiles, the ITOC was mounted on a balsa cargo pallet containing crushable aluminum honeycomb.

In the DYCAST analysis, nonlinear springs derived from detailed models of the fork-lift stirrups and helicopter floor were utilized along with nonlinear spring representations of the soil and honeycomb. In spite of the severity of the impact, structural integrity of the ITOC was maintained, and accelerations were successfully measured on the helicopter section, the ITOC, the containers, and the projectiles. A comparison of the experimental acceleration on the ITOC floor with the pretest DYCAST finite-element model (see insert in the center of the figure) showed a slight overprediction of the acceleration. Because the test results validated the analytical DYCAST model, this model could then be used to predict loading for other impact velocities. These studies showed that the honeycomb would provide a satisfactory cushioning for impact velocities up to 150 ft/s.

(E. L. Fasanella, 44150,
L. E. Jones, and
H. D. Carden)

Aircraft Landing Dynamics Facility

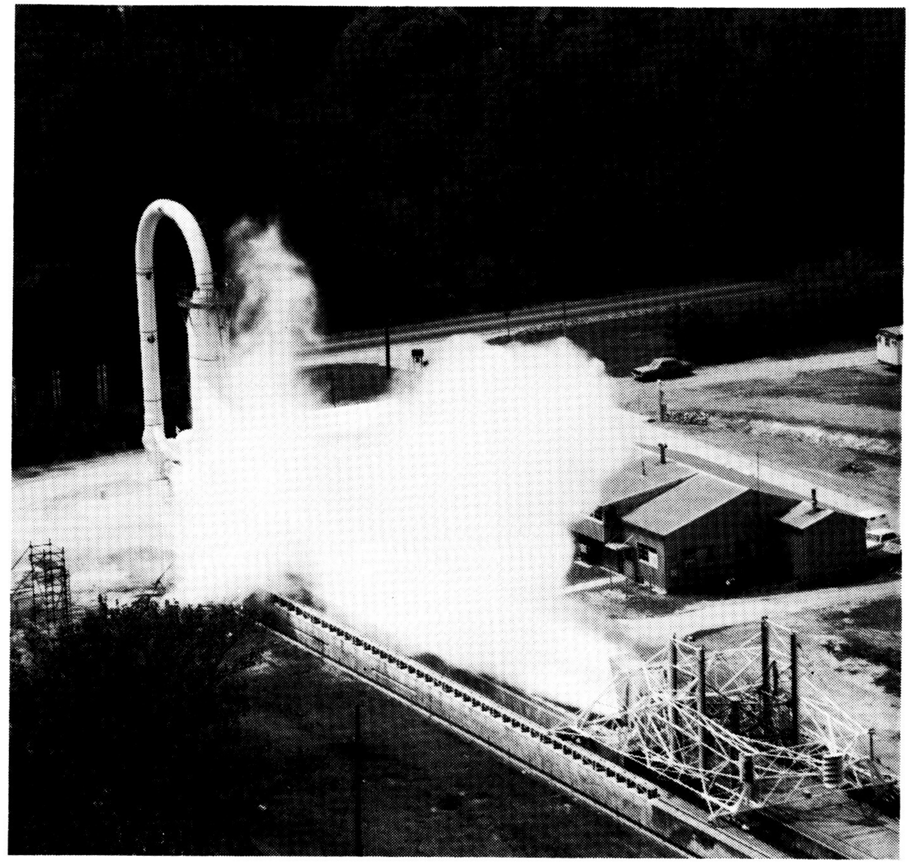

Langley Research Center has recently updated the landing loads track to the Aircraft Landing Dynamics Facility (ALDF) to improve the capability of low-cost testing of wheels, tires, and advanced landing systems. The main features of the updated facility are the propulsion system, the arresting gear system, the high-speed carriage, and the track extension.

The ALDF uses a high-pressure water jet system to propel the test carriage along the 2800-ft track. The propulsion system consists of an L-shaped vessel that holds 28,000 gallons of water pressurized to 3150 lb/in^2 *by an air supply system. A timed, quick-opening shutter valve is mounted on the end of the "L" vessel and releases a high-energy water jet, which catapults the carriage to the desired speed. The propulsion system produces a thrust of* 2×10^6 *lb force, which is capable of accelerating the 108,550-lb test carriage to 220 knots within 400 ft. This thrust creates a peak acceleration of approximately 20 g. The carriage coasts through an 1800-ft test section and decelerates to a velocity of 175 knots or less when it intercepts the five arresting cables that stretch across the track. The arresting system brings the test carriage to a stop in 600 ft or less. Essentially any landing gear can be mounted on the test carriage, including those exhibiting new concepts, and any runway surface and weather condition can be duplicated on the track. Research on slush drag, hydroplaning, tire braking, steering performance, and runway grooving has been conducted in the past.*

Future research programs include the Space Shuttle orbiter main and nose gear tire spin-up wear characteristics and cornering force measurements at high speeds as well as frictional properties of radial and H-type aircraft tires for comparison with conventional bias ply tires. A surface traction program to study the effect of different runway surface textures and various runway grooving patterns on the stopping and steering characteristics of aircraft tires will be conducted. Finally, tests associated with the National Tire Modeling Program will also be conducted.

ORIGINAL PAGE
BLACK AND WHITE PHOTOGRAPH

Carriage with wing section leaving the Heavy Rain Simulator area at ALDF. L-88-9867

Aircraft Landing Dynamics Facility Rain Simulation System.

The potential aerodynamic penalties associated with flying in highly concentrated, short-duration rainfall have been demonstrated utilizing small-scale models in the wind tunnel. However, due to the complexity of the two-phase flow environment of water and air, the established wind tunnel model to full-scale scaling laws may not be applicable in the rain environment. This has motivated the development of a research technique to obtain large-scale aerodynamic data in a simulated natural rain environment. Modifications have been made to the ALDF to accommodate a large-scale wing model and a Rain Simulation System (RSS). A wing mounted to the ALDF carriage has been propelled at speeds from 100 knots to 170 knots with wing angles of attack from 6° to 20°. Lift and drag measurements have been made on the wing for assessment of the rain effects on aerodynamic performance.

The ALDF-RSS is a 500-ft-long, 44-ft-wide overhead distribution system comprised of three parallel 10-in.-diameter irrigation pipes aligned lengthwise along the track and supported every 100 ft at a height of 40 ft above the track. The RSS, shown in operation in the first figure, is presently configured with 1590 nozzles to expel approximately 4000 gal of water in 20 s, or 40 in./hr. By variations in the nozzle arrangement, the RSS will be capable of producing uniform rain rates of 2, 10, 30, or 40 in./hr over an area 15-ft wide by 500-ft long. Rainfall characteristics were determined by measuring the volume of water collected in a series of collector cans spaced beneath the system. This calibration technique has verified the system output of 40 in./hr and the uniformity of the spray region to be within ±10 percent.

The determination of drop diameter and drop distribution data is facilitated by a high-speed photographic technique to "freeze" the action of the near-field falling rain. A typical photograph is shown in the second figure. These photos are digitized into a 1000 by 1000 pixel image with a gray-scale range of 256 intensities using the Eikonix digitizing camera in the Image Processing Laboratory. An interactive thresholding technique is then applied to each image to produce binary (black and white) images. To correct for any drop distortions during the thresholding procedure, binary image overlays onto a gray-scale image are allowed for editing the binary image. Computer-aided analysis of these binary images

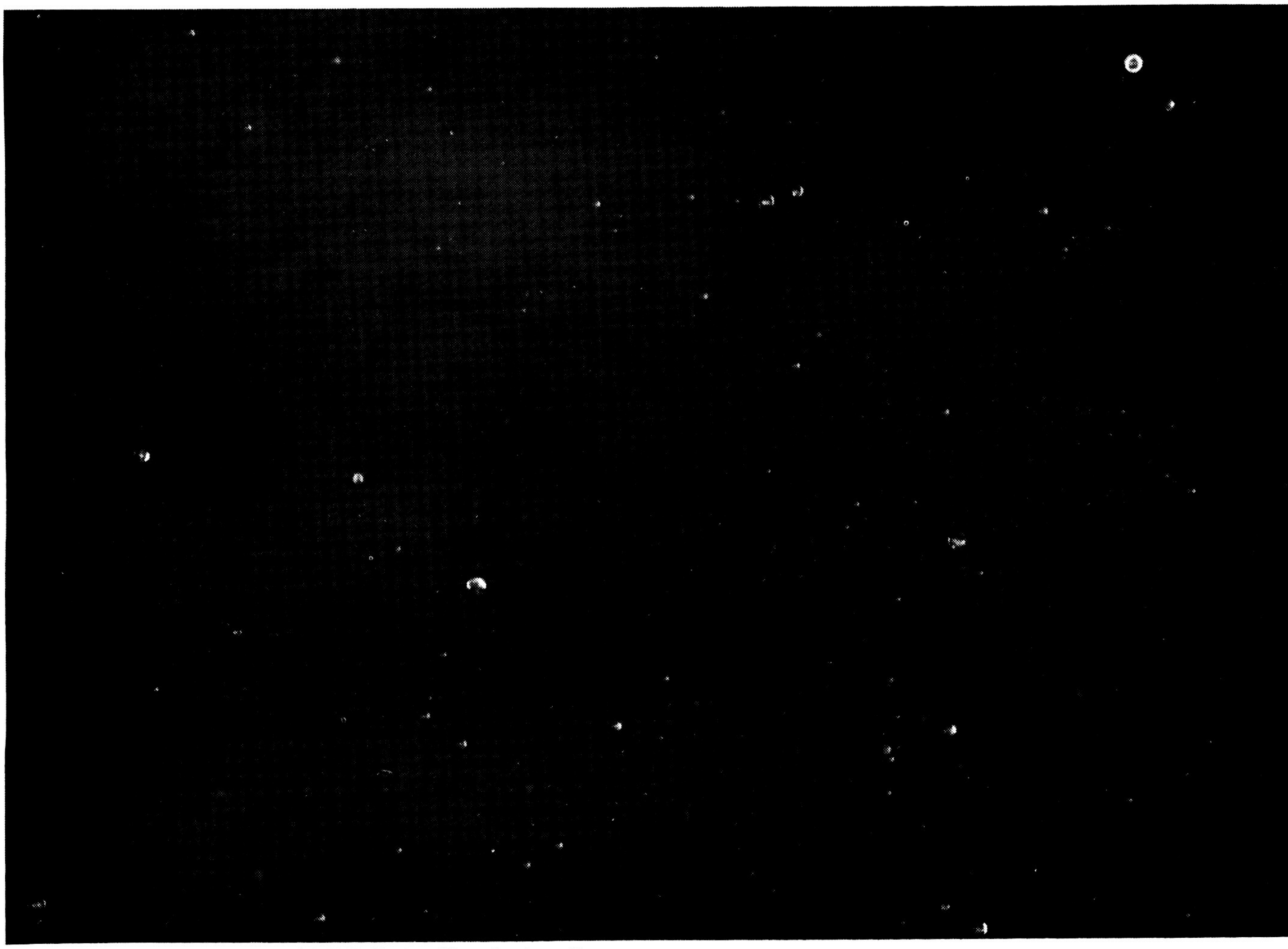

Rain drops simulated at ALDF Rain Simulation System.

will be undertaken to provide the geometric and statistical drop characteristics for the simulated rain rates of 2, 10, 30, and 40 in./hr, which, combined with the volumetric measurements, will allow accurate calibration of the ALDF-RSS.
(B. A. Campbell, 45069, and S. M. Stubbs)

Orbiter Flat-Tire Landing Model

Concerns exist about the consequences of the Space Shuttle orbiter having a flat tire prior to landing. Although this type of failure is extremely remote, tests were conducted at the ALDF to define the drag characteristics of the Space Shuttle orbiter main gear strut assembly during the sequential destruction of its components for a flat-tire landing on a runway. The first tests involved sliding various skid specimens down a simulated concrete runway at higher speeds and bearing pressure than ever tested before. These tests provided data relative to the skidding friction of the orbiter brake stack, axle, or strut piston. Next, tests were conducted on bare orbiter wheels to determine how far they could roll under realistic loads and speeds in the event that the failed tire is ripped off the wheel during the rollout. Wheels with modified flanges were also tested to try to increase the roll distance. Finally a test was conducted which involved landing a deflated tire mounted on the orbiter wheel to determine the rolling friction of this configuration.

Test results given in the figure show that landing with a flat tire produces rolling resistance of 0.2, and after approximately 1000 ft the flat tire destroys itself and leaves behind the tire bead, which causes a rolling resistance of 0.1. After bead failure the wheel loads are high enough to

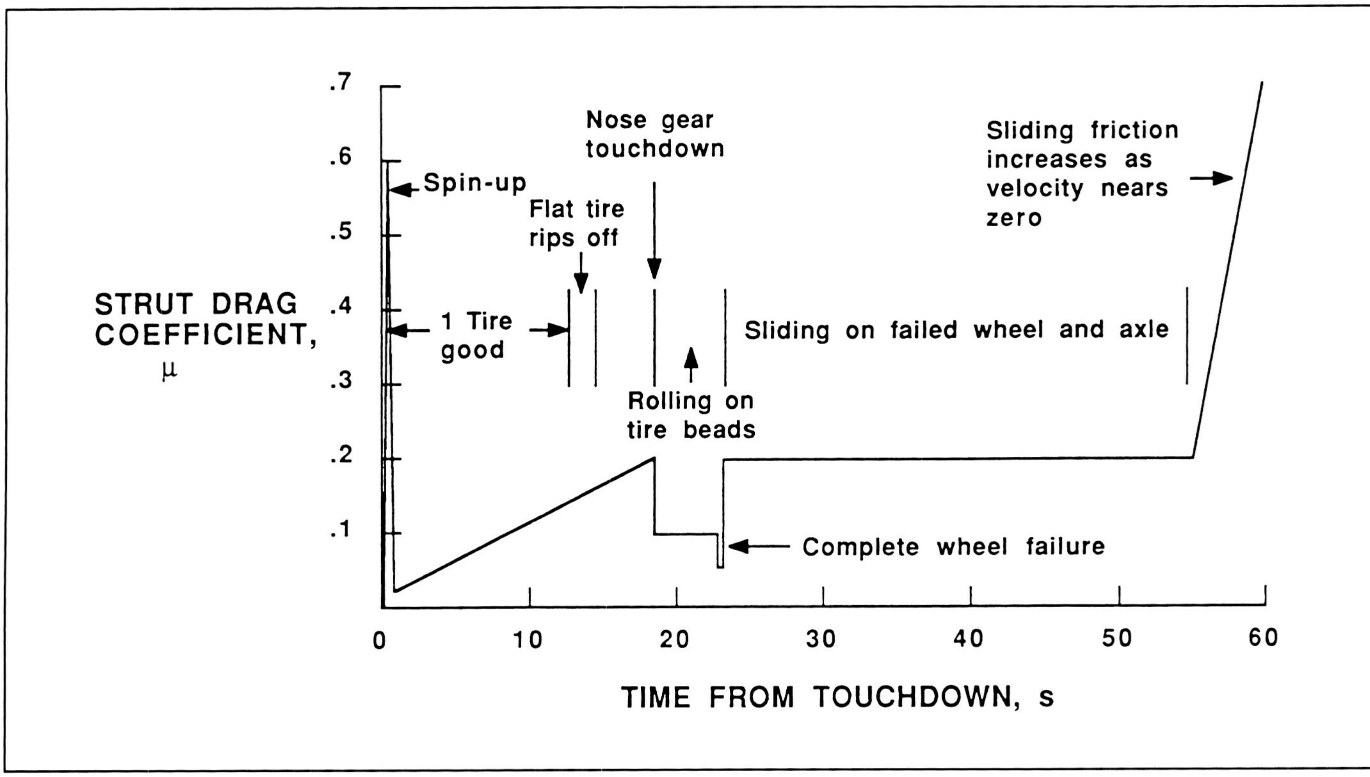

Friction history for flat tire on Space Shuttle orbiter with concrete-surface landing.

fracture the wheel. The wheel was found to survive less than 1 s as shown in the figure. For the remainder of the rollout, modeled by ALDF skid material testing, relatively constant sliding friction is indicated until the speed is fairly low. Based on these data, it was determined that landing with a flat tire is controllable on a concrete runway. The wheel is almost certain to fracture during this type of landing. A review of skid data on lake bed surfaces shows that the skidding friction on a lake bed will be too great for orbiter directional control; therefore, the flat-tire priority runway was changed from the Edwards Air Force Base lake bed to a concrete runway at Edwards. **(R. H. Daugherty, 41309)**

Basic Aerodynamics Research Tunnel

Computational methods are progressing rapidly toward the prediction of the three-dimensional flow field about complex geometries at high angles of attack. These computational methods require a large number of grid points to adequately model the flow field, and they produce large amounts of information. To validate these methods, detailed experimental flow field measurements are required. The Basic Aerodynamics Research Tunnel (BART) is a flow diagnostic facility dedicated to the task of acquiring the detailed data required for code validation and investigating the fundamental character of complex flow fields.

Forward view of BART. L-85-3069

BART is an open-return wind tunnel with a closed test section 28 in. high, 40 in. wide, and 10 ft long. The maximum test section velocity is 220 ft/s, which yields a Reynolds number per ft of 1.4 $\times$ 10^6. The airflow entering the test section is conditioned by a honeycomb, four antiturbulence screens, and an 11-to-1 contraction ratio. These flow manipulators, coupled with an excellent speed controller, provide a low-turbulence, uniform flow in the test section. The level of the longitudinal component of turbulence intensity ranges from 0.05 percent at low speeds to 0.08 percent at a test section dynamic pressure of 45 lb/ft^2.

The timely acquisition of the detailed data required for code validation dictates the use of a highly integrated and fully automated Data Acquisition and Control System (DACS). BART DACS consists of a computer sys-

tem that monitors and controls all test instrumentation. BART instrumentation includes a three-dimensional probe traverse system, an electronic scanning pressure system, a three-component hot wire, and a three-component laser Doppler velocimeter.

Vortical Flow Over 5° Cone With Tip Geometry Variations

To explore the generation of side forces on slender bodies at high angles of attack, an experimental program was conducted to evaluate sectional side forces on a 5° cone with three different nose tips. The baseline nose tip was sharp, and the other two were blunted with tip radii equal to 8.7 percent and 17.5 percent of the cone base radius. Rings of pressure orifices were located at 40 percent and 80 percent of the model length; the model was rolled from ±180° in 9° increments to determine roll dependence. Values of sectional side force were calculated by integrating the pressures measured at the two pressure ring locations.

As had been seen in previous investigations, the cone with the sharp tip exhibited large values of sectional side force; these values were also very dependent on the roll orientation of the model about its own body axis, even though the model was fabricated to be as circular as possible. Testing with the blunted nose tips dramatically reduced the levels of sectional side force although the smaller levels of side force still depended on the roll orientation of the model.

5° cone model being installed in BART. L-88-8138

Along with the pressure data, off-body flow visualization was done using a propylene-glycol seeding mixture. The off-body visualization results demonstrated the complexity of the vortex shedding patterns even from this relatively simple body. Both the visualization and pressure results are expected to be useful for code validation.
**(R. M. Hall, 42883,
S. O. Kjelgaard, and J. Chu)**

Flight Research Facility

The truss-supported roof of the huge hangar of the Flight Research Facility provides a clear floor space with nearly 300 ft in each direction (over 87,000 ft^2).

Door dimensions will allow entry of a Boeing 747. Features such as floor air and electrical power services, radiant floor heating to eliminate corrosion-causing moisture, a modern deluge fire suppression system, energy-saving lighting, modern maintenance spaces, and entry doors and taxiways on either side of the building make this structure equal or superior to any hangar in the country. Extensive and modern maintenance equipment makes it possible to maintain, repair, and modify aircraft ranging in sophistication from modern metal and composite airliners, fighters, and helicopters to fabric-covered light airplanes. Surrounding the hangar are ramp areas with load-bearing capacity sufficient to handle the largest current wide-body jet. The high-power turnup area can also handle a wide variety of aircraft.

The present array of research and research support aircraft includes an airliner, military fighters, trainers, experimental one-of-a-kind designs, helicopters, and single and multiengine light airplanes. This variety enables research to be carried out over a wide range of flight conditions,

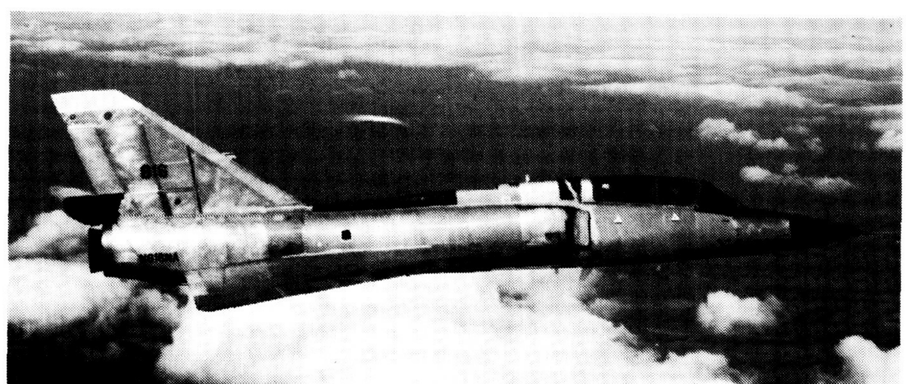

Convair F-106B configured for Storm Hazards Program. L-83-2747

Beech T34C used for flight support. L-80-3923

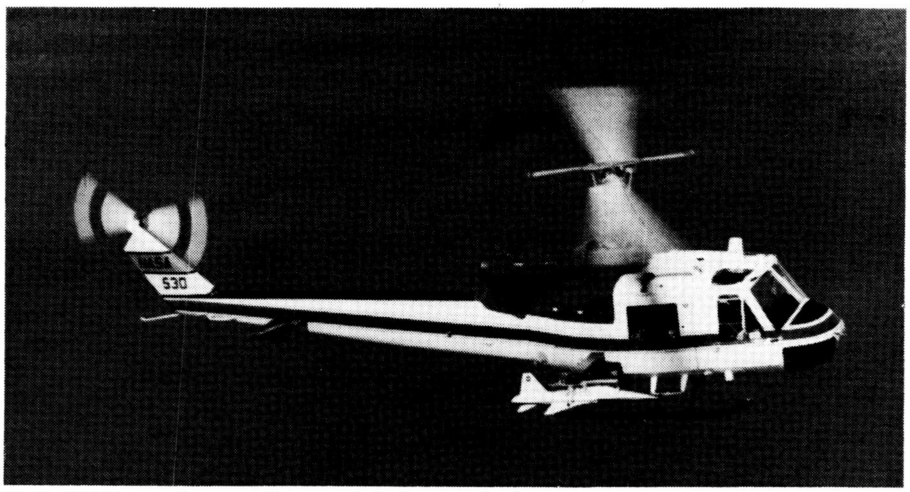

Bell 204B configured for model drop mission. L-76-6425

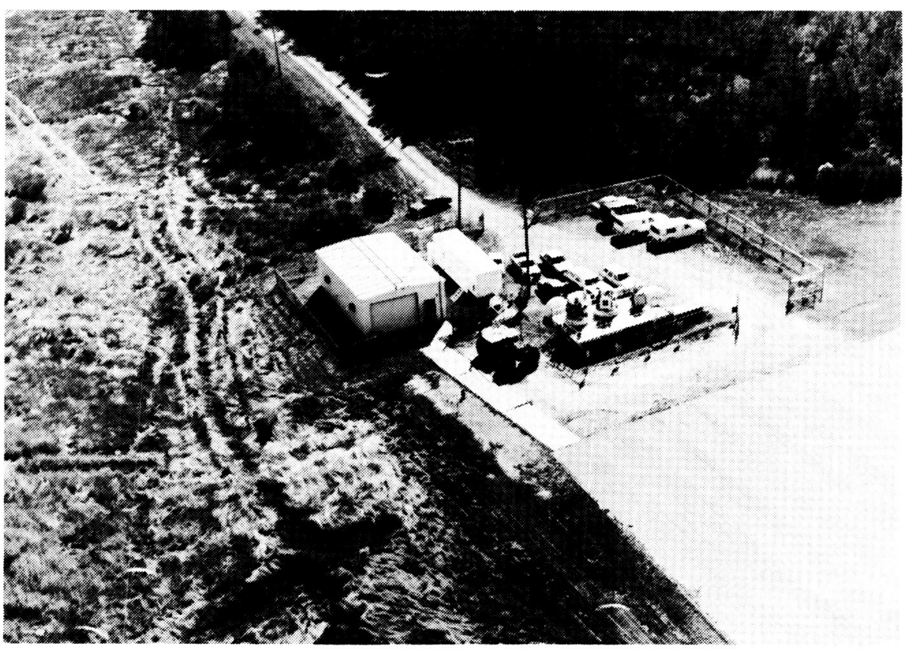

Radio-Controlled Drop Model Facility. L-83-11167

from hover to Mach 2 and from the surface to 60,000 ft. Research pilot currency in this wide spectrum of aircraft is important in conducting credible in-flight experiments as well as in-flight simulator assessments. A variety of research can be conducted in such areas as terminal traffic flow, microwave landing system (MLS) approach optimization, airfoil properties, single-pilot instrument flight rules (IFR), engine noise, turbulence research, natural laminar flow, winglet studies, stall/spin, and severe storm hazards.

One of the support helicopters is used to drop unpowered remotely controlled models of high-performance airplanes to study high-angle-of-attack control characteristics. The Radio-Controlled Drop Model Facility is used to study the low-speed flight dynamic behavior of aerospace vehicles with particular emphasis on high-angle-of-attack characteristics of combat aircraft. The technique consists of launching an unpowered, dynamically scaled, radio-controlled model into gliding flight from the support helicopter, controlling the flight of the model from the ground, and recovering the model with a parachute.

The models are constructed primarily of molded fiberglass and are typically approximately 10-ft long with weights in the range of 200 lb to 300 lb. A comprehensive onboard instrumentation system provides measurements of key flight dynamics parameters that are transmitted to the ground via telemetry and recorded for analysis. The model control loop involves a combination of ground-based and onboard equipment and the required communication links. The heart of the system is a ground-based digital computer into which the control laws are programmed. The processor accepts downlinked feedback signals from the model and commands from the pilot and computes the control surface commands that are then transmitted to the model. Very-high bandwidth electromechanical servoactuators are used to drive the model control surfaces. The pilot flies the model from a ground station that provides the required information on a number of displays. These displays include a high-resolution video image of the model, a map display showing model ground track, and conventional analog instruments presenting key parameters such as angle of attack and airspeed.

The tests are conducted at the Plum Tree Test Site located approximately 5 miles from Langley Research Center. The test site is a marsh approximately 2 miles long and 1 mile wide.

Vortex Flap Flight Experiment

The vortex flap concept, developed computationally and refined by nearly 3000 hours of wind tunnel model testing, progressed to flight testing during 1988. The flap, shown installed on the leading edge of the F-106B aircraft, is being flown to substantiate predictions of large (20-percent) drag reductions when the wing vortex system is shifted to the forward edge of the wing.

The 60° delta wings of the F-106B have been instrumented to measure strain, surface pressures, and structural accelerations. Speed, altitude, and maneuver loading conditions are being increased gradually in a careful expansion of the research test envelope. Vortex-induced flow on the flap is observed via video cameras mounted on the

F-106B with vortex flap deflected 40°. L-88-8864

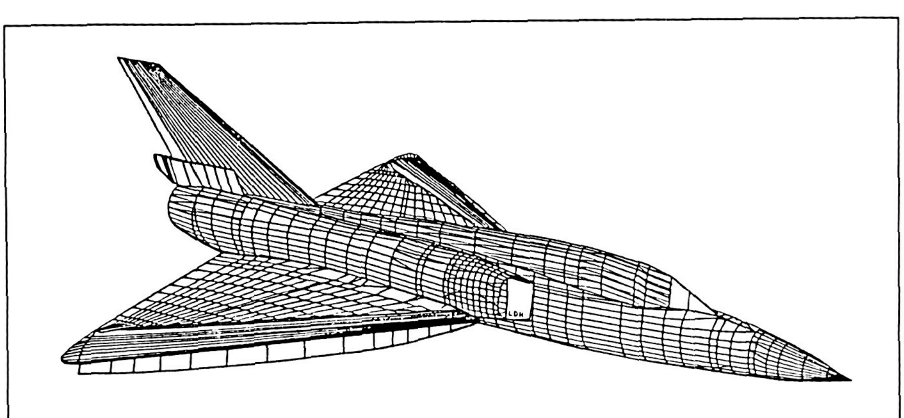

Computer model of F-106B with vortex flap.

upper fuselage and engine-inlet cowl. Flow cones (tufts tipped with slender cones) attached to the flap and wing surfaces indicate motion of the air over these surfaces.

Resultant pressure distribution, wing loading paths, and dynamic structural behavior are being correlated with data from baseline tests of the airplane with the unmodified wing and with results from wind tunnel and computational models of the same F-106B

configuration. After completion of the flight envelope expansion, precise research maneuvers will be flown to gather maneuvering performance data with the vortex flap. The results will be used to validate the computational codes used for aerodynamic design of the flap/wing combination.
(R. H. Smith, 43871, and J. B. Hallissy)

NASA/Bell 204B test helicopter with strakes on. L-88-04861

NASA/ARMY Boom Strake Flight Program

A joint NASA/United States Army flight investigation is under way which utilizes an instrumented NASA/Bell 204B helicopter to determine the effectiveness of tail boom strakes on directional controllability during hovering flight in various crosswinds. The purpose of the strakes is to disrupt or spoil the airflow over the boom during these low-speed crosswind conditions and thus to beneficially alter airloads on the tail boom. Little or no effect in forward flight is expected. Wind tunnel investigations performed in the past on typical helicopter tail boom cross-sectional shapes clearly indicated that the complex flow acting on the boom could generate side forces that would, in turn, produce adverse aircraft yawing moments. Additional yaw control, commanded through the pilot's pedals and produced on the aircraft through the tail rotor, is then necessary to trim these yawing moments created by the airloads on the boom. Under some flight conditions, loss of control of the helicopter is possible when all of the control is being utilized in trying to maintain trimmed flight. The major sources of airflow over the boom are main rotor downwash and ambient wind. Strakes, placed longitudinally along the upper left shoulder (as viewed looking forward, shown in the figure), were found to be effective in disrupting the airflow over the boom and making a significant reduction in the adverse yawing moments caused by this phenomenon.

Instrumentation onboard the test helicopter measured and recorded aircraft control positions, angular velocities, accelerations, rotor r/min, tail rotor power, engine power, airspeed, and angle of attack. Wool tufts were attached to the boom and photographed to indicate airflow conditions with the strakes on and off. A calibrated pace vehicle was used by the pilot to judge each test airspeed. Data were obtained at 5-knot increments of airspeed up to 35 knots for 30° increments in azimuth angle over a range of 0° to 330°. Most of the testing was conducted at the Wallops Flight Facility. The low-speed testing was performed at a skid height of 40 ft to achieve near out-of-ground-effect conditions.

Preliminary results indicate that in a steady crosswind condition of 20 knots and wind direction of 60° off the right of the aircraft nose, a reduction of tail rotor power required of approximately 25 percent (from 117 hp to 86 hp) was achieved. These results agreed with values calculated from wind tunnel results. Increased availability of yaw control offered by this simple device can expand the helicopter operating envelope both in terms of gross weight and altitude. Also, pilot comments indicated that at a crosswind speed of 10 knots to 15 knots with the direction of wind 60° from the left of the nose of the aircraft, the level of aircraft unsteadiness and the difficulty of control were noticeably reduced with the strakes on. Time histories of control positions and aircraft angular velocities confirmed the pilot comments. The increased steadiness with strakes on is probably achieved because the airflow separation is fixed on the

boom and because attachment and reattachment of the air do not occur.
(H. Kelley, 45088, and C. Cook)

Wind Tunnel and Radio-Controlled Flight Test Investigation of USMC Exdrone RPV Configuration

USMC Exdrone RPV configuration at Plum Tree Test Site. L-88-9682

At the request of the United States Marine Corps (USMC), an exploratory investigation was conducted by the Flight Dynamics Branch at Langley Research Center to improve the stability, control, and general flight behavior of the Exdrone RPV (Remotely Piloted Vehicle) configuration.

In order to provide the USMC with an improved Exdrone configuration, an exploratory investigation was conducted in the Langley 12-Foot Low-Speed Tunnel (also see page 1) to determine the configuration's basic aerodynamic characteristics, identify problem areas in stability and control, and identify possible modifications for improvements. Wind tunnel test results indicated that the RPV configuration had limited pitch control authority and weak directional stability characteristics. Configuration modification improvements made during the wind tunnel investigation included increasing elevator size, increasing vertical tail and rudder size, adding wing tip fins, and removing the vertical canard.

As part of the investigation, a follow-up flight test was conducted at the Plum Tree Test Site to provide a qualitative evaluation of the modified configuration's flight characteristics to verify the modification improvements developed from the wind tunnel. Flight tests have indicated that the modified RPV exhibited significant improvements in increased maneuverability, payload performance, and overall flight characteristics for the vehicle. Additional configuration refinements made during the flight test evaluation included increasing roll and yaw control, adjusting thrust alignment, and adding leading-edge droops to the outboard wing tips. With the additional modifications, the vehicle exhibited excellent stability and control characteristics and received excellent ratings from the USMC for satisfying their mission requirements.
(L. P. Yip, 41161)

Biomass Burn Experiment at Merritt Island

Millions of acres of vegetation throughout the world burn each year, thus releasing into the environment many combustion products (gases and aerosols) which are environmentally significant. Although the impact of this burning on regional and global air quality remains largely unknown, the potential for such fires to substantially affect the trace gas composition and chemistry of our atmosphere is large. These fires may significantly alter the Earth's climate through the production of aerosols and greenhouse gases.

Langley Research Center has configured its Cessna 402B fixed-wing aircraft (NASA 503) as a sampling platform for the collection of combustion-produced gases and particulates emanating from forest fires. The instrumented aircraft is used to obtain particle-size distributions, as well

Cessna 402B used for Biomass Burn Experiment. L-88-12243

as chemical composition from the portion of the fire plume where the gases and aerosols have mixed, usually at altitudes from 1000 ft to 10,000 ft. The data collected using NASA 503 will be used to complement and help quantify satellite and remotely sensed images of smoke plume dispersal. The sampling equipment consists of a nephelometer and a quartz crystal microbalance (QCM), which make particle measurements, and a filtered grab sampling system, which obtains gas samples.

On November 7, 1988, a controlled burn of a 2980-acre area on the Merritt Island National Wildlife Refuge in Florida was conducted. The John F. Kennedy Space Center is located on Merritt Island, and a portion of the refuge is burned each year to control the buildup of potential fuel for a wildfire. Langley Research Center participation in the Merritt Island prescribed burn involved the use of a Kennedy Space Center helicopter and NASA 503. The helicopter was used to sample over specific areas of the fire at close range; these areas included "hot" active regions as well as "cold" smoldering ones. NASA 503 was flown at higher altitudes, which allowed the collection of integrated smoke samples for comparison with the helicopter collections. The analysis of the data collected during this and other prescribed burns will allow refinement of the models used to describe and understand the contribution to the atmosphere made by the large number of vegetation fires throughout the world each year.

(R. M. Thomas, Jr., 43913, and W. R. Cofer III)

Image Processing Laboratory

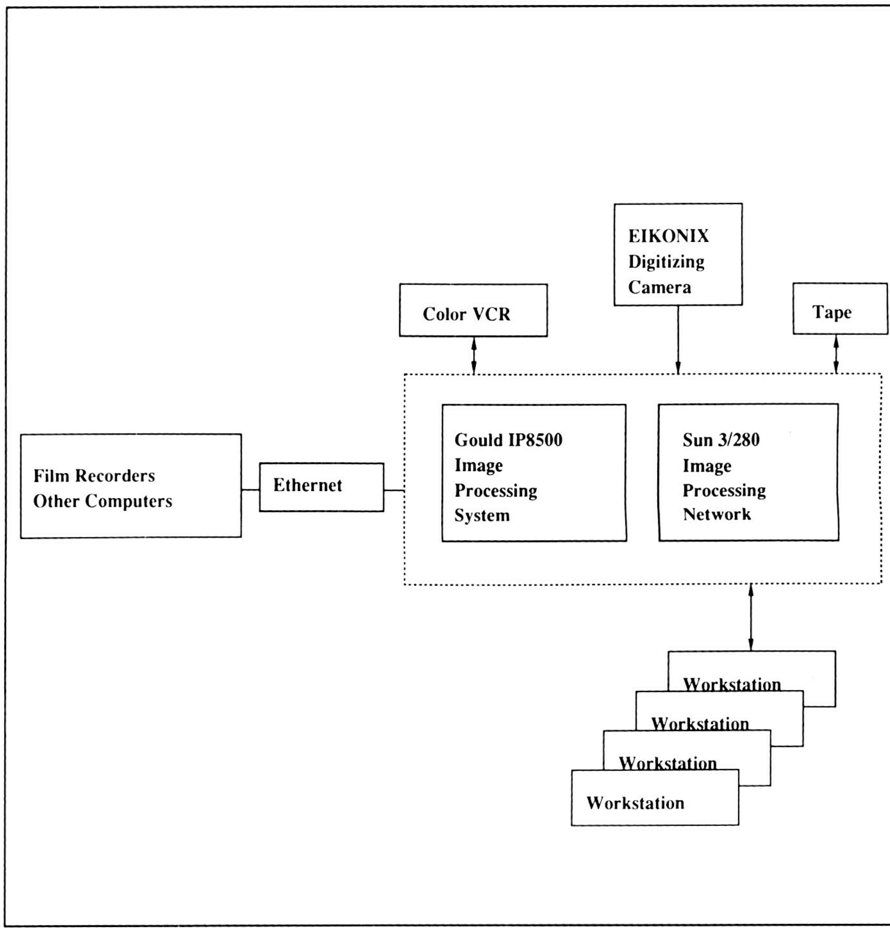

The Image Processing Laboratory (IPL) provides researchers with an interactive capability to produce, process, enhance, and analyze digital images. Typical applications include the enhancement of flow visualization images obtained from wind tunnel or in-flight experiments, analysis of remotely sensed Earth resources imagery, and nonintrusive aerodynamic heat-transfer analysis. To date, many researchers have found the capabilities of the laboratory to be beneficial. Enhanced images and accurate results can be generated in minutes compared to the manual method that took days.

The IPL is undergoing a facility upgrade to provide a state-of-the-art image processing system for Langley Research Center, as shown in the figure. The upgrade includes a Sun 3/280 color workstation featuring a Sun TAAC-1 application accelerator that is specifically designed to dramatically improve imaging and visualization performance. Currently there are several ways of getting images to the Sun for processing. The Eikonix digitizing camera can scan images either on transmissive or reflective material and convert the visual information into a digital array of numbers that can be stored and processed. Also, digital images generated on any computer on the Center's local area network can be transferred to the system via an Ethernet connection, and a nine-track magnetic tape unit can read digital images created at remote locations. The digital images are then analyzed and interactively enhanced using the TAAC-1 application accelerator. A hard copy of the enhanced digital image can be obtained from either the Dicomed or CELCO film recorders. The Gould IP8500 image processing system is still used for capturing a sequence of frames and individual frames on videotape using the color videotape recorder. If desired, these frames can then be transferred to the Sun for processing using the TAAC-1 application accelerator.

The upgrade to the IPL provides researchers with a broader range of processing and analysis capabilities, significantly improved performance, and a more friendly user interface. The new system includes the capability to do volume imaging, a capability

that did not exist on the Gould IP8500 system. The TAAC-1 application accelerator can perform sophisticated operations very fast, thus allowing researchers to quickly analyze and process their image data. The enhanced images provide an effective means of presenting research results for analysis, publication, and presentation. The IPL provides a practical and interactive environment for users to process image data quickly and to obtain a variety of outputs to meet their needs.

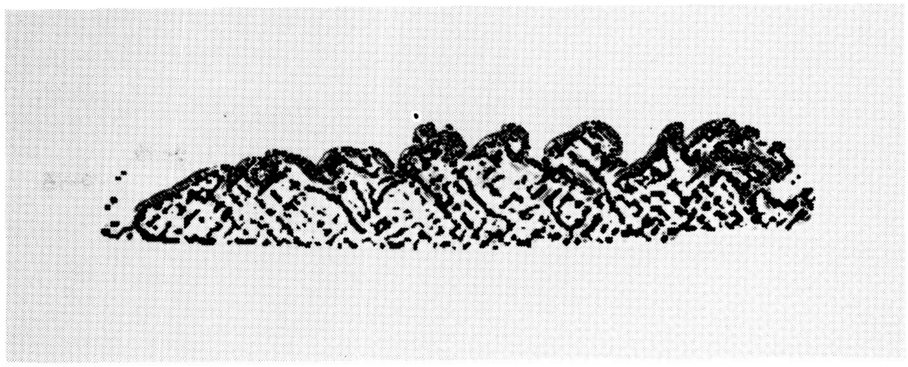

Enhanced final image.

Digital Image Enhancement of Turbulent Boundary-Layer Flow Visualization Pictures

Digital image enhancement techniques have been applied to thin, laser light sheet smoke-flow visualization pictures of an accelerating (low-speed) turbulent boundary layer approaching relaminarization. A local range modification (LRM) technique, developed originally for satellite pictures, has been found to be particularly effective in extracting organized structures, otherwise lying ill-defined, in the fully turbulent regions. The digital image enhancement was done in the IPL.

The bottom figure shows a typical laser light sheet smoke picture obtained in a wind tunnel. The horizontal direction denotes span, and the vertical direction is normal to the surface. The flow is normal to the plane of the figure. The picture is reduced to 1/4 scale. The original picture is a cross-stream section located at the upstream end of the pressure gradient. The mushroom-like organized structures can be recognized at the edges of the boundary layer. However, it is difficult to identify the organization within the turbulent core.

The bottom figure was digitized using the Eikonix digitizing camera in the IPL. The LRM technique uses an adaptive algorithm whose parameters change according to the local image contrast. This technique was applied to the digital image as a first step. The modified image was further enhanced by spatially convolving the image with a digital gradient operator and finally applying contour lines to the digital image by blackening out specified intensity ranges. The final result is shown in the top figure. The most striking feature of the top figure is the presence of crisscross lines lying at ±45° to the vertical. This feature is not obvious in the bottom figure. It is known that a vortex can be stretched most efficiently when it is inclined at 45° to the flow. The presence of the crisscross pattern in a turbulent flow is a new result with considerable significance. This pattern indicates that the effect of an abruptly applied favorable pressure gradient is to stretch the constituent hairpin vortices in a turbulent boundary layer in a most efficient manner.
(P. R. Bandyopadhyay and K. Stacy, 46719)

Original laser light sheet picture obtained in wind tunnel.

ORIGINAL PAGE
BLACK AND WHITE PHOTOGRAPH

16- by 24-Inch Water Tunnel

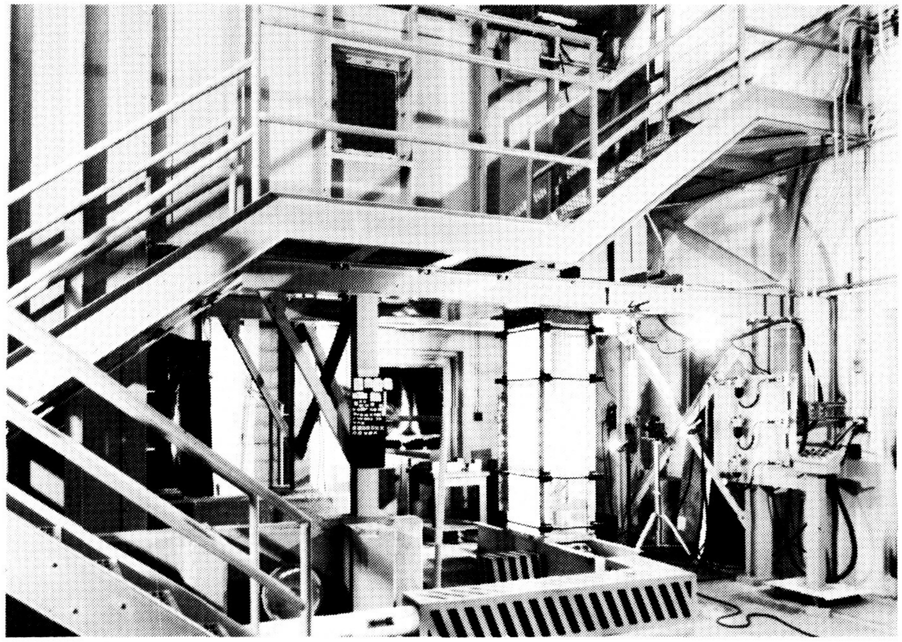

The Langley 16- by 24-Inch Water Tunnel is used for flow visualization studies at low Reynolds numbers. The tunnel has a vertical test section with an effective working length of approximately 4.5 ft. The test section is 16 in. high by 24 in. wide. All four sidewalls are plexiglass to provide optical access. A pump transfers the water from the test section exit to the reservoir upstream of the test section. The test section velocity can be varied from 0 ft/s to 0.75 ft/s. The unit Reynolds number range for water at 78°F for this velocity range is 0 to 7.7 × 10^4/ft. The normal test velocity that produces smooth flow is 0.25 ft/s.

A sting-type model support system positions the model. The model attitude can be varied in two planes over angle ranges of ±33° and ±15°. Operator-controlled electric motors are mounted outside of the test section to control the model position. The model position is read by the operator on a protractor mounted to the model support. Semispan models are mounted on a splitter plate supported by a sting with a lateral offset.

Ordinary food coloring is used as a dye to visualize the flow. The dye is supplied by three reservoirs under pressure so that up to three dye colors may be used. Dye may be ejected from small orifices on the model surface or injected upstream of the test section. The water tunnel was placed in operation in 1987 and has been used to study flows over delta wings and over a rectangular wing with a Gurney flap.

Spanwise Blowing at Wing Tip

Spanwise blowing at the wing tip has been suggested as a means of increasing wing lift. Recent studies of this concept used blowing through one or more discrete jets mounted in the wing tip. The results indicate that spanwise blowing increases the wing lift and changes the intensity and spanwise location of the wing tip vortex. Flow visualization studies detected two counterrotating vortices that formed near the jet exit and turned downstream. The changes in the wing tip vortex intensity and location may be the result of the interaction of the two jet vortices with the wing tip vortex. In order to maintain a subsonic jet exit velocity, the jet-to-free-stream velocity ratio should be approximately 4 or less. Many of the previous studies of wing tip blowing used jet velocity ratios much greater than this. Further studies of the jet path and vorticity as well as the interaction of the jet vortices with the wing tip vortex are needed at these lower jet velocity ratios.

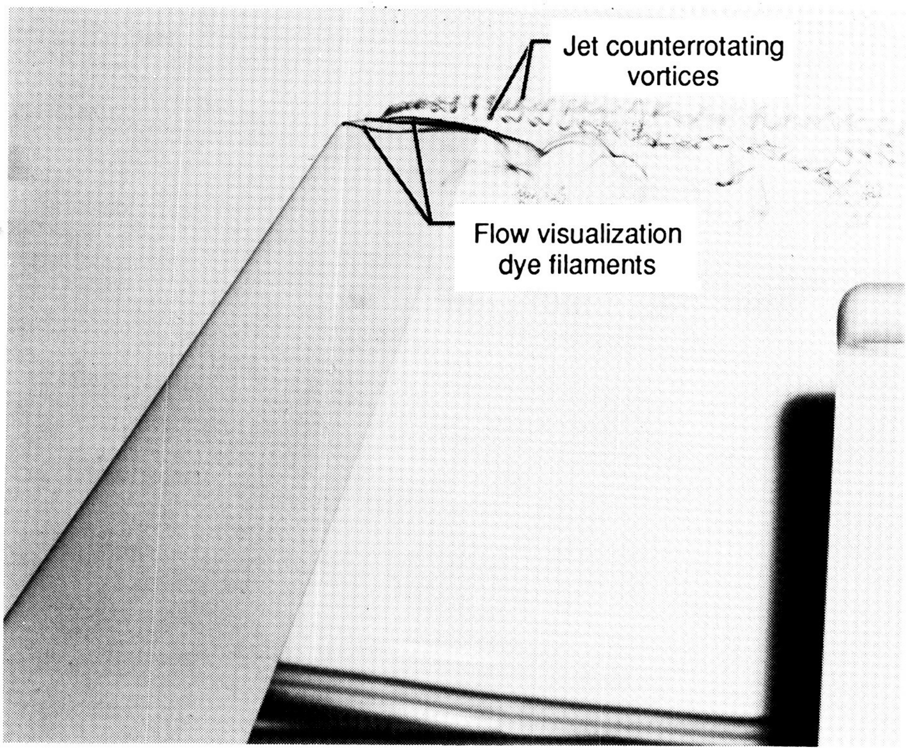

Paths of jet counterrotating vortices for jet velocity ratio of 2 with wing lift.

A water tunnel study of the flow field about a wing with spanwise blowing at the tip was conducted in the 16- by 24-Inch Water Tunnel. The water tunnel model consisted of a semispan wing and four interchangeable wing tips. The wing planform had a leading-edge sweep of 33°, a taper ratio of 0.4, and an aspect ratio of 5.7. The end of the wing tip was rounded. The flow visualization indicated that there was separation near the midchord position. The lower wing circulation prevented visualization of the wing tip vortex. The dye in the jet visualized the jet vortices very well at the lower jet velocity ratios. The jet vortex path moved farther from the wing tip as the jet velocity ratio increased. As the wing lift increased, the vortex path was drawn closer to the wing tip and tended to rotate about the expected path of the wing tip vortex. The tendency of the streamlines to move inboard near the tip is reduced as the jet velocity ratio increased. The strength of the jet vortices decreased rapidly as the vortices became aligned with the free stream. The interaction of the jet vortices with the wing tip vortex needs further study to determine any effect on the tip vortex strength and path.
(R. E. Mineck, 42879, and J. L. Wellons)

Flow Visualization Study of Gurney Flaps

Gurney flaps have been identified as having the potential to improve high lift characteristics of airfoils. Previous studies have shown increases in maximum lift coefficient and lift curve slope, and reductions in the angle of attack for zero lift relative to the clean-trailing-edge configurations. This is similar to how other trailing-edge high-lift devices perform. However, some studies have shown drag reductions (for certain airfoil geometries) which would not normally be expected. This, of course, is a highly desirable characteristic and has provided incentive for further study.

The basic Gurney flap is simply a flat plate located at the airfoil trailing edge perpendicular to the chord line on the pressure side of the airfoil (as shown in the first figure). It has been hypothesized that the drag reduction produced by this device is due to the recirculation region on the downstream side of the flap. This region is thought to induce a downward turning of the flow over the trailing-edge upper surface which keeps the flow attached when it would otherwise be separated. There is therefore a reduced wake momentum deficit and, accordingly, less profile drag. These hypothesized characteristics provided the stimulus for a water tunnel study of Gurney flaps.

A test was conducted in the 16- by 24-Inch Water Tunnel at a chord Reynolds number of 8588. The wing model used was a rectangular planform semispan model with an NACA 0012 airfoil section. Research concentrated on two areas that included visualization of the recirculation region and the effect of the Gurney flap on upper surface trailing-edge separation. A sketch of the results of the flow visualization near the Gurney flap is shown in the second figure. The recirculation region oscillated under the influence of the large laminar wake vortices. The internal structure of this recirculation region was similar

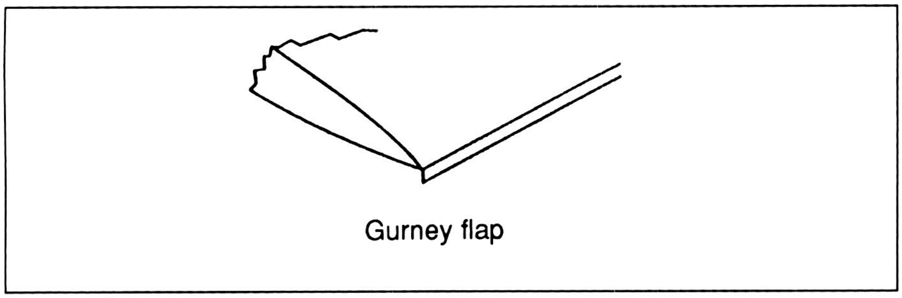

Gurney flap.

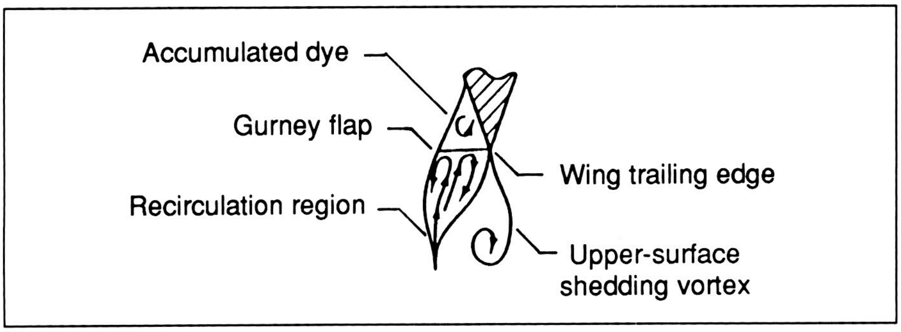

Flow inside recirculation region.

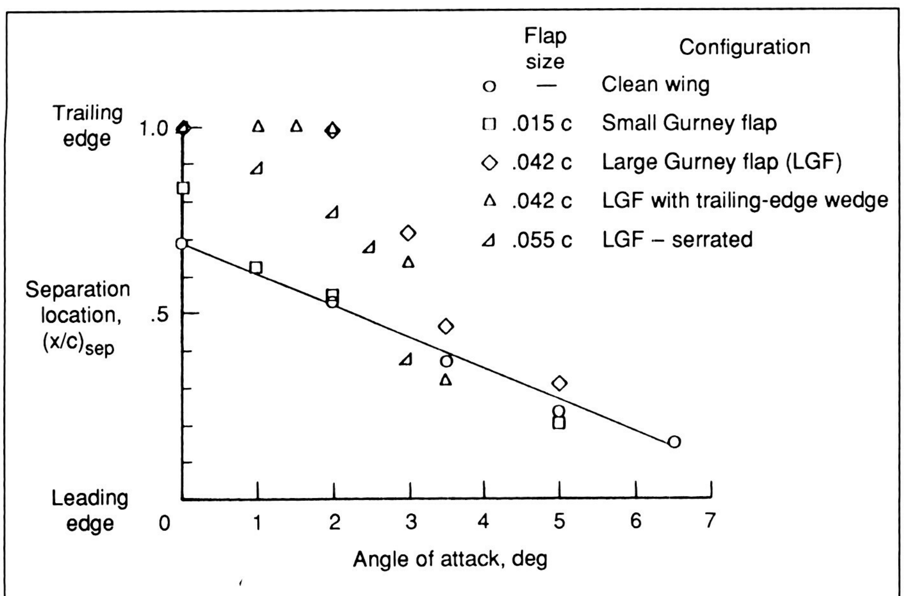

Nondimensional separation locations for clean wing and wing with various Gurney flap configurations.

to that previously hypothesized and indicated significant turning of the flow in the upper surface trailing-edge region.

The effectiveness of the Gurney flap in turning the flow and thereby reducing the trailing-edge separation was determined by examining the wing upper surface separation locations. As indicated in the plot in the third figure, several of the Gurney flap configurations delayed the flow separation to higher angles of attack. This fact implied an acceleration and turning of the flow in the trailing-edge region and possibly a reduction in profile drag due to the reduced wake momentum deficit relative to the separated region on the wing with the clean trailing edge. More detailed study, including studies of various modifications to the Gurney flap, is required to determine appropriate airfoil section shapes for application of this device. Such studies should be done at higher Reynolds numbers in facilities where force and moment and flow field information can be obtained.

(D. H. Neuhart, 43012 , and O. C. Pendergraft, Jr.)

Computer-Generated Animation System

Video system in use at graphics workstation.

A rack-mounted portable video system has been assembled for use in making tape recordings of computer-generated graphics of dynamic physical phenomena such as fluid flows and structural vibrations. The video system can be used with any computer that outputs RS170A RGB (red/green/blue) color signals and a sync signal and has an RS232 port.

A photograph of the video system in use next to a graphics workstation is shown in the above figure. The principal components of the system are sketched in the schematic drawing that shows the system being used with an IRIS workstation.

The animation software executing on the IRIS includes a device driver that communicates with the animation controller through an RS232 port. The animation controller regulates the frame-by-frame recording of graphics drawn on the system console monitor. By recording each frame only after it is fully drawn, the process of actually rendering the scene, however time consuming, is not reproduced on tape, and smooth animations can be achieved of even complicated color images. The transcoder conditions the RGB signals for input to the tape recorders. A sync generator is included for use

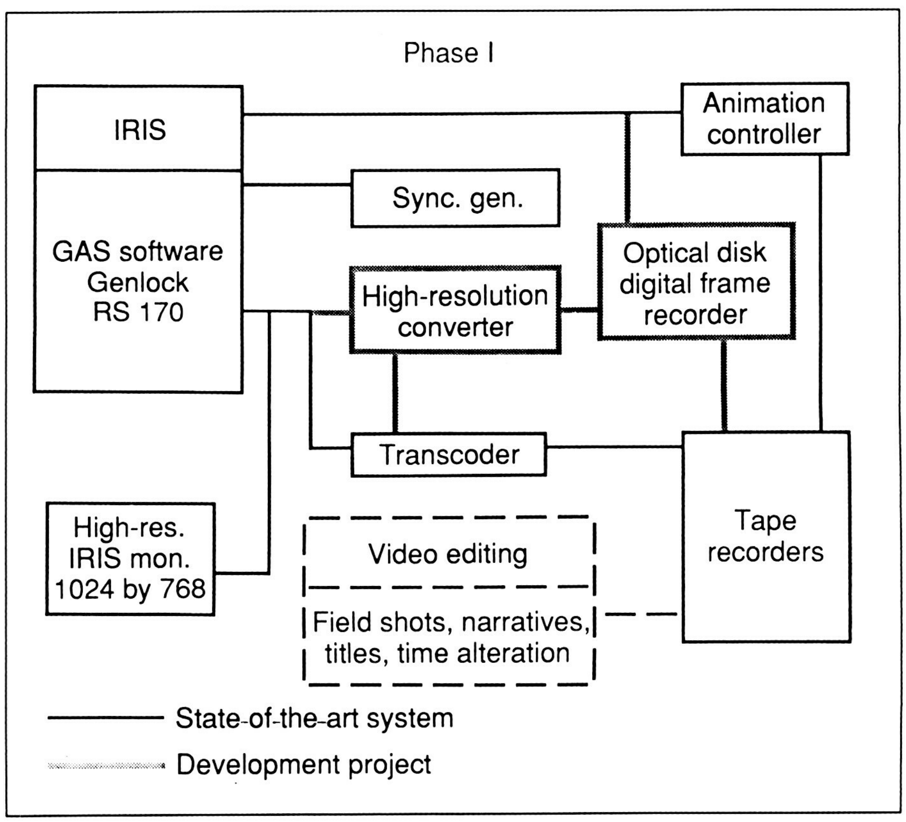

Schematic of video system attached to IRIS workstation.

with workstations that do not provide the proper sync signals themselves.

A high-quality 1/2-in. Betacam recorder/player for producing the master tape and a U-matic SP 3/4-in. recorder for making distribution copies are available. A scan converter, configured for 1024- by 768-pixel screen resolution, has been added to the system. This device antialiases high-resolution graphics in real time to provide good-quality standard video resolution signals for the recorders with no time penalty. A video disk player/recorder capable of holding up to 1 hour of video is being integrated into the system. The video disk will eliminate some tape handling and provide more flexible user access to recorded video frames. These components form an integrated system designed to work as a unit. The system has been configured to operate successfully with Silicon Graphics IRIS 3030 and 4-D workstations, a Lexidata Solidview raster workstation, and an Evans and Sutherland PS 300 color graphics system.

The Betacam recorder is capable of simple manual editing of original rough videos. For professional editing, the videotapes obtained with this system may be processed through the Langley Research Center Research Information and Applications Division video production facility.

The system has been used to produce videotapes of hypersonic inlet flows, boundary-layer transition, grid generation, and pressure distributions on flexible bodies. Groups in the Aeronautics, Structures, Electronics, and Space Directorates have found videotaping useful to convey the results of their computer simulations to a wide audience in the research community.

(D. L. Lansing, 46714)

ORIGINAL PAGE
BLACK AND WHITE PHOTOGRAPH

13-Inch Magnetic Suspension and Balance System

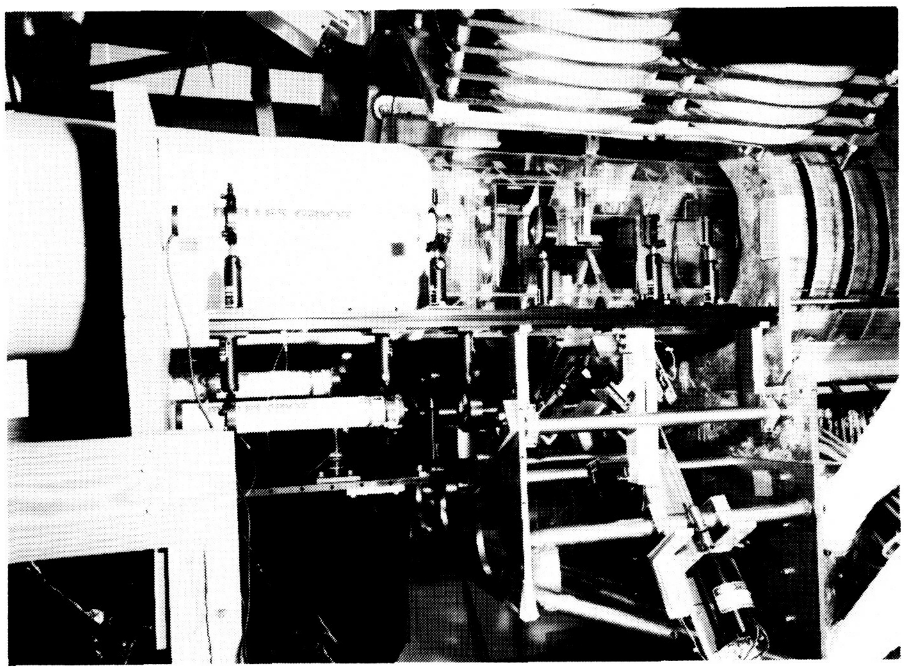

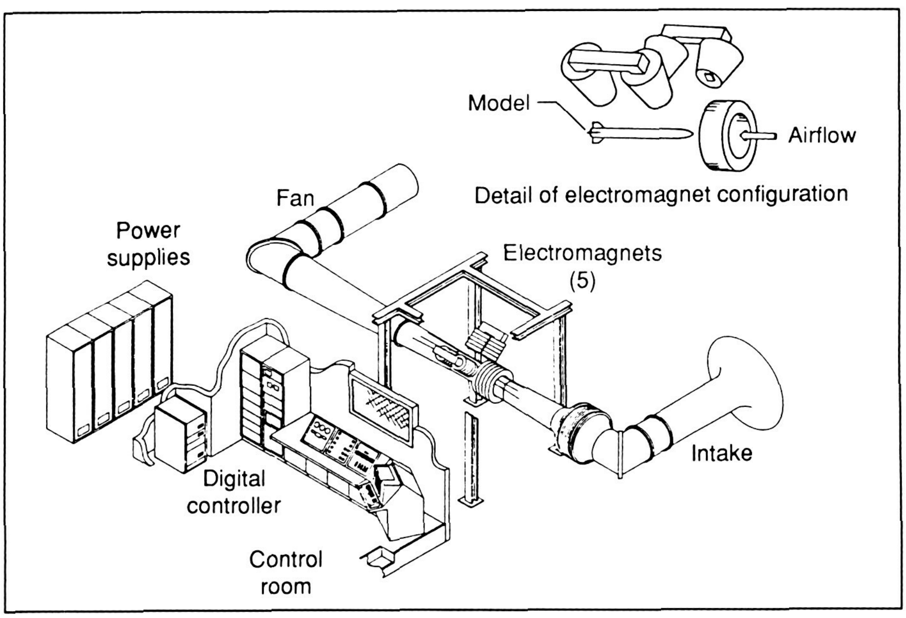

MSBS laboratory schematic.

The Langley 13-Inch Magnetic Suspension and Balance System (MSBS) is a laboratory established to develop technology required for wind tunnel testing that is free of model-support interference. In 1984, the laboratory began operation as a combination of a magnetic suspension and balance system, previously on loan from the United States Air Force, and a small subsonic wind tunnel.

For this system, four electromagnets (arranged in a "V" configuration) above the wind tunnel test section provide the lift force, pitching moment, side force, and yawing moment. A drag electromagnet opposes the drag force. Motion is controlled in these five degrees of freedom with no provision for generation of controlled magnetic roll torque on the model. The 13-Inch MSBS has a lift force capability of approximately 6 lb depending on the size and shape of the iron core in the model. The test section passes through the drag electromagnet.

The tunnel is a continuous-flow, closed-throat, open-circuit design. Ambient air enters the tunnel from the outside through a large bellmouth intake protected from outside contaminants by a screen enclosure. At the end of the tunnel, the flow exhausts to the outdoors. The tunnel is capable of speeds up to Mach 0.5. The transparent test section measures approximately 12.6 in. high and 10.7 in. wide.

Drag Measurements on Modified Prolate Spheroid

Tests have been performed as part of a program primarily aimed at determining the drag force measuring capabilities of the 13-Inch MSBS. The modified prolate spheroid was chosen because of its low drag characteristics and extended run of laminar flow. In addition, a simple support interference study was accomplished by using a dummy sting.

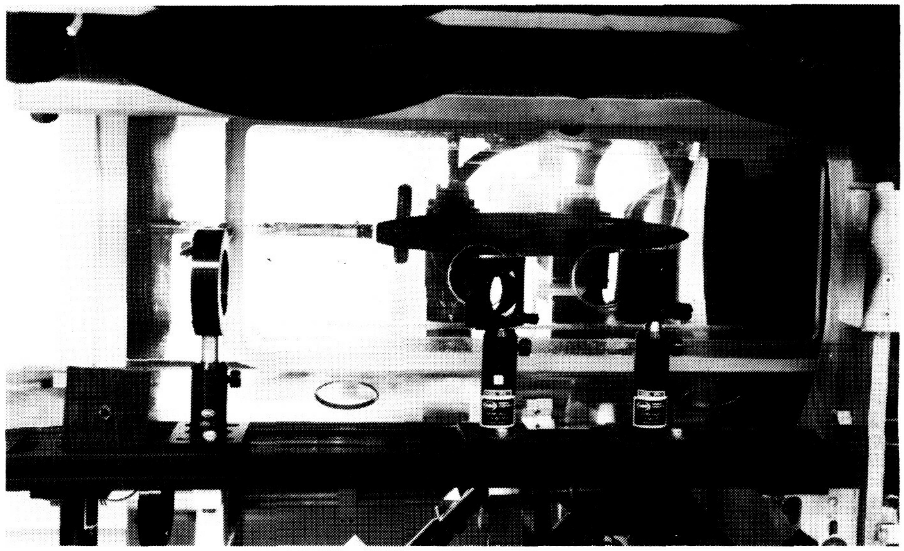

Model in suspension with dummy sting installed. L-88-10341

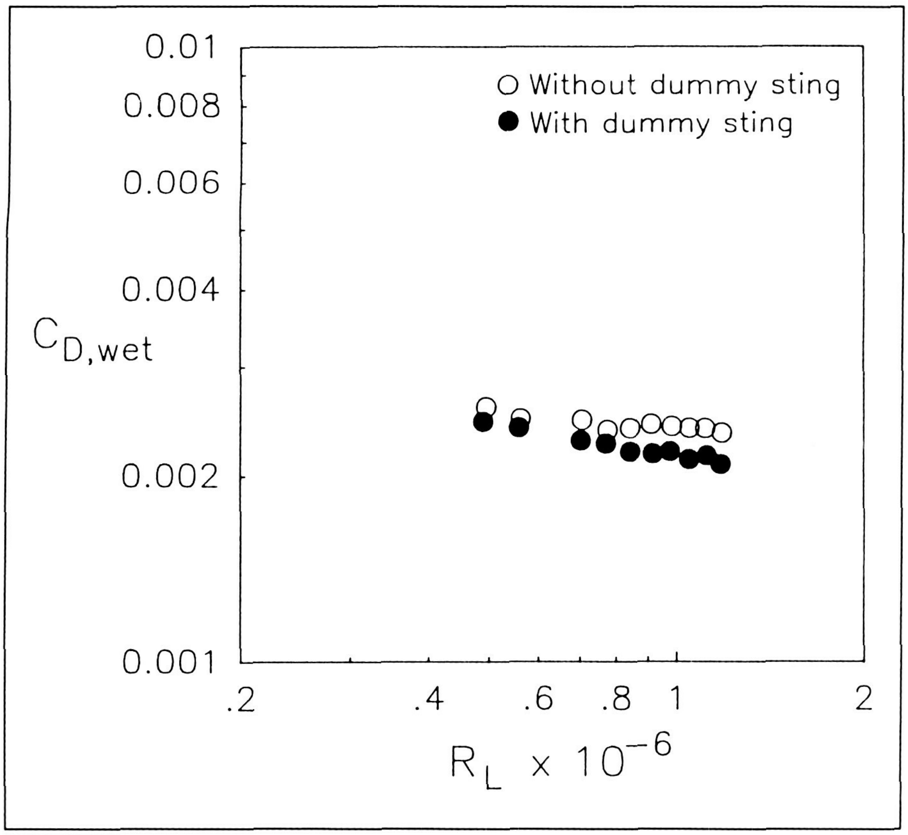

Comparison of drag characteristics with and without dummy sting.

The initial phase of testing consisted of a drag force calibration. The results from this calibration indicate there is no significant hysteresis in the data.

Wind-on drag force measurements (both free and fixed transition) were taken for this body over the Mach number range from approximately 0.06 to 0.26. Comparisons with data from other sources on both the same shape and a similar shape generally show good agreement.

For the tests with the dummy sting, the model was actually "flown" on the sting without contact between them. A gap of approximately 0.04 in. was present between the sting and the model, and the sting extended up into the model approximately 1/16 in. The drag coefficients are lower for the case with the dummy sting present. More significantly, the differences between the two data sets get larger with increasing Reynolds numbers.
(D. A. Dress, 45126)

Cavity/Store Separation

Considerable effort is being expended on modeling of the internal store release problem. A data base exists from tests with the United States Air Force Arnold Engineering Development Center captive-trajectory system; however, no data exist on the

ORIGINAL PAGE
BLACK AND WHITE PHOTOGRAPH

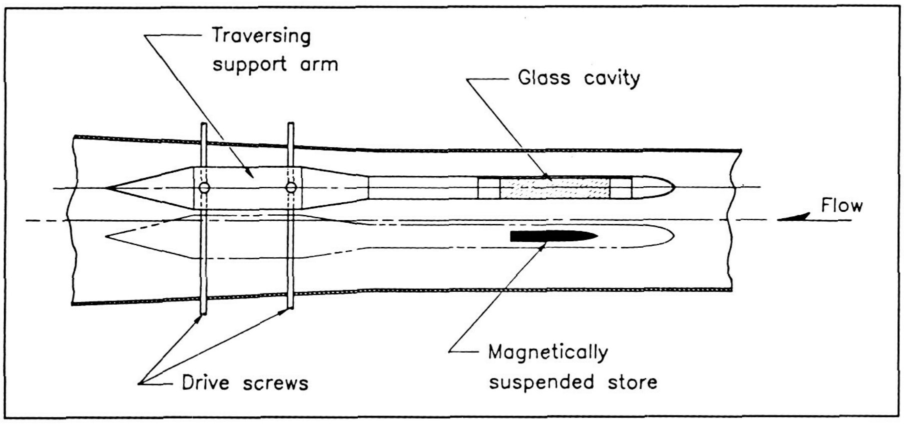

MSBS cavity/store separation demonstration.

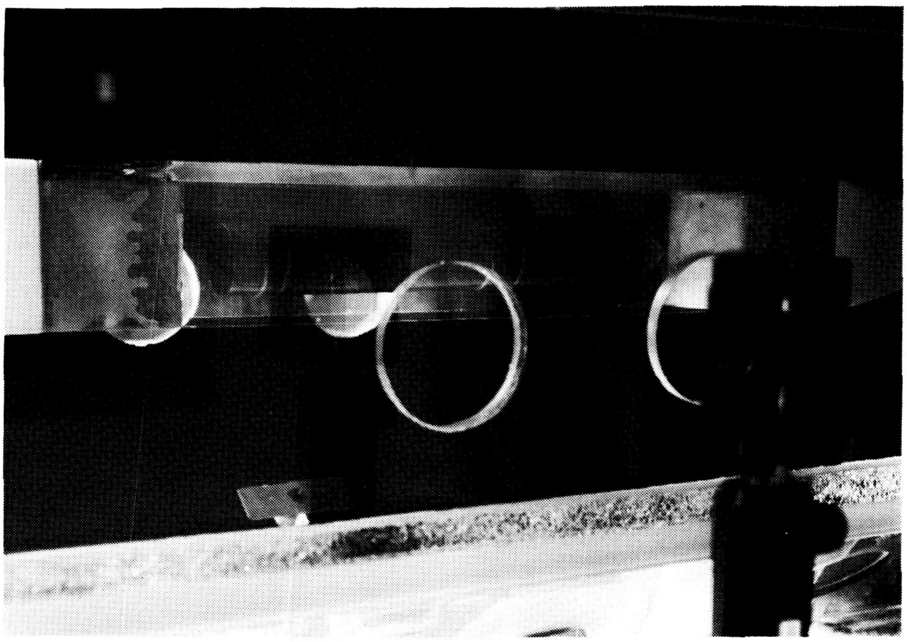

Magnetically suspended store model inside glass cavity with no tunnel flow. L-87-10741

unsteady aerodynamics of the release. Also, there is a severe problem with store damage before release. This damage is probably from vibration due to cavity flow unsteadiness and aeroacoustic loads when the cavity doors are open.

To study both static and dynamic characteristics of the cavity/store separation process, a simple cavity test rig for the 13-Inch MSBS tunnel has been built. The first figure shows this rig. The rig moves the glass cavity to cover and uncover a magnetically suspended store. For the initial tests, a steel rod in a polyvinyl chloride (PVC) tube with a wooden ogive nose serves as the generic store.

A store was successfully suspended and controlled in, partially in, and out of the cavity at several tunnel speeds up to $M = 0.175$. The second figure shows the store suspended in the cavity with no tunnel flow. These tests in the MSBS dramatically showed the effect of the unsteady cavity flow on the enclosed store.

Additional tests will be made at higher speeds with an improved cavity test rig. Improvements to the cavity test rig include a better drive system and clearer optical paths through the test section walls and cavity. Future tests will have dynamic pressure instrumentation installed in the end of the cavity to record fluctuating pressures.

(W. G. Johnson, Jr., 45133)

Slanted-Base Ogive Cylinder Models

The aerodynamic characteristics of a family of slanted-base ogive cylinder models have been examined. Interest in this geometry is due to the abrupt change in drag coefficient occurring around a 45° slant angle. This arises due to a change in wake structure from quasisymmetric closure to a longitudinal vortex flow. Further tests are establishing the effects of a dummy sting support on the aerodynamic behavior. Measurements are made with a dummy sting protruding into a cavity in the model's base, but not in contact with any part of the model.

Early results show a consistent reduction in the drag of the 0° base model with the sting present. Sting cavity pressure

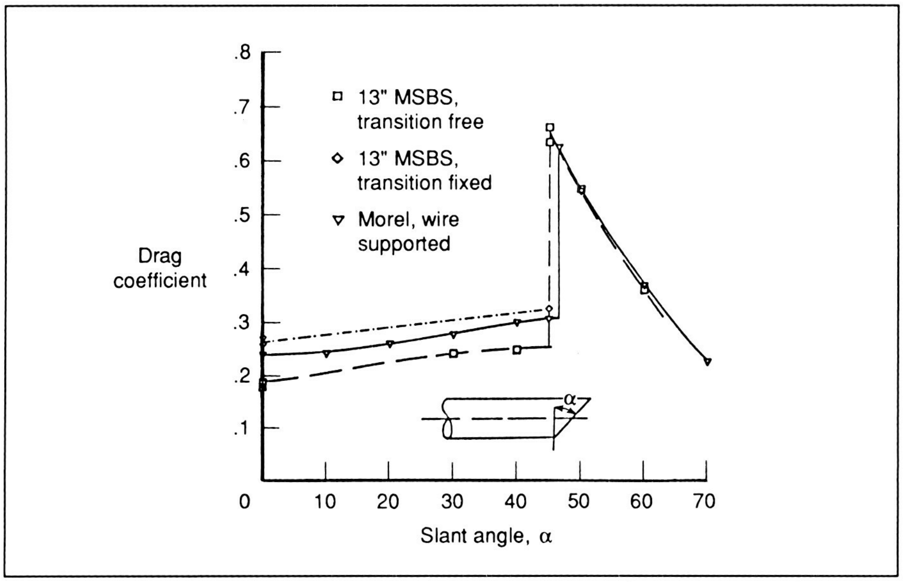

Variation of drag coefficient with base slant angle ($R_{e_D} = 94,000$).

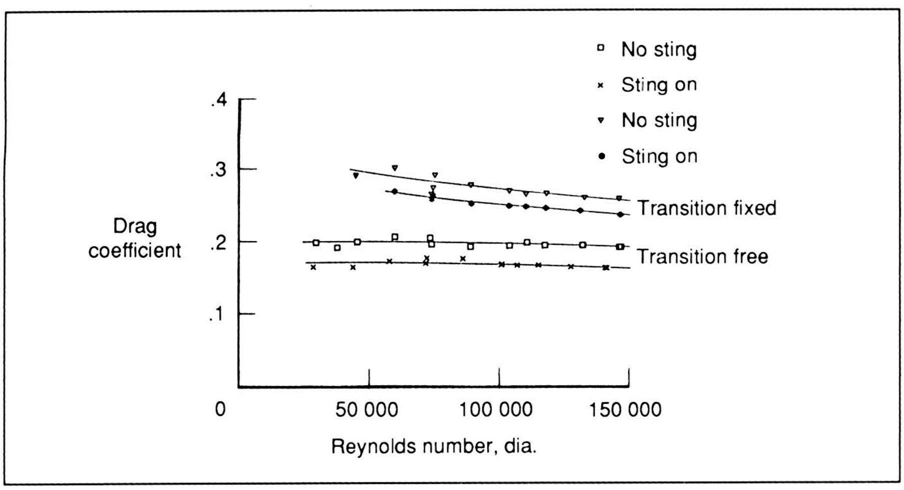

Effect of dummy sting on drag with 0° base.

and base pressure measurements, using remote telemetry, show a correspondingly increased (less negative) base pressure with the sting present. Testing continues with other base slant angles.

(C. P. Britcher and R. P. Boyden, 45160)

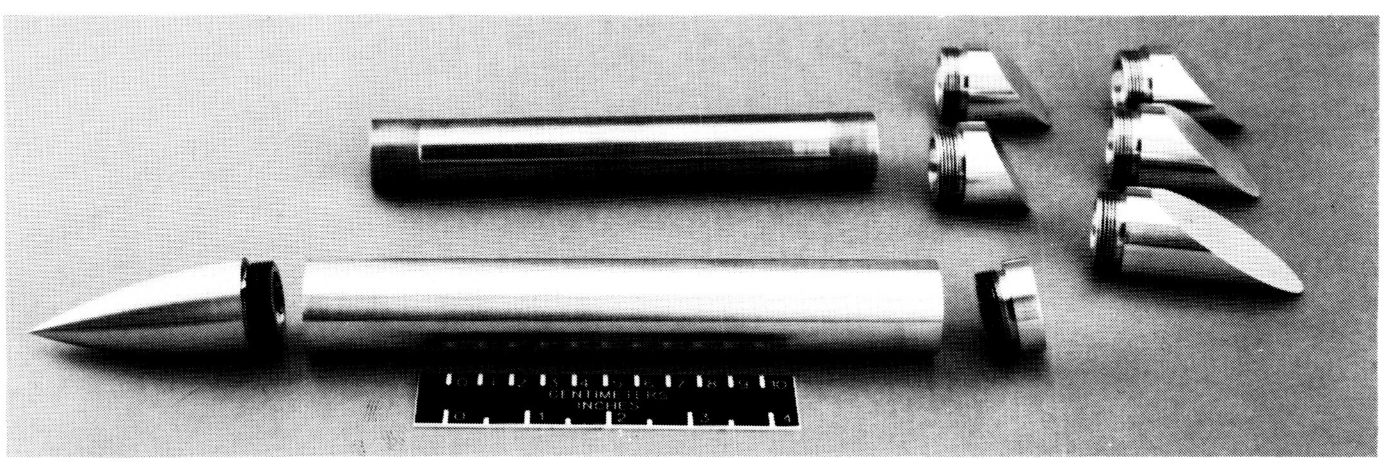

Ogive cylinder model showing interchangeable bases and magnetic core. L-86-11668

Supersonic Low-Disturbance Pilot Tunnel

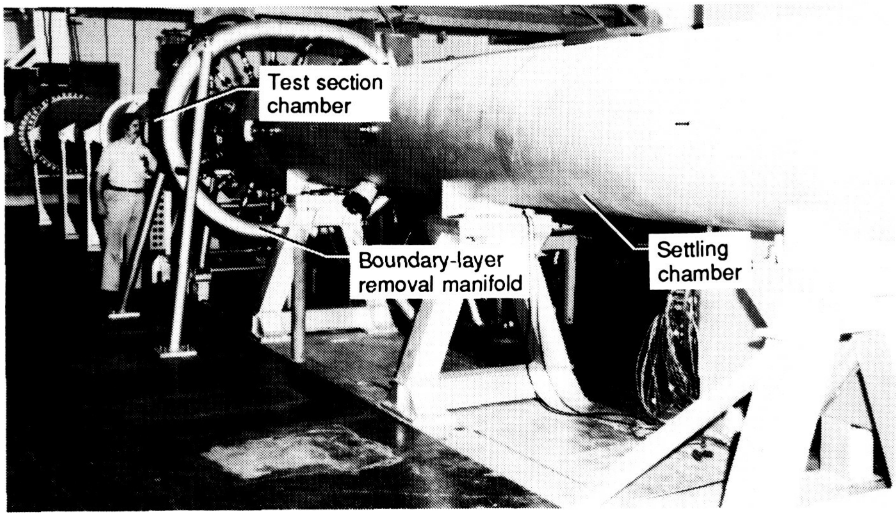

The Supersonic Low-Disturbance Pilot Tunnel (formerly called the Langley Mach 3.5 Low-Disturbance Pilot Tunnel) has been in operation since 1981. The tunnel, which is located in the Gas Dynamics Laboratory, uses high-pressure air from a 4200 psi tank field that is dehydrated to a dew point temperature of -52° F, reduced in pressure by control valves located upstream of the settling chamber, and filtered to remove all particles larger than 1 μm in size.

The predicted locations of transition from laminar-to-turbulent flow in the boundary layers of high-speed, high-altitude flight vehicles are critical design considerations because both friction drag and aerodynamic heating may be greatly affected by uncertainties in these predictions. Unfortunately, transition phenomena are extremely sensitive to noise, which is a known contaminant in conventional high-speed wind tunnels. For Mach numbers >2.5, the predominant sources of this wind tunnel noise are acoustic disturbances radiated into the free stream from the supersonic turbulent boundary layers on the tunnel walls. Other sources of noise in blowdown wind tunnels are pressure-reducing control valves that regulate the settling chamber pressure. The tunnel is a part of an ongoing Langley Research Center program to develop and test methods for eliminating or reducing severe noise problems.

The main figure above shows the settling chamber (visible on the right-hand side) and the open-jet test section chamber (visible on the left-hand side). The tunnel flow exhausts to a vacuum sphere complex that provides up to approximately 1-hr run times for stagnation pressures from 25 psia to 100 psia. At higher pressures, the flow is exhausted to the atmosphere. The settling chamber contains seven antiturbulence screens along with a number of dense porous plates that function as acoustic baffles to attenuate the high-level noise from the control valves and the piping system. These porous plates reduce the incoming noise from approximately 0.2 percent of stagnation pressure to approximately 0.01 percent. The antiturbulence screens reduce the normalized rms velocity fluctuations to approximately 1 percent.

With the input disturbances reduced to these low levels, research has shown that the most successful technique to eliminate the radiated noise is to laminarize the nozzle wall boundary layers by using boundary-layer removal slots just upstream of the nozzle throat and properly tailored expansion nozzles with highly polished walls. The large circular manifold shown in the figure is connected to a vacuum sphere and is used to remove the nozzle inlet boundary layer through a series of 1-in.-diameter pipes. By the use of these techniques, all disturbances have been practically eliminated in three different nozzles for Mach numbers of 3 and 3.5.

Effects of Wind Tunnel Noise on Supersonic Transition

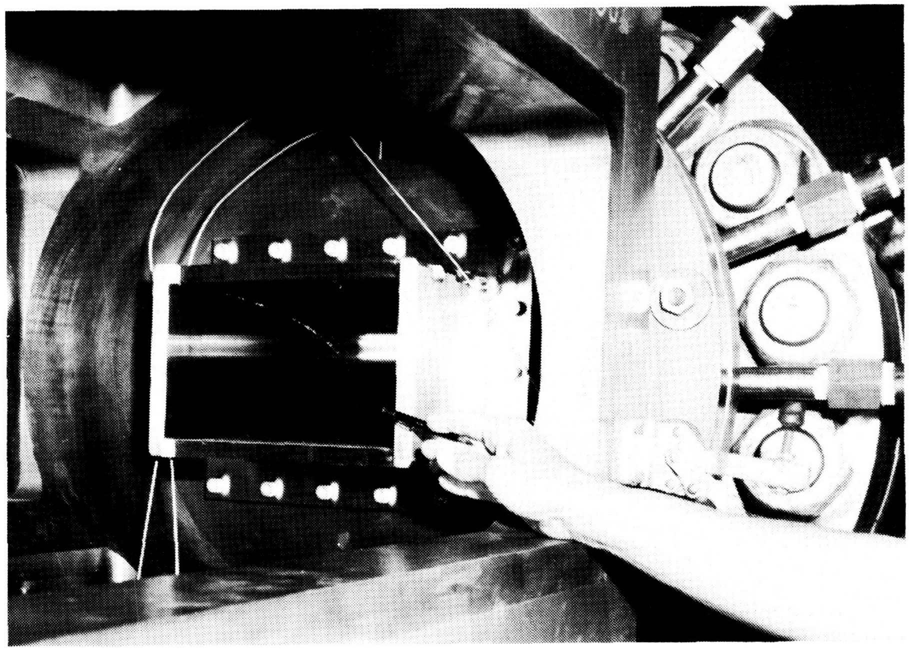

Mach 3.5 two-dimensional nozzle. L-81-4422

Test results in the Supersonic Low-Disturbance Tunnel (formerly called the Langley Mach 3.5 Low-Disturbance Tunnel) obtained on cones at Mach 3.5 show excellent agreement with predictions from linear stability theory and with flight data. This theory also predicts that transition should occur farther downstream on flat plates than on cones at the same test conditions. Conventional wind tunnel data, however, have shown the opposite effect, which caused uncertainty as to the utility of the theory. Recent data from this facility have shown that flat-plate transition does occur farther downstream on flat plates than on cones and is accurately predicted by the theory, thus resolving this long-standing discrepancy. The most important implication of this new result is that the profound effects of wind tunnel noise on transition are different for planar- and conical-type vehicles.

In addition, data obtained on sharp cones at small angles of attack show that wind tunnel noise has a much larger effect on the location of transition on the windward side than on the leeward side. The transition trend with increasing bluntness is in agreement with predictions from linear stability theory for blunt cones at an angle of attack of zero. However, when moderate tunnel noise is present, the trend is modified, and linear theory is no longer applicable.

Finally, wind tunnel noise has been shown to have no effect on transition on the leading edge of a swept wing, provided the surface is smooth and spanwise propagation of disturbances is eliminated. Thus, it is concluded that each configuration must be tested in low-disturbance conditions before the full effects of wind tunnel noise on transition can be determined.

Recent developments in the theory required for the design of advanced hypersonic nozzles with the capability to provide very low-disturbance test flows at high Reynolds numbers now have been experimentally verified. Therefore, the techniques and requirements for the design and fabrication of low-disturbance supersonic/hypersonic wind tunnels have now been developed and tested. These new low-disturbance facilities will be essential for evaluating and controlling viscous flows for a variety of high-speed applications, including the development and testing of laminar-flow control techniques for applications to the second-generation supersonic transport aircraft. Boundary-layer stability and transition prediction codes can be calibrated and validated only in these low-disturbance tunnels over the speed range required for application to supersonic and hypersonic aircraft of the twenty-first century.

The figure shows a view inside the open-jet test section of the tunnel. The exit of a small two-dimensional nozzle is identified by the hand-held pencil. Some of the 1-in.-diameter pipes used to remove the inlet boundary layer are visible on the right side of the figure.

(I. E. Beckwith, 45544)

NASA
National Aeronautics and Space Administration

Report Documentation Page

1. Report No.	2. Government Accession No.	3. Recipient's Catalog No.
NASA TM-101579		

4. Title and Subtitle Langley Aerospace Test Highlights—1988	5. Report Date May 1989
	6. Performing Organization Code
7. Author(s)	8. Performing Organization Report No.
9. Performing Organization Name and Address NASA Langley Research Center Hampton, VA 23665-5225	10. Work Unit No.
	11. Contract or Grant No.
12. Sponsoring Agency Name and Address National Aeronautics and Space Administration Washington, DC 20546-0001	13. Type of Report and Period Covered Technical Memorandum
	14. Sponsoring Agency Code

15. Supplementary Notes

16. Abstract

The role of the Langley Research Center is to perform basic and applied research necessary for the advancement of aeronautics and space flight, to generate new and advanced concepts for the accomplishment of related national goals, and to provide research advice, technological support, and assistance to other NASA installations, other government agencies, and industry. This report highlights some of the significant tests which were performed during calendar year 1988 in Langley test facilities, a number of which are unique in the world. The report illustrates both the broad range of the research and technology activities at the Langley Research Center and the contributions of this work toward maintaining United States leadership in aeronautics and space research. Other highlights of Langley research and technology for 1988 are described in *Research and Technology 1988 Annual Report of the Langley Research Center*. Further information about both reports is available from the Office of the Chief Scientist, Mail Stop 105-A, Langley Research Center, Hampton, Virginia 23665-5225 (804-864-6062).

17. Key Words (Suggested by Authors(s))	18. Distribution Statement
Research and technology Tests Facilities Wind tunnels Models	Unclassified—Unlimited Subject Category 99

19. Security Classif. (of this report)	20. Security Classif. (of this page)	21. No. of Pages	22. Price
Unclassified	Unclassified	165	A08

NASA FORM 1626 OCT 86

NASA-Langley, 1989

For sale by the National Technical Information Service, Springfield, Virginia 22161-2171

dies, and the digestive systems of termites and ruminant animals), and the chlorofluorocarbons, or CFCs, which are still utilized in some parts of the world as spray-can propellants and throughout the industrialized world in plastic-foam manufacture, cleaning of industrial components, air conditioning, and refrigeration.

CFCs and Stratospheric Ozone

The introduction of CFCs into the atmosphere can ultimately lead to depletion of the Earth's stratospheric ozone layer, which shields terrestrial life from harmful solar ultraviolet radiation. Once released into the lower atmosphere, the CFCs migrate upward into the stratosphere, where they are decomposed by ultraviolet sunlight. The chlorine thus freed acts as a catalyst to destroy ozone. There is strong evidence that CFCs are largely responsible for the substantial seasonal declines in ozone levels over Antarctica in recent years, and there is mounting concern that global ozone levels are also being affected. Atmospheric concentrations of the two major CFCs are currently increasing at the alarming rate of 5% per year. Other greenhouse gases, such as methane and nitrous oxide, also play roles in the ozone chemistry of the upper atmosphere.

The United States banned CFCs as aerosol propellants in 1978, and many nations have now agreed to further limit CFC use. However, our knowledge of upper-atmosphere chemistry is at present inadequate for detailed study of the ozone problem, as is our understanding of the dynamical processes and energy balances that are closely coupled to chemical effects. Informed policy decisions of the 1990s will need to draw upon a comprehensive data base furnished by a systematic, global research program targeted at the upper atmosphere. NASA's Upper Atmosphere Research Satellite (UARS) is the centerpiece of that program.

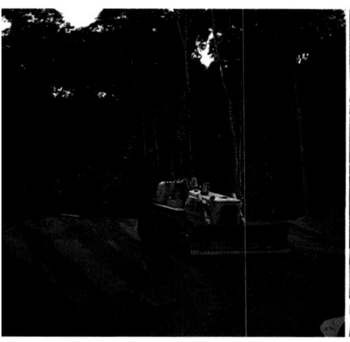

of solar ultraviolet radiation resulting from ozone loss could lead to an increase in human skin cancer from exposure to sunlight. Below, left: volcanic eruptions inject sulfur compounds and other gases and particles into the atmosphere. Below, right: industrial processes alter lower-atmosphere chemistry, eventually affecting upper-atmosphere composition.